



## **DISCLAIMER**

This report has been prepared by the Institute of Geological and Nuclear Sciences Limited (GNS Science) exclusively for and under contract to Christchurch City Council.

The report considers the risk associated with geological hazards. As there is always uncertainty inherent within the nature of natural events GNS Science gives no warranties of any kind concerning its assessment and estimates, including accuracy, completeness, timeliness or fitness for purpose and accepts no responsibility for any actions taken based on, or reliance placed on them by any person or organisation other than Christchurch City Council.

GNS Science excludes to the full extent permitted by law any liability to any person or organisation other than Christchurch City Council for any loss, damage or expense, direct or indirect, and however caused, whether through negligence or otherwise, resulting from any person or organisation's use of, or reliance on this report.

The data presented in this Report are available to GNS Science for other use after the public release of this document.

## **BIBLIOGRAPHIC REFERENCE**

Massey, C. I.; Della Pasqua, F.; Lukovic, B.; Yetton, M. D.; Archibald, G.; Ries, W. 2014. Canterbury Earthquakes 2010/11 Port Hills Slope Stability: Risk assessment for Clifton Terrace. *GNS Science Consultancy Report 2014/76*. 125 p. + Appendices

## **REVIEW DETAILS**

This report in draft form was independently reviewed by Dr L. Richards, Dr J. Wartman and T. Taig. Internal GNS Science reviews of drafts were provided by M. McSaveney and N. Litchfield.

## CONTENTS

<b>EXECUTIVE SUMMARY</b> .....	<b>VII</b>
ES 1 INTRODUCTION.....	VII
ES 2 INVESTIGATION PROCESS AND FINDINGS .....	VIII
ES 3 CONCLUSIONS .....	X
ES3.1 Hazard.....	x
ES3.2 Risk.....	x
ES 4 RECOMMENDATIONS.....	XI
ES4.1 Policy and Planning.....	xi
ES4.2 Short-term actions .....	xi
ES4.3 LONG-TERM ACTIONS.....	XII
<b>1.0 INTRODUCTION</b> .....	<b>1</b>
1.1 BACKGROUND.....	1
1.2 THE CLIFTON TERRACE MASS MOVEMENTS .....	5
1.3 PREVIOUS WORK AT THE CLIFTON TERRACE SITE .....	9
1.4 SCOPE OF THIS REPORT.....	10
1.5 REPORT STRUCTURE .....	11
1.6 METHODS OF ASSESSMENT.....	11
1.6.1 Engineering geology assessment .....	11
1.6.2 Hazard assessment.....	12
1.6.3 Estimation of landslide extent and failure mechanism .....	12
1.6.4 Risk assessment .....	12
<b>2.0 DATA USED</b> .....	<b>15</b>
<b>3.0 SITE ASSESSMENT RESULTS</b> .....	<b>17</b>
3.1 SITE HISTORY.....	17
3.1.1 Aerial photograph interpretation .....	17
3.1.2 Before the 2010/11 Canterbury earthquakes .....	18
3.1.3 During the 2011 Canterbury earthquakes .....	19
3.1.4 After the 2010/11 Canterbury earthquakes .....	20
3.2 SITE INVESTIGATIONS .....	27
3.2.1 Geomorphological mapping .....	27
3.2.2 Subsurface trenching, drilling and probing.....	27
3.2.3 Geophysics.....	30
3.2.4 Surface movement .....	30
3.2.5 Subsurface movement .....	34
3.2.6 Groundwater.....	38
3.3 ENGINEERING GEOLOGICAL MODEL.....	40
3.3.1 Slope materials.....	40
3.3.2 Geotechnical properties .....	51
3.3.3 Rainfall and groundwater response.....	66
3.4 SLOPE FAILURE MODELS .....	72
3.4.1 Landslide types affecting the site .....	72

3.4.2	Failures mechanisms adopted for modelling.....	74
<b>4.0</b>	<b>HAZARD ASSESSMENT RESULTS .....</b>	<b>77</b>
4.1	SLOPE STABILITY – STATIC CONDITIONS.....	77
4.1.1	Model sensitivity to groundwater.....	86
4.2	SLOPE STABILITY – DYNAMIC CONDITIONS.....	89
4.2.1	Amplification of ground shaking .....	89
4.2.2	Back-analysis of permanent slope deformation .....	90
4.2.3	Forecast modelling of permanent slope displacement.....	101
4.3	SLOPE STABILITY – SUMMARY OF RESULTS .....	103
4.3.1	Cross-section 2 (source area A).....	104
4.3.2	Cross-section 3 (source area B).....	105
4.3.3	Landslide hazard .....	106
<b>5.0</b>	<b>RISK ASSESSMENT RESULTS .....</b>	<b>107</b>
5.1	TRIGGERING EVENT FREQUENCIES .....	107
5.2	FREQUENCY OF EARTHQUAKE TRIGGERS .....	107
5.2.2	Frequency of rainfall triggers.....	110
5.2.3	Overall triggering event frequency .....	110
5.3	RISK TO DWELLINGS .....	110
<b>6.0</b>	<b>DISCUSSION.....</b>	<b>115</b>
6.1.1	Annual frequency of the event.....	115
6.1.2	Risk assessment sensitivity to uncertainties .....	115
<b>7.0</b>	<b>CONCLUSIONS .....</b>	<b>117</b>
7.1	HAZARD.....	117
7.2	RISK.....	117
7.2.1	Risk management .....	118
<b>8.0</b>	<b>RECOMMENDATIONS.....</b>	<b>119</b>
8.1	POLICY AND PLANNING.....	119
8.2	SHORT-TERM ACTIONS.....	119
8.2.1	Hazard monitoring strategy .....	119
8.2.2	Surface/subsurface water control.....	119
8.3	LONG-TERM ACTIONS.....	119
8.3.1	Engineering measures .....	119
8.3.2	Reassessment.....	120
<b>9.0</b>	<b>REFERENCES .....</b>	<b>120</b>
<b>10.0</b>	<b>ACKNOWLEDGEMENTS.....</b>	<b>125</b>

## FIGURES

<b>Figure 1</b>	Location map.....	3
<b>Figure 2</b>	Location map showing the locations of the assessed Clifton Terrace mass movement areas A and B.....	7
<b>Figure 3</b>	Aerial view of the Clifton Terrace mass movement (approximate extent within the yellow dashed lines).....	9
<b>Figure 4</b>	Tension cracks, shears and scarps (yellow arrows) formed by the 22 February 2011 earthquakes at the cliff crest cutting across Kinsey Terrace.....	10
<b>Figure 5</b>	Main features identified at the Clifton Terrace site from field mapping and interpretation of aerial photographs.....	19
<b>Figure 6</b>	Site investigation map.....	21
<b>Figure 7</b>	Engineering Geology map.....	22
<b>Figure 8</b>	Engineering geological cross-sections 1–3.....	23
<b>Figure 9</b>	Piezometric head levels recorded above the sensor tip installed in the standpipe in drillhole BH-KSY-2a. The sensor tip is at 4.1 m below ground level and 2.0 m above rock head.....	39
<b>Figure 10</b>	Piezometric head levels recorded above the sensor tip installed in the standpipe in drillhole BH-KSY-8a. The sensor tip is at 9.6 m below ground level, and 0.8 m above rock head.....	39
<b>Figure 11</b>	Drillhole core from BH-CH-03.....	42
<b>Figure 12</b>	Geological face log of the rock slope exposed along Shag Rock Reserve.....	44
<b>Figure 13</b>	Drillhole core of highly weathered basalt lava breccia from BH-CH-03.....	46
<b>Figure 14</b>	Interpolated rock head boundary.....	49
<b>Figure 15</b>	Results from the refraction seismic collected across the head scarp of assessed source area A (Clarke, 2012).....	51
<b>Figure 16</b>	In-ground moisture (water, wt%) content of collected loess samples.....	52
<b>Figure 17</b>	Loess residual shear strength results (from Table 11 and Table 12).....	55
<b>Figure 18</b>	Numerical slope stability back-analysis of the loess material for cross-section 2, representing source area A.....	58
<b>Figure 19a</b>	Numerical slope stability back-analysis of the loess material for cross-section 2, representing source area A.....	59
<b>Figure 19b</b>	Numerical slope stability back-analysis of the mixed colluvium for cross-section 2, representing source area A.....	61
<b>Figure 20</b>	Loess and colluvium shear wave velocity results from dynamic probing reported by Tonkin and Taylor (2012a) for the loess at Clifton Terrace.....	63
<b>Figure 21</b>	Daily rainfalls at Christchurch Botanic Gardens and landslides in the Port Hills.....	67
<b>Figure 22</b>	Rainfall depth-duration-return period relations estimated for Christchurch Gardens by Griffiths et al. (2009) using recorded rainfall data.....	69
<b>Figure 23</b>	Daily rainfall recorded at the GeoNet gauge installed at Clifton Terrace (next to cGPS CLS5, Appendix 2), and piezometric head levels recorded in the standpipe in drillhole BH-KSY-8a (Figure 6).....	70
<b>Figure 24</b>	Daily rainfall recorded at the GeoNet gauge installed at Clifton Terrace (next to cGPS CLS5, Appendix 2), and piezometric head levels recorded in the standpipe in drillhole BH-KSY-8a (Figure 6), for rain event 11–17 August 2012.....	71

<b>Figure 25</b>	Daily rainfall recorded at the GeoNet gauge installed at Clifton Terrace (next to cGPS CLS5, Appendix 2), and piezometric head levels recorded in the standpipe in drillhole BH-KSY-8a (Figure 6), for rain event 3–5 March 2014.....	71
<b>Figure 26</b>	Engineering geological model. ....	75
<b>Figure 27</b>	Failure mechanism 2, upper part of cross-section 2.....	82
<b>Figure 28</b>	Failure mechanism 2, lower part of cross-section 2. ....	83
<b>Figure 29</b>	Failure mechanism 2, entire part of cross-section 2. ....	84
<b>Figure 30</b>	Failure mechanism 2, entire part of cross-section 3. ....	85
<b>Figure 31</b>	Failure mechanism 2, upper part of cross-section 3.....	85
<b>Figure 32</b>	Sensitivity assessment of the slope factor of safety (cross-section 2, source area A) in response to changing piezometric head levels above rock head for slide surface in the lower, upper and entire parts of source area A.....	87
<b>Figure 33</b>	Sensitivity assessment of the slope factor of safety (cross-section 3, source area B) in response to changing piezometric head levels above rock head for slide surfaces in the upper and entire parts of source area B. ....	88
<b>Figure 34</b>	Sensitivity assessment of the lower slope factor of safety (in source area A, section 2) in response to including filled tension cracks in the model. ....	89
<b>Figure 35</b>	Failure mechanism 1. ....	94
<b>Figure 36</b>	Failure mechanism 1. ....	94
<b>Figure 37</b>	Failure mechanism 1. ....	95
<b>Figure 38</b>	Failure mechanism 1. ....	95
<b>Figure 39</b>	Results from the seismic slope-stability assessment for failure mechanism 1, cross-section 2, for the 22 February 2011 earthquake.....	96
<b>Figure 40</b>	Results from the seismic slope-stability assessment for failure mechanism 1, cross-section 3, for the 22 February 2011 earthquake.....	96
<b>Figure 41</b>	Failure mechanisms 2 and 3. ....	97
<b>Figure 42</b>	Failure mechanisms 2 and 3. ....	97
<b>Figure 43</b>	Results from the seismic slope stability assessment for failure mechanisms 2 and 3, cross-section 2, for the 22 February 2011 earthquake.....	98
<b>Figure 44</b>	Failure mechanisms 2 and 3. ....	100
<b>Figure 45</b>	Cross-section 2, failure mechanisms 2 and 3.....	102
<b>Figure 46</b>	Cliff-collapse hazards and the Class II relative hazard exposure area. ....	113

## TABLES

<b>Table 1</b>	Assessed mass movement relative hazard exposure matrix (from the Stage 1 report, Massey et al., 2013).....	5
<b>Table 2</b>	Summary of the data used in the analysis. LiDAR is Light Detecting and Ranging.....	15
<b>Table 3</b>	Summary of observations from aerial photographs used to assess the site history at Clifton Terrace.....	17
<b>Table 4</b>	Summary of the ground investigations carried out at the site by Aurecon NZ Ltd. (Pletz, 2013) and Tonkin and Taylor Ltd. (Tonkin and Taylor, 2012a).....	28
<b>Table 5</b>	Summary of slope displacements inferred from the surveying of cadastral, monitoring and cGPS marks installed on the slope.....	32
<b>Table 6</b>	Measured cumulate crack apertures, which formed mainly during the 22 February, and less so during the 13 June, 2011 earthquakes, measured by GNS Science.....	33
<b>Table 7</b>	Summary of Tonkin and Taylor (2012a) drillhole inclinometer surveys.....	36
<b>Table 8</b>	Installation details for the water level sensors installed in drillholes BH-KSY-2a and BH-KSY-8a.....	38
<b>Table 9</b>	Summary of water levels manually recorded in standpipes.....	40
<b>Table 10</b>	Engineering geological descriptions of the main geological units forming the exposed cliffs in Shag Rock Reserve and in drillhole cores (descriptions as per New Zealand Geotechnical Society, 2005).....	43
<b>Table 11</b>	Shear-strength test results (from Carey et al., 2014).....	56
<b>Table 12</b>	Other published shear tests on loess in the Port Hills.....	57
<b>Table 13</b>	Index-testing results (mean values) on loess and mixed colluvium (from Tonkin and Taylor, 2012a).....	60
<b>Table 14</b>	Range of bulk geotechnical material parameters adopted for Clifton Terrace soils.....	62
<b>Table 15</b>	Shear wave velocity profiles from Port Hills and other loess.....	63
<b>Table 16</b>	Range of adopted rock strength parameters.....	65
<b>Table 17</b>	Shear wave velocity (SWV) and Rock Quality Designation (RQD) per lithology type for drillhole BH-CH-03.....	66
<b>Table 18</b>	Annual frequencies of given rainfall in the Christchurch for four main events following the 2010/11 Canterbury earthquakes.....	68
<b>Table 19</b>	Example results from slope stability assessment of source area A (cross-section 2).....	79
<b>Table 20</b>	Example results from slope stability assessment of source area B (cross-section 3).....	81
<b>Table 21</b>	Material strength parameters used for modelling the permanent coseismic displacements for cross-sections 2 and 3.....	91
<b>Table 22</b>	Results from the dynamic modelling of cross-sections 2 and 3 for failure mechanism 1, with the slide surfaces confined to the loess.....	92
<b>Table 23</b>	Results from the dynamic modelling of cross-section 2 for failure mechanisms 2 and 3, with slide surfaces confined to the mixed colluvium (Coll) and the weathered basalt lava breccia (Dist. breccia).....	93
<b>Table 24</b>	Forecast modelling results from the dynamic slope stability assessment for cross-section 2.....	103
<b>Table 25</b>	The annual frequency of a given peak ground acceleration occurring on rock.....	108

## APPENDICES

<b>A1</b>	<b>APPENDIX 1: METHODS OF ASSESSMENT</b> .....	<b>A1-1</b>
A1.1	METHODS OF ASSESSMENT.....	A1-1
	A1.1.1 Engineering geology assessment methodology.....	A1-1
	A1.1.2 Hazard assessment methodology.....	A1-1
<b>A2</b>	<b>APPENDIX 2: RESULTS FROM SURVEYS OF CADASTRAL AND MONITORING SURVEY MARKS</b> .....	<b>A2-1</b>
<b>A3</b>	<b>APPENDIX 3: CONTINUOUS GPS TIME-SERIES DATA</b> .....	<b>A3-1</b>
<b>A4</b>	<b>APPENDIX 4: RESULTS FROM THE TWO-DIMENSIONAL SITE RESPONSE ASSESSMENT FOR CROSS-SECTION 1</b> .....	<b>A4-1</b>

## APPENDIX FIGURES

<b>Figure A4.1</b>	Amplification relationship between the synthetic free-field rock outcrop input motions ( $A_{FF}$ ) and the modelled cliff crest maximum accelerations ( $A_{MAX}$ ) for cross-section 2.....	A4-2
<b>Figure A4.2</b>	Modelled horizontal peak ground acceleration contours for the 22 February 2011 earthquake at Clifton Terrace, cross-section 2.....	A4-3
<b>Figure A4.3</b>	Relationship between the modelled horizontal and vertical maximum accelerations modelled at the convex break in slope ( $A_{MAX}$ ) for cross-section 2, using the synthetic free-field rock outcrop motions for the Clifton Terrace site by Holden et al. (2014) as inputs to the assessment.....	A4-4
<b>Figure A4.4</b>	Peak ground amplification (PGA) with respect to the reference station in the horizontal (left) and vertical (right) directions recorded between stations at Clifton Terrace (Figure 6 for instrument locations).....	A4-5

## APPENDIX TABLES

<b>Table A4.1</b>	Results from the two-dimensional site response assessment for cross-section 2, using the out-of-phase synthetic free-field rock outcrop motions for the Maffey's Road site by Holden et al. ....	A4-1
-------------------	--	------

## EXECUTIVE SUMMARY

### ES 1 INTRODUCTION

This report combines recent field information collected from the Clifton Terrace mass movement site with numerical slope-stability modelling to assess the risk to people in dwellings from mass movements. The assessment area also includes an area containing cliff-collapse hazards. The risk associated with the cliff-collapse hazards was previously assessed by Massey et al. (2012).

Following the 22 February 2011 earthquakes, extensive cracking of the ground occurred in some areas of the Port Hills. In many areas, the cracks are thought to represent only localised relatively shallow ground deformation in response to earthquake shaking. In other areas however, the density and pattern of cracking and the amounts of displacement across cracks indicated large mass movements.

Christchurch City Council contracted GNS Science to carry out further detailed investigations of the areas of systematic cracking, in order to assess the nature of the hazard, the frequency of the hazard occurring, and whether the hazard could pose a risk to life, a risk to existing dwellings and/or a risk to critical infrastructure. This work on what are termed mass movements is being undertaken in stages. Stage 1 is now complete (Massey et al., 2013) and Stages 2 and 3 are detailed investigations of mass movements from highest to lowest priority.

The Stage 1 report identifies 36 mass movements of concern in the Port Hills project area. Four of these are further subdivided based on failure type, giving a total of 46 mass movements including their sub-areas. Fifteen of these are assessed as being in the Class I (highest) relative hazard-exposure category. Mass movements in the Class I category might cause loss of life if the hazard were to occur, as well as severe damage to dwellings and/or critical infrastructure leading to the loss of services for many people.

Clifton Terrace mass movement area was assessed in the Stage 1 report (Massey et al., 2013) as being in the highest relative hazard exposure category (Class I, involving possible risk to life). Following the 22 February 2011 earthquakes, significant systematic cracking was noted in the loess (soil) slope above the crest of the steep cliff at the Clifton Hill mass movement, and the amount of slope displacement, coupled with the steep slope angles, suggested the slope was susceptible to earth/debris flows.

This report is part of the Stage 2 investigations and presents hazard assessments for the Clifton Terrace Class I and Class II mass movements, as a result of which the Class I mass movement has been reclassified as a Class II (not involving possible risk to life). This report does not reassess the risk associated with cliff-collapse hazards, assessed in an earlier cliff-collapse study (Massey et al., 2012).

## **ES 2 INVESTIGATION PROCESS AND FINDINGS**

Detailed investigations of the Clifton Terrace mass movement, including its history, were carried out by GNS Science. These investigations identified several relict landslides that probably pre-date European settlement (about 1840 AD). Past rockfalls are also evident from the steep rock slope called Shag Rock Reserve in the aerial photographs and newspaper photographs. The evidence suggests that the slope above the cliff crest has moved, albeit at low magnitudes of movement. The areas of inferred past movement coincide with the same areas that were cracked during the 2010/11 Canterbury earthquakes.

The foot of the cliff at Shag Rock Reserve was exposed to marine erosion until the road to Sumner was built. The dangers of the precarious rock slope above the road was a repeated theme of local newspapers until the road and tramway were relocated away from the foot of the cliff to the present location after 1911. The risk to life of people in dwellings from debris avalanches and cliff-top recession hazards (collectively termed cliff collapse) associated with the steep rock slope of Shag Rock Reserve has already been estimated and is reported by Massey et al. (2012); it is not re-considered in this assessment.

The slope above the cliff crest at Clifton Terrace was significantly cracked during the 22 February 2011 earthquakes, and again during the 13 June 2011 earthquakes. Relatively little movement was reported in the other moderate sized earthquakes.

The absolute ground deformation at this site through the 2010/11 Canterbury earthquakes is well characterised via survey markers installed to enable before-and-after measurements. Total recorded permanent deformation is estimated to be slightly more than one metre horizontally, with most of the movement being recorded in the upper and central part of the assessed source areas.

The bulk strengths of the materials forming the slope have been weakened by the cracking; and in particular, open surface cracks make the slope more susceptible to the ingress of run-off water, which can weaken the loess and underlying colluvium and weathered breccia.

The main types of landslide hazard identified at the Clifton Terrace mass-movement site and originating from the loess and colluvium slopes are earth/debris slides, where the debris is likely to move as relatively intact blocks over limited distances of a few metres.

By mapping cracks and relating these to the results of stability assessments, it has been possible to identify two potential earth/debris slide source areas. The assessed source areas are not the only sources of landslides on this slope; the deformation patterns suggest the assessed areas contain a number of smaller slide-blocks which could move separately.

Numerical models were used to assess the stability of the two identified Clifton Terrace earth/debris slide source areas. Analyses have considered both:

- static conditions (without earthquake shaking); and
- dynamic conditions (with earthquake shaking).

### **Earth/debris slides**

The main triggering mechanism for the assessed source areas is considered to be earthquakes. Increases in water levels within the mass associated with very high rainfall could also in principle trigger displacement, but static analysis suggests that the loess and colluvial strengths appear sufficient to prevent slope collapse not only under relatively dry

conditions but also under the maximum water levels recorded at the site from November 2011 to July 2014. Displacement resulting from increased water levels is thus considered of secondary importance to earthquakes as a triggering mechanism for slope movement.

With relatively high static factors of safety under current conditions, the assessed source areas are considered to be acceptably stable and unlikely to reactivate as large intact slides during rain. However, if conditions on the slope were to change in an adverse manner (for example by slope excavation near the toe for road works or other purposes), reactivation of the larger slide mass under rainfall may become a possibility and the slope would need to be reclassified as Class I.

Whether or not the assessed landslide source areas pose a life risk depends on the ability of the landslide mass to break down during a movement episode to form a more mobile flow-type landslide, which is usually a function of the magnitude and speed of movement. Based on past performance, the two identified and assessed sources have historically moved as a “coherent” block slide, where houses are essentially on slide-block rafts within the larger landslide, and where dwellings located in the head scarp (tension) and toe areas (compression) have suffered the most damage.

Results from the assessment indicate that, under current conditions, it is unlikely the slide mass would break down as a result of a coseismic or rainfall triggered movement episode to form a potentially life-threatening earth/debris flow, because: 1) the high static factors of safety suggest reactivation of the larger slide mass is unlikely under static conditions; 2) the assessed coseismic magnitudes of displacement are relatively small with regards to the size of the displaced mass; and 3) should movement occur, the slope angles in the assessed source areas are relatively low and the angles of the assessed slide surfaces are equally low.

In addition to the assessed earth/debris slides, tunnel gulying, gully erosion and earth/debris flows could occur within the assessment area, preferentially along drainage lines and the steep cut slopes along Clifton Terrace. These are likely to be small; historically such slope failures have been less than 100 m<sup>3</sup> in volume in the Port Hills.

### **Movement triggering frequencies**

The frequency of occurrence of the events that could trigger movement of the assessed earth/debris slides is uncertain. Future movements could occur more frequently, i.e., at lower triggering thresholds.

The area has already undergone more than one metre of permanent slope deformation during the 2010/11 Canterbury earthquakes and this movement could have reduced the shear strength of critical materials in the slope, making the slope more susceptible to future earthquakes. At the current time there is no practical way to estimate the numerical value of the “degraded strength”, of the slope.

With the inferred translational slide-surface movement mechanism and the relatively low angle of the larger slope in the area, it is unlikely that the larger slide mass could break down to form a more mobile earth/debris flow under current conditions. It is possible however, that modelled permanent slope displacements, while not a threat to lives, could destroy dwellings on the assessed source areas, even if the debris did not leave the source.

If current conditions were to change adversely, however – for example as a result of earthworks (cutting or filling of material) or modification of drainage – the changes could reduce the stability of the mass, triggering movement, as well as making it more susceptible to smaller rises in piezometric head levels, and therefore larger displacements in future rainstorms and earthquakes. These could pose a risk to life, and the slope would need to be reclassified as Class I.

### **ES 3 CONCLUSIONS**

These conclusions relate to the assessed earth/debris slides in the assessed source areas only. For information on the risk associated with the cliff-collapse hazards refer to Massey et al. (2012).

#### **ES3.1 Hazard**

1. Results from the assessment indicate that, under current conditions, it is unlikely the material in the assessed source areas would break down during a coseismic or rainfall triggered movement episode to form life-threatening earth/debris flows. The runout of debris flows and associated risk to life have, therefore not been assessed.
2. There is potential for reactivation of the assessed source areas to occur as earth/debris slides, where the debris may move as relatively intact blocks over limited distances, e.g., metres. Under current conditions, this hazard presents a significant risk to dwellings and infrastructure but not to life. This hazard is in addition to the cliff-collapse hazards at the site as assessed by Massey et al. (2012).
3. The most likely triggers for the assessed earth/debris slides are strong earthquake shaking, very high rainfall or changes to the conditions of the site as a result of, for example, construction or excavation activities.
4. The frequency of reactivation of the earth/debris slides in the future is difficult to estimate and could be anything from every few years to many hundreds of years.

#### **ES3.2 Risk**

1. Under current conditions reactivation of source areas A and B is considered to pose a risk to dwellings and infrastructure sited on the area (likely via a combination of cracking and undercutting as the ground moves beneath dwellings), but is not considered to pose a risk to life.
2. The area of slope represented by assessed source area A was highlighted in the Stage 1 report as being a Class I area. Based on the further investigation, the area (outside of the cliff collapse risk zones has been re-assessed as currently being in the same risk category as source area B (a Class II area). This classification may need to be reconsidered if circumstances change (see section ES3.1 point 3).
3. A Class II area is defined in the Stage 1 report (Massey et al., 2013) as: Coherent slides and slumps with associated cumulative inferred displacement of the mass of greater than 0.3 m, where dwellings and critical infrastructure are present within the moving mass.

4. Renewed movement in both areas could severely impact critical infrastructure and dwellings. The amount of damage to critical infrastructure and dwellings is likely to be a function of their location on the slide mass. The most hazardous places are the extensional and compressional areas where most of the surface deformation is located. Given the failure mechanisms relevant to this site and the moderate magnitudes of displacement, it is unlikely that damage to dwellings would pose an immediate life risk to building occupants.

### **ES3.2.3 Risk management**

1. A risk-management option of monitoring rainfall, soil moisture, pore-pressure and surface and subsurface movement in the assessed source areas may be of some value in providing warning of changing conditions that could lead to larger displacements.
2. If current conditions were to change – for example as a result of earthworks (cutting or filling of material) or modification of drainage, or undercutting as a result of earthquake-induced cliff collapses’ – the changes could reduce the stability of the mass and make it more susceptible to larger displacements in future earthquakes and rainstorms. This would require the Class II categorisation to be revisited.
3. If conditions were to change, there is also a possibility that the mass could break up to form more rapid failures with longer runout, and potentially loss of life.

## **ES 4 RECOMMENDATIONS**

In order to manage the hazard at this site, and to prevent it from becoming a potential risk to life, GNS Science recommends that based on the results of this study, Christchurch City Council:

### **ES4.1 Policy and Planning**

1. Invoke strict controls on earthworks, drainage and other construction-related activities, as any modification to the slope, may lead earth/debris slides to develop into flows.
2. Require a detailed ground investigation and assessment of how any proposed earthworks, drainage works or other development could affect the stability of the slope.

### **ES4.2 Short-term actions**

#### **ES4.2.1 Hazard monitoring strategy**

1. Include the report findings in a slope-stability monitoring strategy with clearly stated aims and objectives, and list how these would be achieved, aligning with the procedures described by McSaveney et al. (2014).
2. Continue monitoring to identify trends and changes in slope movement. The monitoring network should be reassessed to ensure the main identified assessment areas are adequately monitored.
3. Ensure that the existing emergency management response plan for the area identifies the dwellings that could be affected by movement, and outlines a process to manage a response to renewed movement.

### **ES4.2.3 Surface/subsurface water control**

Reduce water ingress into the slopes, where safe and practicable to do so, by:

1. Identifying all water-reticulation services (water mains, sewer pipes and storm water) inside the assessed source area boundaries and relocating them to locations outside the boundary, in order to control water seepage into the slope. The water main, which currently traverses along Kinsey Terrace is a particular example of such services; and
2. Controlling surface water seepage by filling the accessible cracks on the slope and provide an impermeable surface cover to minimise water ingress.

## **ES4.3 LONG-TERM ACTIONS**

### **ES4.3.1 Engineering measures**

1. Assess the cost, technical feasibility and effectiveness of alternative longer-term engineering stabilisation measures.
2. Any proposed engineering works would require a detailed design to be carried out under the direction of an appropriately certified engineer, and should be independently verified in terms of their risk reduction effectiveness by appropriately qualified and experienced people.

### **ES4.3.2 Reassessment**

Reassess the risk and revise and update the findings of this report in a timely fashion, for example:

1. In the event of any changes in ground conditions; or
2. In anticipation of further development or land-use decisions.

## 1.0 INTRODUCTION

This report brings together recent field information on the Clifton Terrace mass movement site and uses numerical models of slope stability to assess the risk to people in dwellings from the identified earth/debris slide at the site. This report does not reassess the risk associated with cliff collapse hazards, assessed in an earlier cliff-collapse study (Massey et al., 2012).

### 1.1 BACKGROUND

Following the 22 February 2011 earthquakes, members of the Port Hills Geotechnical Group (a consortium of geotechnical engineers contracted to Christchurch City Council to assess slope instability in the Port Hills) identified some areas in the Port Hills where extensive cracking of the ground had occurred. In many areas cracks were thought to represent only localised relatively shallow ground deformation in response to shaking. In other areas however, the density and pattern of cracking and the amounts of displacement across cracks clearly indicated that larger areas had moved systematically *en masse* as a mass movement.

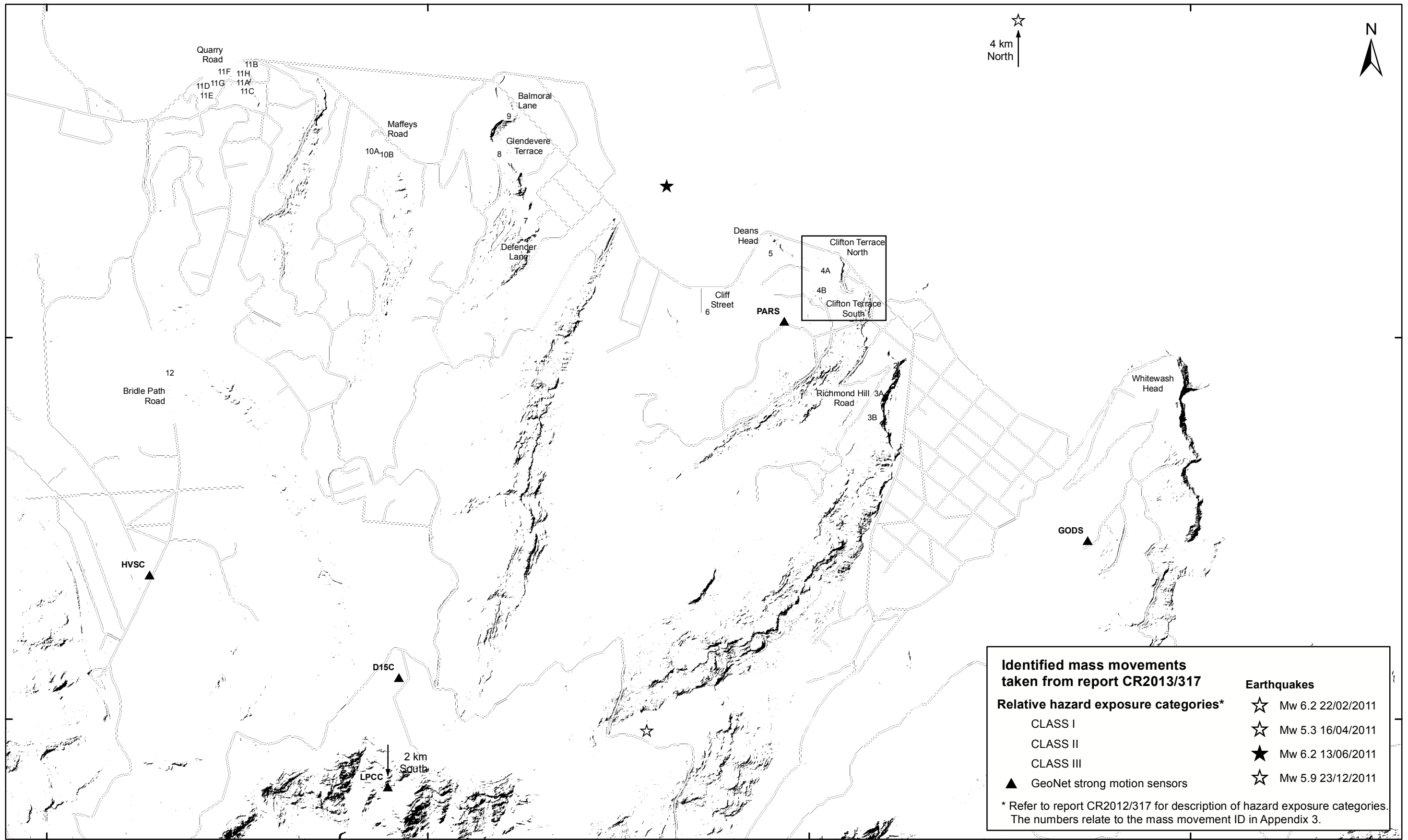
Christchurch City Council contracted GNS Science to carry out detailed investigations of the identified areas of mass movement in order to assess the nature of the hazard, the frequency of the hazard occurring, and whether the hazard could pose a risk to life, a risk to existing dwellings and/or a risk to critical infrastructure (defined as water mains, sewer mains, pump stations, electrical substations and transport routes). This work is carried out under Task 4 of contract No. 4600000886 (December 2011).

The main purpose of the Task 4 work is to provide information on slope-stability hazards in the Port Hills. This is to assist Christchurch City Council land-use and infrastructure planning and management in the area, as well as to establish procedures to manage on-going monitoring and investigation of the hazards.

The Task 4 work is being undertaken in stages. Stage 1 is completed (Massey et al., 2013; hereafter referred to as the Stage 1 report) and comprised: 1) a list of the areas susceptible to significant mass movement; 2) the inferred boundaries of these areas (as understood at the time of reporting); and 3) an initial “hazard-exposure” assessment (Table 1) intended only to prioritise the areas with regards to future investigations.

The Stage 1 report identified 36 mass movements of concern in the Port Hills project area. Four of these were further subdivided based on failure type, giving a total of 46 mass movements including their sub-areas (Figure 1). Fifteen of these were assessed as being in the Class I (highest) relative hazard-exposure category, and the results of their detailed investigation and assessment are presented in Stages 2 and 3, which includes this Stage 2 report on the Clifton Terrace Class I mass movement. Mass movements in the Class I category are described as: “Slides, falls, topples, flows and avalanches of loess, loess and rock or rock, with associated displacement in the source area of greater than 0.3 m leading to cliff top recession. Once triggered the debris has potential to run-out long distances down-slope. In these locations there is potential for dwellings in the source area to be undercut and severely damaged by displacement, and for debris to impact and inundate dwellings, their occupants or road users lower down the slope. Given the velocity and long runout it is possible these types of mass movement could result in the loss of life” (Massey et al., 2013).

The Stage 1 report recommended that mass movements in the Class I relative hazard-exposure category be given high priority by Christchurch City Council for detailed investigations and assessment.



**Identified mass movements taken from report CR2013/317**

**Relative hazard exposure categories\***

- CLASS I
- CLASS II
- CLASS III

▲ GeoNet strong motion sensors

**Earthquakes**

- ☆ Mw 6.2 22/02/2011
- ☆ Mw 5.3 16/04/2011
- ★ Mw 6.2 13/06/2011
- ☆ Mw 5.9 23/12/2011

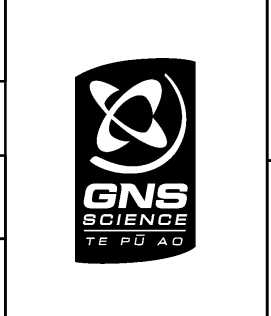
\* Refer to report CR2012/317 for description of hazard exposure categories. The numbers relate to the mass movement ID in Appendix 3.

SCALE BAR: 0 0.5 1 km

**EXPLANATION:**  
 Refer to Appendices 2 and 3 of report CR2012/317 for maps and more details of each mass movement.  
 Background shade model derived from NZAM post earthquake 2011c (July 2011) LiDAR survey resampled to a 1 m ground resolution.  
 Roads provided by Christchurch City Council (20/02/2012).  
 PROJECTION: New Zealand Transverse Mercator 2000

DRW:  
BL

CHK:  
CM



**LOCATION MAP**

**Port Hills  
Christchurch**

**FIGURE 1**

Map 1

**FINAL**

REPORT: CR2014/76	DATE: August 2014
----------------------	----------------------



**Table 1** Assessed mass movement relative hazard exposure matrix (from the Stage 1 report, Massey et al., 2013).

		Hazard Class		
		1. Displacement* greater than 0.3 m and debris runout	2. Displacement* greater than 0.3 m; no runout	3. Displacement* less than 0.3 m; no runout
Consequence Class	1. Life – potential to cause loss of life if the hazard occurs	<b>CLASS I</b>	<b>CLASS III</b>	<b>CLASS III</b>
	2. Critical infrastructure <sup>1</sup> – potential to disrupt critical infrastructure if the hazard occurs	<b>CLASS I</b>	<b>CLASS II<sup>2</sup></b>	<b>CLASS II</b>
	3. Dwellings – potential to destroy dwellings if the hazard occurs	<b>CLASS I</b>	<b>CLASS II</b>	<b>CLASS III</b>

\*Note: Displacements for each assessed mass movements are inferred by adding together the mapped crack apertures (openings) along cross-sections through the assessed mass movements. They are a lower bound estimate of the total displacement, as no account is given for plastic deformation of the mass and not every crack has been mapped.

<sup>1</sup> Critical infrastructure is defined, for the purpose of this report, as infrastructure vital to public health and safety. It includes transport routes (where there is only one route to a particular destination), telecommunication networks, all water related mains and power networks (where there is no redundancy in the network), and key medical and emergency service facilities. Networks include both linear features such as power lines or pipes and point features such as transformers and pump stations.

<sup>2</sup> This relative hazard exposure category is based largely on an assumption that 'critical infrastructure' exists within these areas. Until further assessments are made on the nature of toe slumps and the existence of critical infrastructure in these areas, the relative hazard exposure category of these assessed mass movements has been appropriately assessed as "Class II". It is likely that many of the assessed mass movements in the Class II relative hazard exposure category (where the hazard class is 2 and the consequence class is 2) would be more appropriately classified as "Class III" following further assessments.

## 1.2 THE CLIFTON TERRACE MASS MOVEMENTS

The Clifton Terrace mass-movement area was divided into two areas, A and B, these are shown in Figure 1 and Figure 2. Part of this mass movement area was assessed in the Stage 1 report (Massey et al., 2013) as being in the highest relative hazard exposure category (Class I), labelled 4A in Figure 1. The other part was originally assessed as being in the Class II relative hazard exposure category, labelled 4B in Figure 1. From here onwards these areas are now referred to as source areas A and B.

This report presents the risk-assessment results for both the Clifton Terrace Class I and Class II mass movements located above the cliff crest. The map in Figure 2 outlines the assessment area and the revised assessed source areas A and B, which as a result of these investigations differ slightly to the original boundaries shown in Figure 1.

The assessment area also includes an area containing cliff-collapse hazards. The risk associated with these cliff-collapse hazards has been assessed by Massey et al. (2012) and has not been reassessed in this report.





	Assessed source areas
<b>Slope hazard</b>	
	Earth/debris slide source area
	Rockfall/debris avalanche source area*
	Assessment area

SCALE BAR: 0 50 100 m

EXPLANATION:  
 \* Taken from reports CR2012/57 and CR2012/124  
 Background shade model derived from NZAM post earthquake 2011c (July 2011) LiDAR survey resampled to a 1 m ground resolution.  
 Roads and building footprints provided by Christchurch City Council (20/02/2012).  
 PROJECTION: New Zealand Transverse Mercator 2000

DRW:  
BL  
 CHK:  
CM, FDP



**MASS MOVEMENT LOCATION MAP**

**Clifton Terrace  
Christchurch**

**FIGURE 2**

**FINAL**

REPORT: CR2014/76	DATE: August 2014
----------------------	----------------------



### 1.3 PREVIOUS WORK AT THE CLIFTON TERRACE SITE

Following the 22 February 2011 earthquakes, significant cracks were noted in the slope within the Clifton Terrace mass movement (Figure 3 and Figure 4). Previous investigations of the site comprised:

1. The risk to life of people in dwellings at the cliff crest from debris avalanches and cliff-top recession associated with the steep rock slope (collectively termed cliff-collapse hazards) was previously estimated by Massey et al. (2012);
2. Field mapping of crack distributions was carried out by GNS Science, and the results are contained in the Stage 1 report (Massey et al., 2013);
3. Ground investigation of the site has involved drilling of three fully-cored drillholes, and inclinometer monitoring, carried out by Aurecon NZ Ltd, under contract to Christchurch City Council. The results of the drilling are contained in Pletz (2013); and
4. Ground investigation and field mapping of the site carried out by Tonkin and Taylor Ltd, under contract to the Earthquake Commission (Tonkin and Taylor, 2012a). The ground investigations comprised 30 drillholes (using a number of techniques: cored, open barrel, wash drilling, percussive and push-tube sampling), 16 cone penetration tests (nine were conducted with seismic cones), two test pits, and 17 Scala Penetrometer probes. Records from eight standpipe piezometers and six inclinometers, installed in selected drillholes, are reported by Tonkin and Taylor (2012a).



**Figure 3** Aerial view of the Clifton Terrace mass movement (approximate extent within the yellow dashed lines). Refer to Figure 2 for the mapped extent of source areas A and B (previously referred to in the Stage 1 report as mass movements 4A and 4B). The cliff-collapse hazards shown within the red dashed lines (approximate extent only), have not been assessed in this report; refer to Massey et al. (2012) for details. Photograph C. Massey (GNS Science, March 2011).



**Figure 4** Tension cracks, shears and scarps (yellow arrows) formed by the 22 February 2011 earthquakes at the cliff crest cutting across Kinsey Terrace. Photograph G. Hancox (GNS Science, February 2011).

#### 1.4 SCOPE OF THIS REPORT

The scope of this report as per Appendix A of contract No. 4600000886 (December 2011) is to:

1. Estimate the annual individual fatality risk for affected dwelling occupants from failure of the assessed earth/debris slide source areas A and B, within the shown assessment area in Figure 2.
2. Provide recommendations to assist Christchurch City Council with considered options to mitigate risks, associated with the assessed source areas.

This report does not include any assessment of the cliff-collapse hazards assessed by Massey et al. (2012). Refer to Massey et al. (2012) for information relating to the cliff-collapse hazards.

For the purpose of this risk assessment, all dwellings are considered as timber-framed single-storey dwellings of building importance category 2a (AS/NZS 1170.0.2002). The consequences of the hazards discussed in this report on commercial buildings have not been assessed.

The risk assessments contained in this report supersede the preliminary risk assessments contained in the Working Note 2013/300LR (Massey and Della Pasqua, 2013).

## **1.5 REPORT STRUCTURE**

- Section 1.6 of the report details the methodology.
- Section 2 details the data used in the assessments.
- Sections 3–5 contain the results from the engineering geological, hazard and risk assessments respectively.
- Section 6 discusses the results of the hazard and risk assessment and explores the uncertainties associated with the estimated risks.
- Section 7 summarises the assessment findings.
- Section 8 presents recommendations for Christchurch City Council to consider.

## **1.6 METHODS OF ASSESSMENT**

The site assessment comprised three stages:

1. Engineering geology assessment;
2. Hazard assessment; and
3. Risk assessment.

The methodologies adopted are described in detail in Appendix 1, and summarised in the following sections.

### **1.6.1 Engineering geology assessment**

The findings presented in this report are based on engineering geological models of the site developed by GNS Science. The engineering geological assessment comprised:

1. Interpretation of available aerial photographs covering the period 1940–2011, to determine the land use and development history of the site.
2. Resurveying of cadastral survey marks within and around the mass movement to determine the amounts of ground displacement during the 2010/11 Canterbury earthquakes.
3. Assessment of the results from surveying of monitoring marks installed on the site by Aurecon NZ Ltd. (under contract to Christchurch City Council), following the 22 February 2011 earthquake. This was undertaken to assess the amount of slope displacement relating to the 22 February, 16 April, 213 June and 23 December 2011 earthquakes.
4. Geological and geomorphological field mapping to identify the materials, processes and landforms within the assessment area.
5. Review of previous ground investigations by Aurecon NZ Ltd. (Pletz, 2013) and Tonkin and Taylor Ltd. (Tonkin and Taylor, 2012a).
6. Preparation of an engineering geological model, an engineering geological map and three cross-sections of the site, based on the results from the aerial photograph interpretation, surveying, field mapping, and site investigations. These were used as the basis for the hazard and risk assessments.

### **1.6.2 Hazard assessment**

The hazard assessment method followed two main steps:

**Step 1** comprised assessments of the stability of selected slope cross-sections under static (non-earthquake) and dynamic (earthquake) conditions to determine whether landslides could be triggered under static or dynamic conditions and the likelihood of landslides occurring.

**Step 2** used the results from step 1 to define the likely extent and movement mechanisms of potential landslides, which were combined with the crack patterns and slope morphology and engineering geology mapping to estimate the likely failure geometries and volumes.

The results from this characterisation were then used in the risk assessment.

### **1.6.3 Estimation of landslide extent and failure mechanism**

The results of the engineering geological assessments and the slope stability modelling were used to define the possible future extent and failure mechanism of landslides within the assessment area. The extent of the assessed landslides corresponds to areas where the bulk strength of the slope could permit failure after having been degraded by earthquake-induced cracking.

The most likely extents of future landslides were estimated based on the current surveyed displacement magnitudes, material exposures, crack distributions and slope morphology as well as the numerical analyses of the slope stability. The purpose of these estimations was to constrain the likely depth, width and length of any landslide. This was done by linking the main cracks and pertinent morphological features with the width, length and depth of the failure surfaces derived from the finite-element and limit-equilibrium modelling.

### **1.6.4 Risk assessment**

The risk metric assessed is the annual individual fatality risk for dwelling occupants from the landslides which are mainly earth/debris slides. Cliff-collapse hazards comprising debris avalanches and cliff-top recession within the assessment area are assessed by Massey et al. (2012), and no further assessment of the risk associated with cliff-collapse hazards was carried out for this report.

## Event annual frequencies

The frequency of occurrence of events that could trigger movement of the assessed earth/debris slides is unknown.

- For non-earthquake triggers such as rainfall, a range of pore-pressures within the source areas were assessed, and linked to their corresponding rainfall events and their frequencies of occurrence.
- For earthquake triggers, the annual frequency of a given magnitude of permanent displacement of the assessed source areas was estimated by using:
  - a. A relationship between the yield acceleration ( $K_y$ ) and the maximum average acceleration of the mass ( $K_{MAX}$ ), derived from back-analysing the permanent displacement of the assessed source areas during the 2010/11 Canterbury earthquakes; and
  - b. The Expert Elicitation Seismic Hazard Model for Christchurch (Gerstenberger et al., 2014) based on a modified form of the National Seismic Hazard Model for New Zealand (Stirling et al., 2012), which provides the annual frequencies of free-field rock outcrop peak horizontal ground accelerations ( $A_{FF}$ ) and therefore the annual frequencies of the equivalent maximum average acceleration of the mass ( $K_{MAX}$ ).

The methods are detailed in Appendix 1.



## 2.0 DATA USED

The data and sources of the data used in this report are listed in Table 2.

**Table 2** Summary of the data used in the analysis. LiDAR is Light Detecting and Ranging.

<b>Data</b>	<b>Description</b>	<b>Data source</b>	<b>Date</b>	<b>Use in this report</b>
Post-22 February 2011 earthquake digital aerial photographs	Aerial photographs taken on 24 February 2011 by NZ Aerial Mapping and were orthorectified by GNS Science (0.1 m ground resolution).	NZ Aerial Mapping	Last updated 24 February 2011	Used for base maps and to map extents of landslides and deformation triggered by the 22 February 2011 earthquakes.
Post-13 June 2011 earthquake digital aerial photographs	Aerial photographs taken between 18 July and 26 August 2011, and orthorectified by NZ Aerial Mapping (0.5 m ground resolution).	NZ Aerial Mapping	18 July–26 August 2011	Used to map extents of landslides and deformation triggered by the 13 June 2011 earthquakes.
Historical aerial photographs	Photographs taken in 1940, 1946, 1973, 1975 and 1984 by several sources and orthorectified by NZ Aerial Mapping and GNS Science (at variable ground resolutions).	NZ Aerial mapping and GNS Science	1946, 1975, 1975 and 1984	Used to assess the site history before the 2010/11 Canterbury earthquakes.
LiDAR digital elevation model (2011c)	Digital Elevation Model derived from post-13 June 2011 earthquake LiDAR survey; re-sampled to 1 m ground resolution.	NZ Aerial Mapping	18 July–26 August 2011	Used to generate contours and shade models for the maps and cross-sections used in the report.
Christchurch building footprints	Footprints are derived from aerial photographs. The data originate from 2006 but have been updated at the site by CCC using the post-earthquake aerial photos.	Christchurch City Council	Unknown	Used to identify the locations of residential buildings in the site.
GNS Science landslide database	Approximate location, date, and probably trigger of newsworthy landslides	GNS Science	Updated monthly	Used to estimate the likely numbers and volumes of pre-earthquake landslides in the areas of interest.
Earthquake Commission claims database	Location, date and brief cause of claims made in the Port Hills of Christchurch since 1993.	Earthquake Commission	1993–August 2010	Used to estimate the likely numbers and volumes of pre-earthquake landslides in the areas of interest.

<b>Data</b>	<b>Description</b>	<b>Data source</b>	<b>Date</b>	<b>Use in this report</b>
Synthetic earthquake time/ accelerations	Earthquake time acceleration histories for the four main 2011 earthquakes: 22 February, 16 April, 13 June and 23 December.	GNS Science	February 2014	Used as inputs for the seismic site response analysis.
Rainfall records for Christchurch	Rainfall records for Christchurch from various sources, extending back to 1873.	NIWA archive	1873–present	Used to assess the return periods of past storms triggering landslides of known magnitudes in the Port Hills.
Drillhole and test pit logs	Descriptions of drillhole and test-pit materials, cone penetrometer, and scala penetrometer measurements from the site.	Tonkin and Taylor Ltd. (Tonkin and Taylor, 2012a)	2012	Used to generate the engineering geological map and cross-sections.
Drillhole logs	Results from the logging of three drillholes carried out at the site.	Aurecon NZ Ltd. (Pletz, 2013)	January 2013	Used to generate the engineering geological map and cross-sections.
Downhole shear wave surveys	Downhole shear wave velocity surveys measured in the Aurecon NZ Ltd. drillholes	Southern Geophysical Ltd. (2013)	February 2014	Used to determine the dynamic properties of the materials in the slope for the seismic site response analysis.
Geotechnical laboratory data	Geotechnical strength parameters for selected soil and rocks in the Port Hills.	GNS Science (Carey et al., 2014)	February 2014	Used for static and dynamic slope stability analysis.
Field work	Field mapping of cracks, engineering geology and ground verification of the risk analyses.	GNS Science and the Port Hills Geotechnical group	22 February 2011–present	Used in generating the engineering geological models of the site. Results from field checks used to update risk maps.
Groundwater measurements	The results from groundwater (pore pressure) measurements made in two drillholes carried out by Tonkin and Taylor Ltd.	The instruments were installed by GNS Science (funded by GeoNet)	November 2011–present	Used for the numerical modelling of landslide stability under static conditions
Survey measurements	The results from the resurveys of cadastral (LINZ) markers and monitoring survey marks (Aurecon NZ Ltd.).	GNS Science and Aurecon NZ Ltd.	Post-22 February 2011 earthquake	Used to derive permanent slope displacements in response to the main 2010/11 Canterbury earthquakes

### 3.0 SITE ASSESSMENT RESULTS

The site assessment results and engineering geological conceptual models developed for the site by GNS Science are summarised below. Figure 5 shows the main features identified at the site from field mapping and review of aerial photographs. Figure 6 shows the locations of the various site investigations and Figure 7 presents an engineering geological map for the site. Figure 8 presents three engineering geological cross-sections through the site.

#### 3.1 SITE HISTORY

##### 3.1.1 Aerial photograph interpretation

Aerial photographs of the site are available for various dates since 1940. Table 3 summarises the photograph details and main features noted.

**Table 3** Summary of observations from aerial photographs used to assess the site history at Clifton Terrace.

Date/scale of photo	Resolution	Comments
1940 1:10,000 (approx.)	Poor resolution	<p>Several large arcuate features (concave depressions) – interpreted as relict landslide scars – are apparent at the southern part of the site corresponding to the location of source area B. These appear to have been incised to the north and south by relatively narrow linear drainage lines, indicating past erosion along the drainage lines. No corresponding accumulations of debris are present at the slope toe, but any debris could have been removed (Figure 5). One of these features, to the south, corresponding to the location of source area B (labelled B in Figure 5), has the subdued morphology of a degraded relict landslide where some of the debris appears to have evacuated from the source area in one or more events. Given its subdued nature, it is likely the possible landslide occurred long ago. The slope between the two drainage lines appears to be a relatively intact but possibly displaced block within the larger relict landslide scar.</p> <p>To the north, near the cliff edge, the northern boundary of assessed source area A corresponds to an incised drainage line. Two subtle convex breaks-in-slope extend between this northern drainage line and the more prominent drainage line along the southern boundary of the assessed source area, which together may delineate a large relict and relatively intact but displaced landslide block.</p> <p>Many dwellings were already present on the slope. Clifton Terrace and Kinsey Terrace were already constructed by then.</p>
30/05/1946 1:5,500 (approx.)	Good resolution	<p>At the northern end of the site, there are several recent rockfalls at the toe of the steep cliff in Shag Rock Reserve.</p> <p>Several of the cut slopes (in what appears to be loess) along Clifton Terrace appear eroded (Figure 5).</p>
1973, 1:10,000 (approx.)	Poor resolution	No obvious change. More dwellings have now been constructed on the slope. Clifton Terrace appears to have been widened towards the southern end of the site.
1975, 1:10,000 (approx.)	Poor resolution	No obvious change. More dwellings have been constructed on the slope.
1984, 1:6,000 (approx.)	Good resolution	<p>There appears to be several recent rockfalls apparent at the toe of the steep cliff in Shag Rock Reserve at the northern end of the site.</p> <p>More dwellings have now been constructed on the slope.</p>

### 3.1.1.1 Relict landslides

Review of aerial photographs and field mapping identified several relict landslide scars on the slope within and adjacent to the Clifton Terrace site (Figure 5 and Table 3). The southern one (assessed source area B) is larger and more pronounced than the northern one, possibly indicating it has been more recently active. It is bound to the north and south by drainage lines (labelled 2 and 3 in Figure 5), which are incised to within a few metres of bedrock. Recent (post-2011) tunnel gullying and gully erosion is apparent along these drainage lines. The slope between the two drainage lines appears to be a relatively intact displaced block within a larger relict landslide scar. A possible landslide head scarp extends upslope behind this area. Basalt lava and breccia outcrops in the head scarp area, and underlies the volcanic colluvium and loess, which were exposed in the flanks of the drainage lines. Seepage was noted in the drainage lines and in the head scarp where rock head is inferred (from drillholes and field exposures) to be near the surface. The shape of the possible relict landslide (cross-section 3, Figure 8) is consistent with a translational failure mechanism, with a failure surface sub-parallel to rock head, and with much of the debris remaining in the source area.

The possible landslide scar in the north of the site (assessed source area A) is more subtle; it is bound to the north and south by incised drainage lines (labelled 1 and 2 in Figure 5). Two subtle scarps, marked by rounded concave and convex breaks-in-slope (a few metres high) extend north-south between the two drainage lines. These scarps may have formed due to past slope movement, and the slope between the two drainage lines and scarps may have displaced as a relatively intact block. The scarps are sub-parallel to the strike of rock head (Figure 9), which is consistent with the eastward dip direction (bearing 070–080°) of the volcanic lava, breccia and epiclastic sequences exposed in the cliff face north of the site (Figure 10). This suggests some structural geological control on the morphology of the landslide scars, which is also suggested by the downslope displacement in the dip direction of the volcanic sequences. Given the relatively “intact” appearance of the slope compared to the southern landslide scar, it is unlikely that past displacements were large.

### 3.1.2 Before the 2010/11 Canterbury earthquakes

- No reports of large slope deformation since European settlement (ca. 1840 AD) have been found by searching the “Paperspast” website. No records of complaints from residents in the area have been located in Christchurch City Council that would suggest large scale displacement of the site had occurred post-residential development and before the 2010/11 Canterbury earthquakes.
- Geomorphological expressions of several landslide scars, within the assessment area and on the adjacent slopes, are apparent in the 1940 aerial photographs (the date of the earliest available aerial photographs), and shown on Figure 5. These appear to be relatively old and may pre-date European settlement (1840 AD).
- The cliff, referred to as Shag Rock Reserve, at the northern side of the site was an eroding sea cliff until a road to Sumner was constructed at its foot after 1840. The precariousness of the slope then featured often in local newspapers because of rockfalls. After a large rockfall in 1911, the Sumner tramway and Main Road were relocated to the site of the present Main Road to be further from the foot of the cliff.

- There is no evidence in the aerial photographs (1940, 1946, 1973, 1975, 1984 and 2011) of past quarrying or significant modification to the slopes at the site, other than for the construction of dwellings and the roads Clifton and Kinsey Terraces. Many dwellings were present in the 1940 aerial photographs.
- No cracking was reported or observed following the 4 September 2010 earthquake.

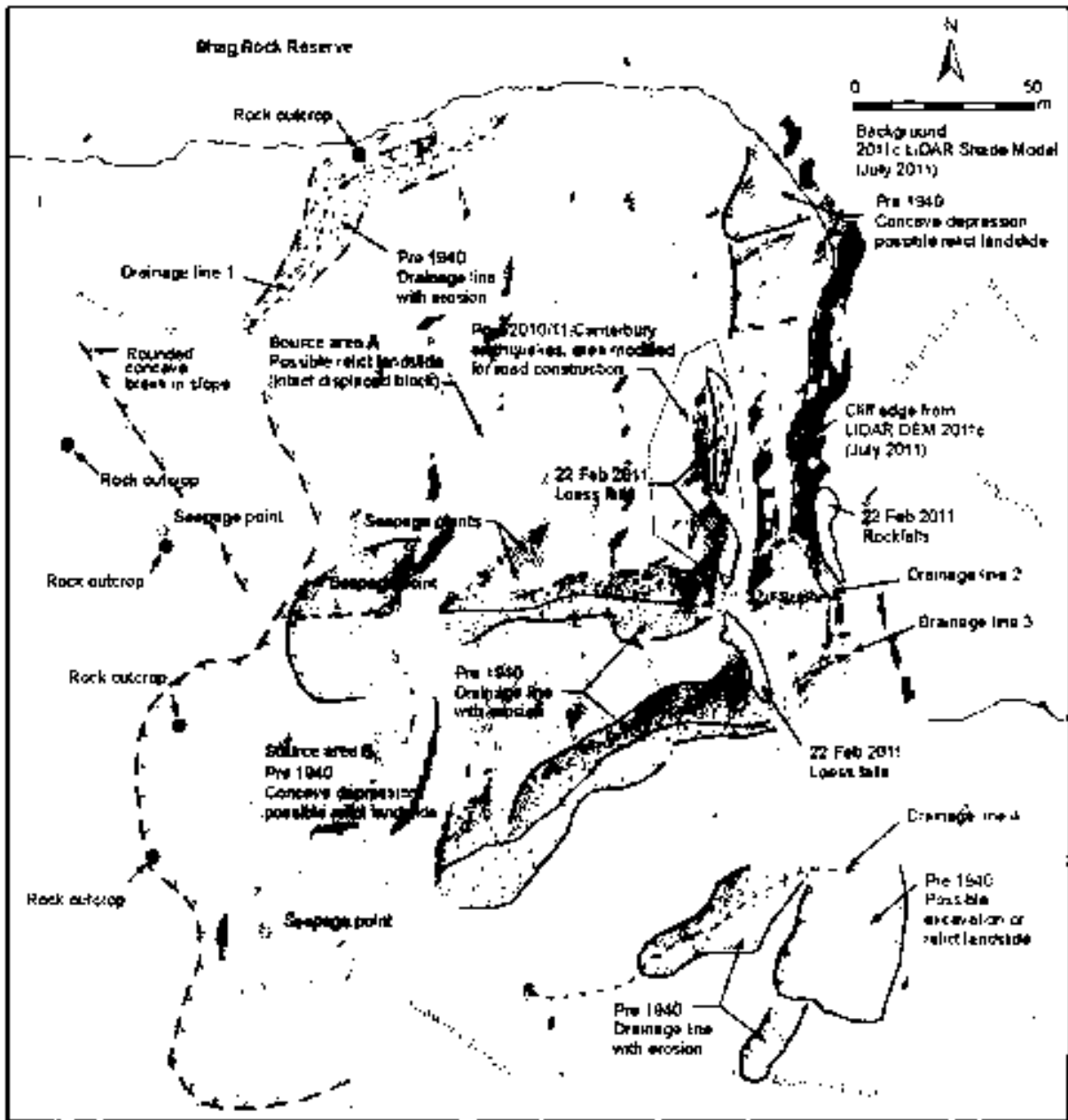


**Figure 5** Main features identified at the Clifton Terrace site from field mapping and interpretation of aerial photographs.

### 3.1.3 During the 2011 Canterbury earthquakes

- *22 February 2011 earthquakes* – the majority of cracks (shown on maps in the Stage 1 report and displacements summarised in Table 5 formed in one or more earthquakes on the 22 February 2011. Permanent ground deformation in the area in this event, inferred from surveying of cadastral survey marks (by GNS Science, Table 4), was in the order of about 0.3–0.7 m (average of 0.49 m) for assessed source area A, and

about 0.2–0.4 m for source area B. Displacements in source area A were towards bearing 070° (east) and displacements in source area B were more towards bearing 080–090°, however, there are limited survey data for source area B. For assessed source area A, the surveyed displacements are consistent in magnitude over much of the site, and the crack pattern suggests the area moved as a coherent block, as most of the vertical displacements correspond to the identified “head scarp” of the area, with predominantly translational movement in the central and lower parts of the displaced mass, at angles sub parallel to the dip of rock head and the volcanic sequence, and with azimuths broadly perpendicular to the head scarp. Compression was also noted along Clifton Terrace. Local failures of steeply cut slopes formed in loess also occurred along Clifton Terrace. Debris from these failures buried several cars parked at the roadside.

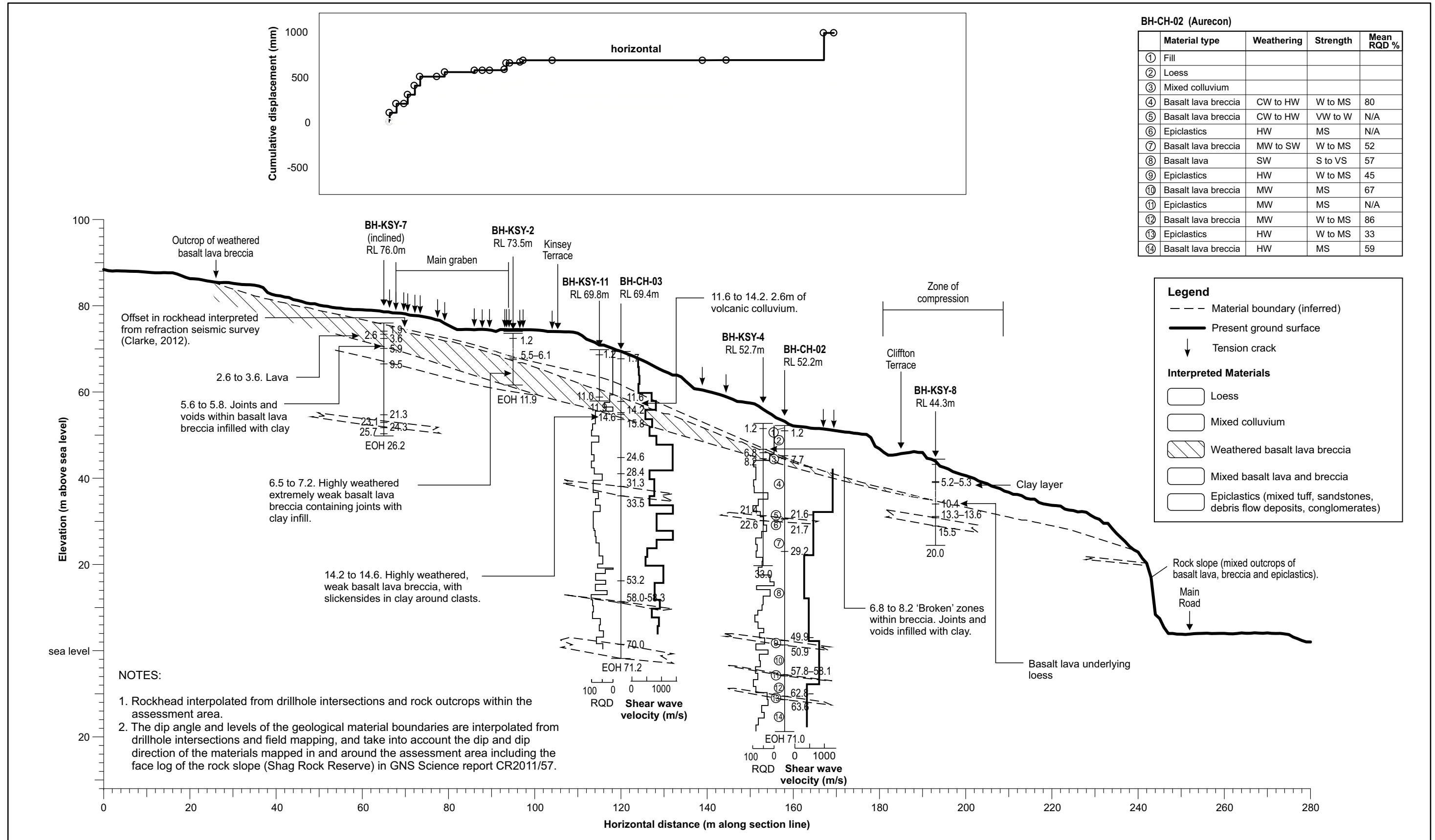
- *16 April 2011 earthquake* – Permanent displacement in source area A, inferred from the survey of monitoring marks (by GNS Science and Aurecon NZ Ltd.), was about 0.01–0.02 m towards a bearing of 070°. Many of the monitoring marks, including those within source area B, show no displacement exceeding the associated errors.
- *13 June 2011 earthquakes* – The cracks near the slope crest of source area A opened further in response to this earthquake. New cracks and areas of compression also formed. Permanent deformation of the area in response to the earthquakes on 13 June 2011 is inferred from the survey of monitoring marks (by GNS Science and Aurecon NZ Ltd.), was about 0.25–0.4 m (average of 0.33 m) towards a bearing of 070–090° (east), with vertical displacement of 0.1 and 0.2 m. Inferred displacement of source area B during this earthquake was about 0.15 m, and was recorded by one survey mark located near a collapsed retaining wall. No obvious signs of reactivation were observed across cracks in this area. These data imply a higher ground shaking movement threshold and stronger overall condition of this area compared to source area A.
- *23 December 2011 earthquake* – Existing cracks near the slope crest of source area A and B showed minor further opening in response to this earthquake. Horizontal displacement of source area A was about 0.05 m towards a bearing of 200° (south), and is attributed to tectonic displacement and not to reactivation of the landslide. If reactivation of the mass movement occurred, it could not be separated from the larger differential tectonic distortion of the land.

#### **3.1.4 After the 2010/11 Canterbury earthquakes**

- No systematic movements of the source areas A and B (outside survey error) have been detected since the 23 December 2011 earthquake.
- Several survey marks have shown small local displacements with no obvious trigger. These displacements are not thought to relate to reactivation of the landslide mass, but instead may be caused by shrinkage and swelling of the soil mass, or collapse of local tension cracks. In many cases the displacements are upslope.
- Evidence of localised displacement has been noted at various locations across the source areas including the inferred toe of source area A. However, these have not been related to systematic movement of the larger landslide mass.
- The loess slopes along Clifton Terrace in the lower part of source area A (Figure 5) have been modified during reconstruction and maintenance of Clifton Terrace. This area, of predominantly cut slopes, shows on-going minor deformation not recorded by survey marks.







**BH-CH-02 (Aurecon)**

	Material type	Weathering	Strength	Mean RQD %
①	Fill			
②	Loess			
③	Mixed colluvium			
④	Basalt lava breccia	CW to HW	W to MS	80
⑤	Basalt lava breccia	CW to HW	VW to W	N/A
⑥	Epiclastics	HW	MS	N/A
⑦	Basalt lava breccia	MW to SW	W to MS	52
⑧	Basalt lava	SW	S to VS	57
⑨	Epiclastics	HW	W to MS	45
⑩	Basalt lava breccia	MW	MS	67
⑪	Epiclastics	MW	MS	N/A
⑫	Basalt lava breccia	MW	W to MS	86
⑬	Epiclastics	HW	W to MS	33
⑭	Basalt lava breccia	HW	MS	59

**Legend**

- Material boundary (inferred)
- Present ground surface
- ↓ Tension crack

**Interpreted Materials**

- Loess
- Mixed colluvium
- Weathered basalt lava breccia
- Mixed basalt lava and breccia
- Epiclastics (mixed tuff, sandstones, debris flow deposits, conglomerates)

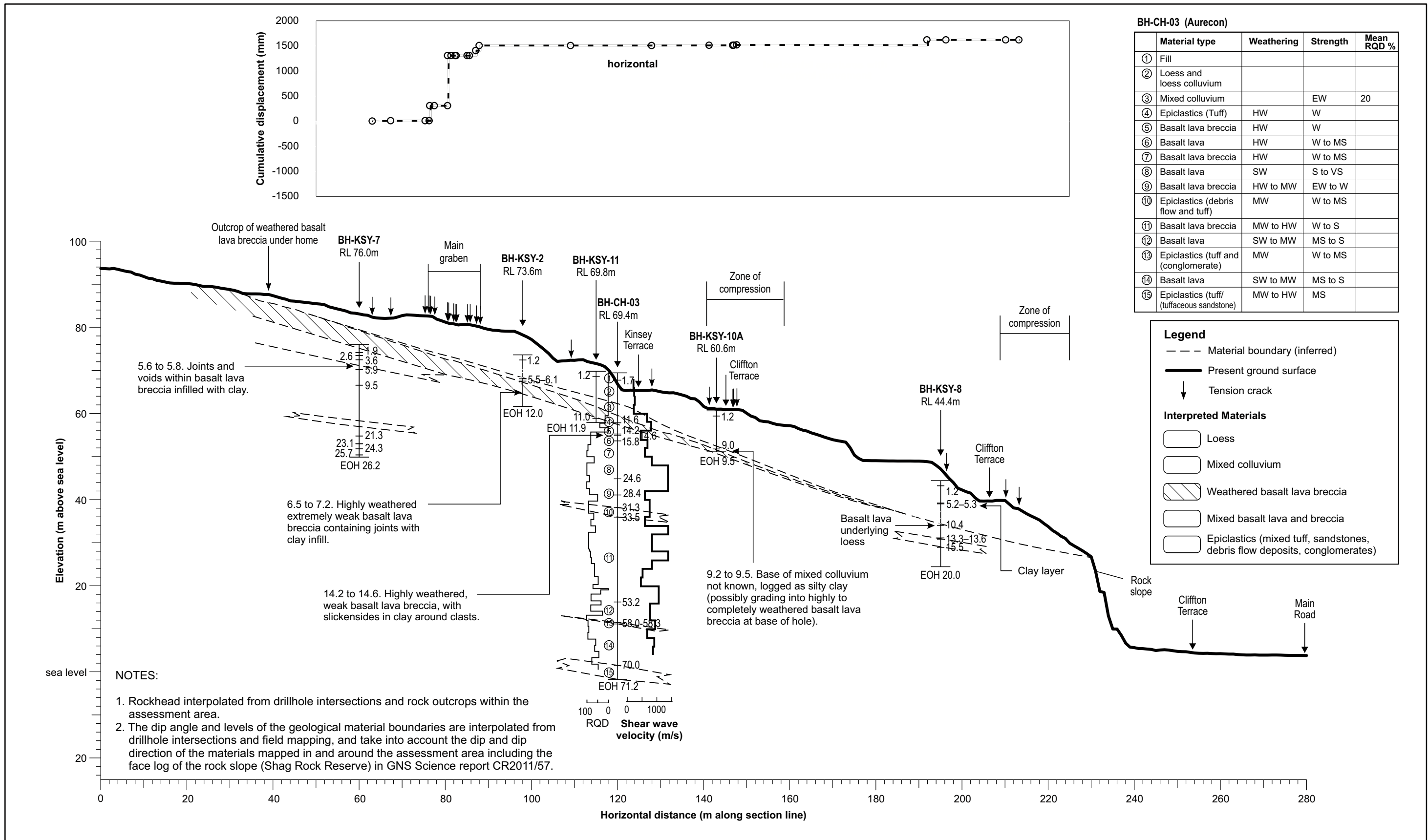
Weathering (adopting NZGS (2005) terminology): CW completely weathered; HW highly weathered; MW moderately weathered; SW slightly weathered; UW unweathered.  
 Rock Strength (field strengths adopting NZGS (2005) terminology): EW extremely weak; VW very weak; W weak; MS moderately strong; S Strong; VS very strong; extremely strong.  
 Soil strength (field strengths adopting NZGS (2005) terminology): Coarse soils – VL very loose; L loose; MD medium dense; D dense; VD very dense. Cohesive soils – H hard; VSt very stiff; St stiff; F firm; So soft; VSo very soft.  
 RQD: Rock quality designation

DRW:  
PC  
CHK:  
FDP/CM

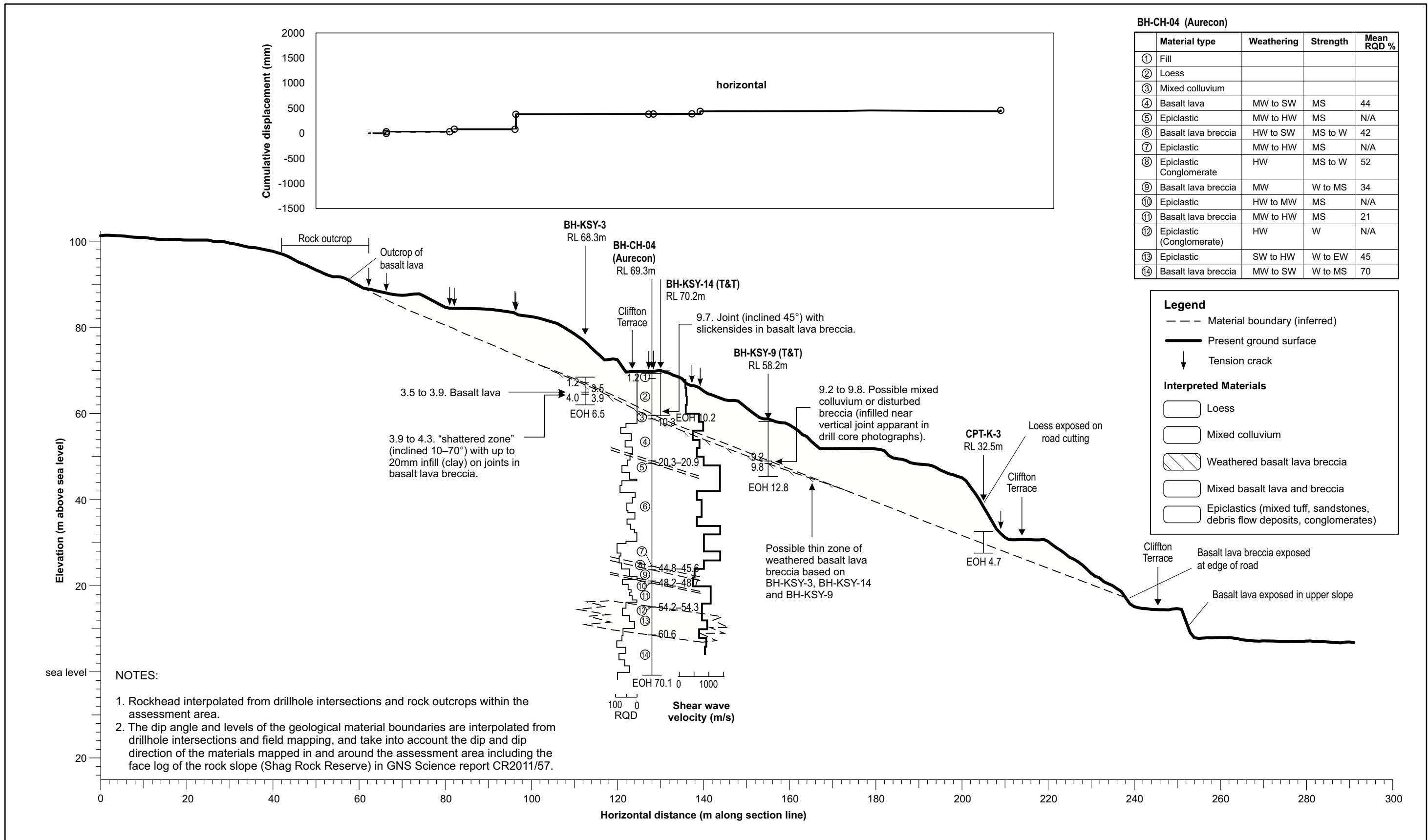


**ENGINEERING GEOLOGY CROSS SECTION 1**

**Clifton Terrace Christchurch**

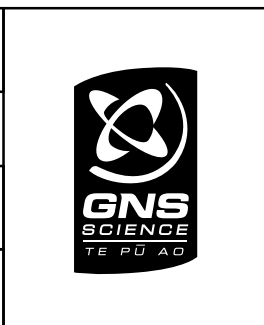


Weathering (adopting NZGS (2005) terminology): CW completely weathered; HW highly weathered; MW moderately weathered; SW slightly weathered; UW unweathered. Rock Strength (field strengths adopting NZGS (2005) terminology): EW extremely weak; VW very weak; W weak; MS moderately strong; S Strong; VS very strong; extremely strong. Soil strength (field strengths adopting NZGS (2005) terminology): Coarse soils – VL very loose; L loose; MD medium dense; D dense, VD very dense. Cohesive soils – H hard; VSt very stiff; St stiff; F firm; So soft; VSo very soft. RQD: Rock quality designation	DRW: PC		<b>ENGINEERING GEOLOGY CROSS SECTION 2</b>		<b>FIGURE 8</b>	
	CHK: FDP/CM		<b>Clifton Terrace Christchurch</b>		REPORT: CR2014/76	DATE: August 2014



Weathering (adopting NZGS (2005) terminology): CW completely weathered; HW highly weathered; MW moderately weathered; SW slightly weathered; UW unweathered.  
 Rock Strength (field strengths adopting NZGS (2005) terminology): EW extremely weak; VW very weak; W weak; MS moderately strong; S Strong; VS very strong; extremely strong.  
 Soil strength (field strengths adopting NZGS (2005) terminology): Coarse soils – VL very loose; L loose; MD medium dense; D dense, VD very dense. Cohesive soils – H hard; VSt very stiff; St stiff; F firm; So soft; VSo very soft.  
 RQD: Rock quality designation

DRW:  
PC  
CHK:  
FDP/CM



**ENGINEERING GEOLOGY CROSS SECTION 3**

**Clifton Terrace Christchurch**

**FIGURE 8**

REPORT: CR2014/76  
DATE: August 2014



## **3.2 SITE INVESTIGATIONS**

### **3.2.1 Geomorphological mapping**

The results from field mapping of slope morphology, interpreted surface materials and their genesis, surface deformation mapping and other relevant information are shown in Figure 6.

The site consists of a symmetric north sloping spur, which ends abruptly at a cliff in the north. The cliff toe was abandoned by the sea following construction of Main Road shortly after 1840. The area below the cliff is locally referred to as “Peacocks Gallop”. Peacock's father John Jenkins, when he rode by horse to and from Lyttelton to Sumner via Evans Pass, is said to have always been afraid of falling rocks, so he galloped along the road at the base of the cliff. After public demand and a large rockfall in 1911, the road and a tramway were relocated away from the base of the cliff to the site of the present Main Road. The area, now called Shag Rock Reserve, comprises the sea stack of Shag Rock and reclaimed land between the high cliffs and the relocated road and former tramway (now Main Road).

Clifton Terrace site is located on the northeast flank of the spur immediately adjacent to the steep cliff. The cliff on the northern side is about 80 m high, 500 m long, with a slope angle of about 60° and overhanging, in parts. The Clifton Terrace site can be divided into three sections based on slope geometry and exposed materials: 1) a toe section, adjacent to Main Road and Clifton Terrace, forming a steep (60° to vertical) slope predominantly in rock, which appears modified probably due to construction of Clifton Terrace; 2) a central section, forming a less steep slope (25–30°) formed predominantly in soil, mainly loess; and 3) an upper section near Kinsey Terrace, forming an even gentler slope (10–20°) formed predominantly in rock.

The central loess slope is deeply incised by several drainage lines, and exposures of loess in slope cuts along Clifton Terrace are greater than six metres high in parts. Dwelling construction has followed the natural contours of the land, but created a series of cut and fill terraces, on which dwellings and associated access drives have been constructed.

### **3.2.2 Subsurface trenching, drilling and probing**

Ground investigation details are summarised in Table 4 and located on Figure 6 and Figure 7. Geological logs and equipment installation details are contained in reports by Aurecon NZ Ltd. (Pletz, 2013) and Tonkin and Taylor Ltd. (Tonkin and Taylor, 2012a). Only seven of the cored drillholes extend to an adequate depth into rock to provide information on the bedrock. Nearly all of the other drillholes and all cone penetrometer holes (Labelled CPT in Table 4) terminate within overburden material at or close to rock head.

**Table 4** Summary of the ground investigations carried out at the site by Aurecon NZ Ltd. (Pletz, 2013) and Tonkin and Taylor Ltd. (Tonkin and Taylor, 2012a).

ID	Data source	Type	Depth (m below ground level)	Instrumentation/depth (m below ground level)
BH-CH-02	Aurecon NZ Ltd.	Cored hole	70.0	Inclinometer (70)
BH-CH-03	Aurecon NZ Ltd.	Cored hole	71.2	Inclinometer (71)
BH-CH-04	Aurecon NZ Ltd.	Cored hole	71.0	Inclinometer (71 m)
BH-KSY-1	Tonkin and Taylor Ltd.	Open barrel	27.0	Inclinometer (26.8 m)
BH-KSY-1a	Tonkin and Taylor Ltd.	Open barrel/Cored	14.1	Standpipe/response zone 14–17 m (bedrock)
BH-KSY-1b	Tonkin and Taylor Ltd.	Open barrel	10.2	Standpipe/response zone 9.6–12.6 m (tunnel gully in loess)
BH-KSY-1c	Tonkin and Taylor Ltd.	Open barrel	9.6	Standpipe/response zone 6.3–9.3 m (loess)
BH-KSY-1d	Tonkin and Taylor Ltd.	Open barrel	8.2	None
BH-KSY-1e	Tonkin and Taylor Ltd.	Open barrel/push tubes	8.8	None
BH-KSY-2	Tonkin and Taylor Ltd.	Open barrel	12.0	Inclinometer (11.3 m)
BH-KSY-2a	Tonkin and Taylor Ltd.	Tri-cone	5.1	Standpipe/response zone 3.4–5.4 m (loess)
BH-KSY-3	Tonkin and Taylor Ltd.	Open barrel	6.5	Inclinometer (11.3 m)
BH-KSY-3a	Tonkin and Taylor Ltd.	Tri-cone	3.7	Standpipe/response zone 1.7–3.7 m (loess)
BH-KSY-4	Tonkin and Taylor Ltd.	Open barrel	33.0	Inclinometer (32.8)
BH-KSY-4a	Tonkin and Taylor Ltd.	Tri-cone	5.0	Standpipe/response zone 1.7–4.7 m (loess)
BH-KSY-7	Tonkin and Taylor Ltd.	HQ Cored	37.0 (length)	None
BH-KSY-8	Tonkin and Taylor Ltd.	Cored	20.0	Inclinometer (19.8 m)
BH-KSY-8a	Tonkin and Taylor Ltd.	Wash drilled	10.5	Standpipe/response zone 7.0–10.0 m (loess)
BH-KSY-8b	Tonkin and Taylor Ltd.	Open barrel	10	None
BH-KSY-8c	Tonkin and Taylor Ltd.	Dry Cored/Push tubes	11.7	None
BH-KSY-9	Tonkin and Taylor Ltd.	Open barrel	12.8	Inclinometer (10.8 m)
BH-KSY-9a	Tonkin and Taylor Ltd.	HQ Cored/push tubes	9.2	Standpipe/response zone 6.7–9.7 m (loess)
BH-KSY-10	Tonkin and Taylor Ltd.	Percussion	9.5	None
BH-KSY-10a	Tonkin and Taylor Ltd.	Open barrel/push tubes	9.5	None

<b>ID</b>	<b>Data source</b>	<b>Type</b>	<b>Depth (m below ground level)</b>	<b>Instrumentation/depth (m below ground level)</b>
BH-KSY-11	Tonkin and Taylor Ltd.	Open barrel	11.9	None
BH-KSY-11a	Tonkin and Taylor Ltd.	Open barrel/push tubes	11.5	None
BH-KSY-12	Tonkin and Taylor Ltd.	Open barrel	4.9	None
BH-KSY-12a	Tonkin and Taylor Ltd.	Open barrel/push tubes	6.0	None
BH-KSY-13	Tonkin and Taylor Ltd.	Percussion	1.2	None
BH-KSY-14	Tonkin and Taylor Ltd.	Open barrel	10.5	None
BH-KSY-14a	Tonkin and Taylor Ltd.	Open barrel/push tubes	9.7	None
BH-KSY-15	Tonkin and Taylor Ltd.	Percussion	4.2	None
BH-KSY-15a	Tonkin and Taylor Ltd.	Percussion	4.4	None
CPT-K-1	Tonkin and Taylor Ltd.	Non-seismic cone	11.4	None
CPT-K-1A	Tonkin and Taylor Ltd.	Seismic cone	12.6	None
CPT-K-3	Tonkin and Taylor Ltd.	Non-seismic cone	4.8	None
CPT-K-4	Tonkin and Taylor Ltd.	Non-seismic cone	11.5	None
CPT-K-4A	Tonkin and Taylor Ltd.	Seismic cone	8.4	None
CPT-K-5	Tonkin and Taylor Ltd.	Non-seismic cone	5.9	None
CPT-K-6	Tonkin and Taylor Ltd.	Non-seismic cone	4.6	None
CPT-K-7	Tonkin and Taylor Ltd.	Non-seismic cone	7.0	None
CPT-K-8	Tonkin and Taylor Ltd.	Non-seismic cone	8.7	None
CPT-K-9	Tonkin and Taylor Ltd.	Seismic cone	7.5	None
CPT-K-10	Tonkin and Taylor Ltd.	Non-seismic cone	1.5	None
CPT-K-11	Tonkin and Taylor Ltd.	Seismic cone	4.5	None
CPT-K-12	Tonkin and Taylor Ltd.	Seismic cone	4.1	None
CPT-K-13	Tonkin and Taylor Ltd.	Seismic cone	5.7	None
CPT-K-14	Tonkin and Taylor Ltd.	Seismic cone	12.4	None
CPT-K-15	Tonkin and Taylor Ltd.	Seismic cone	11.3	None
CPT-K-16	Tonkin and Taylor Ltd.	Seismic cone	8.9	None
TP-K-1	Tonkin and Taylor Ltd.	Test pit	4.5 m	None
TP-K-2	Tonkin and Taylor Ltd.	Test pit	1.9 m	None

### **3.2.3 Geophysics**

Tonkin and Taylor Ltd. (Tonkin and Taylor, 2012a) carried out nine seismic cone penetrometer holes and conducted dissipation tests at their termination depths, which was typically at rock head. The seismic cone penetrometer tests record cone resistance and pore pressure as well as the shear wave velocity of the soil at one metre intervals.

Victoria University of Wellington conducted a refraction seismic line across the head scarp of the area of cracks (Figure 6) in January 2012 (Clarke, 2012). The objectives of this study were to investigate the loess-rock interface (rock head) at the landslide sites and at Clifton Terrace to investigate the thickness of the loess and the shape of rock head across the main area of cracking.

GNS Science maintained a small-scale temporary seismic array comprising five seismometers (K1–K5 on Figure 6) across the cracked area at Kinsey Terrace between 19 June 2011 and 19 January 2012 (Kaiser et al., 2014). The purpose of this work was to characterise the seismic site response and assess the extent to which amplification influenced ground motions at the site.

### **3.2.4 Surface movement**

#### **3.2.4.1 Surveyed slope displacements**

The survey monitoring data are presented in Appendix 2 and are summarised below. There are three datasets:

1. Cadastral survey marks (details held by Land Information New Zealand), for property boundaries and roads footpaths etc.;
2. Monitoring-survey marks installed by Aurecon NZ Ltd., for Christchurch City Council, to specifically monitor surface displacement; and
3. Continuous GPS monitoring at three locations, installed by GeoNet as part of a GNS Science research project investigating coseismic landslide behaviour.

All datasets adopt reference control marks that are outside the area of movement, but still within the local area. Therefore, any regional offsets caused by tectonic displacements should be removed from the data.

#### **3.2.4.2 Cadastral marks (source: LINZ)**

Available cadastral survey marks were remeasured by GNS Science to detect absolute ground movements spanning the earthquake period from before the 22 February 2011 earthquakes (the pre-earthquake survey dates for each cadastral mark vary). Surveys of some of these marks were carried out on 25 March 2011 and 8 September 2011. Any displacements of these cadastral marks therefore, include any displacement of the survey marks in response to the earthquakes within this time period. The results of this survey are contained in Appendix 2.

Vector displacements based on these measurements indicate permanent ground displacements, within the lower and middle part of source area A, that range from 320 to 710 mm, towards bearings 030–100° (east-northeast) (Map 2 Appendix 2). In source area B the magnitude of displacement is less, about 260–490 mm towards bearings 080–090° (Map 2 Appendix 2), for the marks in the central part of the source area.

Calculated total displacements of the cadastral survey marks are summarised in Table 5.

#### **3.2.4.3 Monitoring marks (source: Aurecon NZ Ltd.)**

The displacements calculated from the Aurecon survey data span the period from 24 February 2011 to 25 June 2013. There are from 4–90 observations per mark (average of about 50). Note that the dates covered and the numbers of observations vary between survey marks. The data include any displacement of the survey marks in response to the earthquakes within the time period, mostly in the 16 April, 13 June and 23 December 2011 earthquakes. Several survey marks were installed in lines across areas of cracks, where the displacements were estimated relative to a control mark, which was assumed to be stable. However, in some locations the control mark was inside the area of mapped displacement and therefore the data for these marks cannot be used to infer total permanent displacement of the slope.

#### **3.2.4.4 cGPS marks (GeoNet)**

Surface movement at three locations is monitored by GNS Science using continuous GPS (cGPS) receivers (labelled CLSK, CLS5 and CLS6 on Map 1 in Appendix 2). CLSK was installed on 2 March 2011 and so captured permanent displacements of the slope in response to the 16 April, 13 June and 23 December 2011 earthquakes. CLS5 and CLS6 were installed on 22 June 2011 and 14 October 2011 respectively, by GeoNet (Appendix 2, Map 1), and so capture permanent slope displacements caused by earthquakes after these dates. The data for the cGPS marks are summarised in Appendix 2 and the displacement versus time plots are contained in Appendix 3.

From the survey time series relating to the cadastral, monitoring and cGPS marks it has been possible to determine the magnitudes and bearings of displacements caused by these earthquakes; these are summarised in Table 5. The listed magnitudes of displacements are those outside the estimated survey errors, which are shown as error ellipses on the maps in Appendix 2.

**Table 5** Summary of slope displacements inferred from the surveying of cadastral, monitoring and cGPS marks installed on the slope. Only measurements outside survey error are shown, refer to Appendix 2 for details.

<b>Date</b>	<b>Survey type</b>	<b>Assessed source area A</b>	<b>Assessed source area B</b>
Pre-22 February 2011 (various dates) to either 25 March 2011 or 8 September 2011	Cadastral marks	319–710 mm (horizontal, down slope)	264–493 mm (horizontal, down slope)
22 February 2011	Measured and inferred from the survey of cadastral marks	313–655 mm (horizontal, down slope)	108–337 mm (horizontal, down slope). Inferred by subtracting the displacement of monitoring mark 35 (D16) (154 mm towards bearing 080°) inferred to be mainly caused by the 13 June 2011 earthquake.
16 April 2011	Monitoring marks and cGPS	9–19 mm (horizontal, down slope) Movement only marginally outside error.	No movement outside error
13 June 2011	Monitoring marks and cGPS	245–399 mm (horizontal, down slope)	154 mm (horizontal, down slope)
23 December 2011	Monitoring marks and cGPS	16–46 mm (horizontal) but upslope and attributed to local tectonic displacement caused by the earthquake.	No movement outside error
23 December 2011 to 25 June 2013	Monitoring marks and cGPS	1–16 mm/year creep displacement (horizontal, down slope) in various directions. Thought to be related to local shrink and swell of the soil, and unrelated to the large-scale movement of source area A.	No movement outside error

### 3.2.4.5 Inferred slope displacement patterns from crack apertures

Cumulative displacement of the slope inferred from crack apertures along cross-sections 1–3, in response to the 2010/11 Canterbury earthquakes, was about 0.6–2.2 m for cross-sections 1 and 2, and 0.4–0.5 m for cross-section 3 (Table 6).

**Table 6** Measured cumulate crack apertures, which formed mainly during the 22 February, and less so during the 13 June, 2011 earthquakes, measured by GNS Science. Displacements were obtained from field mapping of tension crack apertures along survey lines. Errors are nominally estimated as being  $\pm 0.01$  m.

Cross-section	Location	Vertical component (mm)	Horizontal component (mm)		Resultant vector <sup>2</sup>		Apparent dip of loess/rock interface from the horizontal (°)
			All apertures	Horizontal with vertical component <sup>1</sup>	Magnitude (mm)	Dip (°)	
1	Head scarp	460	680	430	821	34	13
	Entire cross-section	620	983	433	1,162	32	
2	Head scarp	1,250	1,508	1,503	1,959	40	18
	Entire cross-section	1,432	1,619	1,603	2,161	41	
3	Head scarp	38	380	103	382	6	22
	Entire cross-section	0	458	56	458	0	

<sup>1</sup> The measurements area based on adding the horizontal displacements with vertical displacements, and excluding those with no vertical displacements.

<sup>2</sup> Resultant vectors are calculated using the horizontal displacements for all crack apertures

The tension cracks that formed during the 2010/11 Canterbury earthquakes were mainly confined to the head scarp of the assessed source areas, and correspond to the locations of where the subtle scarp features were identified in the historical aerial photographs (Figure 5). There are only a few tension cracks within the main body of the inferred displaced mass, and displacements across these apertures are small compared to those measured in the head scarp, suggesting the displaced mass moved as a series of large relatively intact blocks.

The displacement vectors along cross-sections 1–3 indicate a steeper angle in the inferred head scarp of the main area of cracking and movement for both source areas. The compression features mapped along Clifton Terrace (Figure 6), along with the extensional cracks at the head scarp suggest the displaced mass had a translational movement mechanism. In the central part of the displaced mass (source area A) the displacement angles (from the horizontal), inferred from the surveying of monitoring marks (20 and 21, Map 1 Appendix 2) are 25–33° and are slightly steeper than the dip of rock head and the volcanic bedrock sequence, which is estimated to vary between 10° and 30° (average of about 20°). Given the uncertainties associated with the measurements, however, the displacement angles are similar to the dip of the volcanic sequence, supporting a predominantly translational displacement mechanism. The horizontal vectors of displacement are also generally sub-parallel to the dip of the loess/colluvium and rock interface, as well as the dip direction of the underlying volcanic sequence.

The total amount of permanent slope displacement inferred from the survey marks (all events) is slightly more than half the total amount inferred from crack apertures. This is thought to be because the amount of displacement inferred from crack apertures has been accumulated along the cross-sections, taking no account of any compression. Therefore the displacements inferred from crack apertures are considered to be upper-bound estimates.

### **3.2.5 Subsurface movement**

Inclinometer tubes installed in drillholes were used to: 1) monitor displacements at depth; 2) assess whether movement was occurring along single or multiple slide-surfaces; and 3) to independently verify the results of surface monitoring. Monitoring was undertaken manually by commercial contract (Geotechnics Ltd.).

Inclinometer tubes are installed in drillholes BH-CH-02, BH-CH-03 and BH-CH04 (Pletz, 2013) and six of the Tonkin and Taylor drillholes: BH-KSY-1, BH-KSY-3, BH-KSY-4, BH-KSY-8 and BH-KSY-1. The inclinometer displacements were monitored at 0.5 m intervals and the inclinometer accuracy is quoted as  $\pm 6$  mm over 25 m of tubing (Slope Indicator, 2005).

Inclinometer measurement details are summarised in Table 7 for the Tonkin and Taylor (2012a) inclinometers. The recorded cumulative displacements of the inclinometer tubes installed in drillholes BH-KSY-1, BH-KSY-3 and BH-KSY-8 show minor displacements that are only slightly larger than the associated errors. The inclinometer tube in drillholes BH-KSY-2 and BH-KSY-9 show no obvious displacements outside of survey error, and the inclinometer tube in drillhole BH-KSY-4 shows a sinusoidal pattern associated with incomplete grouting of the void between the inclinometer tube and the drillhole wall or natural voids in the ground, which at these depths comprises weathered basalt lava breccia. The results in Tonkin and Taylor (2012a) cover the period from installation to 24 December 2011, but contain no tilt change plots. Additional data for these inclinometers, including the tilt change plots, was supplied to GNS Science by Tonkin and Taylor Ltd., for the period 24 December 2011 to 24 June 2013.

The inclinometer installed in drillhole BH-KSY-1, has a deflection in the monitoring tube between the 11.75 and 12.25 m intervals (below the collar elevation), corresponding to the mixed colluvium at its interface with the overlying loess (at approximately 12.3 m below ground level). The inclinometer in drillhole BH-KSY-3, has a deflection in the monitoring tube between the 3.5 and 3.75 m intervals, corresponding to the contact between the loess and the underlying weathered basalt lava breccia (at approximately 3.5 m below ground level). The inclinometer installed in drillhole BH-KSY-8, has a slight deflection in the monitoring tube between the 8.25 and 8.75 m intervals, corresponding to the loess (rock head is at 10.4 m below ground level).

The total cumulative deflection in all inclinometers is relatively small, about 2–5 mm. The bearings of displacement are towards:  $087^\circ$  for BH-KSY-1;  $168^\circ$  for BH-KSY-3 and  $048^\circ$  for BH-KSY-8. The deflections are recorded in multiple surveys. For BH-KSY-1 and BH-KSY-8, the main displacement in the inclinometer tubes occurred between 23 December 2011 and 1 June 2012 surveys and the direction of displacement is consistent with the direction of permanent slope movement during the main earthquakes, inferred from the surface monitoring marks. It is possible that these displacements were in response to the 23 December 2011 earthquake. For BH-KSY-3, there appear to be two main periods of displacement, between the 23 December 2011 to 1 June 2012, and 11 December 2012 and

13 March 2013 surveys. The direction of movement, however, is not consistent with the main direction of slope displacement for the main 2011 Canterbury earthquakes, inferred from surface monitoring marks.

These readings are only marginally in excess of the associated survey error. Given the small magnitude of displacement, it is not known whether these displacements relate to displacement of the slope, or to displacement of the inclinometer tubes within the drillholes, unrelated to slope displacement. Further monitoring is required to resolve this issue.

The inclinometers installed in the Aurecon NZ Ltd. drillholes BH-CH-02, BH-CH-03 and BH-CH-04 (Pletz, 2013) show no displacements that are larger than the associated errors for the monitoring period, between 12 February 2013 and 18 March 2013 (Geotechnics, 2014).

**Table 7** Summary of Tonkin and Taylor (2012a) drillhole inclinometer surveys. Note: m bgl refers to metres below ground level.

Measuring date	Drillhole ID			
	BH-KSY-1	BH-KSY-3	BH-KSY-4	BH-KSY-8
7/07/2011	Baseline	Baseline		
15/07/2011	No data	No data	Baseline	
12/08/2011	No data	No data	No data	Baseline
25/08/2011	No movement outside error	No data	No data	No data
1/09/2011	Slight drift in cumulative displacement plot between 12–17 m bgl of about 3 mm.	Slight drift in cumulative displacement plot between 3.25 and 3.75 m bgl.	No data	No data
9/09/2011	No movement outside error	No data	Sinusoidal displacement pattern between 7.75 and 12.25 m bgl.	No data
15/09/2011	No data	No data	Sinusoidal displacement pattern between 7.75 and 12.25 m bgl.	No data
26/09/2011	No data	No data	No data	No movement outside error
5/10/2011	No data	Slight drift in cumulative displacement plot between 3.25 and 3.75 m bgl.	No data	No movement outside error
12/10/2011	No movement outside error	Slight drift in cumulative displacement plot between 3.25 and 3.75 m bgl.	Sinusoidal displacement pattern between 7.75 and 12.25 m bgl.	No movement outside error
21/10/2011	No movement outside error	Slight drift in cumulative displacement plot between 3.25 and 3.75 m bgl	Sinusoidal displacement pattern between 7.75 and 12.25 m bgl.	No movement outside error
31/10/2011	No data	No data	No data	No data
10/11/2011	No data	No data	No data	No data
18/11/2011	No data	No data	No data	No data
24/11/2011	No data	No data	No data	No data
23/12/2011	Small deflection in the tilt change plot between 11.75 and 12.25 m bgl. 1–2 mm towards bearing 087°.	Small deflection in the tilt change plot between 3.25 and 3.75 m bgl. 1–2 mm towards bearing 168°.	Sinusoidal displacement pattern between 7.75–12.25 m bgl.	No data

Measuring date	Drillhole ID			
	BH-KSY-1	BH-KSY-3	BH-KSY-4	BH-KSY-8
24/12/2011	No data	No data	No data	Small deflection in the tilt change plot between 8.5 and 8.75 m bgl. 1–2 mm towards bearing 048°.
1/06/2012	No movement outside error	No movement outside error	Sinusoidal displacement pattern between 7.75–12.25 m bgl.	No movement outside error
11/12/2012	No movement outside error	Small deflection in the tilt change plot between 3.25 and 3.75 m bgl. 2–3 mm towards bearing 330°.	No data	No movement outside error
12/12/2012	No data	No data	Sinusoidal displacement pattern between 7.75–12.25 m bgl.	No data
13/03/2013	No movement outside error	Small deflection in the tilt change plot between 3.25 and 3.75 m bgl. 2–3 mm towards bearing 168°.	Sinusoidal displacement pattern between 7.75–12.25 m bgl.	No data
15/03/2013	No data	No data	No data	No movement outside error
18/06/2013	No movement outside error	No movement outside error	Sinusoidal displacement pattern between 7.75–12.25 m bgl.	No data
24/06/2013	No data	No data	No data	No movement outside error

### 3.2.6 Groundwater

Drilling-water circulation conditions are not reported in drilling logs by Tonkin and Taylor (2012a). Water loss was recorded in drilling records reported in Pletz (2013) for BH-CH-02, BH-CH-03 and BH-CH-04. These records are for the rock only and report 20–100% water loss, with an average of about 70%, indicating the material is quite permeable. Water levels measured during drilling show that water levels were recorded in all drillholes whilst drilling through the loess, mixed colluvium and rock head, between the ground surface and about 20 m below ground level. The holes were recorded as being predominantly dry whilst drilling at depths 20–60 m below ground level.

Observations made by the drillers that circulation was abruptly lost and gained during drilling (McNeill Drilling Services personal communication, 2012) suggest that tunnel gullies were encountered within the loess. A note in Tonkin and Taylor (2012a) indicates that one of the installed stand pipes in BH-KSY-1b is within an “in filled tunnel gully”. GNS Science mapped several areas of tunnel gulying adjacent to the incised drainage lines (Figure 5). These observations would suggest that the loess is relatively well drained by tunnel gullies.

Six standpipes were installed by Tonkin and Taylor (2012a); their details are contained in Table 4). GeoNet installed water level sensors in Tonkin and Taylor drillholes BH-KSY-2a and BH-KSY-8a, as part of a research project carried out by GNS Science to investigate coseismic landslide displacement patterns. These sensors record the height of water in the standpipe above the sensor tip. Installation details are contained in Table 8, and installation details of the standpipes are contained in Tonkin and Taylor (2012a). Graphs showing the daily mean water levels recorded in the stand pipes are contained in Figure 9 and Figure 10.

**Table 8** Installation details for the water level sensors installed in drillholes BH-KSY-2a and BH-KSY-8a.

Details	Drillhole ID	
	BH-KSY-2a	BH-KSY-8a
Monitoring date (from)	31/10/2011	1/11/2011
Monitoring date (to)	21/07/2014	21/07/2014
Measurement frequency (minutes)	5	5
Data completeness (%)	100%	87%
Sensor tip (metres below ground level)	4.1	9.6
Response zone top (metres below ground level)	3.5	7.0
Response zone bottom (metres below ground level)	5.4	10.0
Drillhole collar elevation (metres above mean sea level)	73.6	44.3
Material type	Loess	Loess
Mean piezometric head level above sensor tip (m)	0.11	0.14
Maximum recorded piezometric head level above sensor tip (m)	2.0	2.5
Maximum recorded piezometric head level above rock head (m)	4.0	3.3
Error on piezometric head level based on barometric pressure variation (metres, at one standard deviation)	±0.1	±0.1
Percentage of days when no water level recorded (%)	69	59

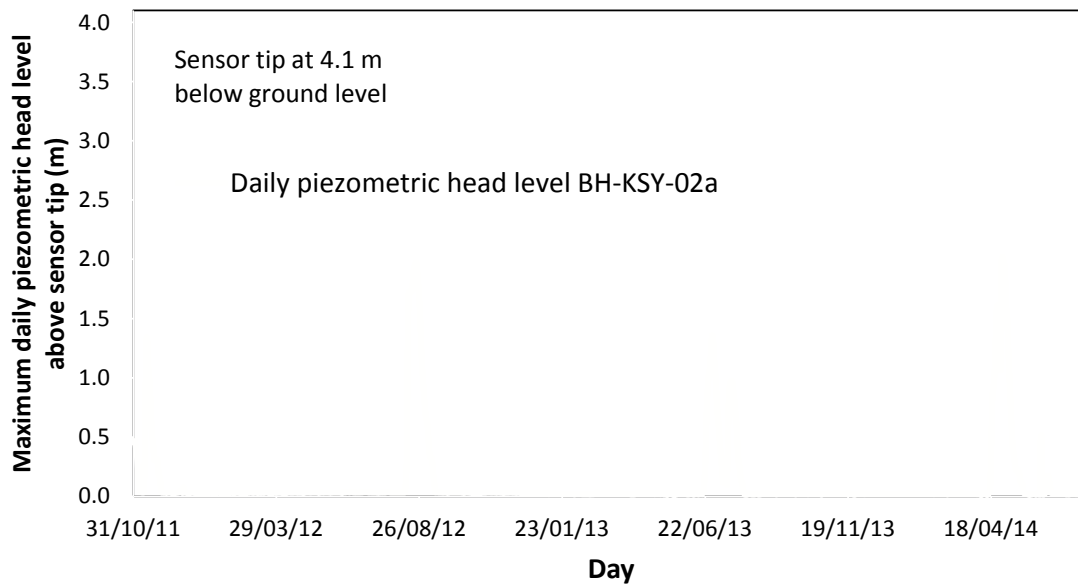


**Figure 9** Piezometric head levels recorded above the sensor tip installed in the standpipe in drillhole BH-KSY-2a. The sensor tip is at 4.1 m below ground level and 2.0 m above rock head.

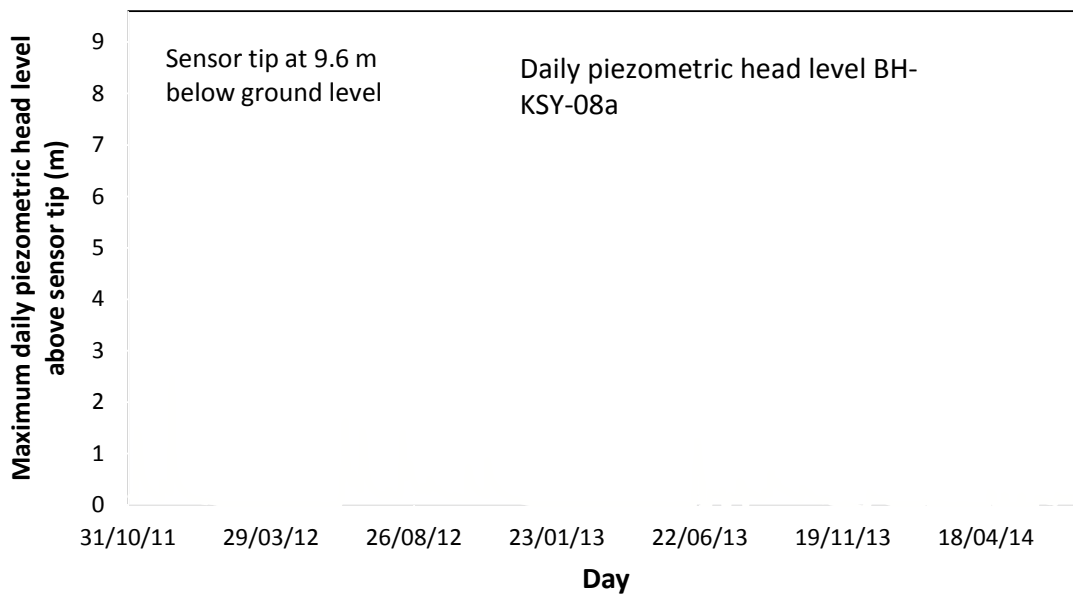


**Figure 10** Piezometric head levels recorded above the sensor tip installed in the standpipe in drillhole BH-KSY-8a. The sensor tip is at 9.6 m below ground level, and 0.8 m above rock head.

Monitoring data from the other standpipes comprised the manual measurement of water. A maximum of 13 measurements were made over the reporting period 3 August 2011–18 July 2012 (Tonkin and Taylor, 2012a), indicating a poor temporal resolution. No more recent data have been provided to GNS Science. A summary of the water level data reported in Tonkin and Taylor (2012a) is contained in Table 9.

**Table 9** Summary of water levels manually recorded in standpipes.

Details	Drillhole ID					
	BH-KSY-1a	BH-KSY-1b	BH-KSY-1c	BH-KSY-3a	BH-KSY-4a	BH-KSY-9a
Number of measurements	13	12	12	16	13	12
Standpipe tip (metres below ground level)	14.1	7.0	9.2	3.6	4.9	8.8
Standpipe tip (metres above rock head)	-1.3	5.8	3.6	-0.1	1.1	1.0
Response zone top (metres below ground level) and material	14 (breccia)	9.6 (loess)	6.3 (loess)	1.7 (loess)	1.7 (loess)	6.7 (loess)
Response zone bottom (metres below ground level)	17 (breccia)	12.6 (mixed colluvium)	9.3 (loess)	3.7 (lava)	4.9 (loess)	9.7 (mixed colluvium)
Maximum recorded piezometric head level above tip (m)	4.5	4.5 (initially 6 m was recorded but after drilling)	0.7	2.6	1.4	1.0
Number of measurements when dry	11	6	8	5	11	7

Field mapping carried out by GNS Science identified several locations within and around the source areas where water was seeping from the surface (these are shown on Figure 5). All seepage points were located in soil overlying rock or soil close to the inferred rock-head level (inferred from field mapping and drillhole logs).

### 3.3 ENGINEERING GEOLOGICAL MODEL

A site-investigation map is presented in Figure 6, engineering geological map in Figure 7 and cross-sections 1–3 in Figure 8. The map and cross-sections are based on the interpretation of features identified in aerial photographs, field mapping and ground investigation data, as summarised in Table 2.

Based on this work the main slope forming materials and groundwater conditions are summarised below.

#### 3.3.1 Slope materials

##### 3.3.1.1 Fill

Modified terrain with local areas of fill relating to building platform construction for residential homes can be found over much of the site. The depths and extents of fill in these areas are unknown. The fill, where encountered in drillholes, is described as soft and relatively weak silt with occasional basalt clasts and concrete rubble. The fill is estimated to be locally up to several metres in places.

### 3.3.1.2 Loess

The loess mantling the slope within the assessment area is similar to that in other areas of the Port Hills. It is a relatively cohesive silt-dominated soil with only minor clay mineral content (less than 10%). Its strength is largely controlled by the soil-moisture content and this has been well studied, e.g., Bell et al. (1986), Bell and Trangmar (1987), McDowell (1989), Goldwater (1990), Yetton (1992) and Carey et al. (2014). In some places, the loess has been reworked by excavation and construction activities. Along Clifton Terrace, the loess has been cut to form relatively steep slopes (typically 60° or greater) of varying height, some greater than six metres. The loess is highly hydrophyllic and when exposed to water (rain) it quickly disintegrates into muddy silt. The thickness of the loess, in drillholes and from field mapping of exposures, varies in thickness from a few metres to about 12 m in this area.

### 3.3.1.3 Mixed loess/volcanic colluvium

A layer of sandy silt containing boulders and gravel with clay, the relative proportions of which are highly variable, was logged and identified as colluvium in many of the drillholes and field exposures across the site. In drillholes and field exposures, the mixed colluvium is highly variable. It ranges from gravel to boulder-sized clasts of volcanic basalt with a loess and clay matrix, where close to the underlying volcanic bedrock, to remoulded loess with occasional gravel and boulders.

In drillhole cores and where exposed in outcrop, the mixed colluvium appears to have slightly higher clay content than the overlying loess. This is shown by the results of index tests (Tonkin and Taylor, 2012a) where its liquid limit, plasticity index and moisture content reflect a higher clay content than the overlying loess. It is thought to represent the deposits of debris from past landslides and other erosion processes. These can be seen in the drillhole cores, where there appear to be distinct layers within the overall layer of mixed colluvium (Figure 11). The material derives mainly from weathered volcanic breccia and lava and remobilised loess, and is similar to the “mixed colluvium” described by Bell and Trangmar (1987).

The thickness of the colluvium in drillholes varies up to 2.6 m (BH-CH-03) in the upper part of source area A (Figure 8), which is unusually thick. In other areas, the colluvium is either thin (less than 0.6 m) or absent from the drillhole cores. However, there is a lack of drillholes in the lower part of the slope in source areas A and B, and so the mixed colluvium could extend, under the loess and above rock head, over much of the site.

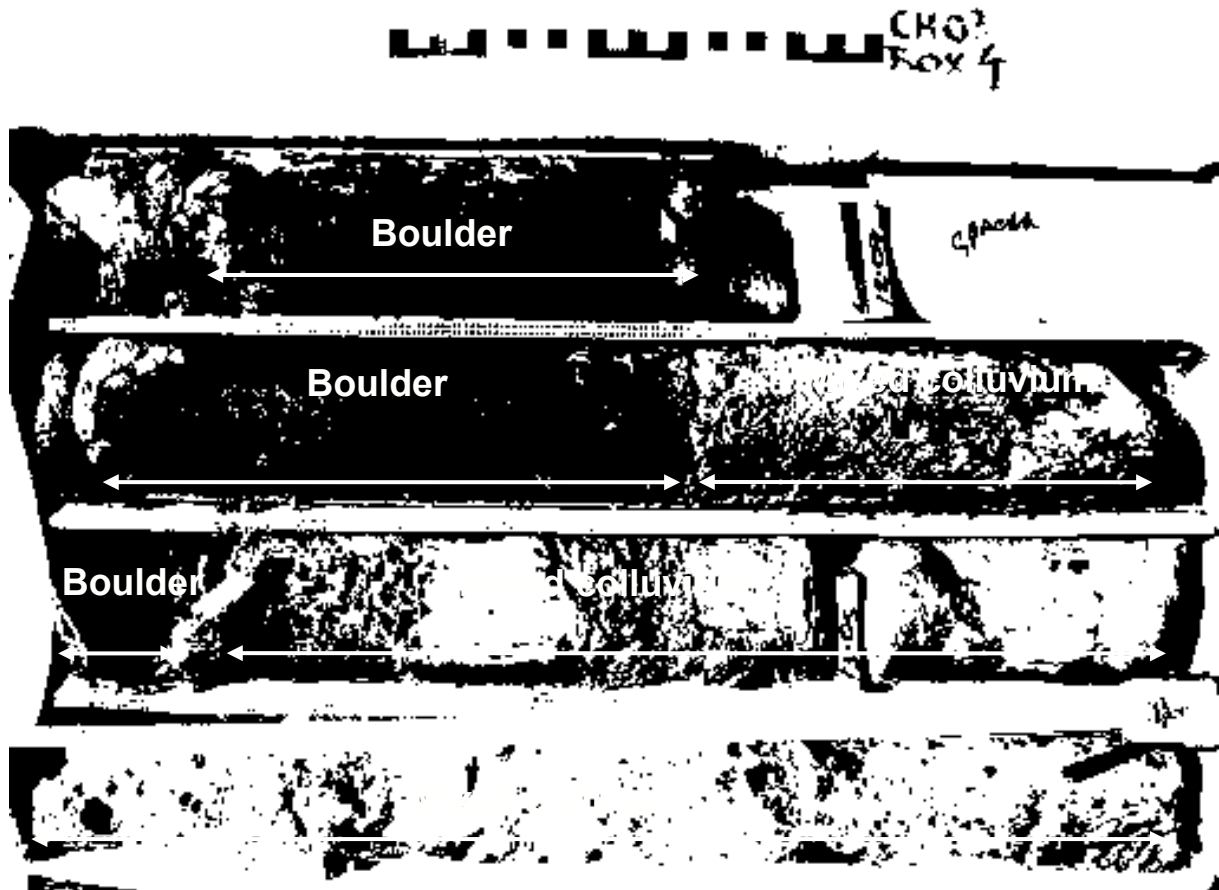


**Figure 11** Drillhole core from BH-CH-03. The depth of the core is 11.6 m below ground level (top left of photograph) to 13.8 m below ground level (bottom right of photograph).

### 3.3.1.4 Bedrock (volcanic basalt lava breccia, basalt lava and epiclastics)

The Clifton Terrace slopes are underlain by mixed layers of weak volcanic basaltic breccia, stronger, but more jointed basalt lava sequences (and channel fills), and occasional thin layers of epiclastic sediments (mainly sandstones, conglomerates) and tuffs. Field mapping of the cliff face along Shag Rock Reserve was carried out by GNS Science and is reported by Massey et al. (2012). The material layering is highly variable both laterally and vertically but the layers are laterally persistent along most of the cliff. Descriptions of the main units are given in Table 10 and shown in Figure 12. The cliff-face logs show that the volcanic sequences generally dip at 10–30° (average of about 20°) with a dip direction of 070–080° (Figure 12). The volcanic and epiclastic layers are continuous over much of the face corresponding to the closest rock outcrop of material beneath source area A (chainage 0–110 m, Figure 12).

**Table 10** Engineering geological descriptions of the main geological units forming the exposed cliffs in Shag Rock Reserve and in drillhole cores (descriptions as per New Zealand Geotechnical Society, 2005).

Unit name	Description
Basaltic lava breccia	<p>Slightly weathered to highly weathered, light grey to dark grey when slightly weathered to orange or red-brown when highly weathered, massive, brecciated basaltic lava fragments, moderately strong to strong (but varies to weak or very weak when highly or completely weathered), with very widely spaced irregular discontinuities.</p> <p>At all sites basaltic lavas have flowed within thick carapaces of brecciated lava, with the breccia often exceeding the thickness of its source lava (brecciated units may be 2 to &gt;10 m thick.). Breccias are poorly graded, angular lava fragments with a fine to coarse matrix supporting unsorted cobbles, blocks and often 1–5 m diameter megablocks of broken lava. Breccia fragments are often more vesicular and scoriaceous than the source lava, and prone to weathering due to high porosity. Bedding is massive, with lower boundaries gradational with the source lava and upper boundaries roughly planar, and joints are typically very widely spaced. Weathering expression is cavernous and spheroidal, of fine and coarse blocks respectively, and in some cases development of cliff-parallel exfoliation joints/cracks. Freshly exposed breccia faces show extensive interstitial clay weathering and deposition of clay within vesicles and between clasts. Many joints are due to recent fracturing of the rock mass during the 2010/11 earthquakes, with very few, if any apparent tectonic discontinuities. Joints are very widely spaced (&gt;2 m), with their persistence varying from a few metres to tens of metres. Joint surfaces tend to be “fair” to “good” adopting the Geological Strength Index classification (Hoek, 1999).</p>
Basalt lava	<p>Dark greenish grey to black, unweathered to moderately weathered, sometimes vesicular, basalt, very strong with variably developed columnar joints, widely to very widely spaced (1.5–5 m), typically giving large to very large block sizes that are columnar in shape. Columnar joints may be radial to flow margins, and lavas have gradational contacts with lava breccia at their upper and lateral margins. Joint faces are generally rough to very rough, stepped or irregular, commonly manganese oxide or calcite coated, and only rarely have clay or silt fill. Joint surfaces therefore tend to be “fair” to “good” adopting the Geological Strength Index classification (Hoek, 1999). Individual flows form lensoidal bodies throughout the cliffs, ranging from 0.5 to 2–4 m thick. Columnar jointing is well expressed where flows are thick, and gives way to thin, platy flow-orientated jointing where flows are thin.</p>
Epiclastic deposits	<p>Moderately to highly weathered or oxidised brown to red-brown or yellow-brown thinly bedded tuff or tuffaceous Sandstone, intercalated with or grading into fine to coarse pebbly Lapilli Tuffs or gravelly sandstone and conglomerate, with occasional cobble-sized blocks and bombs of basalt, moderately strong to weak, very weak to extremely weak when highly weathered. Rarely jointed, prone to cracking on exposed surfaces and easily eroded. Bedding is thin (0.1–2 m) and discontinuous, disrupted by overlying lavas. In all sites, these layers of red-oxidised pyroclastic and epiclastic paleosol material are found between lava flows and breccias, usually at the top of the preceding lava breccia, and oxidised/baked by the overlying lava flow. The thinly bedded ash and lapilli, with occasional blocks and bombs, is discontinuous due to re-working by water-driven epiclastic processes or re-working by overlying lava flows. The pyroclastic material exposed at the cliffs is often vegetated or a focus for fluid flow, being water retentive and relatively impermeable compared to the overlying jointed lavas and porous breccias. Contacts are often gradational into lava breccia or lahar/debris-flow deposits.</p>

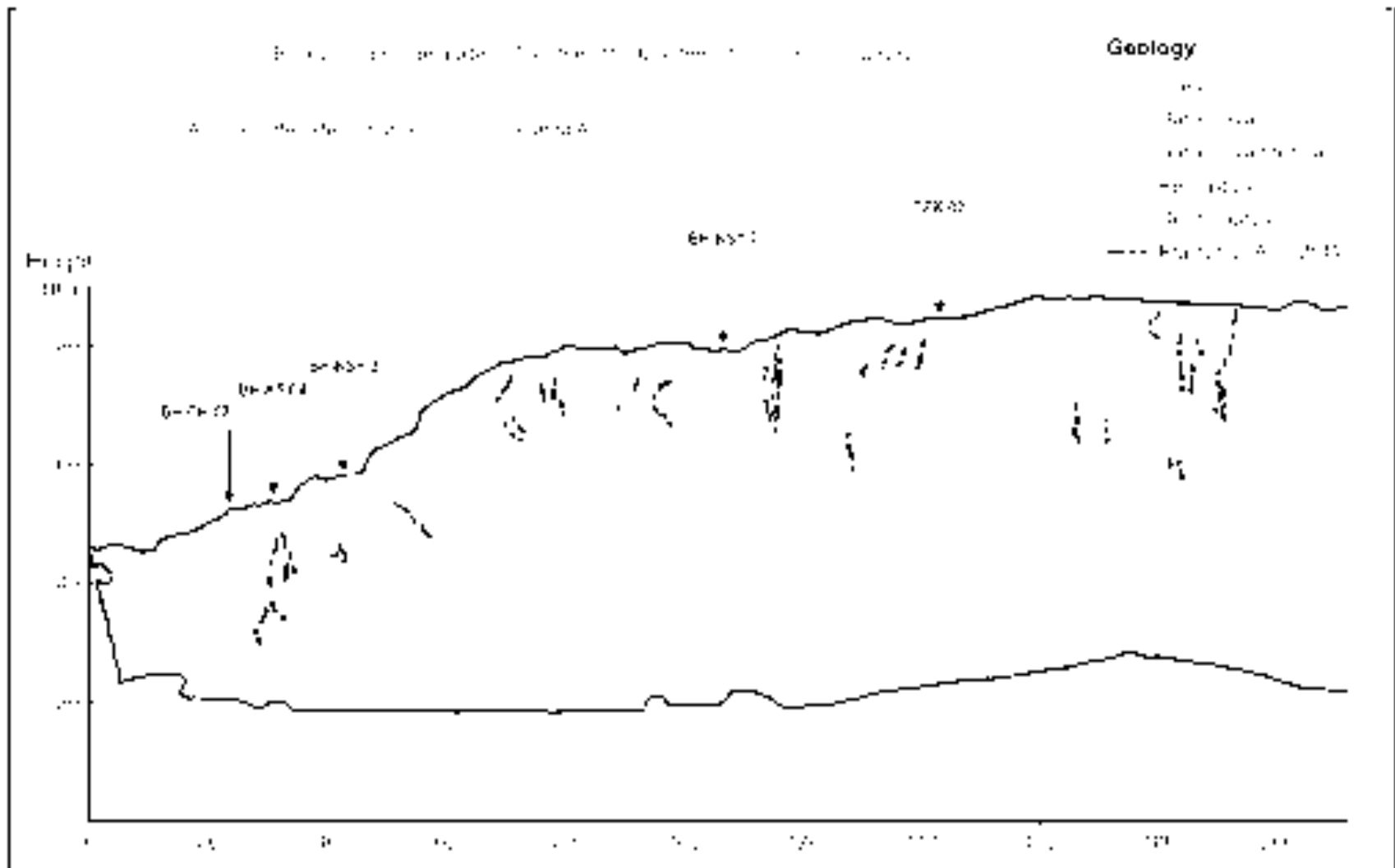


**Figure 12** Geological face log of the rock slope exposed along Shag Rock Reserve. Modified from Massey et al. (2012).

## Weathered basalt lava breccia

Drilling records and field mapping show that much of source area A is underlain by weathered basalt lava breccia. This material is described in drillhole cores (Pletz, 2013) as extremely weak to moderately strong. Rock quality designation values from drillhole BH-DH-02 range between 50 and 100%. The weathering classification system used by Pletz (2013) and Tonkin and Taylor (2012a) uses the New Zealand Geotechnical Society (2005) scheme, which is based on describing the “rock mass”, taking into account the material and defects, and relating this to loss of strength. However, this means that where the rock material is slightly weathered in cores but with defects that are discoloured, the rock mass weathering terms used range from slightly weathered to highly weathered. In such cases the material is slightly weathered, with very little if any loss of intact strength.

Adopting material weathering descriptions as per Eurocode 7 – BS 5930, New Zealand Geotechnical Society (1988) and GeoGuide 3, the basalt lava breccia immediately underlying the loess or mixed colluvium within source area A is typically completely to highly weathered, grading to slightly weathered with increasing depth. Where completely to highly weathered and immediately beneath the overlying loess/mixed colluvium, the matrix of the breccia, around the lava clasts, has weathered to form a clay. In drillhole cores from BH-CH-03, the clay is predominantly smectite and has formed as a product of weathering (A. Reyes personal communication, 2014), and it contains slickensides (evidence of movement), from a few millimetres to centimetres in length (Figure 13).



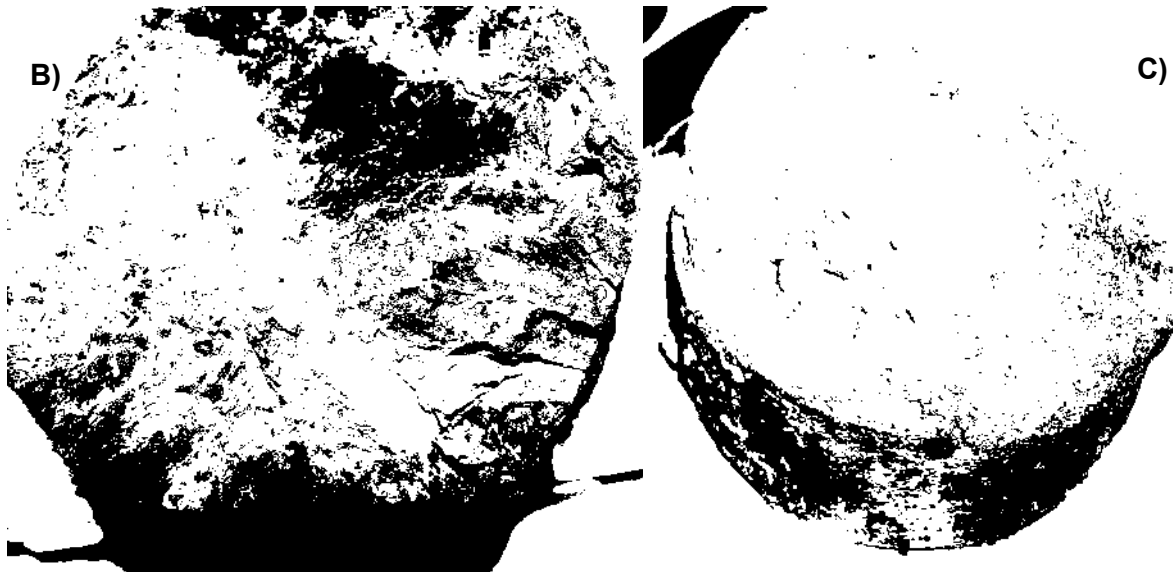


**Figure 13** Drillhole core of highly weathered basalt lava breccia from BH-CH-03. A) Core box from depth 13.8 m below ground level (top left) to 16.1 m below ground level (bottom right). B) and C) show the slickensided clay in the weathered breccia, the samples are taken from the drillhole core within the yellow dashed rectangle shown in photograph A).

The basalt lava exposed in Shag Rock Reserve (Figure 11), in the upper part of source area A, is not present in most of the drillholes. In the drillholes nearest the cliff edge, the lava layer is much thinner (less than two metres) than in the exposure in the cliff face. Highly weathered basalt lava breccia with joints, “broken zones” and voids containing clay has been logged in many of the drillholes, and outcrops, in a zone underlying the loess/mixed colluvium, in most of the upper part of source area A (Figure 8, cross-sections 1 and 2). This zone has been called weathered basalt lava breccia.

In source area B, drillhole logs and field exposures suggest most of this area is underlain by basalt lava and not breccia, and although basalt lava breccia is locally present (e.g., a “shattered zone” with up to 20 mm of clay infill was logged in basalt lava breccia about 0.5 m below rock head), it is not as thick or persistent as it is under source area A (Figure 8, cross-section 3).

### 3.3.1.5 Rock head surface

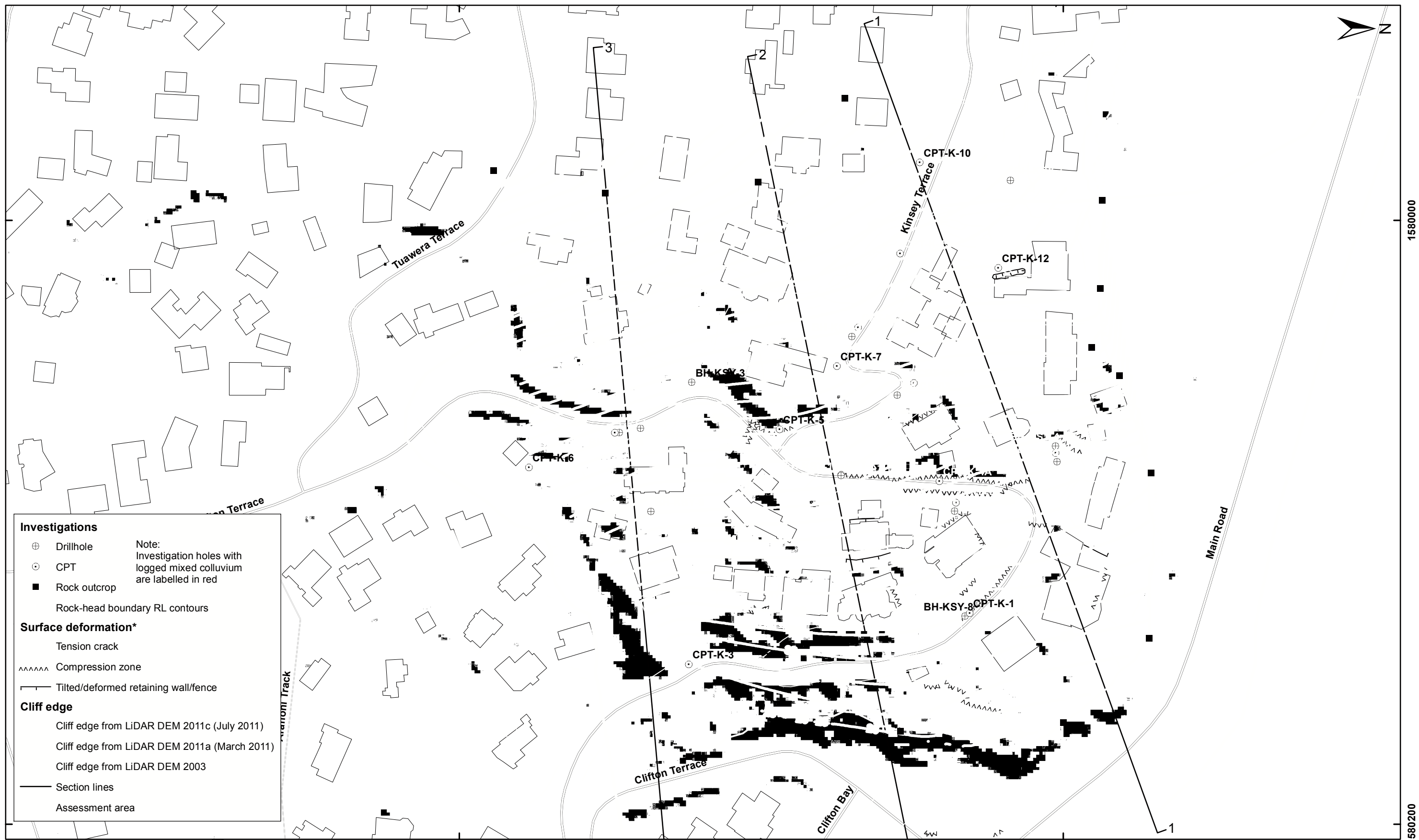
The surface boundary between the base of the mixed colluvium and loess and the underlying volcanic rock (rock head) was interpolated by GNS Science using: 1) drillhole intersections; 2) scala penetrometer test depths of refusal; and 3) field mapped rock outcrop exposures, as control points (Figure 14). In general, rock head shows an overall dip towards the east-northeast (bearing of 070–080°), which is approximately coincident with the ground-surface slope aspect. It should be noted that the overall strike of the main cracks and the strike of rock head are sub-parallel.

For cross-sections 1 and 2 (Figure 8) the dip angle of rock head ranges between 10° and 20°, and is steeper in the upper part of source area A (about 15–20°) than the lower part (about 10–15°). For cross-section 3 (Figure 8), the dip of rock head is uniform (20–25°) over much of source area B. Given that source area A had moved more than the steeper source area B this implies significant differences in the overall shear strength of their respective slide surfaces; refer to section 4 for details.

A vertical step in rock head of about 1.5–2 m was interpreted from geophysical refraction surveys across the head scarp of source area A, in the main area of cracks (Clarke, 2012). Clarke (2012) refers to this step as a “fault scarp”. On the upslope side of the step, outside the main cracked area, the loess is 1–2 m thick, and on the downslope side of the step, in the cracked area, the loess is 4 m or more thick (Figure 15). Tonkin and Taylor (2012a) excavated a test pit (TPK-1) to rock head (about 4 m below ground level) across a prominent tension crack, down slope and offset 20 m from the seismic line. The depth of rock head in the test pit is consistent with the inferred depth from the seismic line. However, no obvious step in rock head was identified in the base of the test pit, although rock head did vary in the base of the pit, from four to five below ground level, across a distance of five metres. The prominent tension crack, exposed in the wall of the test pit, terminated in the loess about one metre above rock head.

The seismic-line data also show a change in the P-wave velocity recorded in the rock downslope of the step in rock head, and within the cracked area. The P-wave velocity in this area was about 500–1,000 m/s, compared to >1,500 m/s for the rock upslope away from the step in rock head and area of cracking (Figure 15).





**Investigations**

- ⊕ Drillhole
- ⊙ CPT
- Rock outcrop

Note:  
Investigation holes with logged mixed colluvium are labelled in red

Rock-head boundary RL contours

**Surface deformation\***

- Tension crack
- ~~~~~ Compression zone
- Tilted/deformed retaining wall/fence

**Cliff edge**

- Cliff edge from LiDAR DEM 2011c (July 2011)
- Cliff edge from LiDAR DEM 2011a (March 2011)
- Cliff edge from LiDAR DEM 2003

— Section lines

— Assessment area



EXPLANATION:

\* Taken from the report 2012/317

Background shade model derived from NZAM post earthquake 2011c (July 2011) LiDAR survey resampled to a 1 m ground resolution.

Roads and building footprints provided by Christchurch City Council (20/02/2012).

PROJECTION: New Zealand Transverse Mercator 2000

DRW:  
BL

CHK:  
FDP, CM



**INTERPOLATED ROCK- HEAD BOUNDARY**

**Clifton Terrace  
Christchurch**

**FIGURE 14**

**FINAL**

REPORT: CR2014/76      DATE: August 2014



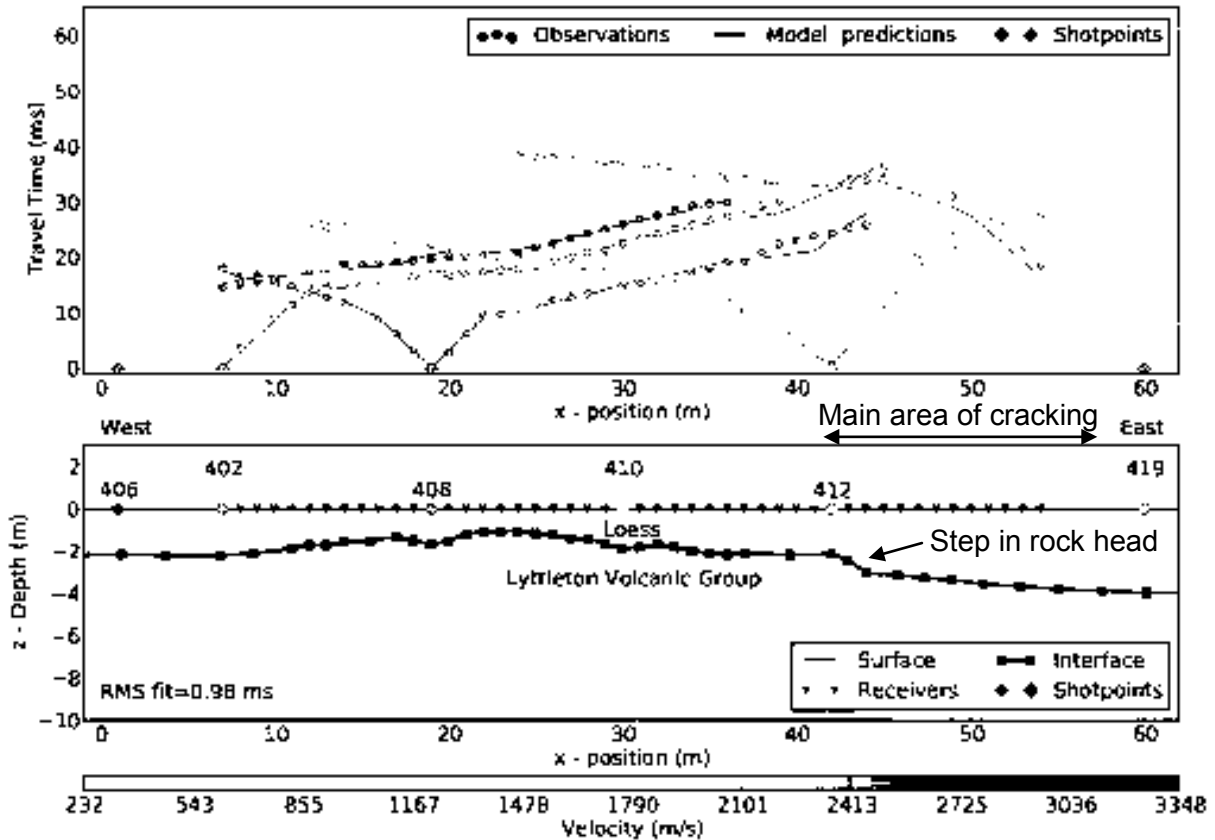


**Figure 15** Results from the refraction seismic collected across the head scarp of assessed source area A (Clarke, 2012). The location of the survey line is shown in Figure 6. The data shown are taken from Clarke (2012) and are Inversion models adopting the root mean squared fit. Note: from x-position 0 to 7 m and from 55 to 60 m there is no data.

### 3.3.2 Geotechnical properties

Material strength parameters were assigned based on the results of in-house (GNS Science) laboratory tests and the published results of testing of samples from the site (Tonkin and Taylor, 2012a) and of similar materials from elsewhere in the Port Hills.

#### 3.3.2.1 Loess

Material parameters for the loess in the assessment area are based on: 1) descriptions of the drillcore materials; 2) Port Hills soil strength test results reported by Carey et al. (2014) and other published data including results from undrained triaxial tests of loess from the site reported in Tonkin and Taylor (2012a); and 3) numerical slope stability back-analysis.

#### *In situ* water contents

A measure of the *in situ* water content (*in situ* meaning the water content of the sample as it was at the time of sampling, and before any testing was carried out) of loess in the slope was derived from *in situ* “block” samples collected from Maffey’s Road, Lucas Lane and Vernon Terrace.

The *in situ* water content of the loess block samples varied mostly between 6 and 10%, with two samples in the 3–5% range (Carey et al., 2014). The samples used for testing were taken from free-draining slopes exposed to the weather, and were sampled between January and February 2013, and January and February 2014, near the end of summer. The *in situ*

water contents are therefore thought to represent the lower end of the seasonal range (Figure 16). The samples were taken from an east-facing loess slope. Even if the samples had been collected in winter, the water contents of the loess at this accessible site would still not be representative of the water content of the loess deeper in the slope, as the outside face of the slope is free draining.

The water contents of the loess in drillhole samples were all substantially higher than those for the block samples. However, drilling uses water to flush the drill bit, and block sampling does not use water (Table 7).

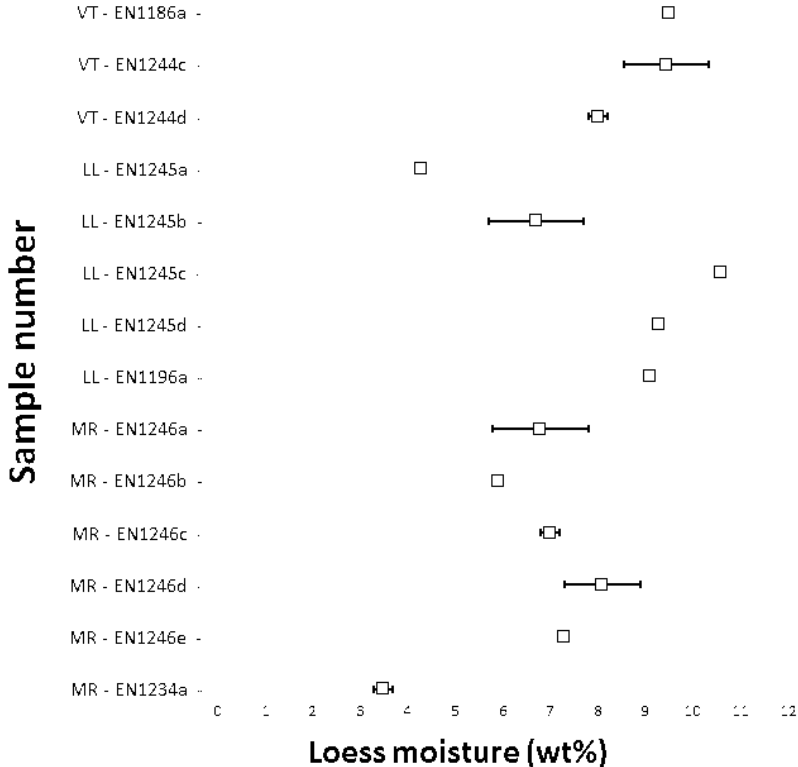


**Figure 16** In-ground moisture (water, wt%) content of collected loess samples.

**In-house shear strength tests**

The shear strength of the loess was tested in-house at GNS Science using two types of ring shear equipment and one type of direct shear equipment (Carey et al., 2014). The results are summarised in Table 11 and 12 and plotted in Figure 17. The results show a wide variability in the tested friction and cohesion values. Where shear box tests indicated peak and residual strength characteristics, both the peak and residual friction and cohesion values have been plotted with “tie” lines joining the data points together.

With the exception of sample EN1243, all tests were carried out in saturated (water-added) conditions (at final post-test water contents of between 16 and 19%). As a consequence, these water contents are higher than those from the tested *in situ* samples. The water contents from the *in situ* samples are thought to better represent the bulk moisture content of the loess in the actual slope.

A shear box test on loess sample EN1243 was carried out without water added (i.e., non-standard testing procedure) at ~3.7% water content, to explore the effect of moisture content on shear strength. The test yielded residual value shear strength values of cohesion ( $c$ ) = 42 kPa and friction ( $\phi$ ) = 48°. This contrasts with the ring shear tests results undertaken for saturated loess, which yield residual shear strengths of  $c$  = 0–6 kPa and  $\phi$  = 27–37°.

Consolidated undrained triaxial test results from a sample of loess taken from drillhole BH-KSY-9a yield peak effective shear strengths of  $c$  = 1–6 kPa and  $\phi$  = 34° (Tonkin and Taylor, 2012a). Ring shear test results from another sample of loess taken from drillhole BH-KSY-9a yield residual shear strengths of  $c$  = 0–10 kPa and  $\phi$  = 31–32° (Tonkin and Taylor, 2012a). These tests were carried out on samples of loess with water contents of between 15 and 20%, which are very close to the liquid limit of the loess. Given the high water contents of the tested materials, these shear strength results, and those in Table 11, are considered to be more representative of the bulk residual strength parameters for the loess slope rather than peak strength parameters.

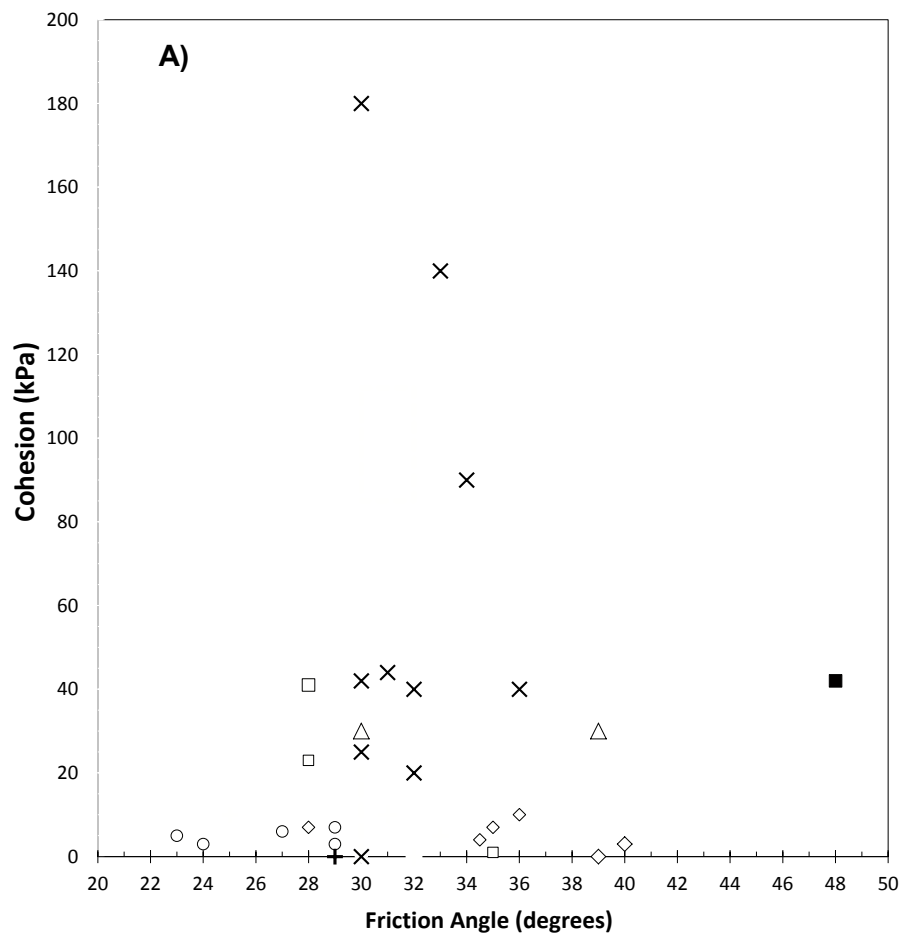
### **Effect of moisture content on loess shear strength**

Comparison can be made with shear strength results from other published Port Hills investigations (Table 12) by plotting them together with the results of the GNS Science tests (Figure 17).

The sensitivities of friction angle ( $\phi$ ) and cohesion ( $c$ ) to change in moisture content have been assessed using both GNS Science testing results (Carey et al., 2014) and results from tests by McDowell (1989), Tehrani (1988) and Tonkin and Taylor (2012a). The results show that, over the interval from 10 to 20 wt% moisture the loess friction angle is less sensitive than the cohesion to changes in water content.

For water contents less than 20 wt% the cohesion of the tested loess is very sensitive to changes in water content. These results illustrate a large variability in the strength parameters of the loess in the Port Hills, and show that the loess strength is critically dependent on water content. These results are consistent with the findings of others (e.g., McDowell, 1989; Goldwater, 1990).

During periods of prolonged wet weather it is feasible for water contents in the loess to increase leading to a reduction in the cohesion and increased susceptibility to failure. The data plotted in Figure 17 probably represent the range of strength parameters at the likely range of moisture contents that could be anticipated in the Port Hills loess.



- Carey et al. (2014) DIRECT SHEAR RESIDUAL ~3wt% water content, No water added during testing
- Carey et al. (2014) DIRECT SHEAR RESIDUAL 16 wt% water content
- Carey et al. (2014) DIRECT SHEAR PEAK 16wt% water content
- Carey et al. (2014) RING SHEAR RESIDUAL 16 to 19 wt% water content
- Goldwater 1990 RESIDUAL water content unknown
- Yetton (1986) DIRECT SHEAR PEAK water content unknown
- △ Tehrani (1988) DIRECT SHEAR PEAK 7wt% water content
- △ Tehrani (1988) DIRECT SHEAR PEAK dry water content
- × MCDowell (1989) TRIAXIAL PEAK 8 - 19 wt% water content
- Tonkin and Taylor & Geotechnics TRIAXIAL PEAK 18 wt% water content
- Tonkin and Taylor & Geotechnics RING SHEAR RESIDUAL 15-20 wt% water content
- Tonkin and Taylor & Geotechnics TRIAXIAL PEAK 21 wt% water content
- + Tonkin and Taylor & Geotechnics RING SHEAR RESIDUAL 19-21 wt% water content
- Tonkin and Taylor & Geotechnics RING SHEAR RESIDUAL 18-21 wt% water content
- ◇ Jowett (1995) DIRECT SHEAR PEAK 10.1-11.5 wt% water content
- ◇ Jowett (1995) DIRECT SHEAR PEAK 12.8-21.5 wt% water content

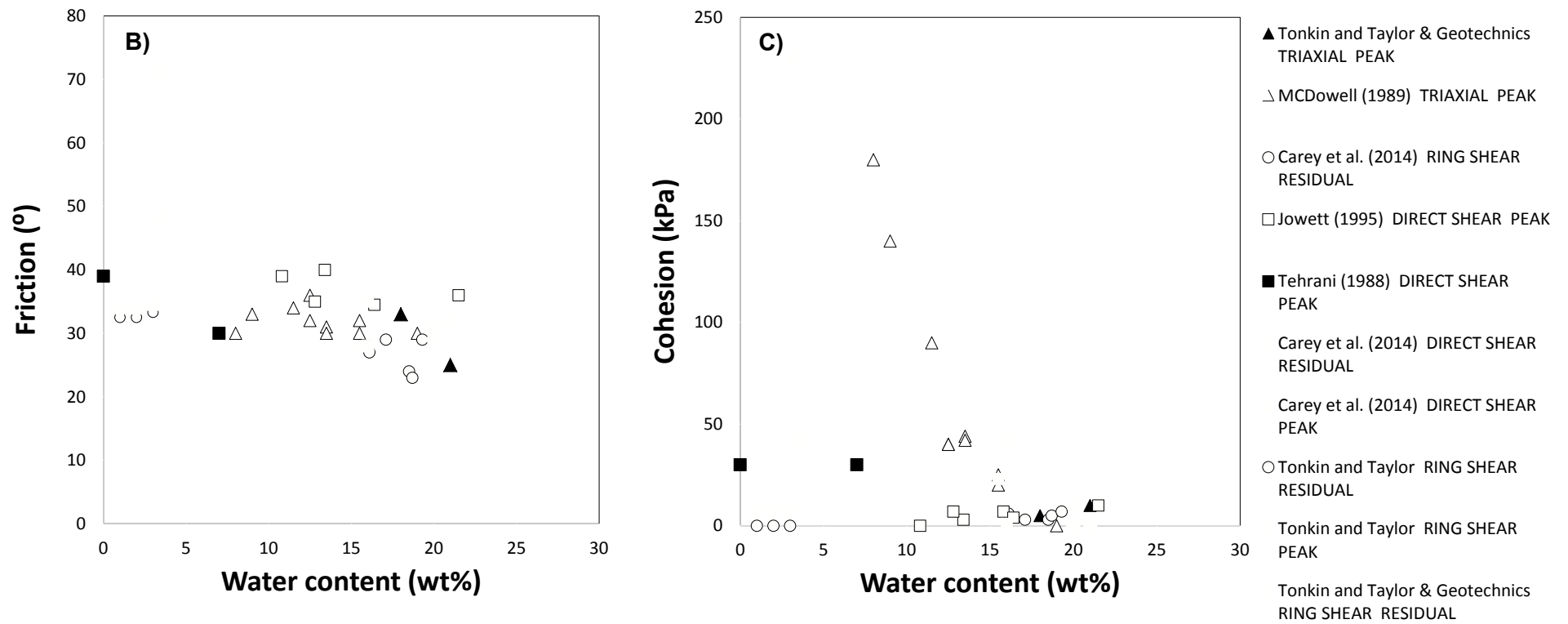


**Figure 17** Loess residual shear strength results (from Table 11 and Table 12). A) Cohesion and friction laboratory results plotted for loess. B) Loess residual cohesion plotted against water content. C) Loess residual friction plotted against water content. The Tonkin and Taylor Ltd. and Geotechnics Ltd. triaxial results are from samples of loess taken from drillhole BH-KSY-9a.

**Table 11** Shear-strength test results (from Carey et al., 2014).

Site	Sample	Sample <i>in situ</i> water content	Test type <sup>1</sup>	Sampling method	Test starting water content <sup>2</sup> (%)	Test final water content (%)	Dry density	Peak cohesion c (kPa)	Peak friction $\phi$	Residual cohesion C (kPa)	Residual friction $\phi$	Lab test number
Lucas Lane <sup>3</sup>	EN1186	n/a	Ring Shear-C	Drillcore	19.8	18.7				3	24	EN1186b
			Ring Shear-C	Drillcore	19.8	18.7				5	23	EN1186d
			Shear Box	Drillcore	13.7	15.5	1.41	41	28	23	28	EN1186a
					13.7	13.7	1.45					EN1186c
Maffey's Road	EN1195	n/a	Ring Shear-C	Block sample	Not reported	16.1				6	27	EN1195b
			Ring Shear-G	Block sample	Not reported	17.9				0	37	EN1195c
Richmond Hill	EN1196	n/a	Ring Shear-C	Drillcore	18.1	17.1				3	29	EN1196b
			Ring Shear-C	Drillcore	17.18	19.3				7	29	EN1196f
			Ring Shear-G	Drillcore	18.1	18.6				6	31	EN1196c
			Ring Shear-G	Drillcore	17.1	16.6				15	35	EN1196e
			Shear Box	Drillcore	16.1	16	134	1	35	1	35	EN1196a
				16.1	13.9	1.32					EN1196d	
Deans Head	EN1230	n/a	Ring Shear-G	Drillcore	17.1	17.9				20	35	EN1230b
Maffey's Road <sup>4</sup>	EN1243	n/a	Shear Box	Block sample		3.3	1.37	230	71	42	48	EN1243a
						3.7	1.36					EN1243b

<sup>1</sup> Two sets of ring shear apparatus were used "C" is Canterbury University, and "G" is GNS Science ring-shear equipment.

<sup>2</sup> This is unrelated to the original sample water content as it has had water added as part of the lab test procedure.

<sup>3</sup> This sample contained a higher clay content than other tested loess samples.

<sup>4</sup> This test was carried out under dry conditions with no added water, and therefore follows a non-standard testing procedure.

**Table 12** Other published shear tests on loess in the Port Hills.

Area	Water content (%wt)	Cohesion c (kPa)	Friction $\phi$ (°)	Data source	Equipment used
Clifton Terrace (effective peak)	18–21	1–6	34	Tonkin and Taylor (2012a) for EQC	Undrained triaxial
Clifton Terrace (residual)	15–20	0–10	31–32		Ring shear
Vernon Terrace	19–21	0	29	Tonkin and Taylor (2012c) for EQC	Ring shear
Maffeys Road (peak)	No data	8	34	Tonkin and Taylor (2012d) for EQC	Ring shear
Maffeys Road (residual)	No data	0	33		
Defender Lane (peak)	No data	8	34	Tonkin and Taylor (2012b) for EQC	Ring shear
Defender Lane (residual)	No data	0	33		
Glendeverre Terrace (peak)	No data	8	34	Tonkin and Taylor (2012e) for EQC	Ring shear
Glendeverre Terrace (residual)	No data	0	33		
Port Hills	No data	85–112	30–35	Yetton (1992)	Direct shear
Not known	No data	30	30–39	Tehrani (1988)	Direct shear
Port Hills	8–19	0–80	29–34	McDowell (1989)	Triaxial
Port Hills	No data	0–20	30	Goldwater (1990)	Not known

### Back-analysis of loess strength

Figure 18 and Figure 19a show the results from numerical slope stability back-analysis for failure surfaces confined to the loess, for cross-section 2 (Figure 8), representing assessed source area A, overlain with the results from the laboratory testing of loess (Figure 17). The failure surfaces adopt the path-search surface function in the RocScience program Slide and no water is included in the model. The purpose of this plot is to show the range in the back analysed slope factor of safety with regards to the range of the laboratory test results, for loess.

A lower estimate of the shear strength of the loess, needed to derive a static factor of safety for the slope of one, was a friction ( $\phi$ ) of 20° and cohesion (c) of 0 kPa, or any other combination of friction and cohesion on the factor of safety = one line. Such values are much lower than the range of shear strengths derived from laboratory testing of the loess, and they are even lower than those test results on samples where water contents were close to the liquid limit of the loess. The slope isn't moving, therefore the factor of safety is greater than 1.0 and the material strength parameters have to be greater than the black dots in Figure 19a.

Typical lower estimates of the bulk shear strength parameters of loess in the Port Hills adopted by local geotechnical consultants are friction ( $\phi$ ) = 30° and cohesion (c) = 10 kPa (Port Hills Geotechnical Group personal communication, 2013). These data are shown as black circles on Figure 19a. The results show that for the typical range of loess parameters adopted by engineering consultants in Christchurch, the factors of safety of slide surfaces in the loess are typically greater than 1.9, under dry conditions.

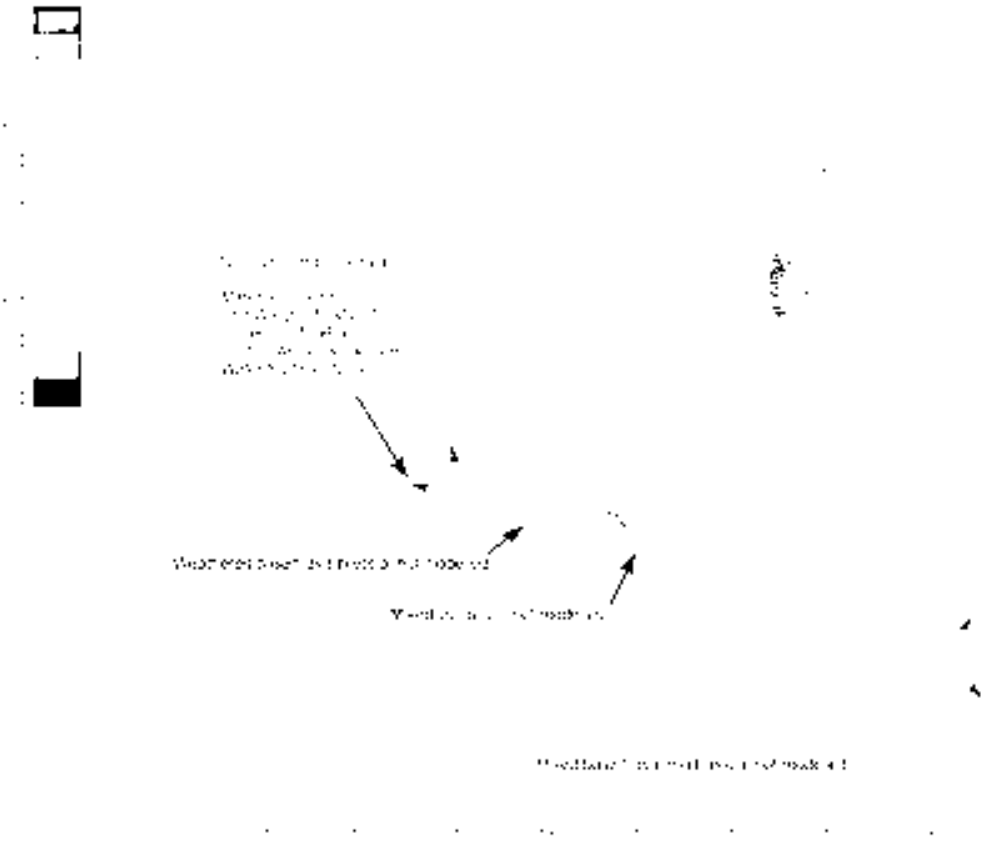
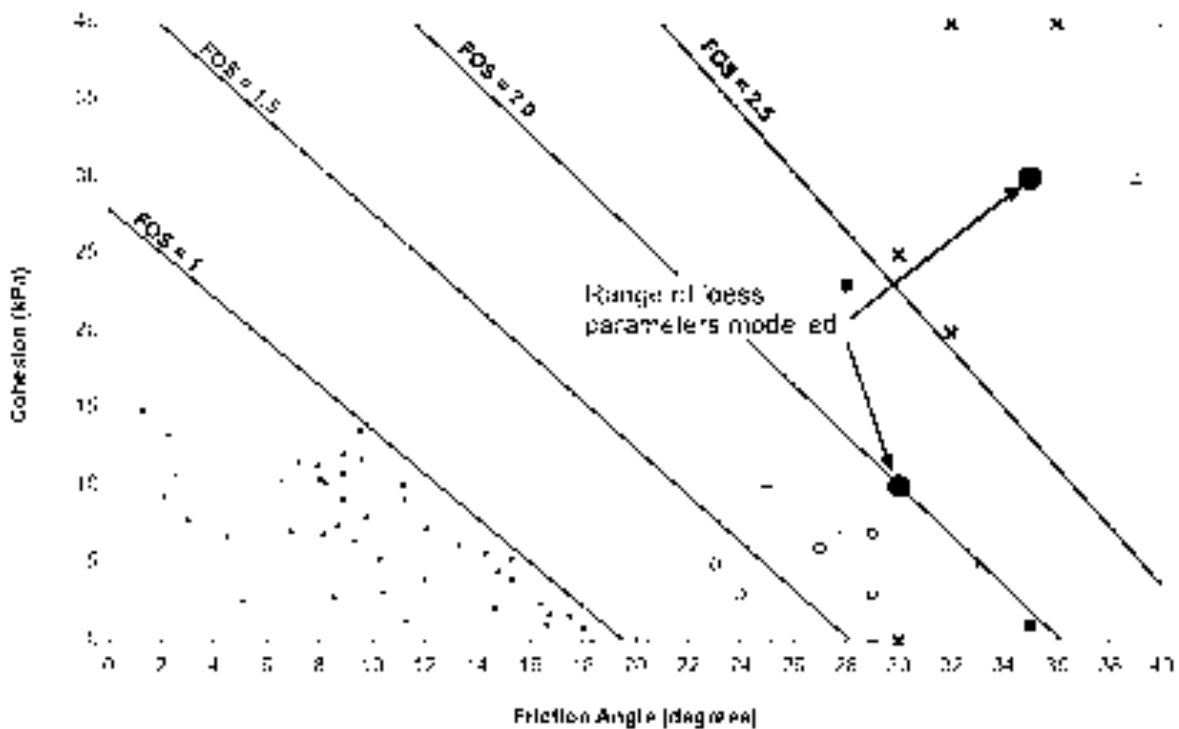


**Figure 18** Numerical slope stability back-analysis of the loess material for cross-section 2, representing source area A. Note: each modelled slide surface adopts the “path search” function.



- Factor of safety (FOS) = 1.0
- Factor of safety (FOS) = 1.5
- Factor of safety (FOS) = 2.0
- Factor of safety (FOS) = 2.5
- Factor of safety (FOS) = 3.0
- Carey et al. (2014): DIRECT SHEAR RESIDUAL (6-16 wt% water content)
- Carey et al. (2014): RING SHEAR RESIDUAL (6-16 wt% water content)
- Golder (1990): RESIDUAL (water content unknown)
- Ibrahim (1998): DIRECT SHEAR PEAK (7 wt% water content)
- Ibrahim (1998): DIRECT SHEAR PEAK (6 wt% water content)
- × Mitchell (1988): TRIAXIAL PEAK (6-16 wt% water content)
- Tokim and Lular & Gede (1984): RING SHEAR RESIDUAL (11-20 wt% water content)
- + Tokim and Taylor & Gede (1984): TRIAXIAL PEAK (21 wt% water content)
- + Tokim and Taylor & Gede (1984): RING SHEAR RESIDUAL (19-21 wt% water content)
- Jewell (1975): DIRECT SHEAR PEAK (10-11 wt% water content)
- Jewell (1975): DIRECT SHEAR PEAK (12.6-21 wt% water content)

**Figure 19a** Numerical slope stability back-analysis of the loess material for cross-section 2, representing source area A. Note: each datapoint represents a modelled slide surface, adopting the geometries shown in Figure 18, at a given combination of cohesion and friction adopted for the loess. Those slide surfaces (adopting the path-search function), shown as black dots, represent those combinations of cohesion and friction that would yield a static factor of safety of less than one. The results from the laboratory testing (Figure 17) are also shown for comparison purposes.

### 3.3.2.2 Mixed colluvium

Material parameters adopted for the mixed colluvium layer underlying the loess material in the assessment area are based on: 1) descriptions of the drillcore materials; and 2) Port Hills soil strength test results reported by Carey et al. (2014) and others.

The mixed colluvium contains varying proportions of reworked loess, and so the results from the laboratory testing of the loess (Figure 17) are likely to be representative of most of the mixed colluvium. However, it was noted from drillhole core samples and field exposures, that the mixed colluvium often contained higher clay content than the loess. This is confirmed by the index tests carried out on the colluvium material by Tonkin and Taylor (2012a) (Table 13).

**Table 13** Index-testing results (mean values) on loess and mixed colluvium (from Tonkin and Taylor, 2012a).

Material	Number of tests	Liquid limit	Plastic limit	Plasticity index	Bulk density (g/cm <sup>3</sup> )	Water content (wt%)
Loess	72	22.3	17.7	5.5	2.0	17.4
Mixed colluvium	4	49.8	20.5	29.3	2.0	19.3

The results from ring-shear testing of the matrix material from a drillcore sample of highly weathered basalt breccia, taken from drillhole BH-CH-03, could be representative of the strength parameters of the more clay-dominated mixed colluvium, as it is thought to derive from the same material. The results reported by Carey et al. (2014) indicate a residual friction angle ( $\phi$ ) of 21° ( $\pm 1^\circ$ ) and cohesion (c) of 15 ( $\pm 2$ ) kPa (errors at one standard deviation). These are consistent with the results of Stark et al. (2005) where the mixed colluvium with 25%  $\leq$  clay content  $\leq$  45%, and liquid limit of about 50 would have a residual friction angle of between 17 and 24°.

### Back-analysis of mixed colluvium strength

Figure 19b show the results from numerical slope stability back-analysis for failure surfaces confined to the mixed colluvium, for cross-section 2 (Figure 8), representing assessed source area A, overlain with the results from the laboratory testing of loess (Figure 17). The failure surfaces adopt the path-search surface function in the RocScience program Slide, and the model assumes the mixed colluvium is continuous, below the loess and above rock head, over the entire length of the slope within source area A.

The results show that by including a weak layer of mixed colluvium in the model the factors of safety of the modelled slide surfaces reduce. A lower estimate of the shear strength of the mixed colluvium, needed to derive a static factor of safety for the slope of one, was a friction ( $\phi$ ) of 15° and cohesion (c) of 0 kPa, or any other combination of friction and cohesion on the factor of safety = one line. Such values are significantly lower than the range of shear strengths derived from laboratory testing of the loess. The slope isn't moving, therefore the factor of safety is greater than 1.0 and the material strength parameters have to be greater than the black dots in Figure 19b.

The results from ring-shear testing of the matrix material from the drillcore sample of clay from the highly weathered basalt breccia (friction ( $\phi$ ) of 21° and cohesion (c) of 15 kPa) are shown on the Figure 19b, and correspond to factors of safety of about 1.5–1.7. Although this material is clay dominated, the lower ranges of results from ring-shear testing of the loess (silt dominated) also yield similar factors of safety.

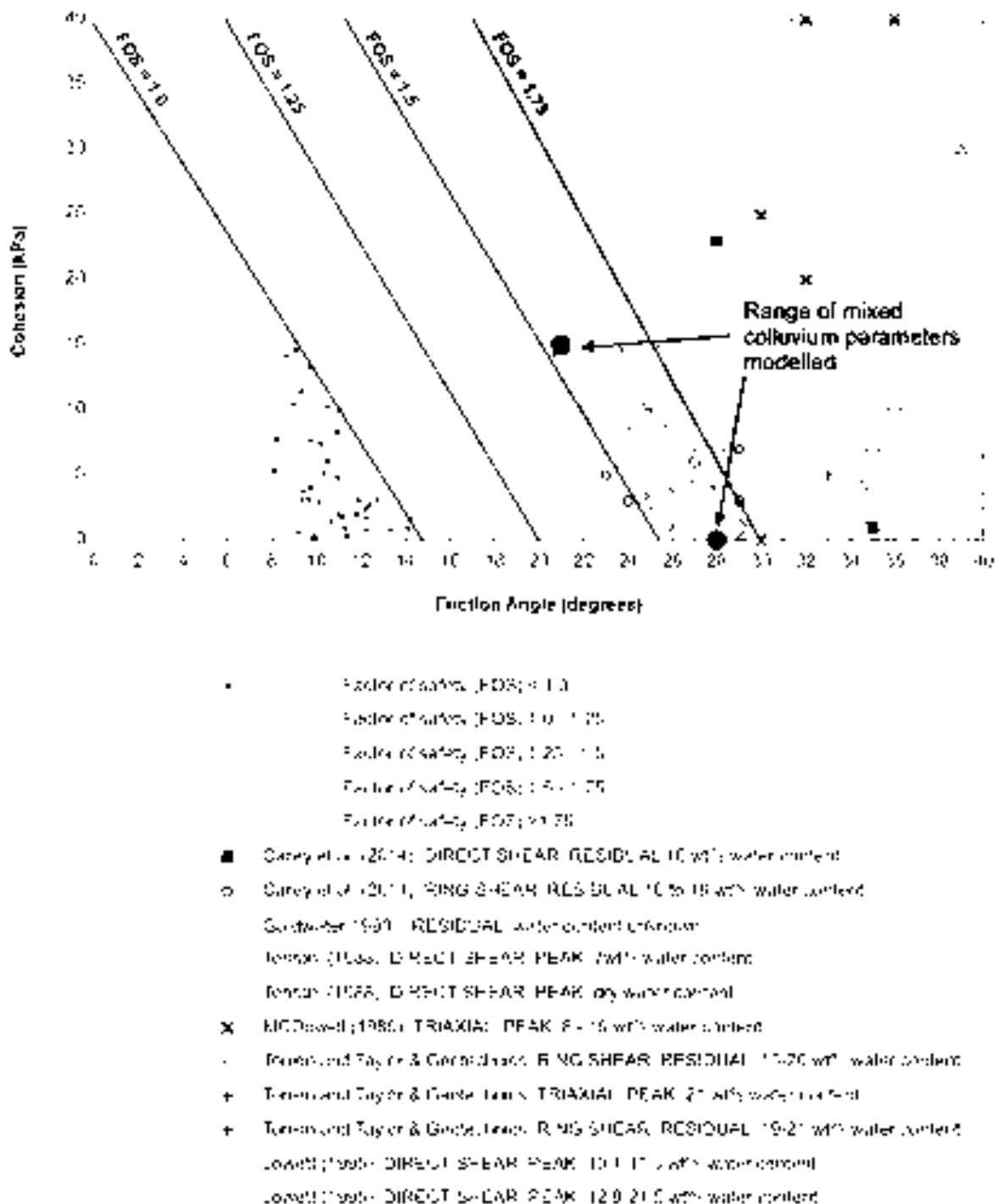


**Figure 19b** Numerical slope stability back-analysis of the mixed colluvium for cross-section 2, representing source area A. Note: each datapoint represents a modelled slide surface, adopting geometries similar to those shown in Figure 18, at a given combination of cohesion and friction adopted for the mixed colluvium. Those slide surfaces (adopting the path-search function), shown as black dots, represent those combinations of cohesion and friction that would yield a static factor of safety of less than one. The results from the laboratory testing (Figure 17) are also shown for comparison purposes.

### 3.3.2.3 Adopted loess and mixed colluvium parameters for numerical models

For the purpose of stability assessment, material strength parameters were selected as shown in Table 14.

**Table 14** Range of bulk geotechnical material parameters adopted for Clifton Terrace soils.

Soil Unit	Unit weight (kN/m <sup>3</sup> )	Intact Young's modulus E <sub>i</sub> (MPa) <sup>1</sup>	Poisson's ratio <sup>1</sup>	Cohesion c (KPa)	Friction φ (°)	Tensile strength (KPa)	Shear wave velocity (m/sec)	Shear modulus <sup>2</sup> G <sub>s</sub> (MPa)
Loess	17	30	0.3	10–30	35	10	200–400	68–272
Mixed Colluvium	17	30	0.3	0–15	21–30	0	200–400	68–272

<sup>1</sup> Derived from published test results.

<sup>2</sup> Shear Modulus G<sub>s</sub> (MPa) derived from dynamic testing of loess and colluvium down-hole shear wave velocity survey of drillholes BH-CH-02 and BH-CH-03.  $G_s = \rho \cdot V_s^2$ . Where  $\rho$  = density (Kg/m<sup>3</sup>) and  $V_s$  = shear wave velocity (m/s).

### 3.3.2.4 Loess and mixed colluvium shear modulus

The *in situ* shear modulus values for the loess and mixed colluvium were derived from:

1. Results from the downhole shear-wave velocity surveys carried out by Southern Geophysical Ltd. (Southern Geophysical Ltd., 2013) based on the survey results from drillholes BH-CH-02 and BH-CH-03; and
2. Results from the seismic cone penetrometer tests carried out by Tonkin and Taylor Ltd. for the Earthquake Commission at Clifton Terrace (Tonkin and Taylor, 2012a) (Table 15)

The results from the dynamic probing are summarised in Figure 20. The mean shear wave velocity is 306 m/s (±93 m/s at one standard deviation) and the mode is 222 m/s. Based on these results reported by Tonkin and Taylor (2012a), there is no measurable difference between the shear wave velocities of the loess and the colluvium, mean velocity of 297 (±121) m/s (errors at one standard deviation), and the data are plotted together in Figure 20.

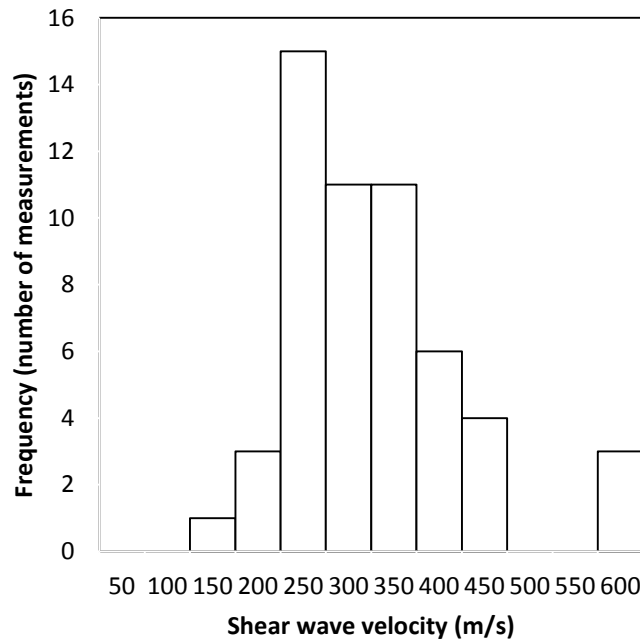


**Figure 20** Loess and colluvium shear wave velocity results from dynamic probing reported by Tonkin and Taylor (2012a) for the loess at Clifton Terrace.

These values are also consistent with shear wave velocity trends defined by Rinaldi et al. (2001) for Argentinean loess as a function of normal stress and moisture content (Table 15) where in the 2–14 m depth range (corresponding to 30–240 kPa range of overburden pressure) the range of loess shear wave velocity was 280–300 m/s, at a water content of ~16 wt%, and 300–320 m/s for a water content of 6.4 wt%.

Applying the relationship for shear wave velocity:

$G = \rho \cdot V_s^2$  Equation 1 Where  $\rho$  is the density of the loess 1,700 kg/m<sup>3</sup> and  $V_s$  is the shear wave velocity from the dynamic probing.

**Table 15** Shear wave velocity profiles from Port Hills and other loess.

Material	Shear wave velocity $V_s$ (m/s)	Data source
Port Hill loess (drillholes BH-CH-02 and BH-CH-03)	295–390	Southern Geophysical Ltd. (2013)
Port Hills loess from Clifton Terrace dynamic probing	126–582	Tonkin and Taylor (2012a)
Loess moisture content ~16 wt%	280–300	Rinaldi et al. (2001)
Loess moisture content 6.4 wt%	300–320	Rinaldi et al. (2001)

### 3.3.2.5 Adopted volcanic bedrock parameters for numerical models

In order to derive rock-mass strength parameters for the volcanic breccia, lava and epiclastic material that take into account the nature of the discontinuities as well as the intact strength of the breccia, lava and epiclastics, the geological strength index (Hoek, 1999) was adopted and the rock mass strength calculated with the Rocscience RocLab software.

The geological strength index values adopted for the breccia are shown in Table 16. Strength tests of Clifton Terrace rock samples from drillholes BH-CH-02 and BH-CH-03 are shown in Table 16, and are taken from Carey et al. (2014). Mohr-Coulomb parameters (cohesion and

friction) were derived from Rocscience RocLab software by line fitting over the appropriate stress range of the slope. Note that epiclastic materials were not tested, but there is little difference between these materials and the breccia, based on the results from laboratory testing of similar materials from elsewhere in the Port Hills (Carey et al., 2014).

For the assessment two main bedrock units were recognised: 1) weathered breccia immediately underlying the loess and mixed colluvium in source area A; and 2) mixed basalt lava breccia, lava and epiclastic layer underlying the weathered basalt breccia in source area A, and underlying the loess and mixed colluvium in source area B.

**Table 16** Range of adopted rock strength parameters.

Laboratory results								Rock mass properties							
Unit		Lab UCS (MPa)	Bulk unit weight (kN/m <sup>3</sup> )	Brazilian Tensile (MPa)	Intact modulus E <sub>i</sub> (MPa)	Poisson's ratio	m <sub>i</sub> <sup>2</sup>	Slope height (m)	GSI	Cohesion <sup>3</sup> c (KPa)	Friction <sup>3</sup> φ (°)	Tensile strength (KPa)	Rock mass modulus E <sub>M</sub> (MPa)	QR4 Shear wave velocity (m/sec)	Shear modulus G <sub>s</sub> <sup>4</sup> (MPa)
Weathered basalt lava breccia (clay matrix) <sup>5</sup>		-	18	-	-	-	-	N/A	N/A	15	21	15	250	570	520
Basalt lava breccia	MIN <sup>1</sup>	1.3	16	0.3	820	0.01	4	20–40	50	50	25	7	251	570	520
	AVG	2.6	18	0.4	1478	0.05	8		65	100	42	23	930	890	1,430
	MAX	3.7	19	0.4	1900	0.11	11		80	220	51	74	1,670	1,200	2,740
Basalt lava	MIN <sup>1</sup>	146	28	9.7	5,470	0.29	13.5	0–20	50	930	67	250	16,800	570	520
	MAX	243	27	16.7	3,880	0.22	21		70	4,500	67	1200	28,600	1,200	2,740

<sup>1</sup> MIN, AVG and MAX represent the range (minimum, average, maximum) of test results and field measurements.

<sup>2</sup> The m<sub>i</sub> values shown, represent the range in the ratio of unconfined compressive strength to tensile strength, derived from tested samples of basalt lavas and basalt lava breccias (Carey et al., 2014), and not the ratio of unconfined compressive strength to tensile values shown in the table.

<sup>3</sup> Mohr-coulomb parameters (cohesion and friction) were derived from RocLab by curve fitting over the appropriate stress range of the slope.

<sup>4</sup> Shear Modulus (G<sub>s</sub>) is derived from down-hole shear wave velocity survey of drillholes BH-CH-02 and BH-CH-03, where G<sub>s</sub>= ρ\*V<sub>s</sub><sup>2</sup> and ρ=density (Kg/m<sup>3</sup>) and V<sub>s</sub> = shear wave velocity (m/s).

<sup>5</sup> Results derived from ring shear testing carried out by GNS Science.

### 3.3.2.6 Volcanic bedrock shear Modulus

The shear moduli for the volcanic lava, breccia and epiclastics were derived from the downhole geophysical surveys carried out by Southern Geophysical Ltd. (Southern Geophysical Ltd., 2013) in drillholes BH-CH-02 and BH-CH-03. These data are shown on cross-sections in Figure 8 and summarised for BH-CH-03 in Table 17.

**Table 17** Shear wave velocity (SWV) and Rock Quality Designation (RQD) per lithology type for drillhole BH-CH-03.

Material type	RQD (%)/ SWV (m/s)	Minimum	Maximum	Mean	Standard deviation	Number of measurements
Epiclastic	RQD	0	100	61	36	10
	SWV	670	949	773	102	4
Basalt lava	RQD	33	100	77	19	15
	SWV	465	1379	817	277	7
Basalt lava breccia	RQD	0	100	71	27	25
	SWV	460	1390	891	324	12

### 3.3.3 Rainfall and groundwater response

In general, there are two main effects that groundwater has on the stability of slopes that need to be considered: 1) rising groundwater within the slope leading to an increase in pore pressures and a reduction in the effective stress of the materials; and 2) infiltration from prolonged rainfall, leading to the deepening of the wetted layer accompanied by a decrease in matric suction (e.g., Kim et al., 2004) and loss of cohesion. Owing to the lack of monitoring data, it is not known which mechanism would be the main contributor to rainfall-induced slope failures in the Port Hills. Loss of cohesion during long duration rainfall is a known cause of instability in fine grained, non-cohesive soils and therefore is likely to be a significant contributory factor to landslides in loess and loess-derived materials.

#### 3.3.3.1 Rainfall and landslides

The relationship between rainfall and landslides in the Port Hills has been summarised by McSaveney et al. (2014). Heavy rain and long-duration rainfall have been recognised as potential landslide triggers on the Port Hills for many years. Loess earth/debris flows were noted frequently, even before the era of wider urban development in the Port Hills. A long historical landslide record has been gathered by searching “Paperspast” (<http://paperspast.natlib.govt.nz>). This electronically searchable record of daily and weekly newspapers in New Zealand was searched over the period 1860–1926, but its landslide information is very incomplete, being only what newspapers of those times considered to be “newsworthy”. A summary of past landslides in the Port Hills and Banks Peninsula is contained in Appendix 4.

McSaveney et al. (2014) examined a list of Earthquake Commission claims for landslide damage for the period 1997–2010 and a Geotech Consulting Ltd. landslide investigations list, which covers the period 1992–2009. Any duplicate records for the period 1997–2009 contained in the data sets were removed. These records, though incomplete with

respect to all of the landslides that occurred over those intervals, may be approximately complete with respect to the episodes of rain associated with landslide occurrences that damaged homes and urban properties (Figure 21).

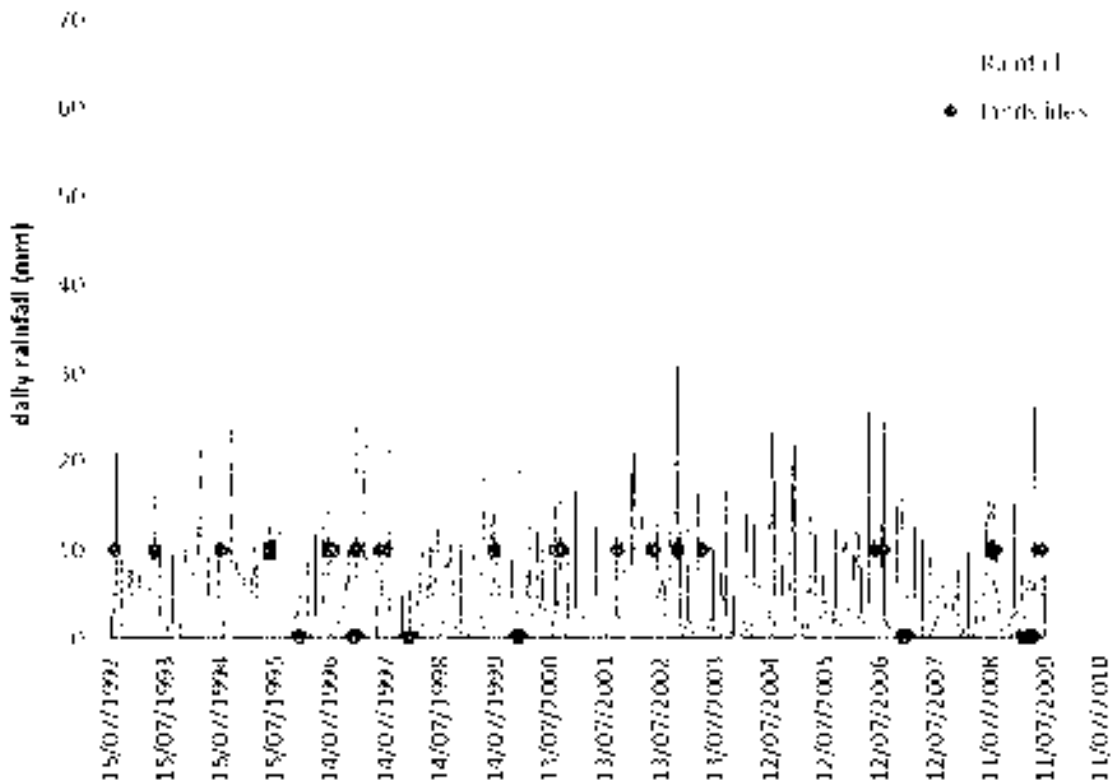


**Figure 21** Daily rainfalls at Christchurch Botanic Gardens and landslides in the Port Hills. Daily rainfalls at Christchurch Botanic Gardens and landslides in the Port Hills investigated by Geotechnical Consulting Ltd, or listed by the Earthquake Commission as causing damage to homes. Landslides without rain are plotted at 0 mm, all others are plotted at 10 mm of rain (the minimum rainfall for triggered landslides).

McSaveney et al. (2014) conclude from comparison of the record of damaging landslides and daily rainfall for the period 1992–2010 that:

1. Landslides can occur without rain, but the probability of landslides occurring increases with increasing intensity of rainfall;
2. Landslides occurred much more frequently on days with rain, but there were many rainy days when no landslides were recorded; and
3. As the amount of daily rainfall increased, a higher proportion of the rainy days had recorded landslides.

Following the 2010/11 Canterbury earthquakes there have been two notable rainfall events (Table 18):

- 11–17 August 2012: occurred at the end of winter following a long period of wet weather. During this period a total of 92 mm of rainfall was recorded at the Christchurch Botanic Gardens. The maximum daily rainfall (24 hourly rainfall recorded 9 am–9 am) during this period was 61 mm on 13 August 2012.
- 3–5 March 2014: occurred at the end of a period of dry weather. During these three days, a total of 118 mm of rain was recorded at the GNS Science rain gauge installed at No. 2 Kinsey Terrace). The maximum daily rainfall during this period occurred on 5 March 2014 and totalled 85.4 mm.

The frequency of high-intensity rainfalls in Christchurch has been well studied (e.g., Griffiths et al., 2009, Figure 22, and McSaveney et al., 2014). Griffiths et al. (2009) use rainfall records for the period 1917–2008 from gauges all over Christchurch. McSaveney et al. (2014) use a composite rainfall record, for the period 1873–2013, mainly from the Christchurch Botanic Gardens gauge (described as Christchurch Gardens from hereafter), but substituting averages for other nearby stations where gaps in the Christchurch Gardens data exist.

The annual frequencies for four rain events, including the two notable events are given in Table 18. Rainfall depth-duration-return period relations for Christchurch Gardens and Van Asch St, Sumner are taken from Griffiths et al. (2009) and for Christchurch Gardens from McSaveney et al. (2014).

**Table 18** Annual frequencies of given rainfall in the Christchurch for four main events following the 2010/11 Canterbury earthquakes (rainfalls are calculated daily from 09:00 to 09:00 NZST).

<b>Date</b>	<b>Total rainfall (mm)</b>	<b>Station</b>	<b>Max daily rainfall/date</b>	<b>Annual frequency Christchurch Gardens Griffiths et al. (2009)</b>	<b>Annual frequency Christchurch Gardens McSaveney et al. (2014)</b>	<b>Annual frequency Van Asch, Sumner Griffiths et al. (2009)</b>
11–17 August 2012	92	Christchurch Gardens (CCC/NIWA)	61 mm 13 August 2011	92 mm = no data available 61 mm = 0.5 (once every 2 years)	92 mm = 0.4 (once every 2.7 years) 61 mm = 5 (5 times per year)	N/A
3–5 March 2014	118	Clifton Terrace (GNS Science)	89 mm 5 March 2014	N/A	N/A	118 mm = 0.1 (once every 10 years) 89 mm = 0.1 (once every 10 years)
3–5 March 2014	141	Christchurch Gardens (NIWA)	130 mm 5 March 2014	141 mm = 0.05–0.02 (once every 20–50 years) 130 mm = 0.02–0.01 (once every 50–100 years)	141 mm = 0.05 (once every 20 years) 130 mm = (>0.01) less than once every 100 years	N/A
18 April 2014	68	Lyttelton (NIWA)	68 mm	N/A	N/A	68 mm = 0.5 (once every 2 years)
29 April 2014	20	Clifton Terrace (GNS Science)	20 mm	N/A	N/A	Greater than 0.5 (occurs frequently every year)

Regardless of the dataset used, both suggest that the heavy rainfalls recorded in the Port Hills following the 2010/11 Canterbury earthquakes were unexceptional. Although the three-day rainfall of 118 mm had an annual frequency of 0.1–0.05 (once every 10–20 years), it occurred at the end of summer when the ground would have had a seasonally low water content.

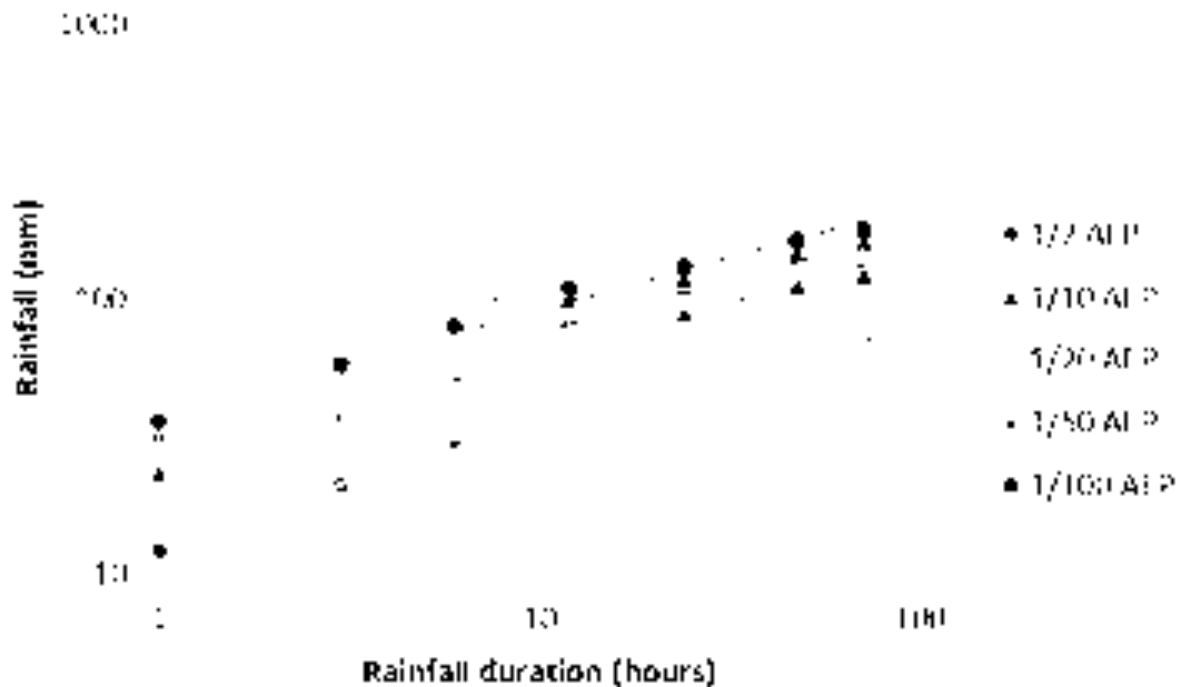


**Figure 22** Rainfall depth-duration-return period relations estimated for Christchurch Gardens by Griffiths et al. (2009) using recorded rainfall data. Error limits of 20% are shown by dotted lines for the 1/2 and 1/100 AEP curves. Shaded area covers the range of 30–75 mm of rainfall over which the expected number of soil landslides in the Port Hills rises from very few to many. Rockfalls can occur without rain, but the probability of rockfalls occurring increases with increasing intensity of rainfall.

There is significant variation in rainfall across Christchurch in individual storms. The return period of the 89 mm of rain recorded at the GNS Science rain gauge at Clifton Terrace on the 5 March 2014 was about 10 years (using the data from Griffiths et al. (2009) for Van Asch Street in Sumner). The return period of the 130 mm of rain recorded at Christchurch Gardens for the same storm on the same day, was between 50 and 100 year (using the data from Griffiths et al. (2009) for the Christchurch Gardens).

At Lyttelton, about 135 mm of rain was recorded on the 5 March 2014, which is considerably higher than the 89 mm recorded at Clifton Terrace, which is only about 5 km north of Lyttelton.

### 3.3.3.2 Groundwater response to rain

Based on the drillhole records and material logs, piezometric head level responses and field mapping of seepages, groundwater in the slope appears to be perched above the base of the weathered basalt lava breccia and or the base of the mixed colluvium, as these materials have higher clay content than the overlying loess. This was confirmed by field mapping of surface water seepage points, as water tended to seep from locations where rock was at or near the ground surface.

The piezometric head level responses recorded by the automated sensors in BH-KSY-2a and BH-KSY-8a indicate a relatively rapid response of piezometric head levels to rainfall. For most of the year (60–70%) the standpipes are recorded as being dry.

The piezometric head level response to significant rainfall events measured in BH-KSY-2a is typically 30-days, between the rise and fall of each response peak, where the increasing and decreasing parts of the response peak are similar in gradient. In comparison, the piezometric head levels recorded in BH-KSY-8a have a steep rising part and a more gradual “exponential” recessional part, typically lasting 30–60 days from peak. These differences are thought to be due to differences in the catchment area, upslope of the drillholes. BH-KSY-2a is located near the slope crest with only limited catchment area, and BH-KSY-8a is near the slope toe with a much larger upslope catchment area.

The response of the piezometric head levels in drillhole BH-KSY-8a in response to rainfall over the monitoring period (2 November 2011–27 July 2014) is shown in Figure 23. The response of piezometric head levels to two notable rain events: 1) 11–17 August 2012; and 2) 3–5 March 2014 (Table 17), are shown in Figure 24 and Figure 25 respectively.

These results show that the larger piezometric response occurred during the rain event 11–17 August 2012, following a period when piezometric head levels were seasonally high. In comparison, the piezometer response to the larger rain event on 3–5 March 2014 was negligible, as this rain occurred when piezometric head levels were seasonally low.

These observations suggest that antecedent water conditions are an important indicator of slope instability. For example, large daily rainfalls occurring during periods of wet weather are more likely to trigger movement and landslides than very high daily rainfalls during long periods of dry weather.

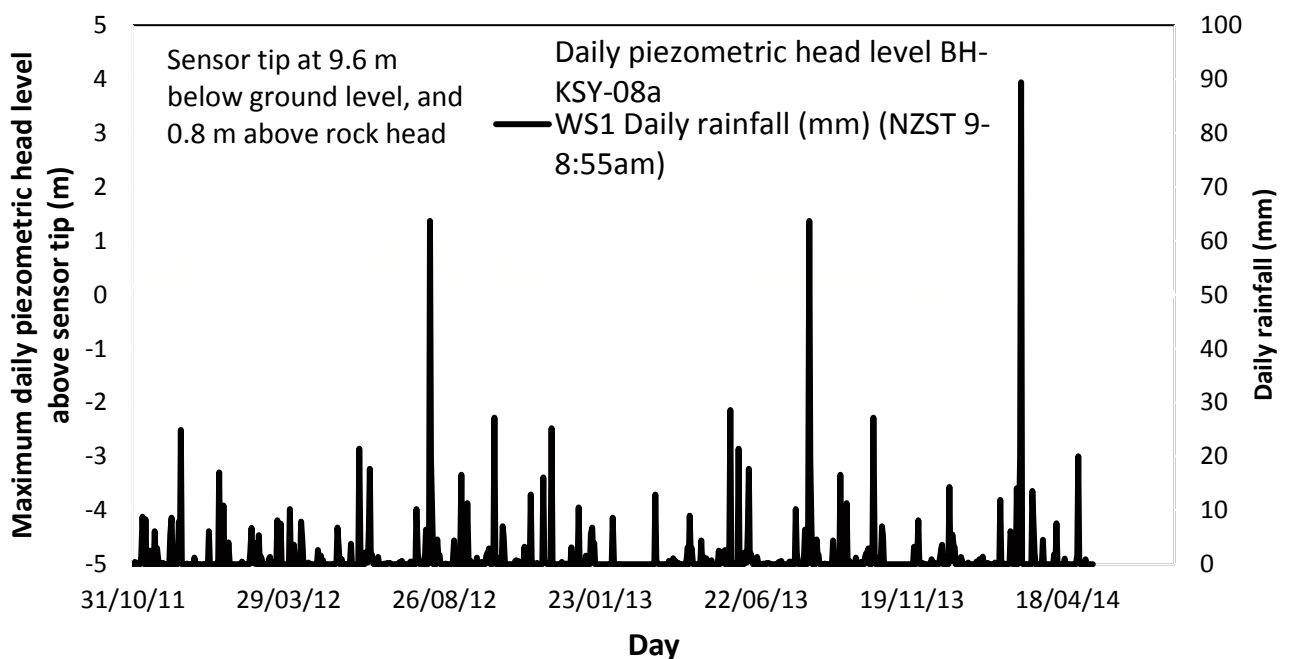


**Figure 23** Daily rainfall recorded at the GeoNet gauge installed at Clifton Terrace (next to cGPS CLS5, Appendix 2), and piezometric head levels recorded in the standpipe in drillhole BH-KSY-8a (Figure 6).

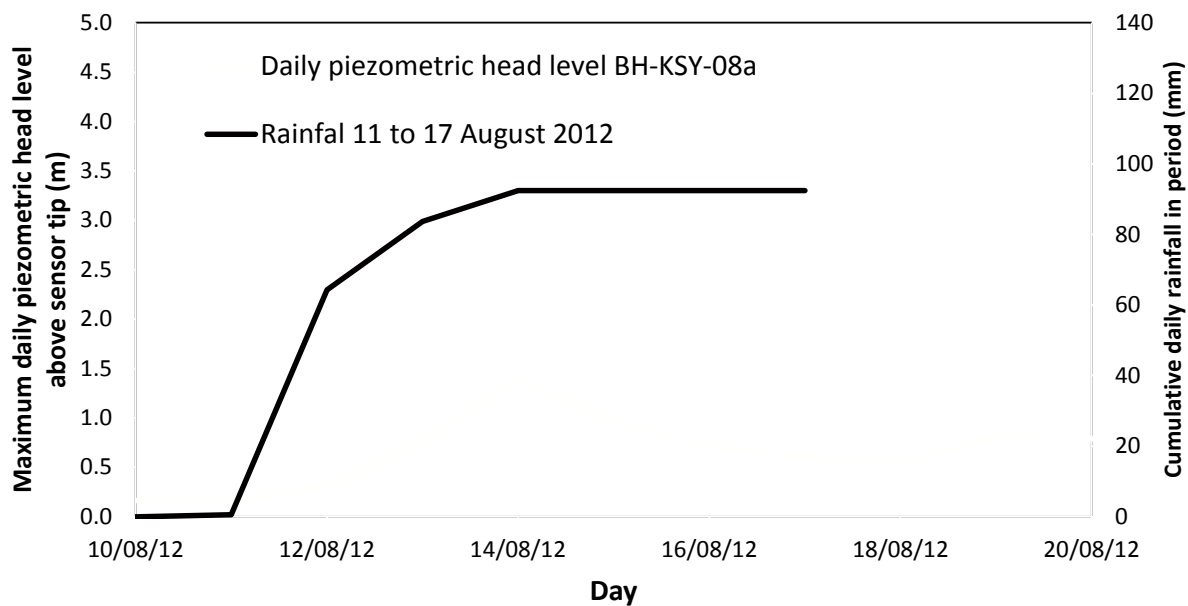


**Figure 24** Daily rainfall recorded at the GeoNet gauge installed at Clifton Terrace (next to cGPS CLS5, Appendix 2), and piezometric head levels recorded in the standpipe in drillhole BH-KSY-8a (Figure 6), for rain event 11–17 August 2012.

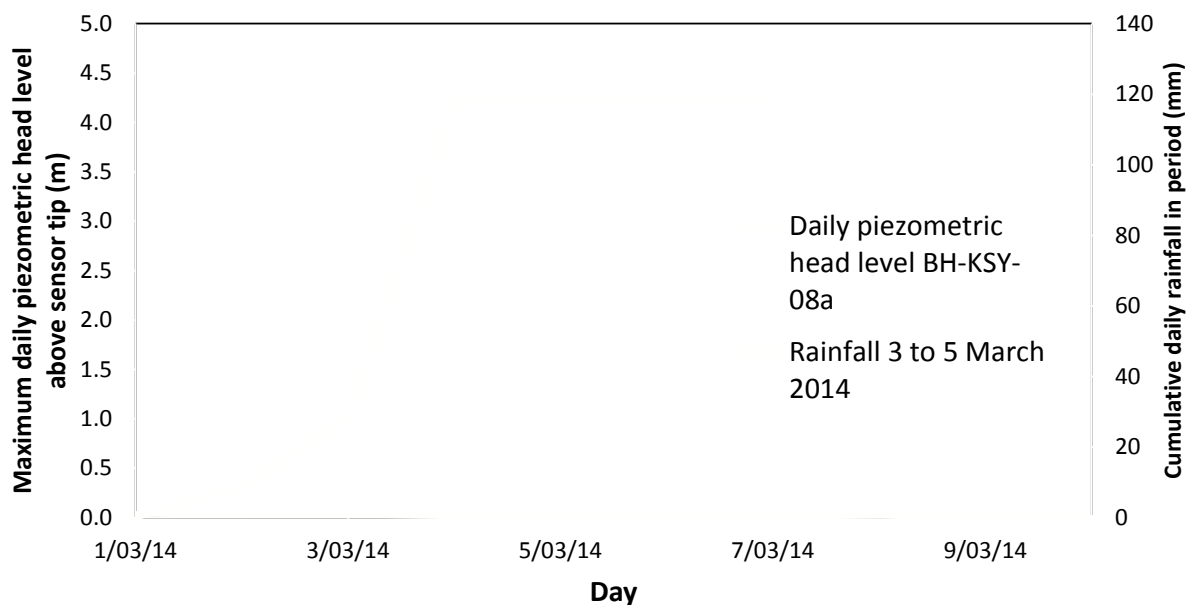


**Figure 25** Daily rainfall recorded at the GeoNet gauge installed at Clifton Terrace (next to cGPS CLS5, Appendix 2), and piezometric head levels recorded in the standpipe in drillhole BH-KSY-8a (Figure 6), for rain event 3–5 March 2014.

### 3.3.3.3 Landslide response to groundwater

No systematic movement, outside of survey error, of source areas A and B has been recorded since the 23 December 2011 earthquake in response to changes in the monitored piezometric head levels.

### 3.4 SLOPE FAILURE MODELS

#### 3.4.1 Landslide types affecting the site

Based on the results from the mapping, monitoring of survey marks, ground investigations and monitoring data, the pattern of slope deformation recorded in the assessment area in response to the 2010/11 Canterbury earthquakes is thought to be consistent with an earthquake-induced coherent “soil block slide” (adopting the scheme of Keefer, 1984), or an earth/debris slide (adopting the scheme of Hungr et al., 2014). Based on the mapped deformation and surveyed displacement patterns, there appear to be several discrete “slide blocks” (mainly source areas A and B) within the overall mass that moved during the 2010/11 earthquakes. Field evidence suggests that a pre-existing landslide was reactivated by the 2010/11 earthquakes.

The main findings from the investigation of the slide are:

##### *Source area A:*

- The total permanent displacement of the area during the 2010/11 Canterbury earthquakes was about one metre. No systematic movement, outside of survey error, has been recorded since the 23 December 2011 earthquake in response to changes in the monitored piezometric head levels.
- It not possible to determine the depth of the basal landslide slide surface from inclinometer records as systematic displacement, relating to obvious landslide movement, has not been identified during the monitoring period. The inclinometer tube in BH-KSY-1, does however, show a slight deflection at a depth corresponding to the mixed colluvium.
- The displacement patterns of the area, inferred from surface monitoring of survey marks and deformation patterns suggest a translational failure mechanism, with predominantly extension (tension cracks) at the head scarp, and areas of compression (ground rolls) near the toe of the displaced area. There is no evidence of any “break-out” of the slope related to the inferred displaced mass, in the steep rock cliffs to the north and northeast of the site. The mapped areas of compression, inferred to be the toe of the displaced mass, are above the crest of the cliff.
- The displacement angles (from the horizontal), inferred from the surveying of monitoring marks are 25–33°, and are slightly steeper than the dip of rock head and the volcanic bedrock layering, which is estimated to vary between 10° and 30° (average of about 20°) and is relatively persistent across the area. Given the uncertainties associated with the measurements, the displacement angles are similar to the dip of the volcanic sequence, supporting a predominantly translational displacement mechanism.
- The bearing of landslide displacement during the earthquakes is mainly 070–090°, which is consistent to the dip direction of rock head and the bedrock layers.
- For cross-sections 1 and 2 the dip angle of rock head is steeper in the upper part of source area (about 15–20°) corresponding to the area of predominantly extension, than the lower part (about 10–15°) corresponding to the area of compression, possibly suggesting that the lower slope may be buttressing the upper slope.
- Logging of drillhole cores and field exposures, indicate the presence of a zone of highly weathered basalt lava breccia underlying the loess and mixed colluvium in the upper and central part of source area A. Within the displaced area, this material appears disturbed possibly as a result of recent and relict slope movement, it contains clay with

slickensides and clay has been noted in several drillholes, infilling joints and voids. This material does not appear to underlie the loess in the lower area, but this cannot be confirmed due to the lack of drillholes in this area.

- The mixed colluvium underlying the loess in this area is unusually thick (>2.5 m) and contains much clay. It is also possible that all or some of the landslide movement could be occurring within this material as it is similar to the slickensided clay within the weathered breccia, and is likely to have derived from it.
- No obvious zones of movement have been logged within the loess material, and the factors of safety for slide surface in the loess are higher than those in the mixed colluvium, assuming reasonable strength parameters for these materials. However, it is unlikely such zones would be visible to the eye, considering the silt-dominated nature of the material.
- The refraction seismic line across the main area of cracking, in source area A, suggests there is a 1.5–2 m step in rock head in this area, which could be consistent with a deeper seated landslide slide surface within the weathered breccia. The seismic line data also shows a change in the P-wave velocity in the rock on the down slope side of the step in rock head, and within the area of cracking, suggesting that the rock within the area of cracking is less dense (and possibly more disturbed).
- Groundwater in the slope appears to be perched within the weathered basalt lava breccia and or above the base of the mixed colluvium, as these materials have higher clay content than the overlying loess. The loess appears to be relatively well drained by tunnel gullies. Groundwater responds rapidly to rain, but the magnitude of the response is linked to the antecedent rainfall and piezometric head levels in the slope at the time of the rain.

#### *Source area B:*

- This area appears more incised and degraded than source area A, with well-developed scarps in parts, inferred to be from past landslide movement or gully erosion.
- The total permanent displacement of the area during the 2010/11 Canterbury earthquakes was about 0.4 m and is significantly less than in source area A, implying significant differences in the overall shear strength of their respective shear surfaces, despite rock head in source area B being notably steeper. No systematic movement, outside of survey error, of the area has been recorded since the 23 December 2011 earthquake in response to changes in the monitored piezometric head levels.
- It not possible to determine the depth of the basal landslide slide surface from inclinometer records as no displacement, relating to landslide movement, has been identified during the monitoring period.
- The displacement patterns of the area, inferred from surface monitoring of survey marks and deformation patterns suggest a translational failure mechanism, with predominantly extension (tension cracks) at the head scarp. No areas of compression have been mapped in the area.
- The displacement angles (from the horizontal), inferred from the surveying of monitoring marks are 25–33° and are slightly steeper than the dip of rock head (20–25°) and the volcanic bedrock layering (average of about 20°).
- The bearing of landslide displacement during the earthquakes is mainly 080–090°, which is consistent to the dip direction of rock head and the bedrock layers.

- Drillhole logs and field exposures suggest most of this area is underlain by basalt lava and not breccia, and although basalt lava breccia is locally present, it is not as weathered, thick or persistent as it is under source area A. The mixed colluvium underlying the loess in this area is also thinner, less than 0.6 m compared to >2.5 m in source area A.
- No obvious zones of movement have been logged within the loess material. However, it is unlikely such zones would be visible to the eye, considering the silt-dominated nature of the material.
- Groundwater in the slope appears to be perched above rock head at the base of the mixed colluvium, as seepage was noted near rock head.

Other landslide types in the assessment area:

- Cliff collapses, comprising debris avalanches and cliff-top recession of the rock mass and overlying loess, located at the crest of the steep rock slopes in Shag Rock Reserve, towards the north and east of the site.
- Localised failures of the cut slopes, in predominantly loess, above and below Kinsey Terrace and along the incised drainage lines.

### 3.4.2 Failures mechanisms adopted for modelling

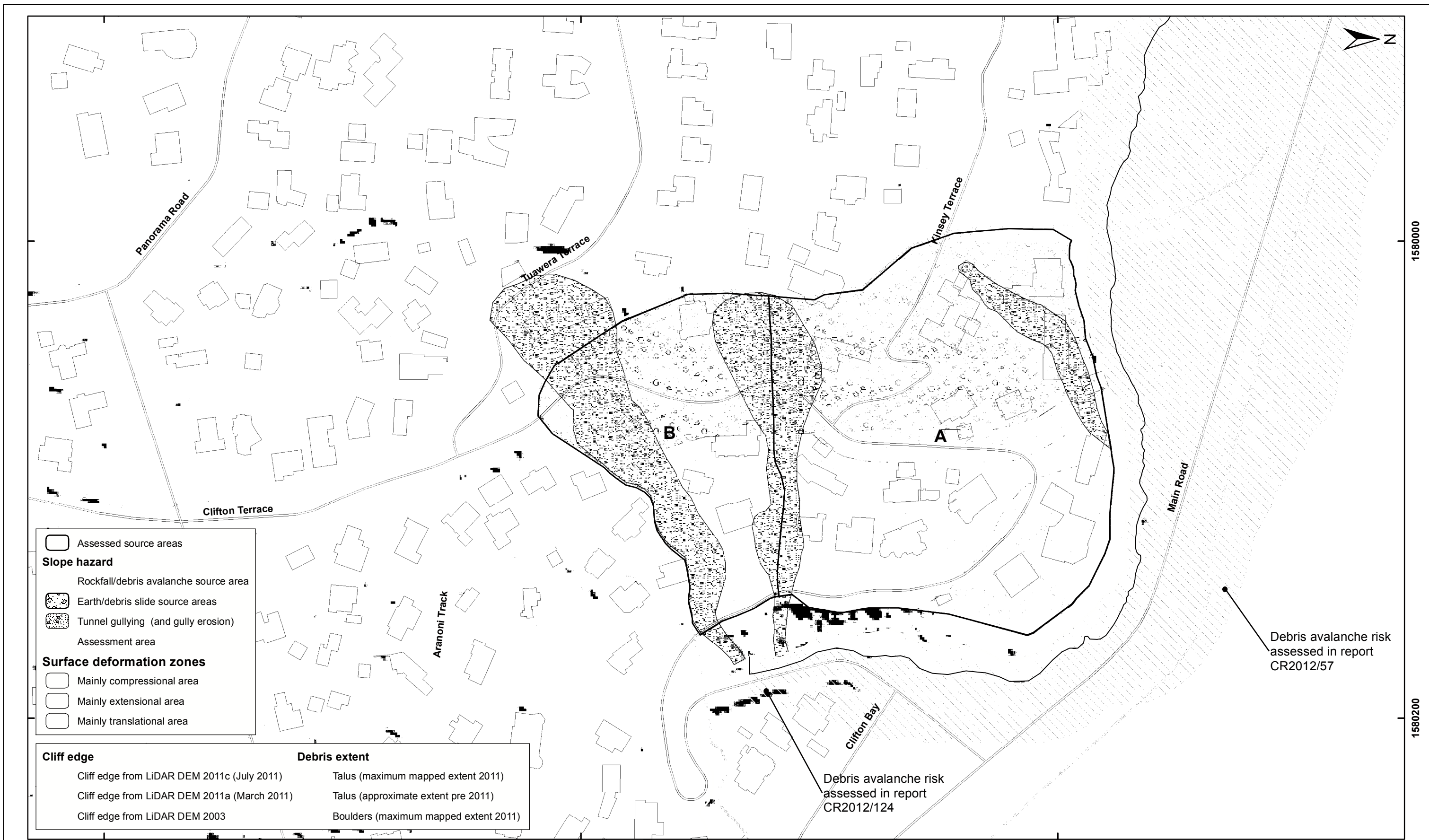
Excluding the cliff-collapse failure mechanisms affecting the site (Massey et al., 2012), the slope-failure mechanisms in source areas A and B that have been adopted for numerical modelling are:

- *Mechanism 1:* Translational failure through the loess of the upper, lower and the entire slope.
- *Mechanism 2:* Deeper translational failure (upper, lower and entire slope) of the loess through the underlying mixed colluvium layer. A colluvium layer was intercepted in all drillholes within the upper and central parts of source areas A and B. For the purpose of the model, it was also assumed that the mixed colluvium layer extends beneath the loess and above the volcanic lava sequences over most of the site. The failure mechanism is thought to be translational, with the failure surface in the mixed colluvium generally being sub parallel to rock head.
- *Mechanism 3:* Deep-seated translational failure (upper, lower and entire slope), through the weathered basalt lava breccia and mixed colluvium (source area A only). The failure mechanism is thought to be mainly translational, with the failure surface anastomosing between the mixed colluvium and weathered basalt lava breccia, but generally being sub-parallel to rock head.

Cliff collapse is another credible failure mechanism, but the risk from such failures is already addressed by Massey et al. (2012) and the risk from cliff collapse is not reassessed in this report.

Localised failures of the cut slopes or retaining walls within source areas A and B were not assessed for this report.

An engineering geological model showing the main landslide hazards affecting the site is presented in Figure 26, which is a simplified version of Figure 7.



SCALE BAR: 0 50 100 m

EXPLANATION:

Background shade model derived from NZAM post earthquake 2011c (July 2011) LiDAR survey resampled to a 1 m ground resolution.  
 Roads and building footprints provided by Christchurch City Council (20/02/2012).  
 PROJECTION: New Zealand Transverse Mercator 2000

DRW:  
BL  
CHK:  
CM, FDP



**ENGINEERING GEOLOGY MODEL**

**Clifton Terrace  
Christchurch**

**FIGURE 26**

**FINAL**

REPORT:  
CR2014/76

DATE:  
August 2014



## 4.0 HAZARD ASSESSMENT RESULTS

### 4.1 SLOPE STABILITY – STATIC CONDITIONS

For assessed source areas A and B, the engineering geological cross-sections in Figure 8 were used as the basis of the numerical slope stability modelling. Geotechnical material strength parameters used in the modelling are from Table 14 and Table 16, and models using variable shear-strength parameters for the key materials were used to assess the sensitivity of the slope – along a given cross-section – to failure.

Graphic examples of stability assessment outputs are shown in Figure 27–Figure 29 for cross-section 2 (source area A) and cross-section 3 (source area B). Cross-section 2 was chosen to represent source area A as it best represents the site conditions where the angle of rock head was steepest, and it is the cross-section closest to where the largest permanent slope displacements were measured from survey marks.

For cross-section 2, models were run to assess the stability of the upper, lower and entire slope. For cross-section 3, models were run to assess the stability of the upper and entire slope.

For cross-section 2 (source area A), piezometric head levels used in the assessment were: 1) the maximum levels recorded in drillholes BH-KSY-2a and BH-KSY-8a (Table 8); 2) the maximum levels needed to reduce the slope factor of safety to 1.0; and 3) dry. For cross-section 3 (source area B), piezometric head levels used in the assessment were: 1) the maximum levels needed to reduce the slope factor of safety to 1.0; and 2) dry.

Table 19 shows the results from the assessment of the three failure mechanisms for source area A. In summary the analysis shows:

- *Mechanism 1 – Failure through the loess:* The results adopting loess shear strength parameters of friction angle ( $\phi$ ) of 30° and cohesion (c) of 10 kPa, (lower bound of the likely loess parameters), suggest that the factor of safety is about 1.9–2.0 for the upper and entire parts of cross-section 2 (source area A), and about 1.5 for the lower part, assuming drained conditions. The lower part corresponds to the cut slope adjacent to Clifton Terrace. The factors of safety for the lower, upper and entire length reduce to 1.4, 1.7 and 1.7 respectively if the maximum recorded piezometric head levels are used in the model.
- *Mechanism 2 – failure through the mixed colluvium layer (Figure 27–Figure 29, cross-section 2):* The presence of the weak mixed colluvium layer results in slide surfaces with a lower factor of safety than those through the loess. When a weak mixed colluvium layer is included in the model, the factor of safety for the upper and entire part of cross-section 2 is about 1.6–1.8 and for the lower part is 1.4, for the range of material parameters assumed, under drained conditions. The factors of safety for the upper and entire parts reduce to 1.3–1.6 and 1.2 for the upper slope if the maximum recorded piezometric head levels are used.

- *Mechanism 3 – Failure through the weathered breccia:* The presence of the weathered breccia results in slide surfaces with a similar factor of safety to those through the mixed colluvium, as the material strength parameters adopted for the weathered breccia are the same as those adopted for the colluvium. The factor of safety for the upper and entire parts of cross-section 2 is about 1.6–1.8 and for the lower part is 1.4, for the range of material parameters assumed, under drained conditions. The factors of safety for the upper and entire parts reduce to 1.3–1.6 and 1.2 for the upper part if the maximum recorded piezometric head levels are used.

The range of friction-angle values used in these assessments is within the range of residual strength values obtained from ring- and direct-shear tests of the loess, and ring shear tests of the clay matrix material within the weathered basalt lava breccia. These values are likely to represent a lower-bound range of the bulk strength conditions of the loess, mixed colluvium and weathered breccia. Nonetheless, the results highlight the sensitivity of the cross-section to the presence of weak layers. The results show that the lower part of cross-section 2, adjacent to Clifton Terrace where the slope was modified by road widening works, has the lowest assessed factors of safety.

Table 19 shows the results from the assessment of the two failure mechanisms for source area B. In summary the analysis shows:

- *Mechanism 1 – Failure through the loess:* The results from the assessment, with loess shear-strength parameters of friction angle ( $\phi$ ) of 30° and cohesion (c) of 10 kPa, representing the lower end of the range of loess parameters thought to be reasonable, suggest that the factor of safety of the upper and entire slope is about 1.7 and 1.6 respectively, under drained conditions. These are lower than the factors of safety estimated for cross-section 2 (source area A) under drained conditions, and are due to the steeper dip angle of rock head.
- *Mechanism 2 – failure through the mixed colluvium layer (Figure 30 and Figure 31, cross-section 3):* the presence of the weak mixed colluvium layer results in slide surfaces with a lower factor of safety than those through the loess. When a weak mixed colluvium layer is taken into account, the factors of safety for the upper and entire slope are about 1.5 and 1.4 respectively, for the range of material parameters assumed, under drained conditions. These are also lower than the factors of safety estimated for cross-section 2 (source area A) under drained conditions, and also are due to the steeper dip angle of rock head.

**Table 19** Example results from slope stability assessment of source area A (cross-section 2).

Simulated failure mechanism	Loess	Mixed colluvium	Weathered basalt lava breccia	Location of assessed slide surfaces along cross-section	Water level	FoS <sup>1</sup> SLIDE	SRF <sup>2</sup> PHASE2	Comment
Mechanism 1, failure through loess	Cohesion (kPa) / Friction (°) 10 / 30	Not simulated	Not simulated	Upper	Drained	2.0	N/A	Maximum water level recorded in standpipes, assumed to be above the base of the loess
				Lower	Drained	1.5	1.8	
				Entire	Drained	1.9	N/A	
				Upper	Max recorded	1.7	N/A	
				Lower	Max recorded	1.4	1.7	
				Entire	Max recorded	1.7	N/A	
Mechanism 2, failure through colluvium	Cohesion (kPa) / Friction (°) 10 / 30	Cohesion <sup>4</sup> (kPa) / Friction (°) 15 / 21	Not simulated	Upper	Drained	1.8	1.9	Assumes the colluvium is continuous across the entire site.
				Lower <sup>3</sup>	Drained	1.4	1.5	
				Entire <sup>3</sup>	Drained	1.6	1.5	
				Upper	Max recorded	1.6	1.6	Maximum water level recorded in standpipes, assumed to be above the base of the colluvium. Assumes the colluvium is continuous across the entire site.
				Lower <sup>3</sup>	Max recorded	1.2	1.2	
				Entire <sup>3</sup>	Max recorded	1.3	1.2	
				Upper	10.0 m	1.0	N/A	Water level above rock head to achieve FoS = 1. Assumes the colluvium is continuous across the entire site.
				Lower <sup>3</sup>	6.1 m	1.0	N/A	
				Entire <sup>3</sup>	7.5 m	1.0	N/A	

Simulated failure mechanism	Loess	Mixed colluvium	Weathered basalt lava breccia	Location of assessed slide surfaces along cross-section	Water level	FoS <sup>1</sup> SLIDE	SRF <sup>2</sup> PHASE2	Comment
Mechanism 3, failure through weathered breccia	Cohesion (kPa) / Friction (°) 10 / 30	Cohesion <sup>4</sup> (kPa) / Friction (°) 15 / 21	Cohesion (kPa) / Friction (°) 15 / 21	Upper	Drained	1.8	1.9	Assumes the colluvium is continuous across the entire site
				Lower	Drained	1.4	1.5	
				Entire <sup>3</sup>	Drained	1.5	1.5	
				Upper	Max recorded	1.5	1.6	Maximum water level recorded in standpipes, assumed to be above the base of the weathered breccia. Assumes the colluvium is continuous across the entire site.
				Lower	Max recorded	1.2	1.2	
				Entire <sup>3</sup>	Max recorded	1.3	1.2	
				Upper	10.0 m	1.0	N/A	Water level above rock head to achieve FoS = 1. Assumes the colluvium is continuous across the entire site.
				Lower	6.1 m	1.0	N/A	
				Entire <sup>3</sup>	7.5 m	1.0	N/A	

<sup>1</sup> FoS is the factor of safety derived using the general limit equilibrium method of Morgenstern and Price (1965), adopting the path search function.

<sup>2</sup> The finite element model was also used for comparison. Where the slope has been assessed using the finite element model, the stability of the slope is assessed in terms of the Stress Reduction Factor. Note: the shear strength reduction method is used to determine the stress reduction factor (SRF) or factor of safety value that brings a slope to the verge of failure (Dawson et al., 1999).

<sup>3</sup> Assumes the colluvium is continuous above rock head over the entire length of the slope.

<sup>4</sup> Assessments were also run with strength parameters for the colluvium of cohesion (c) = 0 kPa and friction ( $\phi$ ) = 28°. The results with these parameters are similar to those using the parameters of c = 15 kPa and  $\phi$  = 21° and so are not reported in the table.

**Table 20** Example results from slope stability assessment of source area B (cross-section 3).

Simulated failure mechanism	Loess	Mixed colluvium	Weathered basalt lava breccia	Location of assessed slide surfaces along cross-section	Water level	FoS <sup>1</sup> SLIDE	Comment
Mechanism 1, failure through loess	Cohesion (kPa) / Friction (°) 10 / 30	Not simulated	Not simulated	Upper	Drained	1.7	
				Entire	Drained	1.6	
				Upper	7.5 m	1.0	Water level above rock head to achieve FoS = 1
				Entire	5.5 m	1.0	
Mechanism 2, failure through colluvium	Cohesion (kPa) / Friction (°) 10 / 30	Cohesion <sup>3</sup> (kPa) / Friction (°) 15 / 21	Not simulated	Upper	Drained	1.5	
				Entire	Drained	1.4	
				Entire	Drained	1.2	Assumes the colluvium is continuous across the entire site
				Upper	7.5 m	1.0	Water level above rock head to achieve FoS = 1
				Entire	5.5 m	1.0	
				Entire	3.5	1.0	Assumes the colluvium is continuous across the entire site

<sup>1</sup> FoS is the factor of safety derived using the general limit equilibrium method of Morgenstern and Price (1965), adopting the path search function.

<sup>2</sup> The finite element model was also used for comparison. Where the slope has been assessed using the finite element model, the stability of the slope is assessed in terms of the Stress Reduction Factor. Note: the shear strength reduction method is used to determine the stress reduction factor (SRF) or factor of safety value that brings a slope to the verge of failure (Dawson et al., 1999).

<sup>3</sup> Assessments were also run with strength parameters for the colluvium of cohesion (c) = 0 kPa and friction ( $\phi$ ) = 28°. The results with these parameters are similar to those using the parameters of c = 15 kPa and  $\phi$  = 21° and so are not reported in the table.

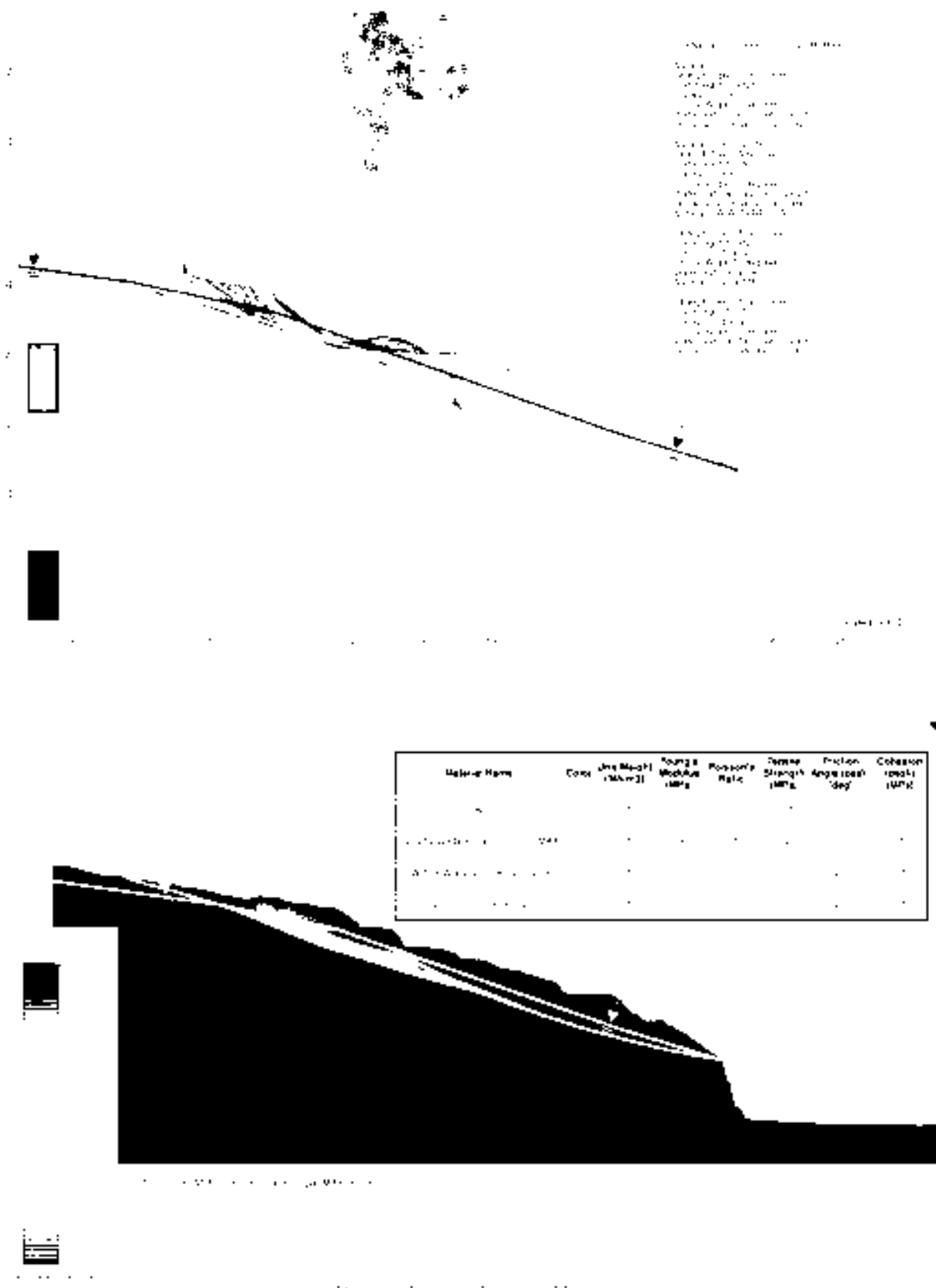


**Figure 27** Failure mechanism 2, upper part of cross-section 2. Example of limit equilibrium and finite element modelling results for cross-section 2, representing failure of colluvium in source area A, adopting the maximum recorded piezometric head levels.

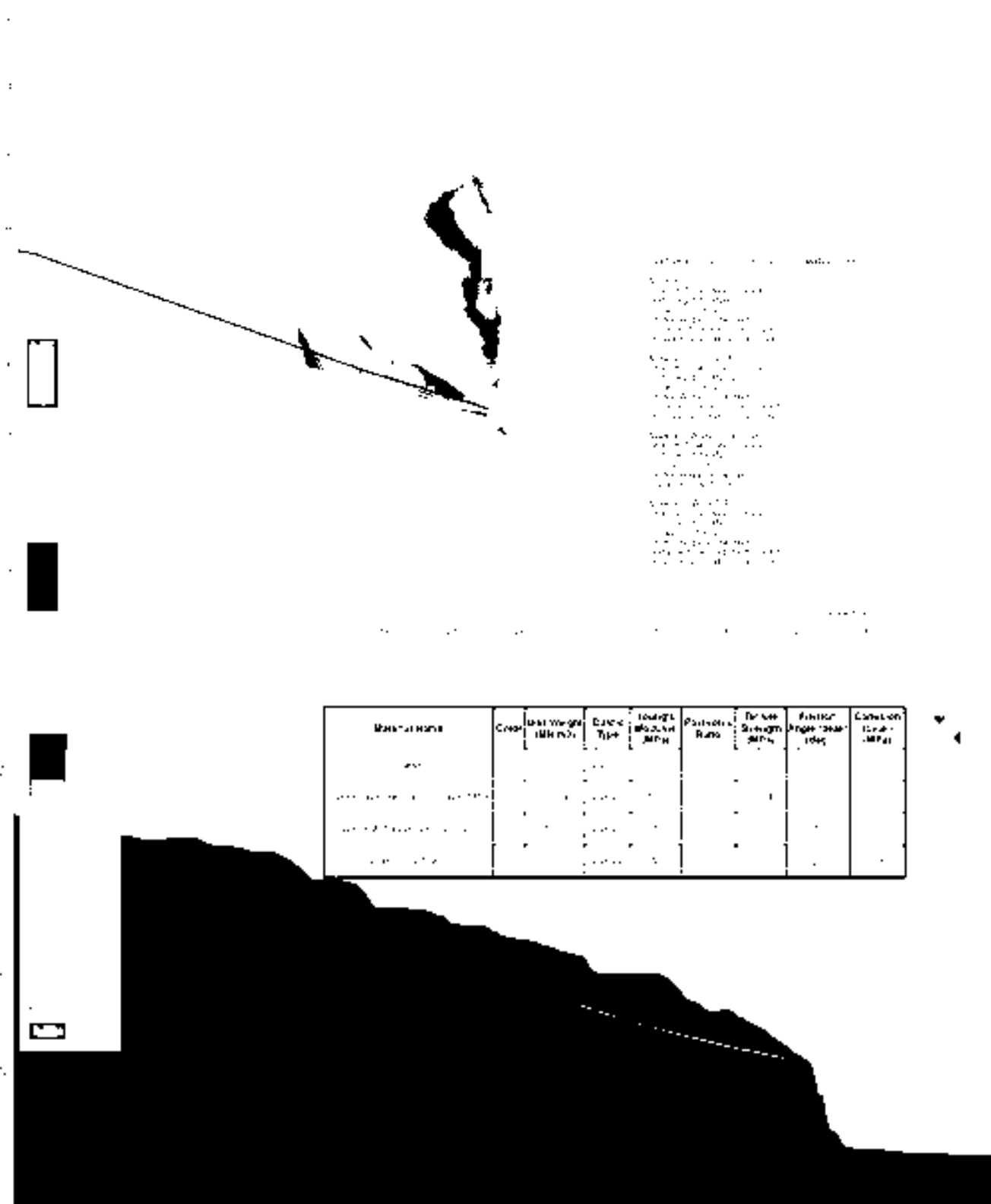


**Figure 28** Failure mechanism 2, lower part of cross-section 2. Example of limit equilibrium and finite element modelling results for cross-section 2, representing failure of colluvium in source area A, assuming the colluvium layer extends across the entire slope, adopting the maximum recorded piezometric head levels.

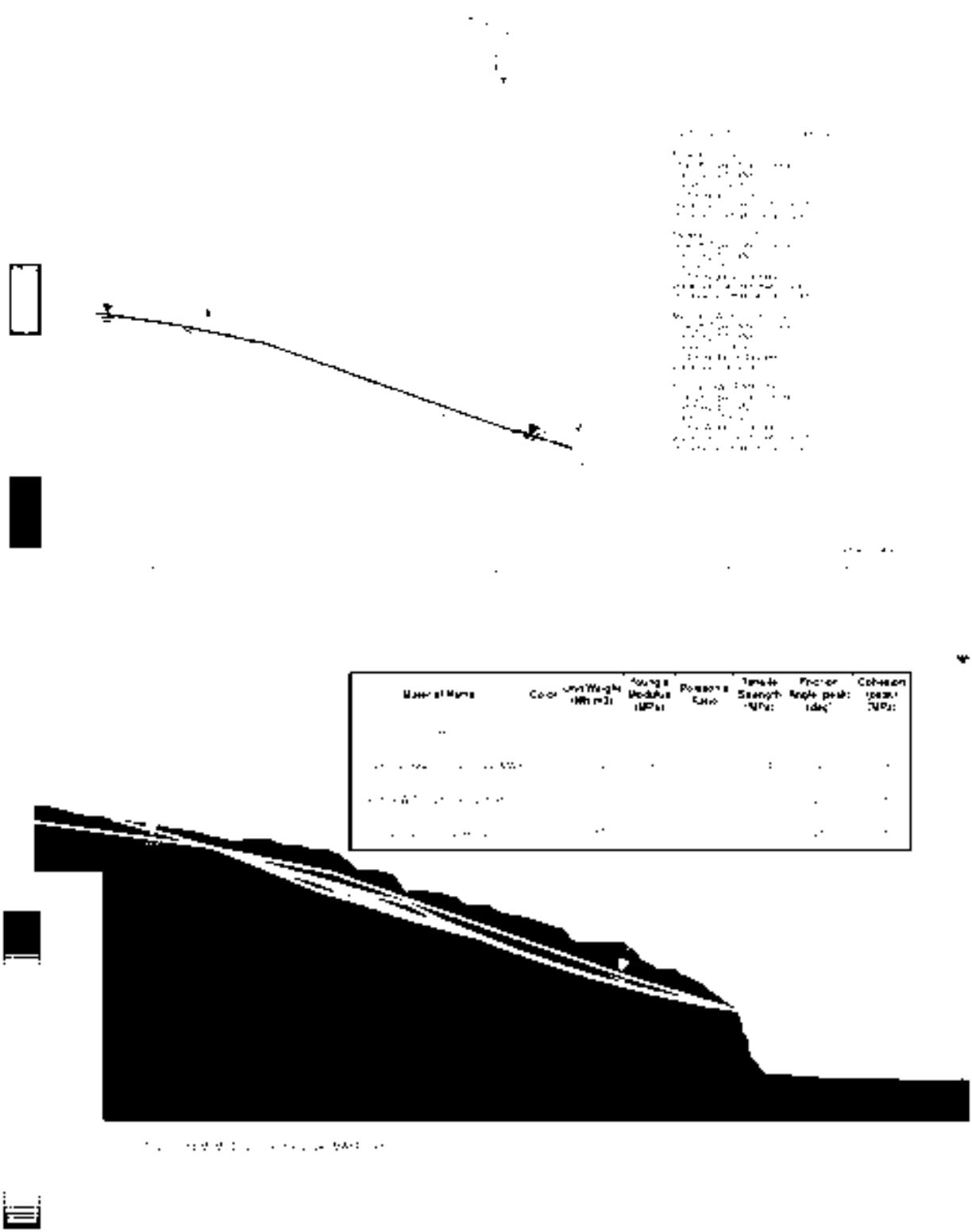


**Figure 29** Failure mechanism 2, entire part of cross-section 2. Example of limit equilibrium and finite element modelling results for cross-section 2, representing failure of colluvium in source area A, adopting the maximum recorded piezometric head levels.

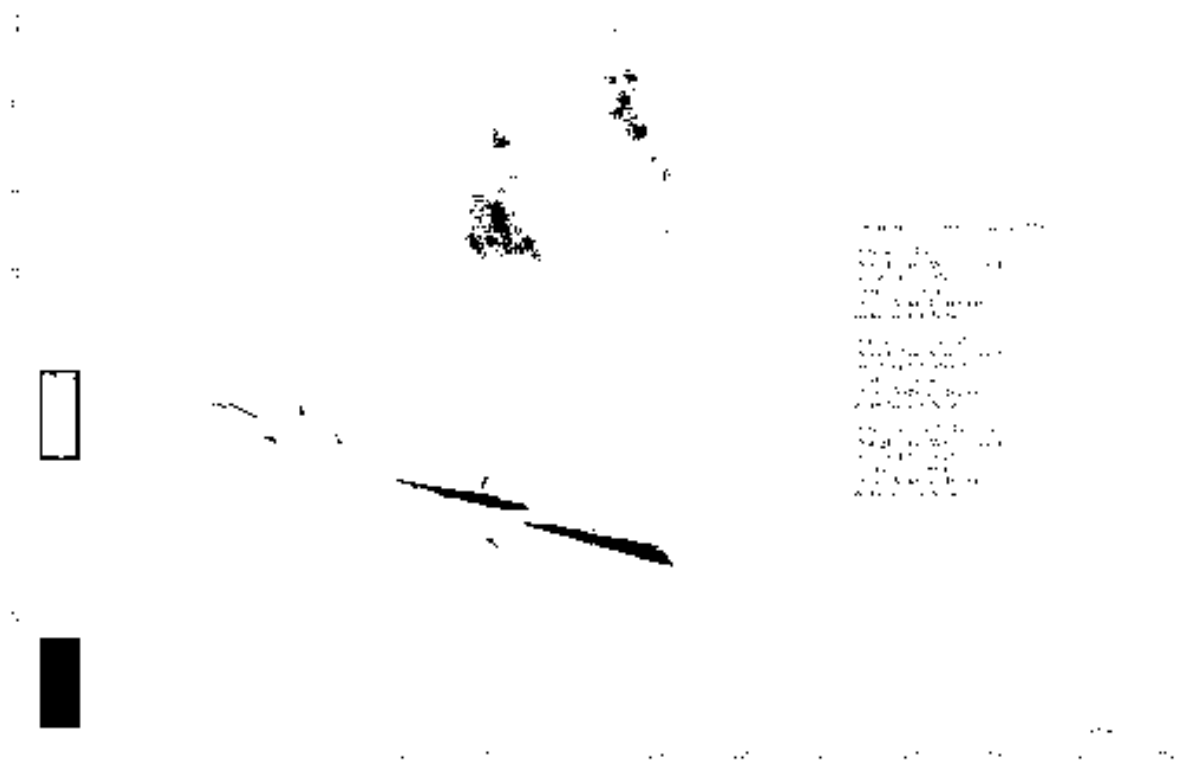


**Figure 30** Failure mechanism 2, entire part of cross-section 3. Example of limit equilibrium results for cross-section 3, representing failure of colluvium in source area B, and adopting dry conditions.

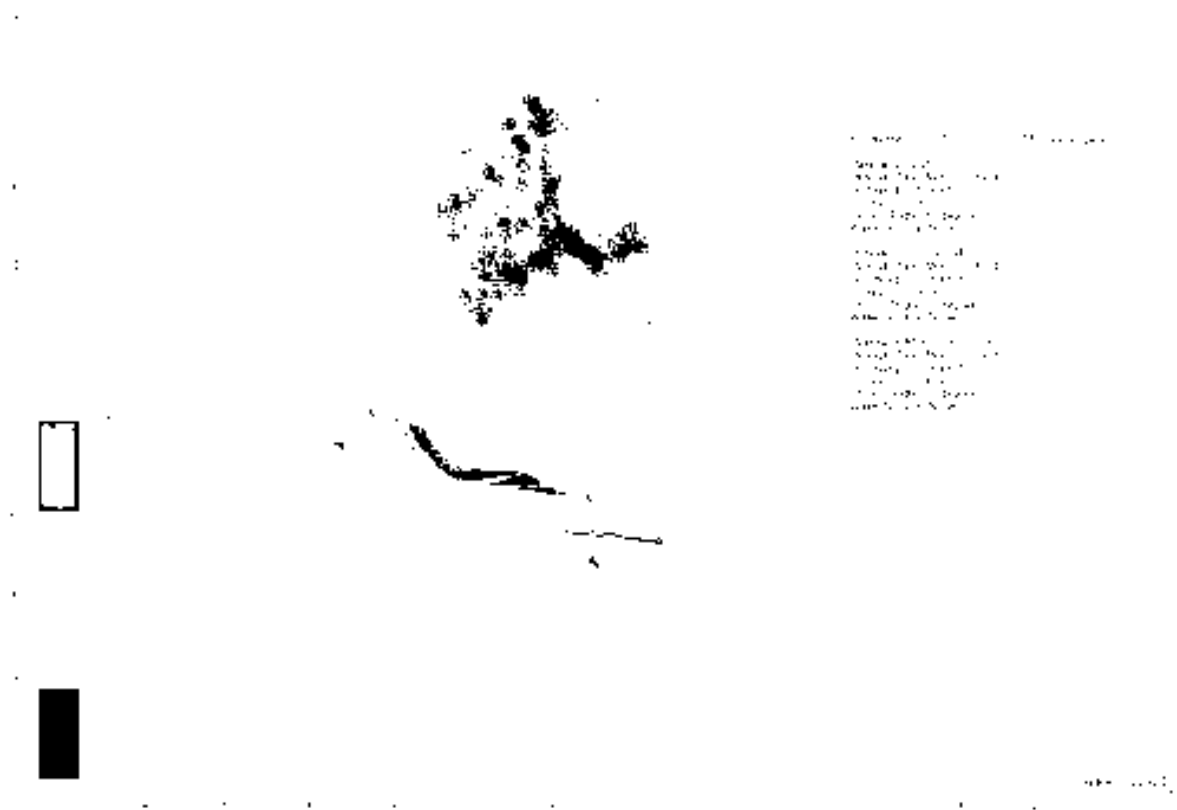


**Figure 31** Failure mechanism 2, upper part of cross-section 3. Example of limit equilibrium results for cross-section 3, representing failure of colluvium in source area B, and adopting dry conditions.

#### **4.1.1 Model sensitivity to groundwater**

The sensitivity of the static factor of safety to changes in transient ground water (pore pressure) for mechanisms 1–3, was simulated by modelling: 1) an initial piezometric line at rock head and by increasing the piezometric head levels from the initial starting level, at given increments, assuming any material below the piezometric line is saturated; and 2) pore pressures acting within tension cracks, where the tension cracks are assumed to extend from the surface to rock head. Results are shown in Figure 32, Figure 33 and Figure 34 for cross-sections 2 and 3.

If failure of the slope were to occur under static conditions, it is more reasonable to assume that it would be through a combination of: 1) reducing shear-strength parameters of the loess, colluvium or weathered breccia in response to increasing water content linked to rainfall; 2) water infilling tension cracks; and 3) the development of a continuous pore pressure surface within the slope leading to a reduction in the effective stress within the saturated materials.

##### **4.1.1.1 Source area A**

For failure surfaces in the loess (mechanism 1), the results show that an increase in piezometric head levels of about 7–8 m above rock head reduces the factor of safety to about one, adopting the lower estimates of the loess shear strength (cohesion ( $c$ ) = 10 kPa and friction ( $\phi$ ) = 30°). Adopting the maximum recorded piezometric head levels, the factor of safety is between 1.4 and 1.7 for the upper, lower and entire parts of cross-section 2.

For failure surfaces in the colluvium and weathered breccia (mechanisms 2 and 3), the results show that an increase in piezometric head levels of about 6–10 m above rock head reduces the factor of safety to about one, adopting the lower estimates of the colluvium and weathered breccia shear strength (cohesion ( $c$ ) = 0-15 kPa and friction ( $\phi$ ) = 21–28°). Adopting the maximum recorded piezometric head levels, the factor of safety is between 1.2 and 1.5 for the upper, lower and entire parts of cross-section 2.

The groundwater levels recorded by GeoNet in standpipe piezometers (BH-KSY-2a and BH-KS8a) in loess, have reached levels of 4.0 and 3.3 m above rock head respectively, which are significantly lower than those needed to initiate movement (factor of safety equal to one).

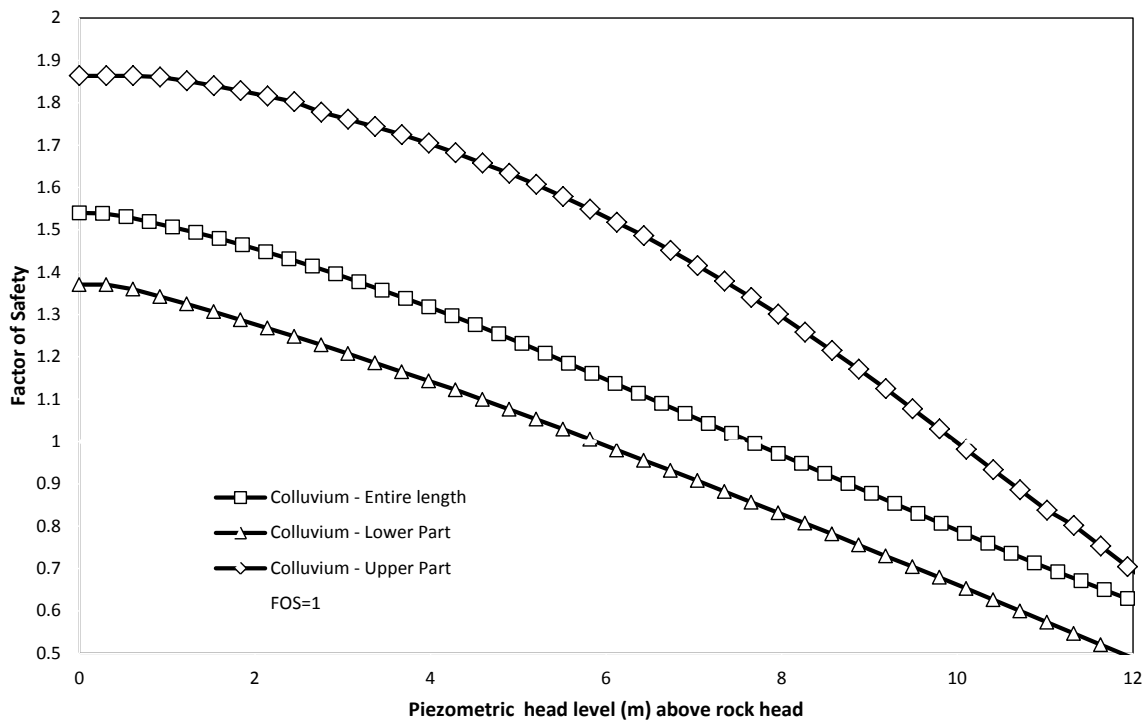


**Figure 32** Sensitivity assessment of the slope factor of safety (cross-section 2, source area A) in response to changing piezometric head levels above rock head for slide surface in the lower, upper and entire parts of source area A. The assessment assumes pore pressures increase uniformly across the entire rock head boundary.

#### 4.1.1.2 Source area B

For failure surfaces in the loess or colluvium (mechanisms 1 and 2), the results show that an increase in piezometric head levels of about 5.5–7.5 m above rock head reduces the factor of safety to about one, for the lower estimates of the loess and colluvium shear strength (cohesion ( $c$ ) = 10 kPa and friction ( $\phi$ ) = 30°).

There are currently no groundwater records from this area of the site. Therefore it is not known whether a piezometric head level rise of between 5.5 and 7.5 m above rock head and across the entire slope is feasible, or under what weather conditions such increases might occur. The groundwater levels in this area are not currently being monitored.

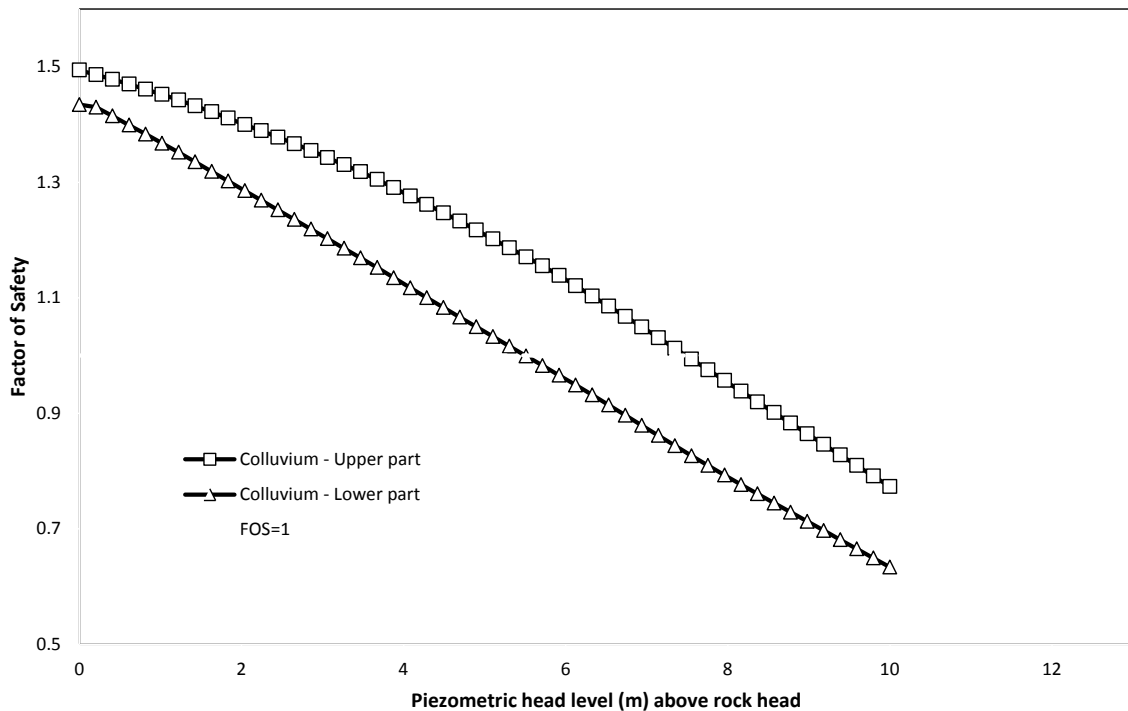


**Figure 33** Sensitivity assessment of the slope factor of safety (cross-section 3, source area B) in response to changing piezometric head levels above rock head for slide surfaces in the upper and entire parts of source area B. The assessment assumes that pore pressures increase by a given amount across the entire rock head boundary.

#### 4.1.1.3 Water filled tension cracks

Water filled tension cracks have been included in the model as a zone extending from the surface to rock head. It should be noted that the mapped tension cracks logged in test pits do not extend all the way down to the base of the loess. The inclusion of water filled tension cracks within the model reduces the piezometric head levels needed to yield a factor of safety of one, for slide surfaces in the lower part of assessed source area A, from 6 m to about 2.5 m, when adopting colluvium shear strengths of cohesion ( $c$ ) of 15 kPa and friction ( $\phi$ )  $21^\circ$ . However, 3.3 m of piezometric head, above rock head, has been recorded in drillhole BH-KSY-8a, in the lower slope near the section line, and no such slope movement has been recorded.

The results show that the factor of safety for the modelled slide surfaces is sensitive to the inclusion of water filled tension cracks in the model. However, the absolute modelled factors of safety are thought to be conservative, as it has been inferred that the weak colluvium extends into the lower slope, although drillhole records do not support this, and that the lower slope contains tensions cracks, which have not been mapped on the ground. Further work is needed to quantify the effects tension cracks have in the model.

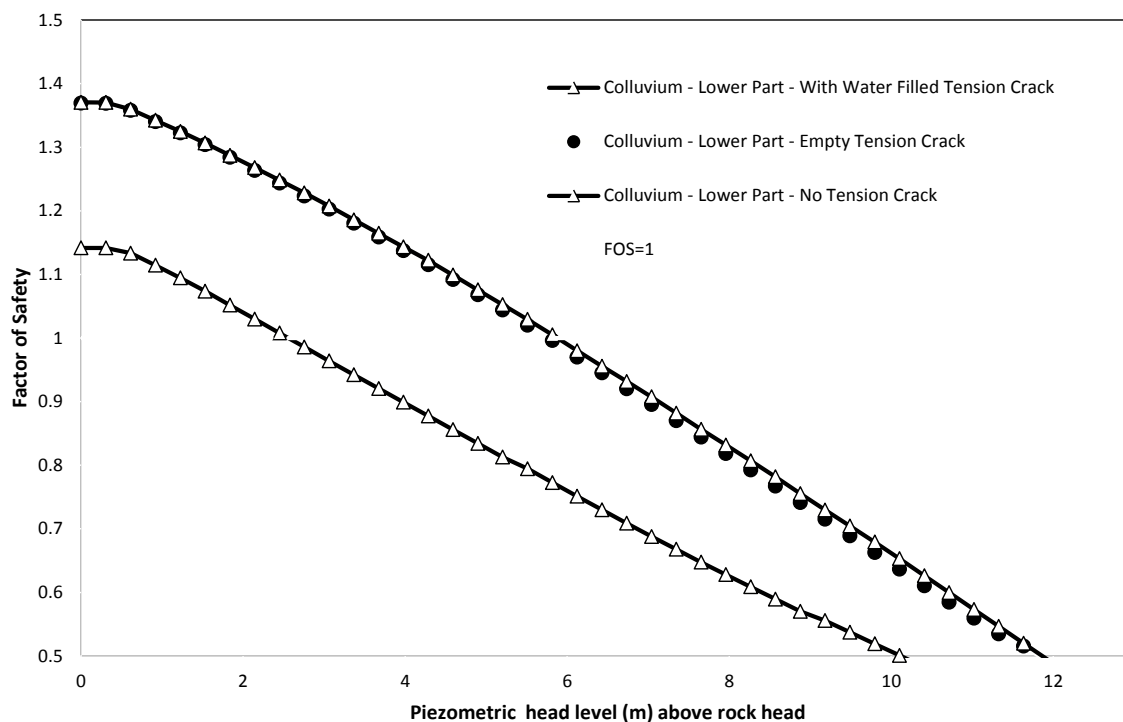


**Figure 34** Sensitivity assessment of the lower slope factor of safety (in source area A, section 2) in response to including filled tension cracks in the model. Tension cracks were assumed to be 100% filled.

## 4.2 SLOPE STABILITY – DYNAMIC CONDITIONS

Dynamic stability assessment comprised: 1) back-analysing the performance of the slope during the 2010/11 Canterbury earthquakes to calibrate the models and verify that the calculated displacements were consistent with those recorded during the earthquakes; and 2) using the calibrated models to forecast the likely displacements under possible future peak ground acceleration scenarios. Cross-sections 2 and 3 have been assessed under dynamic conditions, with and without groundwater.

### 4.2.1 Amplification of ground shaking

The first stage of the assessment was to calculate the maximum acceleration at the slope crest ( $A_{MAX}$ ) to quantify any amplification effects caused by topography and or contrasting materials between the peak ground acceleration of the free field rock input motion and the peak acceleration at the slope crest ( $A_{MAX}$ ). The slope crest is defined as the convex break in slope between the lower steeper slope and the upper less steep slope, and it corresponds to about the middle of the displaced mass. Results from the dynamic site response assessment are contained in Appendix 4.

The results in Appendix 4 suggest that modelled peak acceleration at the slope crest ( $A_{MAX}$ ) vary approximately linearly with the peak ground acceleration of the free-field input motion. Over the range of modelled peak horizontal accelerations, the peak ground acceleration amplification factor ( $S_T$ ) with respect to the free-field peak accelerations ( $A_{FF}$ ) for cross-section 1, is about 2.7 ( $\pm 0.2$ ) for horizontal motions and 1.9 ( $\pm 0.1$ ) for vertical motions. The input peak accelerations are those derived from the out-of-phase synthetic free-field rock outcrop earthquake time acceleration histories described by Holden et al. (2014).

Results from analysis of the data collected by the seismic array instruments installed on Clifton Terrace reported by Kaiser et al. (2014) show significant differences in mean peak ground acceleration amplification between stations of up to 1.7 times horizontal and 2.4 times vertical (Figure A4.4 in Appendix 4). Kaiser et al. (2014) report that their results show that the stations located on source area A (station K1 and K3, Figure 6) have higher amplification factors than the ones located outside the area of cracking (K4 and K5), possibly due to the increased thickness of the loess and mixed colluvium and the weathered breccia in this area.

The results from cross-section 2, showing the response of the slope during the 22 February 2011 earthquake (Figure A4.2 in Appendix 4), suggest that the impedance contrasts between the different materials contribute most to the amplification of shaking, but that the peak horizontal accelerations (for all modelled earthquakes) concentrate around the convex break in slope, defined as  $A_{MAX}$ .

Given the amplification of shaking within the loess and colluvium, coupled with the coseismic landslide displacement inferred from surveying, it is likely that the basal slide surface is coincident with the boundary between the mixed colluvium and the underlying rock, and may include the weathered basalt lava breccia. In experimental data, as the slope moves during an earthquake, the mass above the slide surface can become isolated in part from the shaking below, resulting in lower levels of shaking and displacement. This may be one reason why the calculated amplification factors are near the upper bound of published topographic amplification factors. Assessment of this is outside the scope of this report.

#### **4.2.2 Back-analysis of permanent slope deformation**

Earthquake-induced permanent displacements were calculated using the decoupled method (Makdisi and Seed, 1978) and the Slope/W software. The three failure mechanisms assessed were: 1) failure through the loess (mechanism 1); 2) failure through the mixed colluvium (mechanism 2); and 3) failure through the weathered breccia (mechanism 3). Cross-section 2 was also assessed assuming a piezometric head level consistent with the maximum recorded levels within the drillholes BH-KSY-2a and BH-KSY-8a.

For each failure mechanism, a range of slide surfaces were assessed adopting the “block search” function, assuming a translational failure mechanism. Permanent displacements were estimated along each slide surface, where the displacing mass was treated as rigid-plastic body and no internal plastic deformation of the mass was accounted for, and the mass accrued no displacement at accelerations below the yield acceleration.

The out-of-phase synthetic rock outcrop earthquake time acceleration histories from the 22 February and 13 June 2011 earthquakes were used in the modelling, as permanent coseismic displacement of the Clifton Terrace slopes were recorded during these events. The synthetic rock outcrop earthquake time acceleration histories from the 16 April and 23 December 2011 earthquakes were also modelled to ensure that either no modelled movement or very minor movement of the slopes occurred, as per the magnitudes inferred from survey monitoring. Variable material strength parameters were used for the critical materials present, which were calibrated from the dynamic back-analysis of the inferred permanent displacements; these are listed in Table 21.

For these assessments the displacements inferred from the cadastral and monitoring surveys were assumed to represent the coseismic permanent displacement of the slope, along cross-sections 2 and 3, during the 22 February, 13 June and 23 December 2011 earthquakes. The results from each modelled scenario were then compared with the recorded coseismic permanent slope displacements for each earthquake.

**Table 21** Material strength parameters used for modelling the permanent coseismic displacements for cross-sections 2 and 3. Coseismic displacements are inferred from survey records and field mapping of cracks.

Mechanism	Earthquake	Material	Cohesion (c) (kPa)	Friction ( $\phi$ ) (degrees)	Water Level	Total inferred coseismic displacement (m)
1	22 February and 13 June 2011	Loess	10–30	30–35	Dry	0.1–0.7 (22 Feb)
		Mixed colluvium	0–15	21–30		0.2–0.4 (13 Jun)
		Weathered breccia	0–45	21–30		
		Mixed basalt lava and breccia	110	30		
2 and 3	22 February, 13 June, 16 April, and 23 December 2011	Loess	10–30	30–35	Dry	0.1–0.7 (22 Feb)
		Mixed colluvium	0–15	21–30		0.2–0.4 (13 Jun)
		Weathered breccia	0–45	21–30		<0.01 (16 Apr)
		Mixed basalt lava and breccia	110	30		<0.01 (23 Dec)
2 and 3 (section 2 only)	22 February and 13 June, 2011	Loess	10–30	30–35	Maximum recorded	0.1–0.7 (22 Feb)
		Mixed colluvium	15	21		0.2–0.4 (13 Jun)
		Weathered breccia	15	21		
		Mixed basalt lava and breccia	110	30		

The results from the modelling of the 22 February and 13 June 2011 earthquakes, using the strength parameters listed in Table 19, are summarised in Table 22 and 23 and Figure 35–Figure 44 show the results for the different failure mechanisms:

- Mechanism 1 (cross-sections 2 and 3) – Failure through the loess above the mixed colluvium and weathered basalt lava breccia;
- Mechanism 2 (cross-sections 2 and 3) – Failure through the mixed colluvium; and
- Mechanism 3 (cross-section 2 only) – failure through the weathered basalt lava breccia.

Cross-section 2 was also modelled using the 22 February and 13 June 2011 earthquakes with the lower bound strength parameters for the mixed colluvium and weathered basalt lava breccia (mechanism 2 and 3), but with the maximum recorded piezometric head levels.

**Table 22** Results from the dynamic modelling of cross-sections 2 and 3 for failure mechanism 1, with the slide surfaces confined to the loess. Total inferred coseismic displacements are from measurements of survey marks. Yield accelerations and permanent displacements are calculated from the decoupled assessment and represent the modelled slide surface with the lowest yield acceleration for the given material parameters and failure mechanism. Those rows highlighted in grey represent the material parameters that gave the closest match between the modelled and recorded permanent displacements, for a given earthquake and failure mechanism. Modelled displacements are rounded to the nearest 0.1 m.

Cross-section	Failure mechanism	Earthquake	Critical material	Water level (m)	Cohesion c (kPa)	Friction $\phi$ (°)	Lowest yield acceleration (g)	Modelled coseismic displacement (m)	Total inferred coseismic displacement (m)
2	Translational block slide	22 February 2011	Loess	Dry	10	30	0.35	0.8	0.3–0.7
2	Translational block slide	22 February 2011	Loess	Dry	30	35	0.62	0.2	0.3–0.7
3	Translational block slide	22 February 2011	Loess	Dry	10	30	0.15	2.0	0.1–0.4
3	Translational block slide	22 February 2011	Loess	Dry	30	35	0.40	0.5	0.1–0.4
2	Translational block slide	13 June 2011	Loess	Dry	10	30	0.35	<0.1	0.2–0.4
2	Translational block slide	13 June 2011	Loess	Dry	30	35	0.62	0.0	0.2–0.4
3	Translational block slide	13 June 2011	Loess	Dry	10	30	0.15	0.4	0.0–0.2
3	Translational block slide	13 June 2011	Loess	Dry	30	35	0.40	<0.1	0.0–0.2
3	Translational block slide	13 June 2011	Loess	1 m	30	35	0.36	0.1	0.0–0.2

**Table 23** Results from the dynamic modelling of cross-section 2 for failure mechanisms 2 and 3, with slide surfaces confined to the mixed colluvium (Coll) and the weathered basalt lava breccia (Dist. breccia). Total inferred coseismic displacements are from measurements of survey marks. Yield accelerations and permanent displacements were calculated from the decoupled assessment and represent the modelled slide surface with the lowest yield acceleration for the given material parameters and failure mechanism. Those rows highlighted in grey represent the material parameters that gave the closest match between the modelled and recorded permanent displacements, for a given earthquake and failure mechanism. Modelled displacements are rounded to the nearest 0.1 m.

Cross-section	Failure mechanism	Earthquake	Critical material	Water level	Cohesion c (kPa)	Friction $\phi$ (°)	Lowest yield acceleration (g)	Modelled coseismic displacement (m)	Total inferred coseismic displacement (m)
2	Translational block slide	22 February 2011	Coll/Dist. breccia <sup>1</sup>	Dry	22	45	0.47	0.4	0.3–0.7
2	Translational block slide	22 February 2011	Coll/Dist. breccia <sup>1</sup>	Dry	10	30	0.44	0.4	0.3–0.7
2	Translational block slide	22 February 2011	Coll/Dist. breccia <sup>1</sup>	Dry	0	28	0.35	0.7	0.3–0.7
2	Translational block slide	22 February 2011	Coll/Dist. breccia <sup>1</sup>	Dry	15	21	0.31	0.8	0.3–0.7
2	Translational block slide	22 February 2011	Coll/Dist. breccia <sup>1</sup>	Max recorded <sup>3</sup>	15	21	0.18	1.8	0.3–0.7
2	Translational block slide	13 June 2011	Coll/Dist. breccia <sup>1</sup>	Dry	0	28	0.35	<0.1	0.2–0.4
2	Translational block slide	13 June 2011	Coll/Dist. breccia <sup>1</sup>	Dry	15	21	0.31	0.1	0.2–0.4
2	Translational block slide	13 June 2011	Coll/Dist. breccia <sup>2</sup>	Dry	15	21	0.25	0.2	0.2–0.4
2	Translational block slide	13 June 2011	Coll/Dist. Breccia <sup>1</sup>	Max recorded <sup>3</sup>	15	21	0.18	0.4	0.2–0.4
3	Translational block slide	22 February 2011	Colluvium <sup>1</sup>	Dry	15	21	0.22	1.2	0.1–0.4
3	Translational block slide	13 June 2011	Colluvium <sup>1</sup>	Dry	15	21	0.22	0.2	0.0–0.2
3	Translational block slide	22 February 2011	Colluvium <sup>2</sup>	Dry	15	21	0.1	2.8	0.1–0.4
3	Translational block slide	13 June 2011	Colluvium <sup>2</sup>	Dry	15	21	0.1	0.8	0.0–0.2

<sup>1</sup> Assumes loess parameters of cohesion (c) = 30 kPa and friction ( $\phi$ ) = 35°

<sup>2</sup> Assumes loess parameters of cohesion (c) = 10 kPa and friction ( $\phi$ ) = 30°

<sup>3</sup> Piezometric head levels used in the assessment were the maximum levels recorded in drillholes BH-KSY-2a and BH-KSY-8a

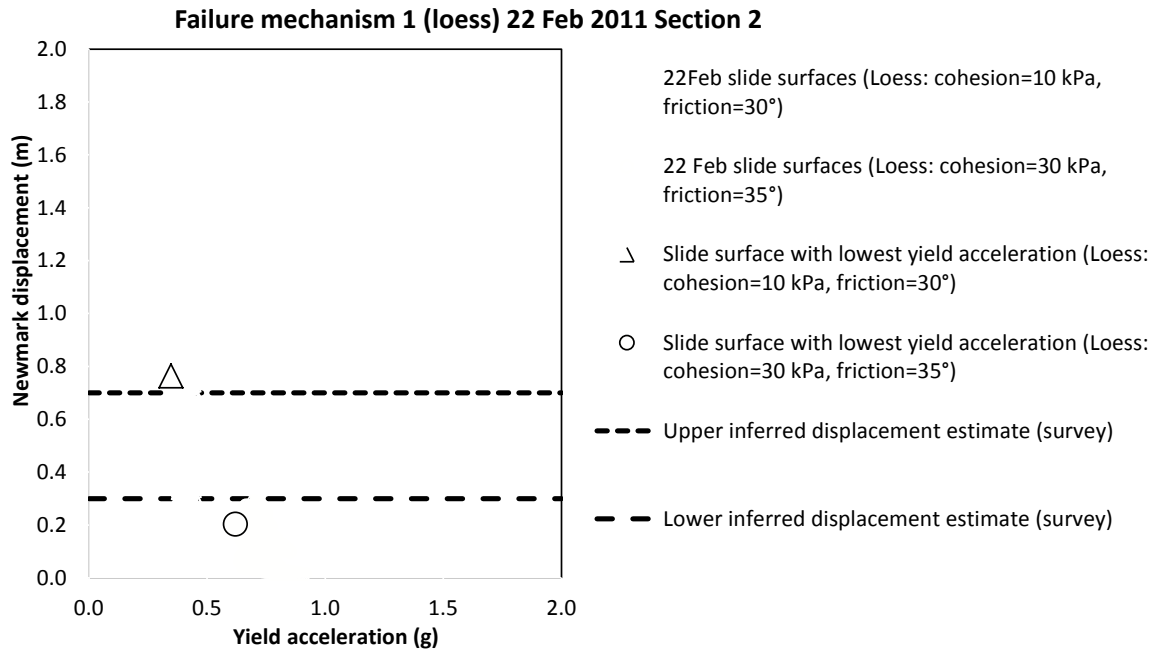


**Figure 35** Failure mechanism 1. Modelled Slope/W decoupled displacements of cross-section 2 for the 22 February 2011 earthquake and adopting variable estimates of the material strength of the loess. Each data point represents a modelled slide surface and the corresponding estimate of its displacement as a result of the 22 February 2011 earthquake – adopting the synthetic free-field rock outcrop earthquake acceleration time histories. The dashed lines represent the total inferred coseismic permanent displacement of the slope along the cross-section during the given earthquake.

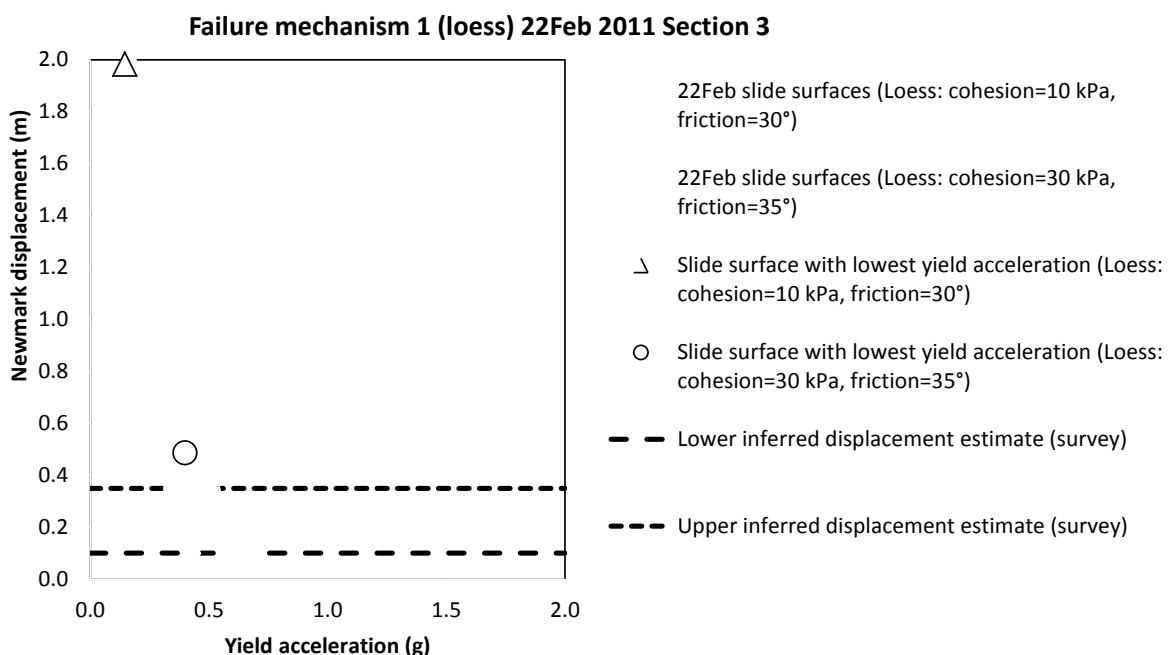


**Figure 36** Failure mechanism 1. 22 February 2011 earthquake, modelled Slope/W decoupled displacements for cross-section 3, and adopting variable estimates of the material strength of the loess. Each data point represents a modelled slide surface and the corresponding estimate of its displacement as a result of the 22 February 2011 earthquake – adopting the synthetic free-field rock outcrop earthquake acceleration time histories. The dashed line represents the inferred coseismic permanent displacement of the slope along the cross-section during the given earthquake.

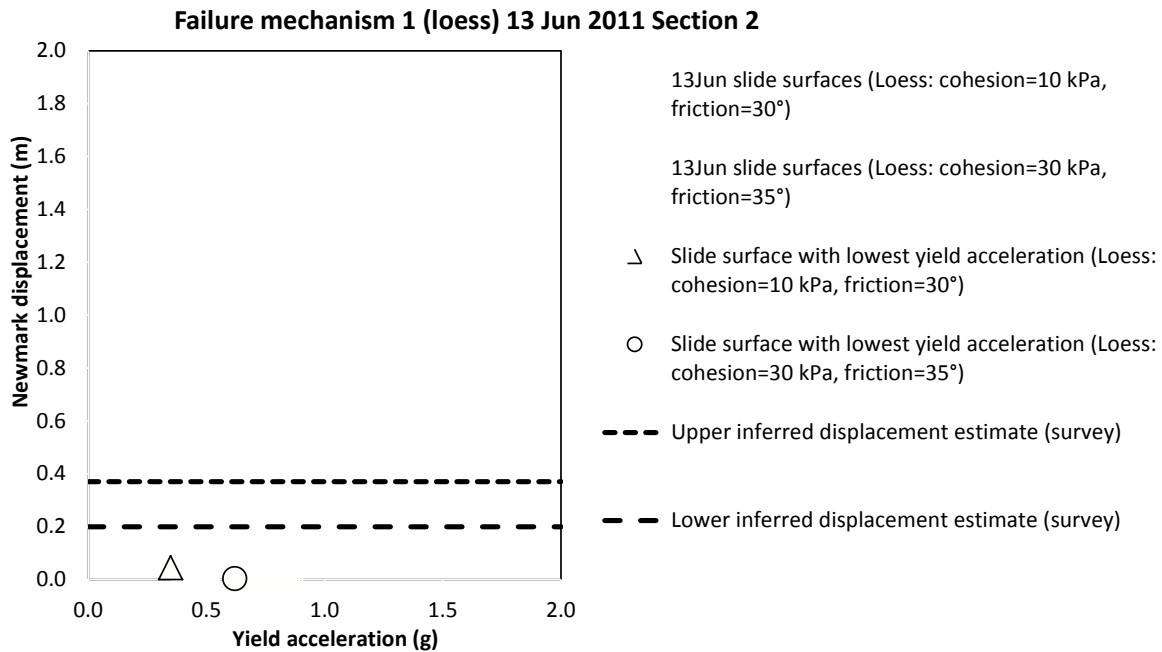


**Figure 37** Failure mechanism 1. Modelled Slope/W decoupled displacements of cross-section 2 for the 13 June 2011 earthquake and adopting variable estimates of the material strength of the loess. Each data point represents a modelled slide surface and the corresponding estimate of its displacement as a result of the 13 June 2011 earthquake – adopting the synthetic free-field rock outcrop earthquake acceleration time histories. The dashed lines represent the total inferred coseismic permanent displacement of the slope along the cross-section during the given earthquake.

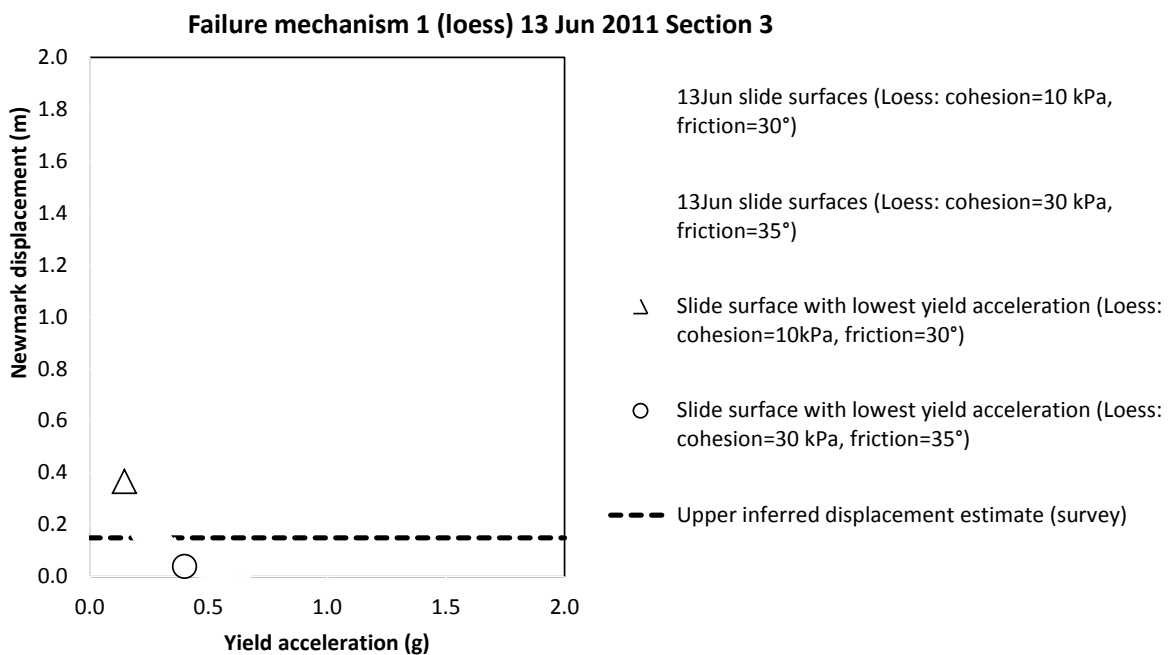


**Figure 38** Failure mechanism 1. Modelled Slope/W decoupled displacements of cross-section 3 for the 13 June 2011 earthquake and adopting variable estimates of the material strength of the loess. Each data point represents a modelled slide surface and the corresponding estimate of its displacement as a result of the 13 June 2011 earthquake – adopting the synthetic free-field rock outcrop earthquake acceleration time histories. The dashed lines represent the total inferred coseismic permanent displacement of the slope along the cross-section during the given earthquake.

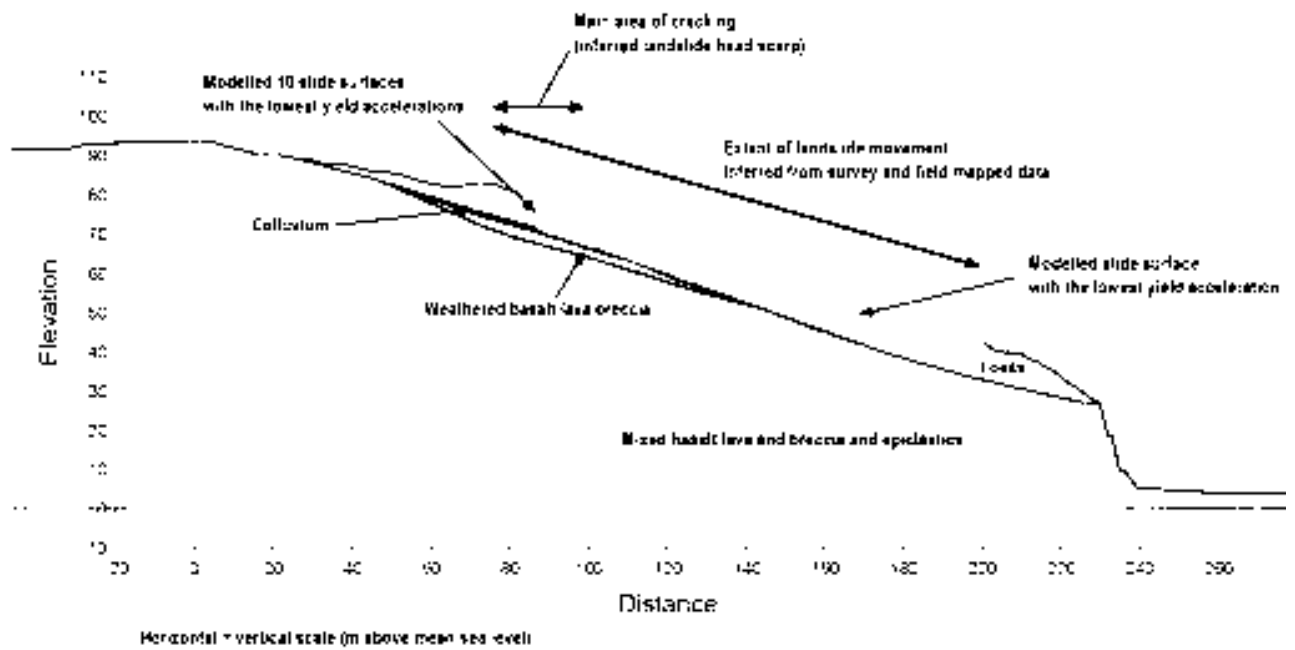


**Figure 39** Results from the seismic slope-stability assessment for failure mechanism 1, cross-section 2, for the 22 February 2011 earthquake.

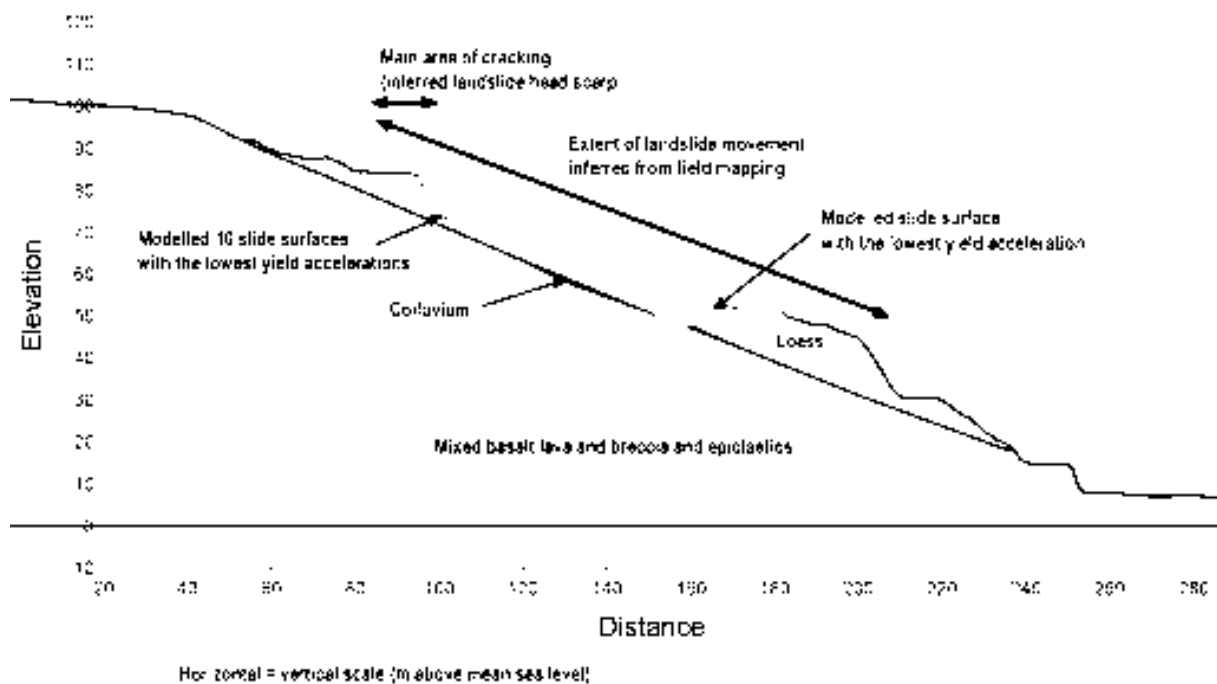


**Figure 40** Results from the seismic slope-stability assessment for failure mechanism 1, cross-section 3, for the 22 February 2011 earthquake.

### Failure mechanisms 2 and 3, 22Feb 2011 Section 2

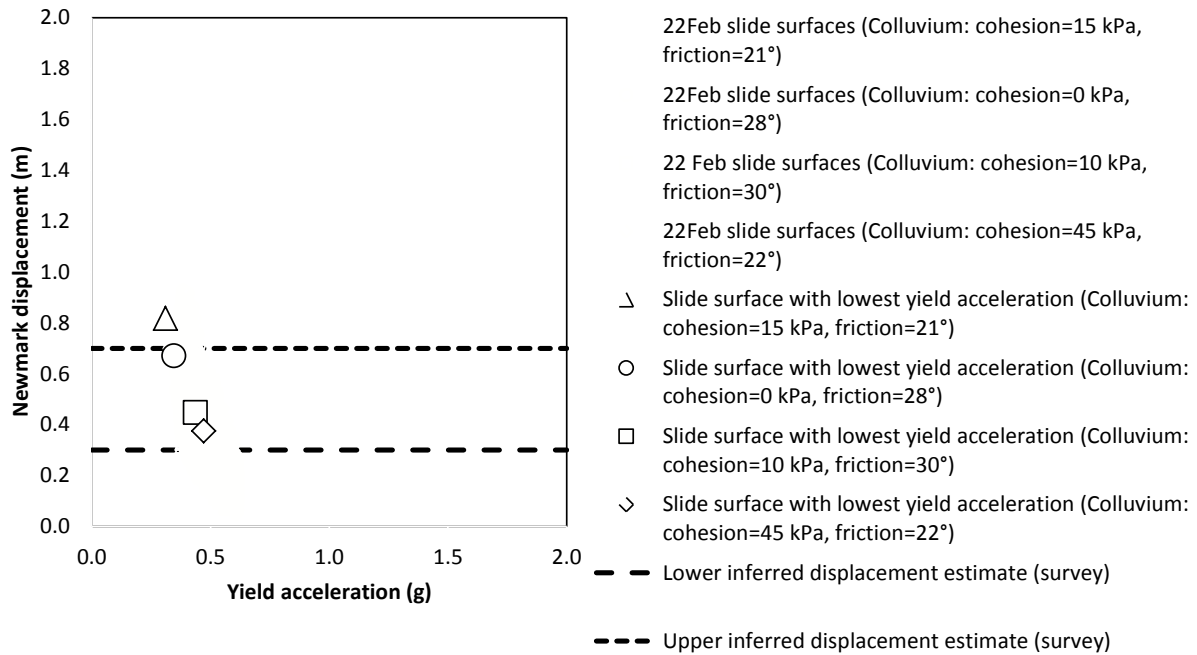


**Figure 41** Failure mechanisms 2 and 3. Modelled Slope/W decoupled displacements of cross-section 2 for the 22 February 2011 earthquake and adopting variable estimates of the material strength of the colluvium and weathered breccia. Each data point represents a modelled slide surface and the corresponding estimate of its displacement as a result of the 22 February 2011 earthquake – adopting the synthetic free-field rock outcrop earthquake acceleration time histories. The dashed lines represent the total inferred coseismic permanent displacement of the slope along the cross-section during the given earthquake.

### Failure mechanisms 2 and 3, 13 Jun 2011 Section 2

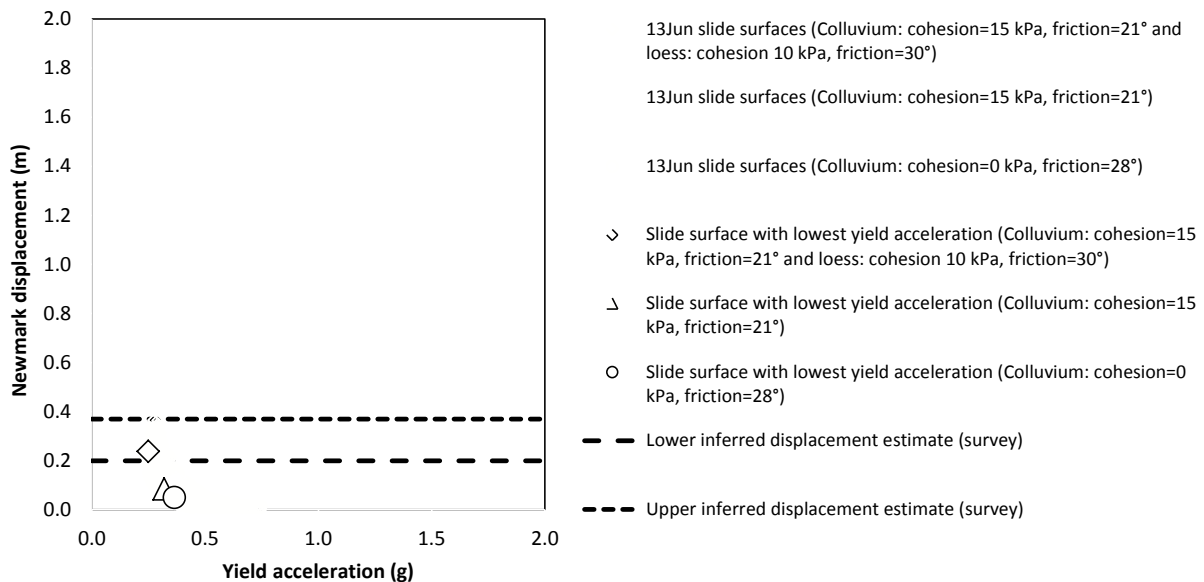


**Figure 42** Failure mechanisms 2 and 3. Modelled Slope/W decoupled displacements of cross-section 2 for the 13 June 2011 earthquake and adopting variable estimates of the material strength of the colluvium and weathered breccia. Each datapoint represents a modelled slide surface and the corresponding estimate of its displacement as a result of the 13 June 2011 earthquake – adopting the synthetic free-field rock outcrop earthquake acceleration time histories. The dashed lines represent the total inferred coseismic permanent displacement of the slope along the cross-section during the given earthquake.

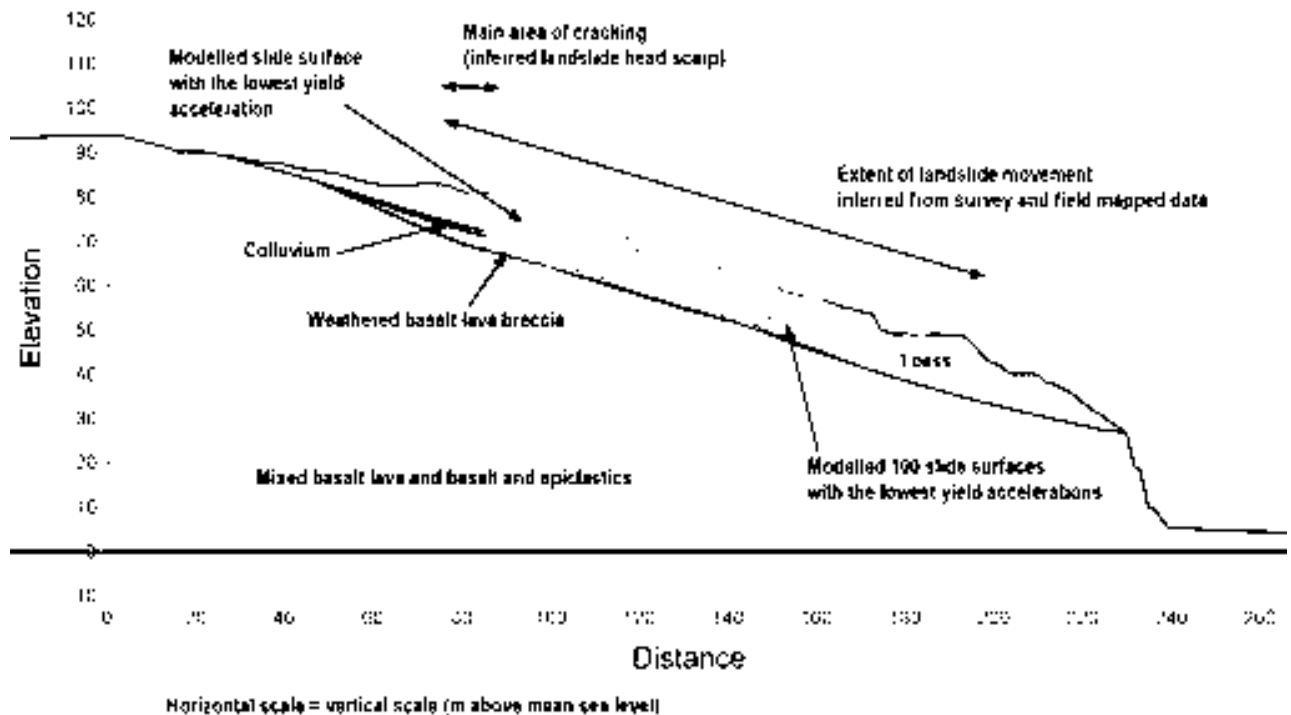


**Figure 43** Results from the seismic slope stability assessment for failure mechanisms 2 and 3, cross-section 2, for the 22 February 2011 earthquake.

The results show that:

#### 4.2.2.1 Failure mechanism 1 (loess)

##### Cross-section 2:

- A good match between the recorded permanent coseismic displacements and modelled displacements of the slope for the 22 February 2011 earthquakes was obtained for modelled slide surfaces with shear strength parameters for the loess of cohesion ( $c$ ) of 10 kPa and friction ( $\phi$ ) of  $30^\circ$ . However, the estimated permanent coseismic displacements for the 13 June 2011 earthquake, adopting the same loess parameters, were less than the measured displacements associated with this earthquake.

##### Cross-section 3:

- A good match between the recorded permanent coseismic displacements and modelled displacements of the slope for the 22 February 2011 earthquakes was obtained for modelled slide surfaces with shear strength parameters for the loess of cohesion ( $c$ ) of 30 kPa and friction ( $\phi$ ) of  $35^\circ$ . However, the estimated permanent coseismic displacements for the 13 June 2011 earthquake, using the same loess strength parameters, are less than the measured displacements associated with this earthquake. If parameters of cohesion ( $c$ ) of 10 kPa and friction ( $\phi$ ) of  $30^\circ$  are used, the modelled displacements significantly exceed those inferred from surveying.

## Both cross-sections

- The displacement results, adopting the same loess strength parameters for both cross-sections, are not consistent between the cross-sections. The failure surfaces through the loess along cross-section 3 have lower yield accelerations (0.2 g) and larger modelled permanent displacements than those along cross-section 2 (yield acceleration of 0.4 g). However, the largest displacements during all earthquakes were measured along cross-section 2. These differences are thought to be due to the angle of rock head, which is steeper along cross-section 3.
- Modelled permanent displacements of both cross-sections adopting the 16 April and 23 December 2011 earthquakes were less than 0.01 m, for shear strength parameters for the loess of (c) 10 kPa and friction ( $\phi$ ) of 30°.
- For both cross-sections there is a good match between the locations and shape of the slide surfaces derived from the limit equilibrium and finite element static stability modelling, and those from the dynamic modelling.
- The largest permanent slope displacements are for slide surfaces that pass through the entire length of the inferred mass movement source areas (A and B). These locations are consistent with those survey marks showing the largest recorded permanent slope displacements, and surface deformation patterns.

### 4.2.2.2 Failure mechanisms 2 and 3 (colluvium and weathered breccia)

#### Cross-section 2:

- A good match between the recorded permanent coseismic displacements and modelled displacements of the slope for the 22 February and 13 June 2011 earthquakes was obtained for modelled slide surfaces with shear strength parameters for the mixed colluvium and weathered basalt lava breccia of cohesion (c) of 0–10 kPa and friction ( $\phi$ ) of 21–28°. However, the estimated permanent coseismic displacements for the 13 June 2011 earthquake (0.1 m), with the same parameters, were at the lower end of the range of measured displacements (0.2–0.4 m) associated with this earthquake.
- A better match between the recorded permanent coseismic displacements and modelled displacements for the 13 June 2011 earthquake was obtained for modelled slide surfaces adopting shear strength parameters for the colluvium and weathered basalt lava breccia of cohesion (c) of 0–10 kPa and friction ( $\phi$ ) of 21–28°, along with the maximum recorded piezometric head levels. However, the estimated permanent coseismic displacements for the 22 February 2011 earthquake, adopting the same material parameters and water levels, are significantly greater than the measured displacements associated with this earthquake.
- The results where water levels (Figure 44) were included in the modelling suggest, as expected, permanent displacements would be greater when the slope is wet, as the factors of safety and therefore yield accelerations reduce (from 0.3 to 0.2 g) when modelled using the maximum recorded piezometric head levels.

- The results show a good match between the recorded permanent coseismic displacement and modelled displacements for the 22 February and 13 June earthquakes, with the lower bound colluvium and weathered basalt lava breccia material strength parameters, if slope conditions are assumed to have been dry at the time of the 22 February 2011 earthquake (which occurred in summer) (Figure 41), and wet during the 13 June 2011 earthquake (which occurred in winter) (Figure 44).

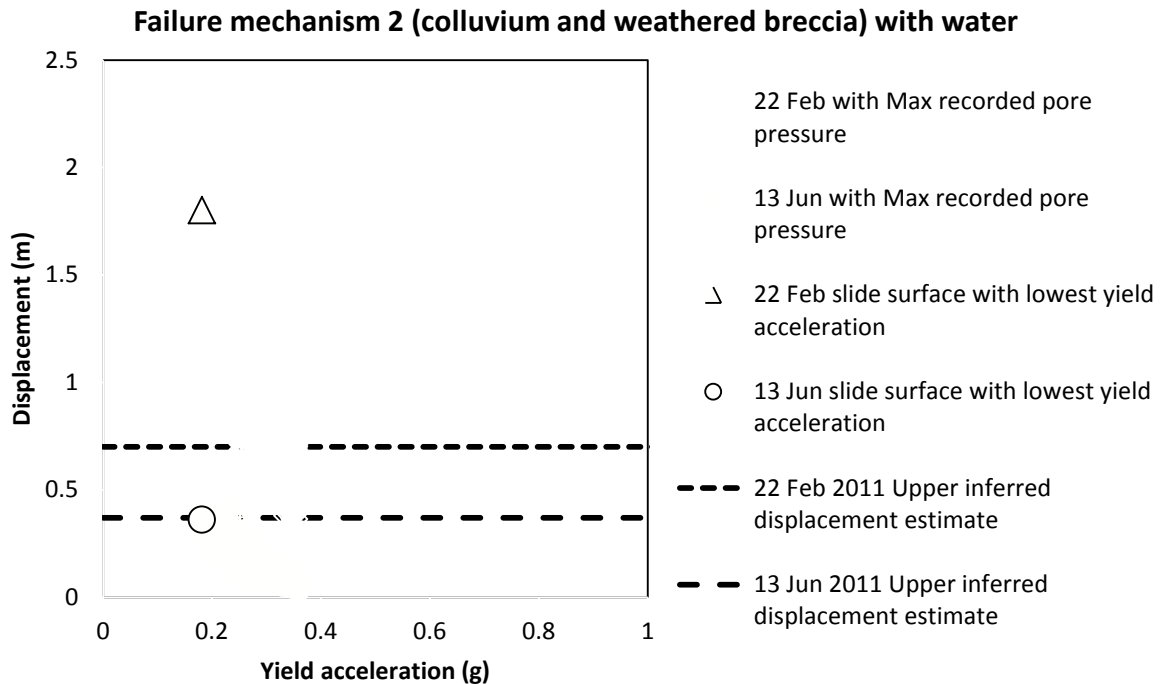


**Figure 44** Failure mechanisms 2 and 3. Modelled Slope/W decoupled displacements of cross-section 2 for the 22 February and 13 June 2011 earthquakes. Adopting the maximum recorded piezometric head levels and material strength parameters for the mixed colluvium and weathered basalt lava breccia of cohesion ( $c$ ) = 15 kPa, and friction ( $\phi$ ) = 21°, and for the loess of cohesion = 30 kPa and friction = 35°. Each data point represents a modelled slide surface and the corresponding estimate of its displacement as a result of the modelled earthquakes – adopting the synthetic free-field rock outcrop earthquake acceleration time histories. The dashed lines represent the total inferred coseismic permanent displacement of the slope along the cross-section during the given earthquake.

### Cross-section 3:

- A good match between the recorded permanent coseismic displacements and modelled displacements of the slope for the 13 June 2011 earthquake was obtained for modelled slide surfaces adopting shear strength parameters for the colluvium of cohesion ( $c$ ) of 10 kPa and friction ( $\phi$ ) of 21°. However, the estimated permanent coseismic displacements for the 22 February 2011 earthquakes, adopting the same parameters, were significantly larger (1.2 m) than the measured displacements (0.1–0.4 m) associated with this earthquake.

## Both cross-sections

- Modelled permanent displacements for both cross-sections adopting the 16 April and 23 December 2011 earthquakes were less than 0.01 m, for shear strength parameters for the mixed colluvium, and weathered breccia (section 2 only) of cohesion (c) 0–10 kPa and friction ( $\phi$ ) of 21–28°.
- For both cross-sections there is a good match between the locations and shape of the slide surfaces derived from the limit equilibrium and finite element static stability modelling, and those from the dynamic modelling.
- The largest permanent slope displacements were for slide surfaces that pass through the entire length of the inferred mass movement source areas (A and B). These locations are consistent with those survey marks showing the largest recorded permanent slope displacements and the surface deformation patterns.

### 4.2.3 Forecast modelling of permanent slope displacement

#### 4.2.3.1 Cross-section 2

Permanent displacements, from the decoupled assessment results from the 22 February and 13 June 2011 modelled earthquakes, were calculated for a range of slide-surface geometries with different ratios of yield acceleration ( $K_y$ ) to the maximum average acceleration of the failure mass ( $K_{MAX}$ ). The maximum average acceleration ( $K_{MAX}$ ) was calculated for each selected slide surface by taking the maximum value of the average acceleration time history from the response to the synthetic earthquake. About 1,000 slide surfaces were used to represent the results from each earthquake input motion. The results use estimates of the shear strength of the mixed colluvium and weathered basalt lava breccia of cohesion (c) = 0–15 kPa and friction ( $\phi$ ) of 21–28° (listed in Table 19), and assume the slope is dry.

The results from the assessment, adopting failure mechanisms 2 and 3, are shown in Figure 45, for those slide surface shown in Figure 39. The results indicate that between  $K_y/K_{MAX}$  values of 0.1 and 0.6, and  $K_y/A_{FF}$  values of 0.2 and 0.7, the data are well fitted to a straight line (an exponential trend line) in semi-log space. The coefficient of determination ( $R^2$ ) is 0.96 for  $K_y/K_{MAX}$  and 0.95 for  $K_y/A_{FF}$ , and includes all of the plotted data (N = 2000).

The peak ground acceleration of the input motion ( $A_{FF}$ ) does not take into account amplification caused by the slope geometry, or at this site, the material contrasts within the slope, between the loess/colluvium and the underlying rock (Appendix 4). From the data in Figure 45, the mean ratio of  $K_{MAX}$  to  $A_{FF}$  for cross-section 2 is 1.6 ( $\pm 0.1$  at one standard deviation), meaning that  $K_{MAX}$  is 1.7 times greater than the peak horizontal ground acceleration of the input motion, if assuming the mean plus one standard deviation of the mean.

For ratios of  $K_y/A_{FF}$  in Figure 45, the estimated displacements are consistent with those reported by Jibson (2007), where these data plot between the ranges for earthquakes of M6.5–7.5 as reported by Makdisi and Seed (1978) and plotted by Jibson (2007).

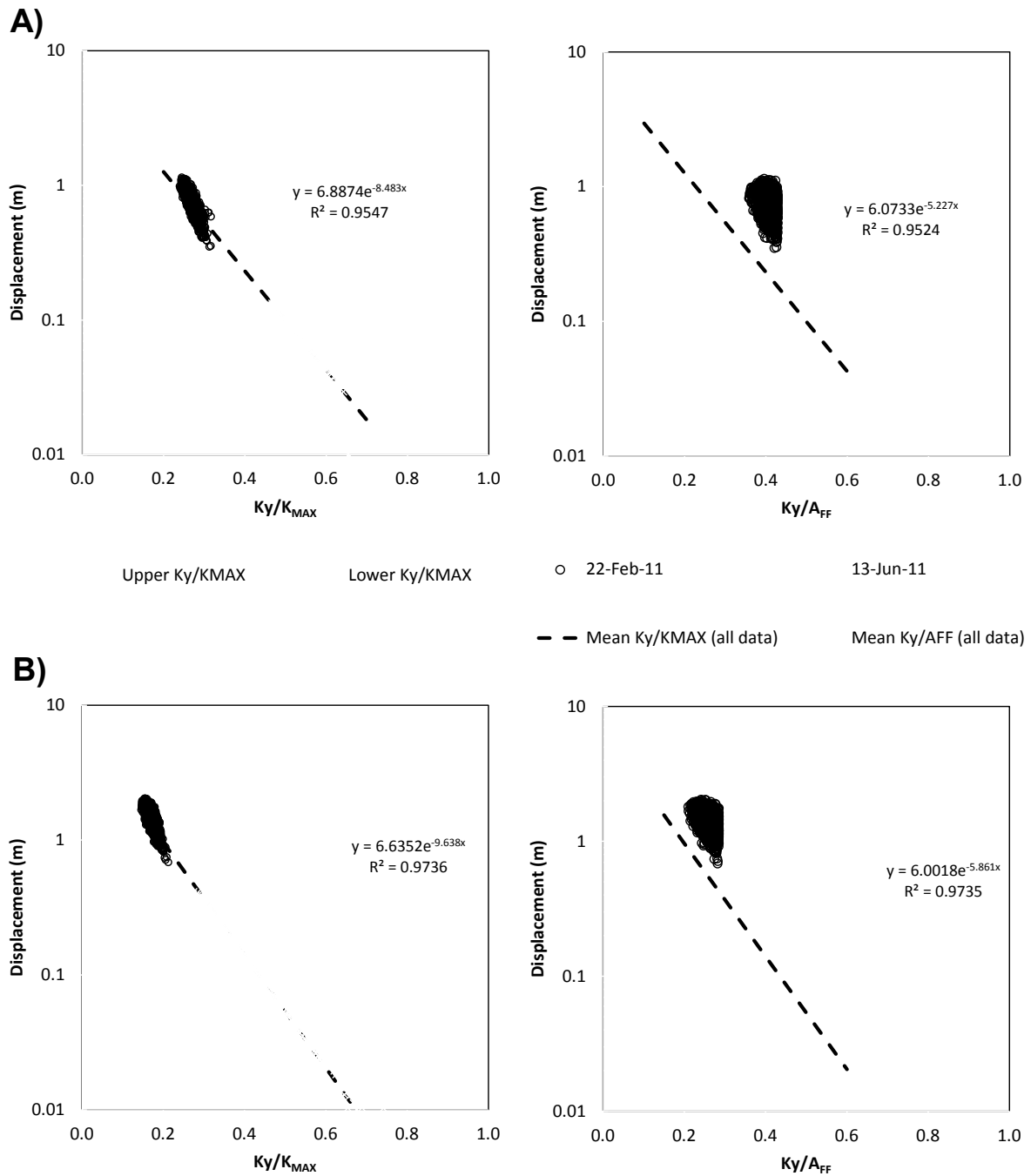


**Figure 45** Cross-section 2, failure mechanisms 2 and 3. Decoupled Slope/W displacements calculated for different ratios of yield acceleration to maximum average acceleration of the mass ( $Ky/K_{MAX}$ ), and maximum acceleration of the mass ( $Ky/A_{MAX}$ ), for selected slide-surface geometries, and material shear strength parameters of cohesion ( $c$ ) of 0-15 kPa and friction ( $\phi$ ) of 21-28°.  $A_{FF}$  is the peak acceleration of the input earthquake time acceleration history. Synthetic rock outcrop time acceleration histories for the 22 February and 13 June 2011 earthquakes were used as inputs for the assessment ( $N = 2000$ ). The dashed lines are exponential trend lines fitted to the semi-log data. The formula and the coefficient of determination ( $R^2$ ) for the trend lines are shown. **A)** Results for dry conditions. **B)** Results for when the slope is wet, when piezometric head levels are at the maximum recorded levels.

The results from the decoupled assessment show that the magnitude of permanent slope displacement during an earthquake will vary in response to the:

1. shear strength of the loess and volcanic colluvium at the time of the earthquake;
2. failure mechanism;
3. pore pressures within the slope at the time of the earthquake; and
4. duration and amplitude of the earthquake shaking.

The relationship between the yield acceleration and the maximum average acceleration (from Figure 45) was used to determine the likely range of displacements of a given failure mass with an adopted yield acceleration ( $K_y$ ) at given levels of peak free field horizontal ground accelerations ( $A_{FF}$ ) and the equivalent maximum average ground acceleration ( $K_{MAX}$ ). The results are shown in Table 24. Conservative yield accelerations were adopted to take account of the possibility that the current shear strength of the materials has degraded as a result of past displacement.

Displacement of the slide mass will not occur at maximum average accelerations ( $K_{MAX}$ ) less than the critical yield acceleration. However, the critical yield acceleration depends upon the strength of the slide surface and any pore pressures present at the time of the earthquake.

**Table 24** Forecast modelling results from the dynamic slope stability assessment for cross-section 2. Estimated displacements are rounded to the nearest 0.1 m, assumes “dry” and “wet” conditions when piezometric head levels are at the maximum recorded levels.

Cross-section	2			
Adopted yield acceleration ( $K_y$ ) (g)	Dry = 0.3, and Wet = 0.2			
Free field peak ground acceleration ( $A_{FF}$ ) (g)	0.2	0.5	0.7	1.0
Adopted $K_{MAX}$ to $A_{FF}$ <sup>1</sup> ratio	1.7 (mean + 1 standard deviation)			
Equivalent $K_{MAX}$	0.3	0.8	1.2	1.7
Estimated displacements DRY (m) based on the mean and upper trend lines fitted to the data	<0.1	0.3–0.6	0.8–1.2	1.5–2.1
Estimated displacements WET (m) based on the mean and upper trend lines fitted to the data	<0.1–0.1	0.7–1.3	1.3–2.0	2.0–3.0

<sup>1</sup>  $A_{FF}$  represents the peak horizontal ground acceleration of the free field input motion.

### 4.3 SLOPE STABILITY – SUMMARY OF RESULTS

Under current conditions, it is possible for failure of the trial slide surfaces, those representing the entire length of cross-sections 2 and 3, and corresponding to the area of mapped deformation, to occur under dynamic conditions. However, it should be noted that material strengths – and therefore the slope factors of safety – may vary through time (weathering), water content, and further movement of the slope under either static or dynamic conditions.

#### 4.3.1 Cross-section 2 (source area A)

With reference to Tables 19, 20 and 22, the main findings from the assessments are:

1. The modelled slide surfaces through the mixed colluvium and weathered basalt lava breccia (mechanisms 2 and 3), underlying the loess, best simulated the locations of cracks and compression features mapped in the field.
2. Based on the dynamic back-analysis of slope stability the minimum values of friction ( $\phi$ ) and cohesion ( $c$ ) of the mixed colluvium and/or weathered basalt lava breccia are about 21–28° and 0–15 kPa, to achieve the displacements of the slope during the 2010/11 Canterbury earthquakes, inferred from survey results.
3. The results show that the magnitudes of displacement would likely be more than double those recorded during the 22 February 2011 earthquakes, which occurred in summer, if the maximum recorded piezometric head levels were present at the time of the earthquake.
4. The static factor of safety of the assessed slope, adopting the maximum recorded piezometric head levels of 3.3 and 4.0 m above rock head, is thought to range between 1.2–1.6 and 1.4–1.8 when dry, for the failure mechanisms and range of material parameters assessed. The results indicate that the lower part of cross-section 2, adjacent to Clifton Terrace at the toe of the mapped area of deformation, has the lowest factor of safety if the colluvium and/or the weathered basalt lava breccia are assumed to be continuous along the entire length of slope. However, the presence of compression features in this lower area indicates that this part of the slope may be buttressing the upper part, implying that the mixed colluvium and weathered basalt lava breccia are not continuous over the entire slope. Given these uncertainties any changes to the stability of the lower slope could lead to movement and more rapid failure of the upper slope.
5. For failure of the assessed slide surfaces to occur under static conditions, approximately six to ten metres of piezometric head above rock head, would be needed to achieve a factor of safety of about one. It is not known whether such a piezometric head level rise is feasible, or under what weather conditions such increases might occur. It might perhaps occur if movement in an earthquake were to rupture a water main. No systematic movement, outside of survey error, of the area has been recorded since the 23 December 2011 earthquake in response to changes in the monitored piezometric head levels.
6. Given the relatively high static factors of safety (1.4–1.5) when adopting the maximum recorded piezometric levels, the assessed source area A is considered to be acceptably stable. For comparison purposes, the Hong Kong Geotechnical Engineering Office recommends for existing slopes a minimum factor of safety of 1.2, against loss of life for a ten-year return period rainfall (refer to Table 2 of GEO, 2009).
7. Under current conditions source area A is unlikely to reactivate as a large intact slide during rain. However, if conditions on the slope were to change, reactivation of the larger slide mass under very high rainfall is a possibility.
8. Smaller more localised failures of slide-blocks (and deformed retaining walls) within the overall larger area of mapped deformation (within source area A), could occur under very high rainfall, especially within the drainage lines and areas of tunnel gullying, and along Clifton Terrace where the slopes have been steeply cut in loess. Assessment of such failures is outside the scope of this report.

9. Given the moderately low yield acceleration of the slope (estimated to be in the range of about 0.2–0.3 g) it is likely that future earthquakes could reactivate the slope, leading to permanent displacements that could be quite large, especially if the slope is wet at the time of earthquake. The magnitude of any coseismic permanent displacements will depend upon:
  - a. The shear strength of the materials at the time of the earthquake;
  - b. The pore pressure/water content conditions within the slope at the time of the earthquake as affected by antecedent rainfall; and
  - c. The duration and amplitude of the earthquake shaking at the site.

#### **4.3.2 Cross-section 3 (source area B)**

With reference to Tables 19, 20 and 22, the main findings from the assessments are:

1. The modelled slide surfaces through the loess and mixed colluvium (mechanisms 1 and 2), above rock head, best simulated the locations of cracks and compression features mapped in the field.
2. Based on the dynamic back-analysis the best match between the modelled displacements and recorded displacements associated with the 22 February 2011 earthquake were for slide surfaces within the loess, with loess strength parameters of friction ( $\phi$ ) 35° and cohesion (c) 30 kPa, and assuming the mixed colluvium has the same strength parameters as the loess. With these parameters the critical yield acceleration is about 0.4 g and the static factors of safety are greater than two. However, results from modelling the 13 June 2011 earthquake, with these strength parameters, indicate that the modelled displacements are at the lower end of those recorded. By including piezometric head levels of one metre above rock head in the model (as the earthquake occurred in winter), the yield acceleration reduces to about 0.36 (equivalent to a static factor of safety of about 1.7) and the modelled displacements better match the recorded displacements.
3. Models using lower strength parameters for the loess, e.g., friction ( $\phi$ ) of 30° and cohesion (c) of 10 kPa, significantly overestimate the magnitudes of displacement for the 22 February 2011 earthquake and slightly overestimate the displacements for the 13 June 2011 earthquake. If a weak zone of mixed colluvium or weathered basalt lava breccia is included in the model underlying the loess in the central part of the slope (with friction ( $\phi$ ) 21–28° and cohesion (c) 0 – 15 kPa, the displacements for both 22 February and 13 June 2011 earthquakes are significantly greater (three metres and one metre respectively) than the recorded displacements.
4. The static factor of safety of the assessed slope, under dry conditions is thought to range between 1.6 and 1.7 for failure surface confined to the loess and adopting the lower strength of the loess of friction ( $\phi$ ) of 30° and cohesion (c) of 10 kPa. By including a thin layer of weak material such as colluvium or weathered basalt lava breccia (friction ( $\phi$ ) = 21–28° and cohesion (c) = 0–10 kPa) in the model, the static factor of safety reduces to about 1.4–1.5, and to 1.2 if these layers are assumed to be continuous across the entire site. Although a thin layer of mixed colluvium underlain by a thin zone of weathered basalt lava breccia has been identified in drillhole records in the central part of this section, it is considerably thinner, less weathered and not as continuous as similar materials located in drillholes in the adjacent source area A. These factors of safety are therefore thought to be at the lower end of the range considered to be reasonable. The presence of such a layer, with these low shear strengths, however, is not supported by the results from the dynamic back analysis.

5. For failure of the assessed slide surfaces to occur under static conditions, and assuming a weak layer of mixed colluvium and/or weathered basalt lava breccia in the model, approximately four to eight metres of piezometric head above rock head would be needed to achieve a factor of safety of about one. It is not known whether such a piezometric head level rise is feasible, or under what weather conditions such increases might occur. Again, it perhaps could occur if a water main ruptured. No systematic movement, outside of survey error, of the area has been recorded since the 23 December 2011 earthquake. Piezometric head levels and soil moisture conditions are currently not being monitored in this area.
6. Given the relatively high static factors of safety for the assessed failure surfaces, the assessed source area B is considered to be acceptably stable under static conditions (GEO, 2009).
7. Under current conditions source area B is unlikely to reactivate as a large intact slide during rain. However, if conditions on the slope were to change, reactivation of the larger slide mass under very high rainfall is a possibility.
8. Smaller more localised failures of slide-blocks (and deformed retaining walls) within the overall larger area of mapped deformation (within source area B), could occur under extreme rainfall events, especially within the drainage lines and areas of tunnel gullying. Assessment of such failures is outside the scope of this report.
9. Given the moderately low yield acceleration of the slope, estimated to be in the range of about 0.3–0.4 g when adopting loess strength parameters of cohesion = 30 kPa and friction = 35° (as per the results that gave the best match between modelled and recorded displacements), it is likely that future earthquakes could reactivate the slope, leading to permanent displacements that could be moderately large, especially if the slope is wet at the time of earthquake. The magnitude of any coseismic permanent displacements will depend upon:
  - a. The shear strength of the materials at the time of the earthquake;
  - b. The pore pressures and water content within the slope at the time of the earthquake as affected by antecedent rainfall; and
  - c. The duration and amplitude of the earthquake shaking at the site.

### 4.3.3 Landslide hazard

Figure 26, from earlier in the report, is a map showing the locations of the different types of landslide hazard identified in the assessment area. These landslide hazards are:

1. Cliff-collapse hazards, comprising debris avalanches and cliff-top recession. These are anticipated to occur from anywhere along the steep cliff. The risk from cliff-collapse hazards is addressed for this site in Massey et al. (2012). Re-assessment of the risk from these hazards was not undertaken for this report.
2. Earth/debris slides, represented by source areas A and B, and including small slides within these larger areas.
3. Tunnel gullying, gully erosion and earth/debris flows (Figure 46, Map 2), could occur from anywhere within the assessment area, but are more likely to occur along the drainage lines and the steep cut slopes along Clifton Terrace. They are likely to be small in volume (historically less than 100 m<sup>3</sup> in the Port Hills).

## 5.0 RISK ASSESSMENT RESULTS

Whether or not the assessed landslide source areas pose a life risk depends on the ability of the landslide mass to break down during a movement episode to form a more mobile flow-type landslide, which is usually a function of the magnitude and speed of movement. Based on past performance, the landslide is moving as a “coherent” block slide, where houses are essentially on slide-block rafts within the larger landslide, and where dwellings located in the head scarp (tension) and toe areas (compression) have suffered the most damage.

Results from the assessment indicate that, under current conditions it is unlikely the slide mass would break down during a coseismic or rainfall triggered movement episode to form an earth/debris flow, because: 1) the high static factors of safety suggest reactivation of the larger slide mass is unlikely under static conditions; 2) the assessed coseismic magnitudes of displacement are relatively small with regards to the size of the displaced mass; and 3) should movement occur, the slope angles in the assessed source areas are relatively low and the angles of the assessed slide surfaces are equally low.

This section describes the results from the assessment of the earth/debris slides only; it does not assess the runout of debris associated with earth/debris flows, as the potential for such flows to occur has been assessed as low. For the risk associated with the cliff collapse hazards refer to Massey et al. (2012).

### 5.1 TRIGGERING EVENT FREQUENCIES

Movements of the earth/debris slides in the assessed source areas are thought to mainly be triggered by earthquakes (dynamic conditions) and possible increased pore pressures in response to very heavy rain, although movement in response to rain has not yet been measured.

### 5.2 FREQUENCY OF EARTHQUAKE TRIGGERS

For earthquake triggers, the frequency of a given free-field peak ground acceleration occurring was obtained from the Expert Elicitation Seismic Hazard Model for Christchurch (Table 25) (Gerstenberger et al., 2014). The increased level of seismicity in the Christchurch region is incorporated in a modified form of the 2010 version of the National Seismic Hazard Model (Stirling et al., 2012).

#### 5.2.1.1 Peak ground acceleration and permanent slope displacement

For these assessments, peak ground acceleration is used to represent earthquake shaking intensity, as peak ground acceleration is the ground-motion parameter directly related to the forces involved in coseismic landslide initiation (Wartman et al., 2013).

The estimated magnitude of permanent slope displacement of the source areas in a future earthquake was based on the decoupled assessment results from cross-section 2. The permanent displacement of each source area at a given level of free-field peak ground acceleration ( $A_{FF}$ ) was estimated from the relationship between the yield acceleration ( $K_y$ ) and the maximum average acceleration of the mass ( $K_{MAX}$ ) (Figure 45). Different levels of peak ground acceleration were used and each multiplied by the site-specific ratio of  $K_{MAX}$  to

$A_{FF}$  (assuming the mean plus one standard deviation) to estimate the equivalent maximum average acceleration of the mass ( $K_{MAX}$ ) for the given value of  $A_{FF}$ . For example, an  $A_{FF}$  of 0.2 g would have an equivalent  $K_{MAX}$  of 0.3 g, assuming a ratio of 1.7.

**Table 25** The annual frequency of a given peak ground acceleration occurring on rock (site class B) for different years adopting the Expert Elicitation Seismic Hazard Model for Christchurch (Gerstenberger et al., 2014), and the associated estimated permanent displacement of cross-section 2. Note: these are free-field rock outcrop peak ground accelerations (equivalent to  $A_{FF}$ ).

<b>Free field peak horizontal ground accelerations (<math>A_{FF}</math>)<sup>1</sup> (g)</b>	<b>0.2</b>	<b>0.5</b>	<b>0.7</b>	<b>1.0</b>
Year 2016 annual frequency of event (from NSHM)	0.090	0.0157	0.0059	0.00164
Year 2016 return period (years)	11	64	169	610
Next 50-year average annual frequency of event (from the NSHM)	0.042	0.0072	0.0027	0.00076
Next 50-year average return period (years)	24	139	370	1316
Adopted $K_{MAX}$ <sup>2</sup> to $A_{FF}$ ratio	1.7 (mean + 1 STD)			
Equivalent $K_{MAX}$ for the given $A_{FF}$	0.3	0.8	1.2	1.7
<b>Estimated displacements DRY (m) for Yield acceleration (<math>K_y</math>) of 0.2 (g)</b>	<b>0.1–0.1</b>	<b>0.3–0.6</b>	<b>0.8–1.2</b>	<b>1.5–2.1</b>
<b>Estimated displacements WET (m) for Yield acceleration (<math>K_y</math>) of 0.3 (g), with maximum recorded piezometric head levels</b>	<b>&lt; 0.1</b>	<b>0.7–1.3</b>	<b>1.3–2.0</b>	<b>2.0–3.0</b>

<sup>1</sup>  $A_{FF}$  represents the peak horizontal ground acceleration of the free field synthetic input motion.

<sup>2</sup>  $K_{MAX}$  represents the maximum average acceleration of the failure mass taken from the relationship in Figure 45.

### 5.2.1.2 Permanent slope displacement and likelihood of catastrophic slope failure

It is difficult to estimate the probability of triggering a failure leading to catastrophic slope collapse where the debris forms an earth/debris flow which runs out down slope. Given the inferred translational movement mechanism of the assessed slide surfaces and the relatively low angle of the larger slope in the area, it is unlikely, under current conditions, that the larger slide mass would break down to form a more mobile earth/debris flow. It is possible that permanent slope displacements could cause substantial damage to dwellings located on the assessed source areas, even if the debris does not leave the source.

The predicted levels of displacement that have been used to differentiate between safe and unsafe behaviour (Abramson et al., 2002) for various structures sited on landslides range from 0.05 m to 0.3 m. Some examples are:

- a. Hynes-Griffin and Franklin (1984) suggest that up to 0.1 m displacements may be acceptable for well-constructed earth dams.
- b. Wieczorek et al. (1985) used 0.05 m as the critical parameter for a landslide hazard map of San Mateo County, California.
- c. Keefer and Wilson (1989) used 0.1 m for coherent slides in southern California.
- d. Jibson and Keefer (1993) used a 0.05–0.1 m range for landslides in the Mississippi Valley.
- e. The State of California (1997) finds slopes acceptable if the Newmark displacement is less than 0.15 m. A slope with a Newmark displacement greater than 0.3 m is considered unsafe. For displacements in the “grey” area between 0.15 and 0.3 m, engineering judgement is required in assessment.

Permanent slope displacements during the 2010/11 Canterbury earthquakes estimated from survey marks were about 0.7 to >1.0 m, and the slope did not fail catastrophically (i.e., with the debris running out as an earth/debris flow), but dwellings were significantly damaged. However, the position of the dwelling on the displaced mass is critical to the level of damage it may sustain. For example, dwellings located in the head scarp area of cracking and compressional area in the toe of the displaced mass sustained more damage than those dwellings located in the central more intact, but displaced area.

The relationship in Figure 45 is based on past performance of the slope. However, the slope moved about one metre during the 2010/11 Canterbury earthquakes and so future displacements may be larger, given the material strengths may have been lowered by past movement, and a future larger earthquake could occur in winter when the slope is wet.

The displacements at different ratios of  $K_y/K_{MAX}$  were calculated using the synthetic earthquake acceleration time histories for the 22 February and 13 June 2011 earthquakes, which were both near-field earthquakes of short duration but high amplitude. The calculated displacements in Figure 45 represent displacements in response to these earthquakes (adopting failure mechanisms 2 and 3). Earthquakes of longer duration may affect the site in different ways. For example, the response of the loess and colluvium (at higher water contents representative of winter conditions) may be non-linear and could lead to larger permanent displacements. Conversely, the peak amplitudes relating to longer duration earthquakes from more distant sources are likely to be lower and may be insufficient to trigger displacement of the slope.

### **5.2.1.3 Deaggregation of the National Seismic Hazard Model**

The seismic performance of the slope in future earthquakes was inferred from assessing its performance in past earthquakes, mainly the 22 February, 16 April, 13 June and 23 December 2011 earthquakes, using the relationship established between peak ground acceleration and the amount of permanent slope displacement. These earthquakes varied in magnitude between M5.2 and M6.3 and were “near-field”, i.e., their epicentres were very close, within 5 km, of the Clifton Hill site.

The annual frequencies of a given level of peak ground acceleration occurring in the area are given by the National Seismic Hazard Model (Stirling et al., 2012). The National Seismic Hazard Model combines all of the various earthquake sources that could contribute to the seismic hazard at a given location. The National Seismic Hazard Model estimates for the Port Hills are based on a combination of different earthquake sources: 1) subduction interfaces; 2) mapped active faults; and 3) unknown or “background” earthquakes. For the risk assessment it is important to deaggregate the national seismic hazard model to assess which earthquake sources contribute the most to it.

R. Buxton and G. McVerry (personal communications 2014) suggest that it is magnitude M5.3–6.3 earthquakes on unknown active faults within 20 km of the site that contribute most to the seismic hazard. The earthquakes of the 22 February, 16 April 13 June and 23 December 2011 are representative of such earthquakes.

### 5.2.2 Frequency of rainfall triggers

The return period of the rainfall that could initiate failure is unknown because:

- There is evidence of historical and prehistorical landslides at the site, but these do not appear to have the morphology associated with more rapid earth/debris flows.
- The 5 March 2014 rainstorm in Lyttelton (130 mm) triggered several large earth/debris flows. The return period of the rainfall at Lyttelton was about 100 years, but the lower amount of rainfall at the Clifton Terrace site (89 mm) had a return period of only about 10–20 years;
- The monitored piezometric head levels at the site showed little response to this rain, as it occurred when the slope was relatively dry.
- It is possible that parts of the larger source areas could reactivate during rain, especially along the drainage lines and cut slope. The relatively high factors of safety for the assessed cross-sections suggest that reactivation of the entire source areas is unlikely to occur during rain, unless piezometric head levels rise to considerably higher levels than those monitored over the recent period. It is not known whether such rises are feasible, as there is no precedent, in the area, on which to base the assessment.

### 5.2.3 Overall triggering event frequency

Given the relatively low yield accelerations in the source areas (estimated to be in the range of about 0.3–0.4 g), along with their displacements during the 2010/11 Canterbury earthquakes, it is likely that future earthquakes could reactivate the slope, leading to permanent displacements that could be large enough to damage dwellings in this area.

## 5.3 RISK TO DWELLINGS

The area of slope represented by assessed source area A was highlighted in the Stage 1 report as being a Class I area. A Class I area was defined as:

- Slides, falls, topples, flows and avalanches of loess, loess and rock or rock with associated displacement in the source area of greater than 0.3 m. Once triggered the debris has potential to run-out long distances down-slope. In these locations there is potential for dwellings in the source area to be undercut and severely damaged by displacement, and for debris to impact and inundate dwellings, their occupants or road users lower down the slope. Given the velocity and long runout it is possible these types of mass movement could result in the loss of life.

Based on the results of the hazard assessment, it is unlikely that the material within the assessed source areas would break down during a coseismic or rainfall triggered movement episode to form a mobile earth/debris flow, where the debris could run-out long distances down-slope. Under current conditions this area is now re-assessed as being a Class II area, similar to source area B. A Class II area is defined in the Stage 1 report (Massey et al., 2013) as:

- Coherent slides and slumps of predominantly loess with associated cumulative inferred displacement of the mass of greater than 0.3 m, where dwellings and critical infrastructure are present within the moving mass. It is possible that renewed movement may severely impact critical infrastructure and dwellings. The level of disruption to critical infrastructure and dwellings is likely to be a function of where they are within the feature. The most hazardous places are the mainly extensional and compressional areas. Given the magnitudes of displacement it is unlikely that damage to dwellings would pose an immediate life risk to their occupants.

A 10-m wide zone is included around the boundary of the Class II hazard exposure area, where the area of slumping and cracking may enlarge in the future in an up-slope or lateral direction beyond the currently recognised boundary. This has been termed a “Class II relative hazard exposure 10 m enlargement area” (Figure 46).

The estimated displacements of the Class II area in a future earthquake depend on the nature of earthquake shaking and the critical yield acceleration of the slope, which is a function of the bulk shear strength of the loess, colluvium and other materials, at the time of the earthquake. Estimated permanent coseismic displacements of cross-section 2 were calculated for various values of peak free field ground accelerations ( $A_{FF}$ ), and these have been compared to annual frequencies of the given ground accelerations occurring.





SCALE BAR: 0 50 100 m

**EXPLANATION:**

\* Modified from reports CR2012/57 and CR2012/124  
 \*\* Taken from report CR2012/317

Background shade model derived from NZAM post earthquake 2011c (July 2011) LiDAR survey resampled to a 1 m ground resolution.  
 Roads and building footprints provided by Christchurch City Council (20/02/2012).  
 PROJECTION: New Zealand Transverse Mercator 2000

DRW:  
BL  
 CHK:  
CM, FDP



**CLIFF COLLAPSE HAZARD MAP**

**Clifton Terrace  
Christchurch**

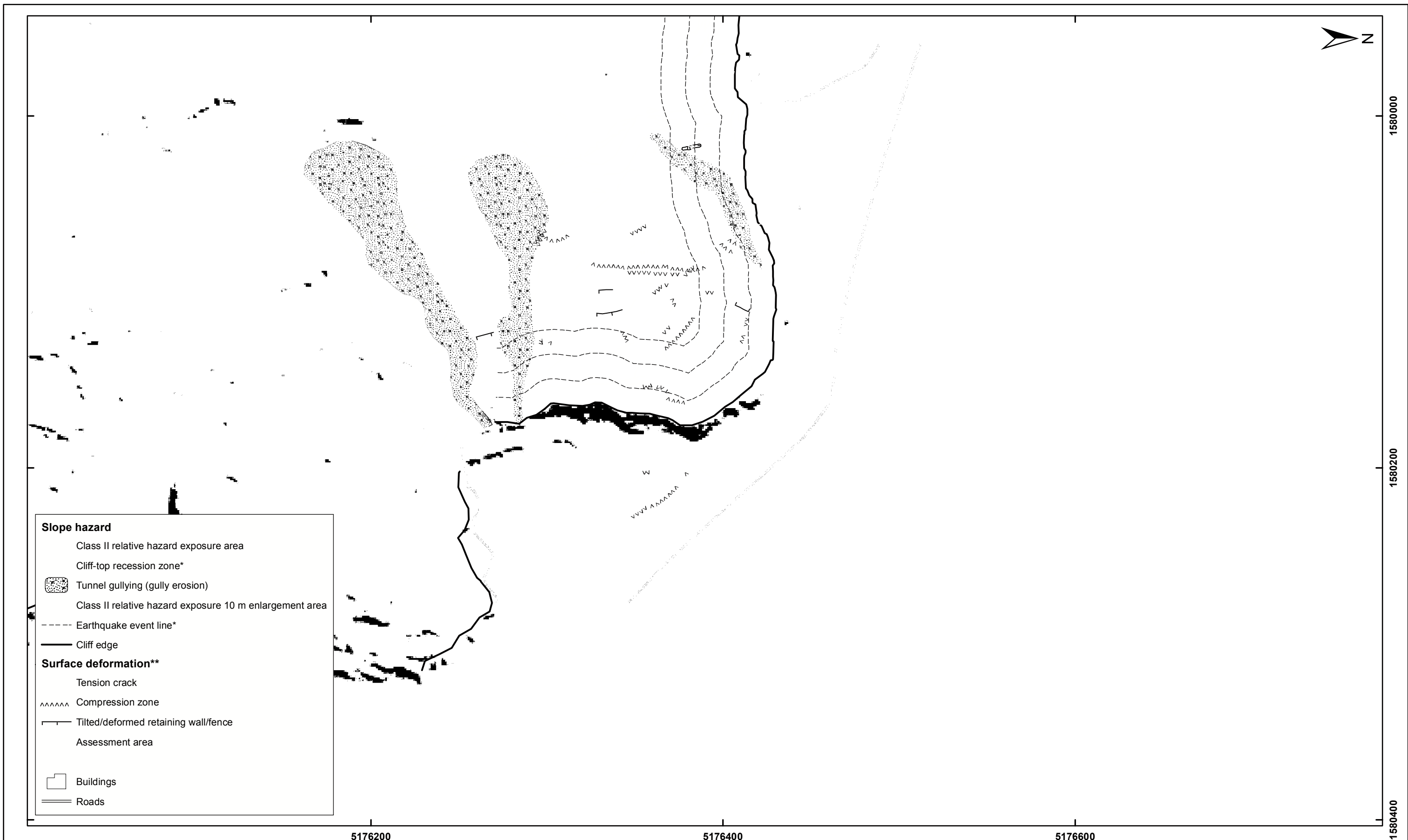
**FIGURE 46**

Map 1

**FINAL**

REPORT:  
CR2014/76

DATE:  
August 2014



**Slope hazard**

- Class II relative hazard exposure area
- Cliff-top recession zone\*
- Tunnel gullying (gully erosion)
- Class II relative hazard exposure 10 m enlargement area
- Earthquake event line\*
- Cliff edge

**Surface deformation\*\***

- Tension crack
- ^^^^ Compression zone
- Tilted/deformed retaining wall/fence
- Assessment area

Buildings

Roads

SCALE BAR: 0 50 100 m

EXPLANATION:  
 \* Modified from reports CR2012/57 and CR2012/124  
 \*\* Taken from report CR2012/317  
 Background shade model derived from NZAM post earthquake 2011c (July 2011) LiDAR survey resampled to a 1 m ground resolution.  
 Roads and building footprints provided by Christchurch City Council (20/02/2012).  
 PROJECTION: New Zealand Transverse Mercator 2000

DRW:  
BL  
 CHK:  
CM, FDP



**CLASS II RELATIVE HAZARD EXPOSURE AREA**

**Clifton Terrace  
Christchurch**

**FIGURE 46**

Map 2

**FINAL**

REPORT: CR2014/76      DATE: August 2014

## **6.0 DISCUSSION**

### **6.1.1 Annual frequency of the event**

The frequency of occurrence of events that could trigger the assessed displacements is uncertain due to the variability in the material properties and location of the slide surface. It is therefore difficult to estimate annual frequencies of movement with a high degree of confidence.

Future displacement at these sites could be more frequent, i.e., occurring at lower triggering thresholds. The area has already undergone more than one metre of permanent slope displacement during the 2010/11 Canterbury earthquakes and this displacement may have reduced the shear strength of critical materials in the slope, making the slope more susceptible to future earthquakes. At the current time there is no practical way to estimate the amount of strength reduction of the slope in terms of cohesion and friction angle.

The stability of the slope under static conditions is a function of the shear strength of the materials and the amount of water in the slope, however:

- It is more likely that failure would occur through specific zones within the loess and mixed colluvium, e.g., through more permeable zones where water contents are likely to increase more readily, or above permeability boundaries such as soil fragipans, or the mixed colluvium and weathered basalt lava breccia layer.
- Significant pore pressure above rock head and within the mixed colluvium and loess, as well as water within open cracks would also reduce the slope factor of safety.
- Given the now-cracked nature of the slopes, it is feasible that water contents of the loess and colluvium could increase more quickly and reach higher values in response to rainfall, as water can more readily enter the slope via the cracks and broken services.
- The assessed source areas appear to be part of a relict landslide. Much of the debris is still within the source areas, indicating relatively limited past displacement, although source area B appears more incised and could possibly be older or have been more incised by gully erosion, than source area A.
- Rainfall or snowmelt runoff and ingress of water through tension cracks could saturate the loess and colluvium overlying rock head, causing loss of strength leading to localised earth/debris flows with limited runout of debris. This type of failure has occurred in the past at the site, but failure volumes appear to have been relatively small. The significance of these has not been assessed.

### **6.1.2 Risk assessment sensitivity to uncertainties**

Under current conditions reactivation of source areas A and B is only thought to pose a risk to dwellings and infrastructure sited on the area, likely to be a combination of cracking and undercutting as the ground moves beneath the dwelling. Reactivation does not appear to pose a risk to life.

Guidance used by the Hong Kong Geotechnical Engineering Office (GEO, 2009), suggests a factor of safety of 1.2 should be used as the "recommended minimum factor of safety against loss of life for a ten-year return period rainfall" for category 1 slopes (where people are living on the slope).

The slopes in the assessed source areas experienced a 20-year return period rainfall in March 2013, but the rain occurred when the slope was dry and the ground water levels, which are a much better indicator of stability, did not increase. Therefore caution should be applied when comparing rainfall return period to slope stability. However, the modelled lowest factors of safety for source area A, which displaced the furthest during the main 2011 Canterbury earthquakes, are about 1.2 when adopting the maximum recorded piezometric head levels, and a continuous weak layer under the entire slide mass. About 6–10 m of piezometric head (above rock head) would be needed to reduce the factor of safety to one. For source area B the lowest modelled factors of safety based on the dynamic back analysis of modelled versus recorded displacements are about 1.7 under drained conditions. About 6–8 m of piezometric head, above rock head, would be needed to reduce the factor of safety to one. Given these high factors of safety and relatively high piezometric head levels needed to initiate movement, it is unlikely movement of source areas A and B would occur under static conditions.

If current conditions were to change adversely, however – for example as a result of earthworks (cutting or filling of material) or modification of drainage – the changes could reduce the stability of the mass, triggering movement, as well as making it more susceptible to smaller rises in piezometric head levels, and therefore larger displacements in future rainstorms and earthquakes. This could pose a risk to life, and the slope would need to be reclassified as Class I.

Conditions could also change if the steep rock cliffs, around the toe of the assessed source areas, were to fail (cliff collapse) in a future strong earthquake. Such failures in the toe of the assessed source areas could lead to undercutting of the toe, and larger displacement of the earth/debris slides, which could pose a life risk to people living on or below the assessed source areas. It is therefore important for Council to control changes and development in the assessed source areas.

## 7.0 CONCLUSIONS

These conclusions relate to the assessed earth/debris slides in the assessed source areas only. For information on the risk associated with the cliff-collapse hazards refer to Massey et al. (2012). With reference to source area boundaries as show in Figure 2, the conclusions of this report are:

### 7.1 HAZARD

1. Results from the assessment indicate that, under current conditions, it is unlikely the material in the assessed source areas would break down during a coseismic or rainfall triggered movement episode to form life-threatening earth/debris flows. The runout of debris flows and associated risk to life have, therefore not been assessed.
2. There is potential for reactivation of the assessed source areas to occur as earth/debris slides, where the debris may move as relatively intact blocks over limited distances, e.g., metres. Under current conditions, this hazard presents a significant risk to dwellings and infrastructure but not to life. This hazard is in addition to the cliff-collapse hazards at the site as assessed by Massey et al. (2012).
3. The most likely triggers for the assessed earth/debris slides are strong earthquake shaking, very high rainfall or changes to the conditions of the site as a result of, for example, construction or excavation activities.
4. The frequency of reactivation of the earth/debris slides in the future is difficult to estimate and could be anything from every few years to many hundreds of years.

### 7.2 Risk

1. Under current conditions reactivation of source areas A and B is considered to pose a risk to dwellings and infrastructure sited on the area (likely via a combination of cracking and undercutting as the ground moves beneath dwellings), but is not considered to pose a risk to life.
2. The area of slope represented by assessed source area A was highlighted in the Stage 1 report as being a Class I area. Based on the further investigation, the area (outside of the cliff collapse risk zones has been re-assessed as currently being in the same risk category as source area B (a Class II area). This classification may need to be reconsidered if circumstances change (see section ES3.1 point 3).
3. A Class II area is defined in the Stage 1 report (Massey et al., 2013) as: Coherent slides and slumps with associated cumulative inferred displacement of the mass of greater than 0.3 m, where dwellings and critical infrastructure are present within the moving mass.
4. Renewed movement in both areas could severely impact critical infrastructure and dwellings. The amount of damage to critical infrastructure and dwellings is likely to be a function of their location on the slide mass. The most hazardous places are the extensional and compressional areas where most of the surface deformation is located. Given the failure mechanisms relevant to this site and the moderate magnitudes of displacement, it is unlikely that damage to dwellings would pose an immediate life risk to building occupants.

### **7.2.1 Risk management**

1. A risk-management option of monitoring rainfall, soil moisture, pore-pressure and surface and subsurface movement in the assessed source areas may be of some value in providing warning of changing conditions that could lead to larger displacements.
2. If current conditions were to change – for example as a result of earthworks (cutting or filling of material) or modification of drainage, or undercutting as a result of earthquake-induced cliff collapses’ – the changes could reduce the stability of the mass and make it more susceptible to larger displacements in future earthquakes and rainstorms. This would require the Class II categorisation to be revisited.
3. If conditions were to change, there is also a possibility that the mass could break up to form more rapid failures with longer runout, and potentially loss of life.

## **8.0 RECOMMENDATIONS**

In order to manage the hazard at this site, and to prevent it from becoming a potential risk to life, GNS Science recommends that based on the results of this study, Christchurch City Council:

### **8.1 POLICY AND PLANNING**

1. Invoke strict controls on earthworks, drainage and other construction-related activities, as any modification to the slope, may lead earth/debris slides to develop into flows.
2. Require a detailed ground investigation and assessment of how any proposed earthworks, drainage works or other development could affect the stability of the slope.

### **8.2 SHORT-TERM ACTIONS**

#### **8.2.1 Hazard monitoring strategy**

1. Include the report findings in a slope-stability monitoring strategy with clearly stated aims and objectives, and list how these would be achieved, aligning with the procedures described by McSaveney et al. (2014).
2. Continue monitoring to identify trends and changes in slope movement. The monitoring network should be reassessed to ensure the main identified assessment areas are adequately monitored.
3. Ensure that the existing emergency management response plan for the area identifies the dwellings that could be affected by movement, and outlines a process to manage a response to renewed movement.

#### **8.2.2 Surface/subsurface water control**

Reduce water ingress into the slopes, where safe and practicable to do so, by:

1. Identifying all water-reticulation services (water mains, sewer pipes and storm water) inside the assessed source area boundaries and relocating them to locations outside the boundary, in order to control water seepage into the slope. The water main, which currently traverses along Kinsey Terrace is a particular example of such services; and
2. Controlling surface water seepage by filling the accessible cracks on the slope and provide an impermeable surface cover to minimise water ingress.

### **8.3 LONG-TERM ACTIONS**

#### **8.3.1 Engineering measures**

1. Assess the cost, technical feasibility and effectiveness of alternative longer-term engineering stabilisation measures.
2. Any proposed engineering works would require a detailed design to be carried out under the direction of an appropriately certified engineer, and should be independently verified in terms of their risk reduction effectiveness by appropriately qualified and experienced people.

### 8.3.2 Reassessment

Reassess the risk and revise and update the findings of this report in a timely fashion, for example:

1. In the event of any changes in ground conditions; or
2. In anticipation of further development or land-use decisions.

## 9.0 REFERENCES

- Abramson, L.W., Thomas, L.S., Sharma, S., Glenn, M.B. 2002. Slope stability and stabilisation methods. 2nd Edition. John Wiley and Sons Inc.
- Ashford, S.A., Sitar, N. 2002. Simplified method for evaluating seismic stability of steep slopes. *Journal of Geotechnical and Geoenvironmental Engineering* 128: 119–128.
- Bell, D.H., Glassey, P.J., Yetton, M.D. 1986. Chemical stabilisation of dispersive loessical soils, Banks Peninsula, Canterbury, New Zealand. *Proceedings of the 5th International Congress of the International Engineering Geological Society* 1: 2193–2208
- Bell, D.H., Trangmar, B.B. 1987. Regolith materials and erosion processes on the Port Hills, Christchurch, New Zealand. *Fifth International Symposium and Field Workshop on Landslides. Lausanne, A.A. Balkema. Volume 1: 77–83.*
- Bray, J.D., Rathje, E.M. 1998. Earthquake-induced displacements of solid-waste landfills. *Journal of Geotechnical and Geoenvironmental Engineering* 124: 242–253.
- Bray, J.D., Travararou, T. 2007. Simplified procedure for estimating earthquake-induced deviatoric slope displacements. *Journal of Geotechnical Engineering and Environmental Engineering*. DOI: 10.1061/(ASCE)1090-0241(2007)133:4(381)
- California, State of 1977. Analysis and Mitigation of Earthquake-Induced Landslide Hazards, Guidelines for Evaluation and Mitigation of Seismic Hazards in California, Division of Mines and Geology, California Department of Conservation Special Publication 117, Chapter 5, 15 p.
- Carey, J., Misra, S., Bruce, Z., Barker, P. 2014. Canterbury Earthquakes 2010/11 Port Hills Slope Stability: Laboratory testing factual report. GNS Science Consultancy Report CR2014/53.
- Choi, W.K. 2008. Dynamic properties of Ash-Flow Tuffs. PhD thesis, The University of Texas at Austin.
- Chopra, A.K. 1966. Earthquake effects on dams. PhD thesis, University of California, Berkeley.
- Clarke, M. 2012. Seismic refraction survey in the Port Hills of Christchurch, New Zealand. Victoria University post-graduate thesis.
- Dawson, E.M., Roth, W.H., Drescher, A. 1999. Slope stability analysis of by strength reduction. *Geotechnique* 122(6): 835–840.
- Del Gaudio, V., Wasowski, J. 2010. Advances and problems in understanding the seismic response of potentially unstable slopes. *Engineering Geology*, doi:10.1016/j.enggeo.2010.09.007.
- Eurocode 8. EN1998-5. 2004. Design of structures for earthquake resistance Part 5: Foundations, retaining structures and geotechnical aspects.
- Geotechnical Engineering Office. 2009. Geotechnical Manual for Slopes Guidance on Interpretation and Updating. Appendix 109.
- Geotechnics Ltd. 2014. GNS Science, Port Hills Inclinerometers, Christchurch. Job No. 720085.001/REP.

- Gerstenberger, M., McVerry, G., Rhoades, D., Stirling, M., 2014. Seismic hazard modelling for the recovery of Christchurch. *Earthquake Spectra* 30: 17–29.
- Goldwater, S. 1990. Slope Failure in Loess. A detailed Investigation, Allendale, Banks Peninsula. MSc thesis, University of Canterbury.
- Griffiths, G., Pearson, C., McKerchar, A.I. 2009. Review of the frequency of high intensity rainfalls in Christchurch. NIWA Client Report: CHC2009-139 for Christchurch City Council. 26 pp.
- Hoek, E. 1999. Putting Numbers to Geology – an Engineer’s Viewpoint. The Second Glossop Lecture, *Quarterly Journal of Engineering Geology* 32(1): 1–19.
- Holden, C., Kaiser, A., Massey, C.I. 2014. Broadband ground motion modelling of the largest M5.9+ aftershocks of the Canterbury 2010–2011 earthquake sequence for seismic slope response studies. GNS Science Report 2014/13.
- Hynes-Griffin, M.E., Franklin, A.G. 1984. Rationalizing the seismic coefficient method. Miscellaneous Paper No. G.L. 84-13, U.S. Army Engineer Waterways Experiment Station, Vicksburg, Mississippi.
- Ishibashi, I., Zhang, X. 1993. Unified dynamic shear moduli and damping ratios of sand and clay. *Soils and Foundations* 3(1): 182–191.
- Jibson, R.W. 2007. Regression models for estimating coseismic landslide displacement. *Engineering Geology* 91: 209–218.
- Jibson, R.W., Keefer, D.K. 1993. Analysis of the seismic origin of landslides: Examples from the New Madrid Seismic Zone. *Geological Society of America Bulletin* 21: 521–536.
- Jowett, T.W.D. 1995. An investigation of the geotechnical properties of loess from Canterbury and Marlborough. MSc thesis, University of Canterbury.
- Kaiser, A. E.; Holden, C.; Massey, C. I. 2014. Site amplification, polarity and topographic effects in the Port Hills during the Canterbury earthquake sequence, GNS Science Consultancy Report 2014/121. 33 p.
- Keefer, D.K. 1984. Landslides caused by earthquakes. *Geological Society of America Bulletin* 95(4): 406–421.
- Keefer, D.K., Wilson, R.C. 1989. Predicting earthquake-induced landslides, with emphasis on arid and semi-arid environments. *Proceedings of Landslides in a Semi-Arid Environment, Vol. 2*, Inland Geological Society, Riverside, California, pp. 118–149.
- Kim, J., Jeong, S., Park, S., Sharma, J. 2004 Influence of rainfall-induced wetting on the stability of slopes in weathered soils. *Engineering Geology* 75: 251–262.
- Kramer, S.L. 1996. *Geotechnical earthquake engineering*. Prentice Hall, Upper Saddle River, New Jersey.
- Makdisi, F.I., Seed, H.B. 1978. Simplified procedure for evaluating embankment response. *Journal of Geotechnical Engineering Division. American Society of Civil Engineers* 105(GT12): 1427–1434.
- Massey, C.I., McSaveney, M.J., Yetton, M.D., Heron, D., Lukovic, B., Bruce, Z.R.V. 2012. Canterbury Earthquakes 2010/11 Port Hills Slope Stability: Pilot study for assessing life-safety risk from cliff collapse. GNS Science Consultancy Report 2012/57.
- Massey, C.I., Yetton, M.J., Carey, J., Lukovic, B., Litchfield, N., Ries, W., McVerry, G. 2013. Canterbury Earthquakes 2010/11 Port Hills Slope Stability: Stage 1 report on the findings from investigations into areas of significant ground damage (assessed source areas). GNS Science Consultancy Report 2012/317.

- Massey, C.I., Della Pasqua, F. 2013. Canterbury Earthquakes 2010/11 Port Hills Slope Stability: Working Note 2013/05 on the interim findings from investigations into the Clifton Terrace mass movement. GNS Science report 2013/300LR.
- McDowell, B.J. 1989. Site investigations for residential development on the Port Hills, Christchurch. MSc Thesis, University of Canterbury.
- McSaveney, M.J., Litchfield, N., Macfarlane, D. 2014. Canterbury Earthquakes 2010/11 Port Hills Slope Stability: Criteria and procedures for responding to landslides in the Port Hills. GNS Science Consultancy Report 2013/171.
- Morgenstern, N.R., Price, V.E. 1965. The analysis of the stability of general slip surface. *Geotechnique* XV(1): 79–93.
- New Zealand Transport Agency (NZTA), 2013. Bridge manual (SP/M/022). 3rd edition. July 2013.
- Newmark, N. 1965. Effects of earthquakes on dams and embankments. *Geotechnique* 15: 139–160.
- Pletz, Z. 2013. Project: Clifton Hill ground investigation report. Aurecon New Zealand Ltd. 22 August 2013. Document ID: 218782-012-03-01.
- Rinaldi, V.A., Claria, J., Santamarina, J.C. 2001. The small-strain shear modulus ( $G_{max}$ ) of Argentinean loess. IV<sup>th</sup> ICSMFE 1: 495–498.
- Schanbel, P.B., Lysmer, J. Seed, H.B. 1972. SHAKE; a computer program for earthquake response analysis of horizontally layered sites. Report No. EERC 72-12, University of California, Berkeley.
- Slope Indicator 2005. Digitilt inclinometer probe. Data sheet. Geo Slope Indicator. <http://www.slopeindicator.com/pdf/digitilt-vertical-inclinometer-probe-datasheet.pdf>
- Slope/W 2012. Stability modelling with Slope/W. An engineering methodology. November 2012 Edition. GEO-SLOPE International Ltd.
- Stark, T. D., Choi, H., and McCone, S. 2005. Drained shear strength parameters for analysis of landslides. *Journal of geotechnical and geoenvironmental engineering*. pp. 575 – 588. DOI: 10.1061/(ASCE)1090-0241(2005)131:5(575)
- Stirling, M., McVerry, G., Gerstenberger, M., Litchfield, N., Van Dissen, R., Berryman, K., Barnes, P., Wallace, L., Bradley, B., Villamor, P., Langridge, R., Lamarche, G., Nodder, S., Reyners, M., Rhoades, D., Smith, W., Nicol, A., Pettinga, J., Clark, K., Jacobs, K. 2012. National Seismic Hazard Model for New Zealand: 2010 Update. *Bulletin of the Seismological Society of America* 102: 1514–1542.
- Southern Geophysical Ltd. 2013. Geophysical investigation: Borehole shear-wave testing, Port Hills, Christchurch. Southern Geophysical Ltd. Report for GNS Science.
- Tehrani, B.H. 1988. Chemical stabilisation of Whaka Terrace Loess, Christchurch. MSc Thesis, University of Canterbury.
- Tonkin and Taylor 2012a. Christchurch Earthquake Recovery Geotechnical Factual Report Kinsey / Clifton. Report prepared for the Earthquake Commission. Ref 52010.0400.
- Tonkin and Taylor 2012b. Christchurch Earthquake Recovery Geotechnical Factual Report Defender Hill. Report prepared for the Earthquake Commission. Ref 52010.0400.
- Tonkin and Taylor 2012c. Christchurch Earthquake Recovery Geotechnical Factual Report Vernon / Rapaki. Report prepared for the Earthquake Commission. Ref 52010.0400.
- Tonkin and Taylor 2012d. Christchurch Earthquake Recovery Geotechnical Factual Report Maffey's / LaCosta. Report prepared for the Earthquake Commission. Ref 52010.0400.
- Tonkin and Taylor 2012e. Christchurch Earthquake Recovery Geotechnical Factual Report Balmoral / Glendever. Report prepared for the Earthquake Commission. Ref 52010.0400

- Wartman, J., Dunham, L., Tiwari, B., Pardel, D. 2013. Landslides in eastern Honshu induced by the 2011 Tohoku Earthquake. *Bulletin of the Seismological Society of America* 103: 1503–1521, doi: 10.1785/0120120128.
- Wieczorek, G.F., R.C. Wilson, Harp, E.L. 1985. Map showing slope stability during earthquakes in San Mateo County, California. *Miscellaneous Investigations Map I-1257-E*, U.S. Geological Survey.
- Yetton, M.D. 1986. *Investigation and Remedial Methods for Subsurface Erosion Control in Banks Peninsula Loess*. MSc thesis, University of Canterbury.
- Yetton, M.D. 1992. Engineering Geological and geotechnical factors affecting development on Banks Peninsula and surrounding areas – Field guide. Bell, D.H. (ed.): *Landslides – Proceedings of the Sixth International Symposium*, Christchurch, 10–14 February 1992, Rotterdam, A.A. Balkema, Vol. 2(3).



## **10.0 ACKNOWLEDGEMENTS**

The authors thank Dr Nicola Litchfield and Dr Mauri McSaveney (GNS Science) for reviewing this report; and Dr Laurie Richards, Dr Joseph Wartman and Tony Taig for their independent reviews.



## **APPENDICES**



## **A1 APPENDIX 1: METHODS OF ASSESSMENT**

### **A1.1 METHODS OF ASSESSMENT**

#### **A1.1.1 Engineering geology assessment methodology**

The findings presented in this report are based on engineering geological models of the site developed by GNS Science.

The scope of the investigation works comprised: 1) engineering geological and geomorphological mapping of the site; 2) construction of four cross-sections through the site area; 3) interpretation of aerial photographs from 1940–2011; and 4) assessment of available LiDAR data for the site and the construction of a digital terrain model.

#### **A1.1.2 Hazard assessment methodology**

##### **A1.1.2.1 Slope stability modelling**

The key output from the static stability assessment is a factor of safety of the given volume, while the key output from the dynamic assessment is the magnitude of permanent slope displacement expected at given levels of earthquake-induced ground acceleration. These two assessments are then used to determine the likely volumes of material that could be generated under the different conditions.

##### **A1.1.2.2 Static slope stability**

If a slope has a static factor of safety of one or less, the slope is assessed as being unstable. Slopes with structures designed for civil engineering purposes are typically designed to achieve a long-term factor of safety of at least 1.5 under drained conditions, as set out in the New Zealand Transport Agency (NZTA) 3rd edition of the bridge manual (NZTA, 2013).

Static assessment of the slope was carried out by limit equilibrium method using the Rocscience SLIDE<sup>®</sup> software and the general limit equilibrium method (Morgenstern and Price, 1965). The failure surfaces were defined using the path search feature in the SLIDE<sup>®</sup> software, and a zone of tension cracks was modelled corresponding to mapped crack locations on the surface and in exposures. For the assessment, tension cracks were assumed to extend to the rock head.

Models were run based on geological cross-sections 2 and 3. The critical slide surface was determined based on the lowest calculated factor of safety. Sensitivity analyses were run assuming a range of geotechnical material strength parameters based on the estimates of their strength to test model sensitivity. These were derived from in-house laboratory testing on samples of materials taken from the site, and samples of similar materials taken from other sites in the Port Hills and published information on similar materials. Strength parameters were also assessed by back-analysis in the limit equilibrium and dynamic analyses.

The finite element modelling adopts the shear strength reduction technique for determining the stress reduction factor or slope factor of safety (e.g., Dawson et al., 1999). Finite element modelling was undertaken on the same cross-sections adopted for the limit equilibrium

modelling assessment, using the Rocscience Phase<sup>2</sup> finite element modelling software. This was done to check the outputs from the limit equilibrium modelling, because the finite element models do not need to have the slide-surface geometries defined.

### **A1.1.2.3 Dynamic stability assessment (decoupled method)**

In civil engineering, the serviceability state of a slope is that beyond which unacceptably large permanent displacements of the ground mass take place (Eurocode 8, EN-1998-5, 2004). Since the serviceability of a slope after an earthquake is controlled by the permanent deformation of the slope; analyses that predict coseismic slope displacements (permanent slope displacements under earthquake loading) provide a more useful indication of seismic slope performance than static stability assessment alone (Kramer, 1996).

The dynamic (earthquake) stability of the slope was assessed with reference to procedures outlined in Eurocode 8 (EN-1998-5, 2004) Part 5. For the Clifton Terrace assessed source areas the magnitude of earthquake-induced permanent displacements was assessed for selected cross-sections adopting the decoupled method and using different synthetic earthquake time-acceleration histories as inputs.

The decoupled seismic slope deformation method (Makdisi and Seed, 1978) is a modified version of the classic Newmark (1965) sliding block method that accounts for the dynamic response of the sliding mass. The “decoupled” assessment is conducted in two steps:

1. A dynamic response assessment to compute the “average” accelerations experienced at the base by the slide mass (Chopra, 1966); and
2. A displacement assessment using the Newmark (1965) double-integration procedure using the average acceleration time history as the input motion.

The average acceleration time history is sometimes expressed as the horizontal equivalent acceleration time history (e.g., Bray & Rathje, 1998), but they are both the same thing. The average acceleration time history represents the shear stress at the base of the potential sliding mass, as it captures the cumulative effect of the non-uniform acceleration profile in the potential sliding mass. The method assumes that the displacing mass is a rigid-plastic body, and no internal plastic deformation of the mass is accounted for.

The two steps above are described below in more detail.

1. Dynamic response assessment:
  - a. Two-dimensional dynamic site response assessment using Quake/W was carried out adopting synthetic time acceleration histories for the four main earthquakes known to have triggered debris avalanches, cliff-top deformation and cracking in the Port Hills. The modelled versus actual displacements inferred from survey results and crack apertures were compared to calibrate the models.
  - b. Synthetic out-of-phase free-field rock-outcrop time acceleration histories (vertical and horizontal) for the site – at 0.02 second intervals for the 22 February, 16 April, 13 June and 23 December 2011 earthquakes – were used as inputs for the assessment (refer to Holden et al. (2014) for details).
  - c. The equivalent linear soil behaviour model was used for the assessment, using drained conditions. Strain-dependent shear-modulus reduction and damping functions for the rock materials were based on data from Schanbel et al. (1972) and Choi (2008). At present, GNS Science do not have dynamic test data for the loess– dynamic testing is currently being carried out by GNS Science as part of a

research project. Therefore for loess shear modulus and damping ratio functions from Ishibashi and Zhang (1993) were adopted assuming a plasticity index of five (Carey et al., 2014) and variable confining (overburden) stress, based on the overburden thickness of the loess at each cross-section assessed.

- d. Shear wave velocity surveys were carried out by Southern Geophysical Ltd. for GNS Science (Southern Geophysical Ltd., 2013). These works comprised the surveying of a surface-generated shear wave signal at 2 m intervals between the surface and the maximum reachable depth inside nearby drillholes at Clifton Terrace.

## 2. Displacement assessment steps:

- a. The dynamic stress response computed with Quake/W – from each input synthetic earthquake time history – were assessed using Slope/W Newmark function to examine the stability and permanent deformation of the slope subjected to earthquake shaking using a procedure similar to the Newmark (1965) method (detailed by Slope/W, 2012).
- b. For the Slope/W assessment, a range of material strength parameters was adopted for the rock, colluvium and loess (based on the results from laboratory strength testing, published information and static back-analysis of slope stability), to assess the sensitivity of the modelled permanent deformation to changing material strength.
- c. For each trial slide surface, Slope/W uses: 1) the initial lithostatic stress condition to establish the static strength of the slope (i.e., the static factor of safety); and 2) the dynamic stress (from Quake/W) at each time step to compute the dynamic shear stress of the slope and the factor of safety at each time step during the modelled earthquake. Slope/W determines the total mobilised shear arising from the dynamic inertial forces. This dynamically driven mobilised shear force is divided by the total slide mass to obtain an average acceleration for a given slide surface at a given time step. This average acceleration response for the entire potential sliding mass represents one acceleration value that affects the stability at a given time step during the modelled earthquake.
- d. For a given trial slide surface Slope/W:
  - i. Computes the average acceleration corresponding to a factor of safety of one. This is referred to as the yield acceleration. The critical yield acceleration of a given slide mass is the minimum acceleration required to produce movement of the block along a given slide surface (Kramer, 1996). The average acceleration of the given slide mass, at each time step, is then calculated along the slide surface (base of the slide mass).
  - ii. Integrates the area of the average acceleration (of the trial slide mass) versus time graph when the average acceleration is at or above the yield acceleration. From this it then calculates the velocity of the slide mass at each time interval during the modelled earthquake.
  - iii. Estimates the permanent displacement, by integrating the area under the velocity versus time graph when there is a positive velocity.

- e. To calibrate the results, the permanent displacement of the slide mass for a given trial slide surface geometry (for a given cross-section) was compared with crack apertures and survey mark displacements, and also with the geometry and inferred mechanisms of failure that occurred during the 2010/11 Canterbury earthquakes. Those soil strength parameters that resulted in modelled displacements of similar magnitude to the recorded or inferred slope displacements were then used for forecasting future permanent slope displacements under similar earthquakes.

#### **A1.1.2.4 Forecasting permanent slope displacements**

To forecast likely slope displacements in future earthquakes, the relationship between the yield acceleration ( $K_y$ ) and the maximum (peak) acceleration ( $K_{MAX}$ ) of the average acceleration of a given slide mass, was used. Using the results from the decoupled (Slope/W) assessment, the maximum average acceleration ( $K_{MAX}$ ) was calculated for each selected slide surface (failure mass), from the average acceleration versus time plot – where the average acceleration versus time plot is the response of the given slide mass to the input acceleration history. The decoupled assessment uses the 22 February and 13 June 2011 synthetic earthquake acceleration histories as inputs (Holden et al., 2014), and the calibrated material strength parameters derived from back-analysis (bullet 2. e. above).

The  $K_y/K_{MAX}$  relationship was used to determine the likely magnitude of permanent displacement of a given failure mass – with an associated yield acceleration ( $K_y$ ) – at a given level of average acceleration within the failure mass ( $K_{MAX}$ ).

Permanent coseismic displacements were estimated for a range of selected trial slide surfaces from each cross-section. These results were then used in the risk assessment to assess the probability of failure of a given range of slide surfaces.

**A2 APPENDIX 2: RESULTS FROM SURVEYS OF CADASTRAL AND  
MONITORING SURVEY MARKS**



PlotID	Mark name	Source	Method	PlotID	Mark name	Source	Method
1	A20	Aurecon	TS	66	H7	Aurecon	TS
2	A21	Aurecon	TS	67	H8	Aurecon	TS
3	A22	Aurecon	TS	68	H9	Aurecon	TS
4	A23	Aurecon	TS	69	H10	Aurecon	TS
5	A24	Aurecon	TS	70	CLS5	GeoNet	cGPS
6	A25	Aurecon	TS	71	CLS6	GeoNet	cGPS
7	A26	Aurecon	TS	72	CLSK	GeoNet	cGPS
8	A27	Aurecon	TS	73	IR3	LINZ	RTK GPS
9	A25A	Aurecon	TS	74	Peg VI	LINZ	RTK GPS
10	B120	Aurecon	TS	75	IT XXXIV	LINZ	RTK GPS
11	B121	Aurecon	TS	76	O Nail XVI	LINZ	RTK GPS
12	B122	Aurecon	TS	77	Peg XI	LINZ	RTK GPS
13	B123	Aurecon	TS	78	III	LINZ	RTK GPS
14	B124	Aurecon	TS	79	IR I DP 384556	LINZ	RTK GPS
15	C10	Aurecon	TS	80	LP II	LINZ	RTK GPS
16	C11	Aurecon	TS	81	IT III	LINZ	RTK GPS
17	C12	Aurecon	TS	82	Peg VI DP 8514	LINZ	RTK GPS
18	C13	Aurecon	TS	83	LP XI	LINZ	RTK GPS
19	C14	Aurecon	TS	84	Peg XIa	LINZ	RTK GPS
20	C15	Aurecon	TS	85	Nail (no rec)	LINZ	RTK GPS
21	C16	Aurecon	TS	86	Peg1	LINZ	RTK GPS
22	C17	Aurecon	TS	87	Peg2	LINZ	RTK GPS
23	C18	Aurecon	TS	88	Peg3	LINZ	RTK GPS
24	C19	Aurecon	TS	89	Peg5	LINZ	RTK GPS
25	C20	Aurecon	TS	90	Peg6	LINZ	RTK GPS
26	C21	Aurecon	TS	91	Peg7	LINZ	RTK GPS
27	C22	Aurecon	TS	92	Peg8	LINZ	RTK GPS
28	C23	Aurecon	TS	93	Peg9	LINZ	RTK GPS
29	D10	Aurecon	TS	94	Peg10	LINZ	RTK GPS
30	D11	Aurecon	TS	95	Peg11	LINZ	RTK GPS
31	D12	Aurecon	TS	96	Peg12	LINZ	RTK GPS
32	D13	Aurecon	TS	97	IR2 DP 384556	LINZ	RTK GPS
33	D14	Aurecon	TS				
34	D15	Aurecon	TS				
35	D16(22)	Aurecon	TS				
36	D20	Aurecon	TS				
37	D21	Aurecon	TS				
38	E10	Aurecon	TS				
39	E11	Aurecon	TS				
40	E12	Aurecon	TS				
41	E13	Aurecon	TS				
42	E14	Aurecon	TS				
43	E15	Aurecon	TS				
44	E16	Aurecon	TS				
45	E20	Aurecon	TS				
46	E21	Aurecon	TS				
47	F1	Aurecon	TS				
48	F2	Aurecon	TS				
49	F3	Aurecon	TS				
50	F4	Aurecon	TS				
51	F5	Aurecon	TS				
52	F6	Aurecon	TS				
53	G1	Aurecon	TS				
54	G2	Aurecon	TS				
55	G3	Aurecon	TS				
56	G4	Aurecon	TS				
57	G5	Aurecon	TS				
58	G6	Aurecon	TS				
59	G7	Aurecon	TS				
60	H1	Aurecon	TS				
61	H2	Aurecon	TS				
62	H3	Aurecon	TS				
63	H4	Aurecon	TS				
64	H5	Aurecon	TS				
65	H6	Aurecon	TS				

**Survey marks**

- Monitoring (Aurecon)
- △ cGPS (GeoNet)
- Cadastral (LINZ)
- Cliff edge

**Surface deformation\***

- Tension crack
- ~~~~~ Compression zone
- Tilted/deformed retaining wall/fence
- Assessment area



<p>SCALE BAR: 0 50 100 m</p> <p>EXPLANATION: * Taken from the report CR2012/317</p> <p>Background shade model derived from NZAM post earthquake 2011c (July 2011) LiDAR survey resampled to a 1 m ground resolution. Roads and building footprints provided by Christchurch City Council (20/02/2012). PROJECTION: New Zealand Transverse Mercator 2000</p>	<p>DRW: BL</p> <p>CHK: CM, GA, FDP</p>		<p><b>SURVEY MARKS</b> Index Map</p> <p><b>Clifton Terrace</b> Christchurch</p>	<p><b>APPENDIX 2</b></p> <p>Map 1</p> <p><b>FINAL</b></p>	<p>REPORT: CR2014/76</p> <p>DATE: August 2014</p>
---	--	---	---	---	---

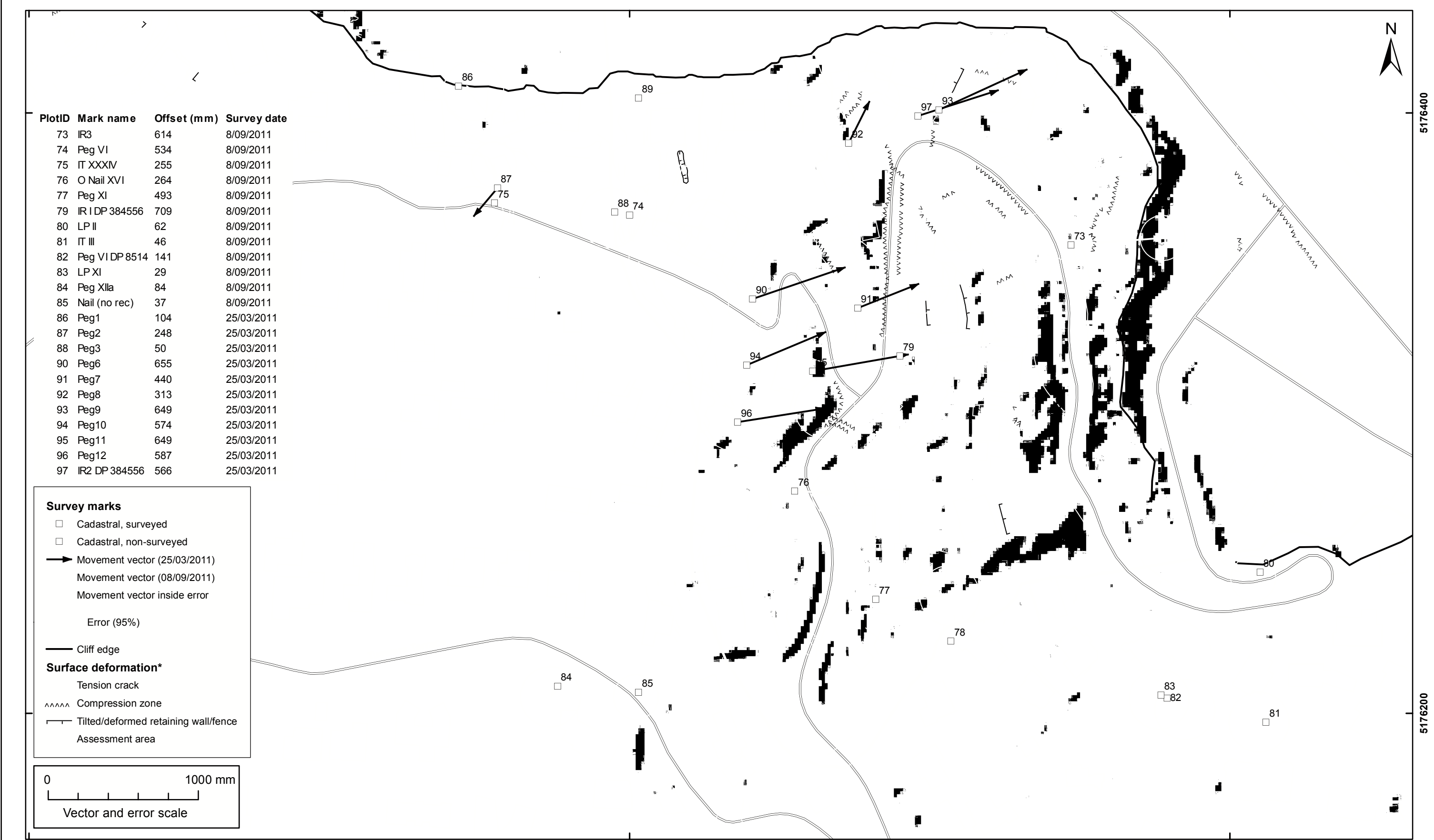
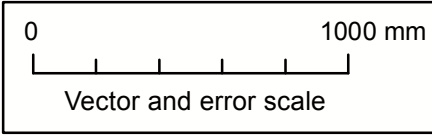
PlotID	Mark name	Offset (mm)	Survey date
73	IR3	614	8/09/2011
74	Peg VI	534	8/09/2011
75	IT XXXIV	255	8/09/2011
76	O Nail XVI	264	8/09/2011
77	Peg XI	493	8/09/2011
79	IR I DP 384556	709	8/09/2011
80	LP II	62	8/09/2011
81	IT III	46	8/09/2011
82	Peg VI DP 8514	141	8/09/2011
83	LP XI	29	8/09/2011
84	Peg Xlla	84	8/09/2011
85	Nail (no rec)	37	8/09/2011
86	Peg1	104	25/03/2011
87	Peg2	248	25/03/2011
88	Peg3	50	25/03/2011
90	Peg6	655	25/03/2011
91	Peg7	440	25/03/2011
92	Peg8	313	25/03/2011
93	Peg9	649	25/03/2011
94	Peg10	574	25/03/2011
95	Peg11	649	25/03/2011
96	Peg12	587	25/03/2011
97	IR2 DP 384556	566	25/03/2011

**Survey marks**

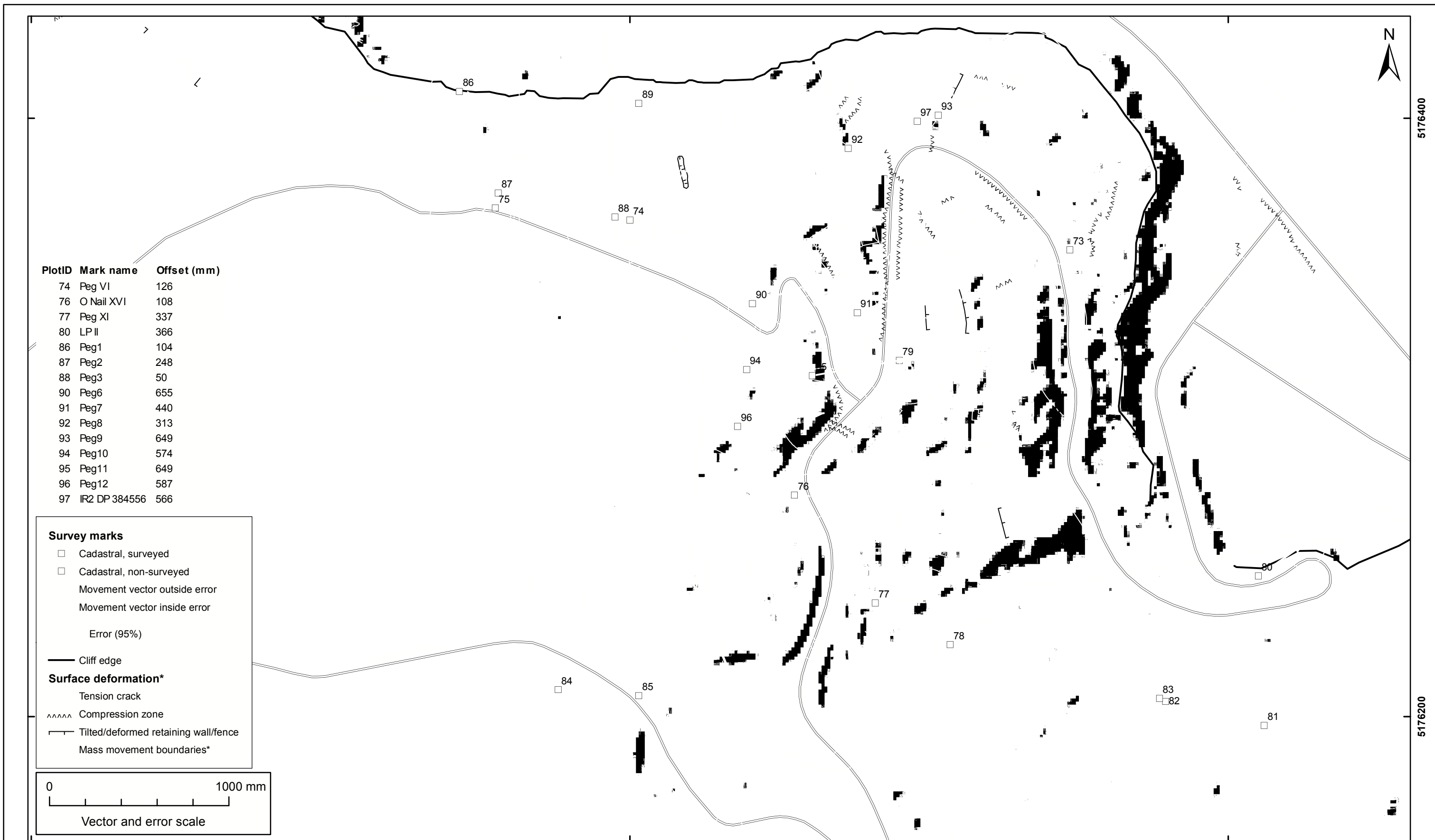
- Cadastral, surveyed
- Cadastral, non-surveyed
- Movement vector (25/03/2011)
- Movement vector (08/09/2011)
- Movement vector inside error
- Error (95%)
- Cliff edge

**Surface deformation\***

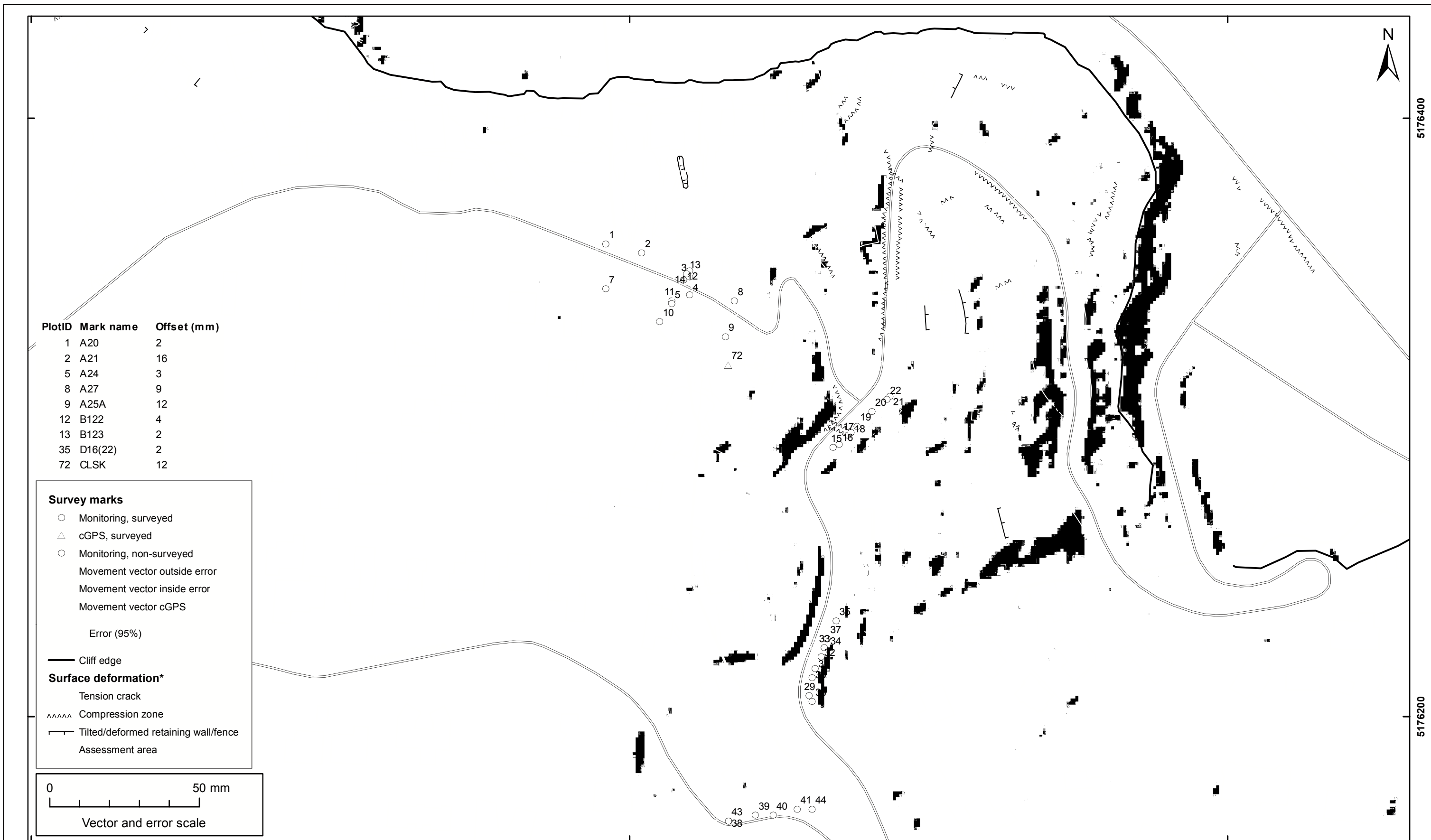
- Tension crack
- AAAAA Compression zone
- Tilted/deformed retaining wall/fence
- Assessment area



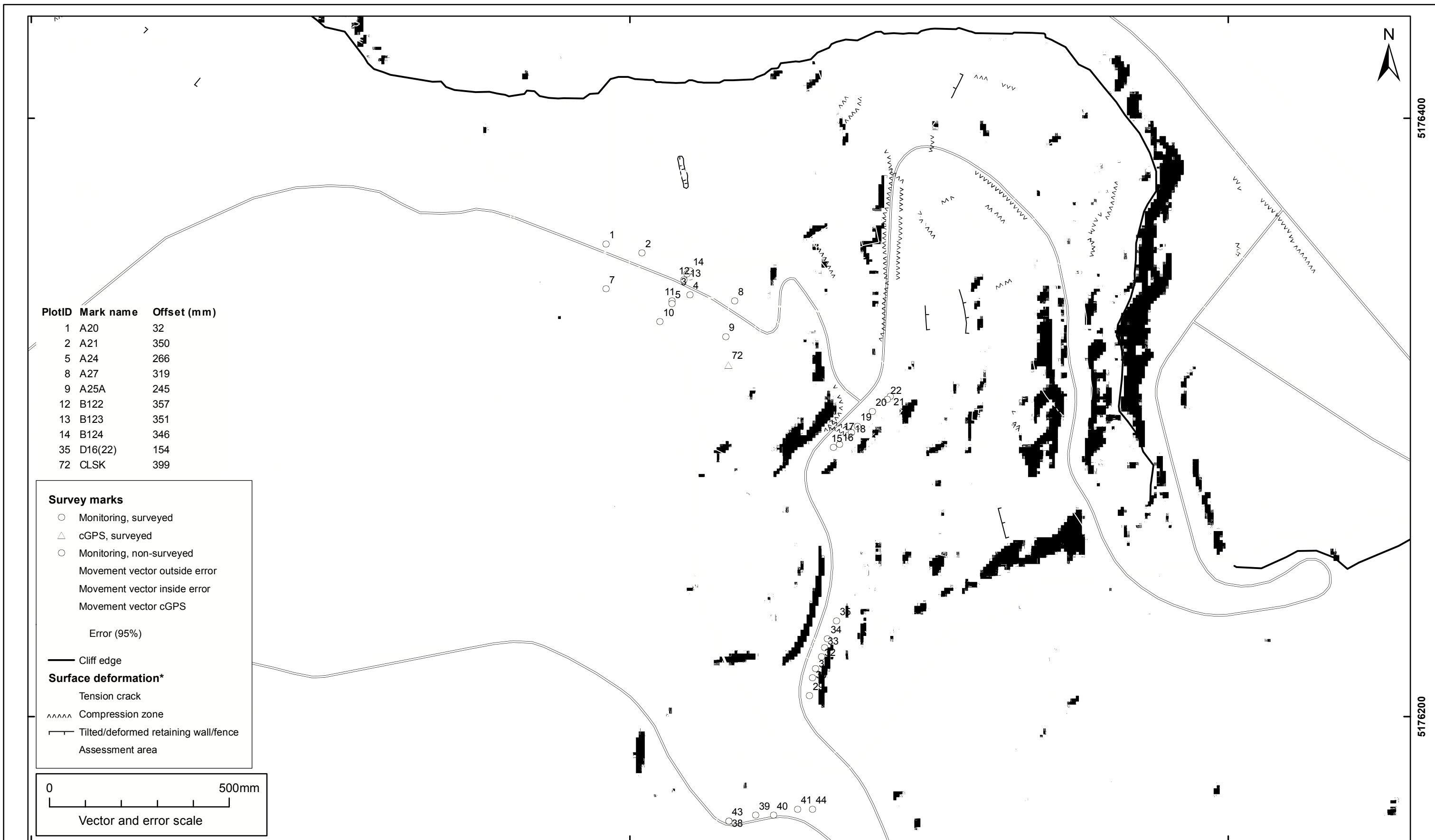
SCALE BAR: 0 50 100 m			<b>MOVEMENT VECTORS</b> <b>Cadastral Marks (Source: LINZ)</b> <b>Total Movement - Pre 22-02-2011 to the survey date</b>		<b>APPENDIX 2</b>		
EXPLANATION: * Taken from the report CR2012/317			DRW: BL	<b>Clifton Terrace</b> <b>Christchurch</b>		Map 2	
Background shade model derived from NZAM post earthquake 2011c (July 2011) LiDAR survey resampled to a 1 m ground resolution. Roads and building footprints provided by Christchurch City Council (20/02/2012). PROJECTION: New Zealand Transverse Mercator 2000			CHK: CM, GA, FDP			<b>FINAL</b>	
			REPORT: CR2014/76	DATE: August 2014			



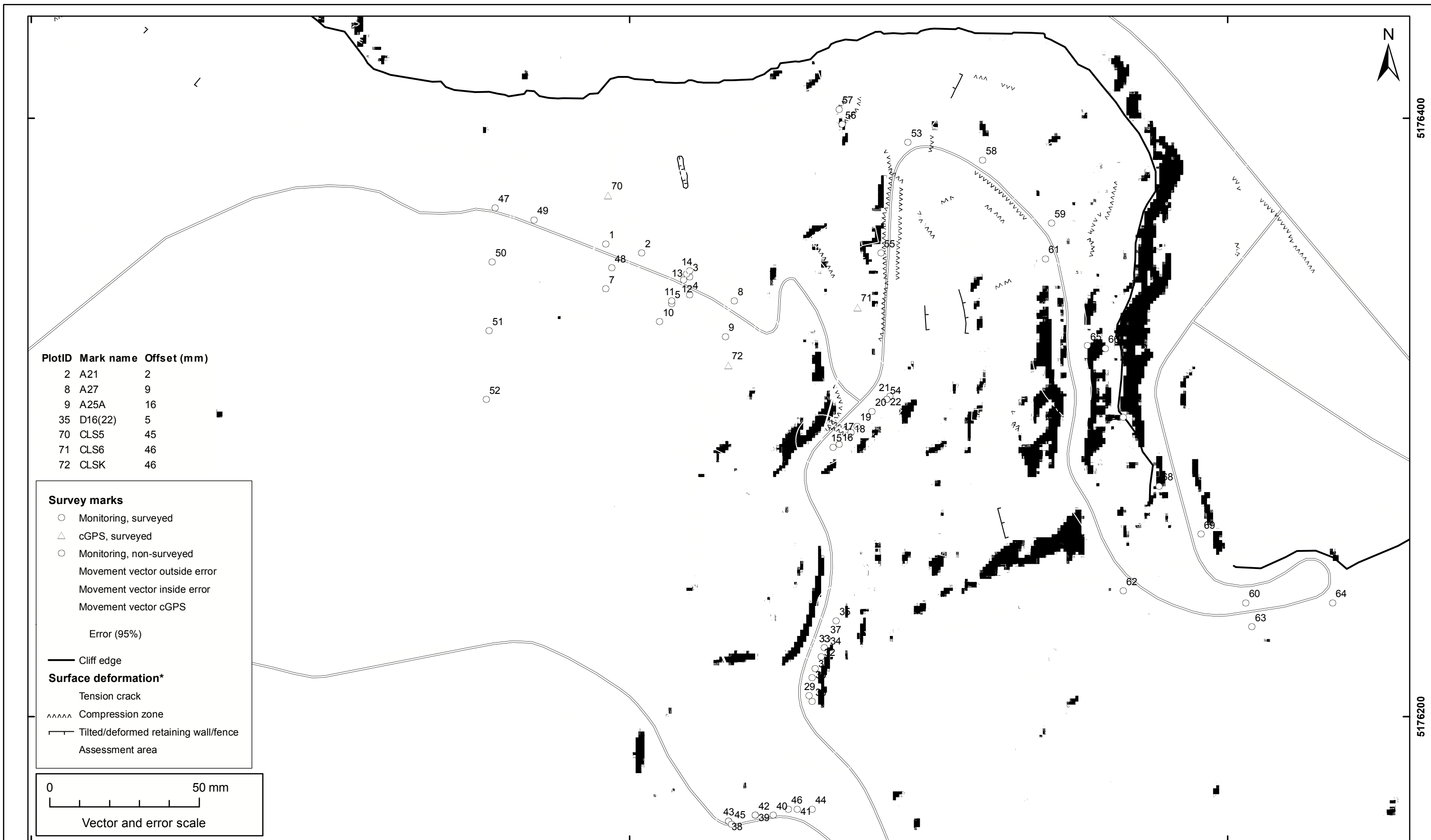
SCALE BAR: 0 50 100 m			<b>MOVEMENT VECTORS</b> <b>Cadastral Marks (Source: LINZ)</b> <b>Earthquake Related Movement - 22 Feb 2011 (M 6.2)</b>		<b>APPENDIX 2</b>		
EXPLANATION: * Taken from the report CR2012/317 Background shade model derived from NZAM post earthquake 2011c (July 2011) LiDAR survey resampled to a 1 m ground resolution. Roads and building footprints provided by Christchurch City Council (20/02/2012). PROJECTION: New Zealand Transverse Mercator 2000			DRW: BL	<b>Clifton Terrace</b> <b>Christchurch</b>		Map 3	
			CHK: CM, GA, FDP			<b>FINAL</b>	
					REPORT: CR2014/76	DATE: August 2014	



1579800		1580000		1580200			
SCALE BAR: 0 50 100 m			<b>MOVEMENT VECTORS</b> <b>Monitoring and cGPS Marks (Source: Aurecon, GeoNet)</b> <b>Earthquake Related Movement - 16 Apr 2011 (M 5.3)</b>			<b>APPENDIX 2</b>	
EXPLANATION: * Taken from the report CR2012/317 Background shade model derived from NZAM post earthquake 2011c (July 2011) LiDAR survey resampled to a 1 m ground resolution. Roads and building footprints provided by Christchurch City Council (20/02/2012). PROJECTION: New Zealand Transverse Mercator 2000						DRW: BL	
			CHK: CM, GA, FDP		<b>FINAL</b>		
			<b>Clifton Terrace</b> <b>Christchurch</b>		REPORT: CR2014/76	DATE: August 2014	



SCALE BAR: 0 50 100 m			<b>MOVEMENT VECTORS</b> <b>Monitoring and cGPS Marks (Source: Aurecon, GeoNet)</b> <b>Earthquake Related Movement - 13 Jun 2011 (M 6.0)</b>		<b>APPENDIX 2</b> Map 5	
EXPLANATION: * Taken from the report CR2012/317 Background shade model derived from NZAM post earthquake 2011c (July 2011) LiDAR survey resampled to a 1 m ground resolution. Roads and building footprints provided by Christchurch City Council (20/02/2012). PROJECTION: New Zealand Transverse Mercator 2000						
		DRW: BL			REPORT: CR2014/76	DATE: August 2014
		CHK: CM, GA, FDP				



SCALE BAR: 0 50 100 m			<b>MOVEMENT VECTORS</b> <b>Monitoring and cGPS Marks (Source: Aurecon, GeoNet)</b> <b>Earthquake Related Movement - 23 Dec 2011 (M 5.9)</b>		<b>APPENDIX 2</b>	
EXPLANATION: * Taken from the report CR2012/317 Background shade model derived from NZAM post earthquake 2011c (July 2011) LiDAR survey resampled to a 1 m ground resolution. Roads and building footprints provided by Christchurch City Council (20/02/2012). PROJECTION: New Zealand Transverse Mercator 2000			DRW: BL	<b>Clifton Terrace</b> <b>Christchurch</b>		Map 6
		CHK: CM, GA, FDP			<b>FINAL</b>	
					REPORT: CR2014/76	DATE: August 2014

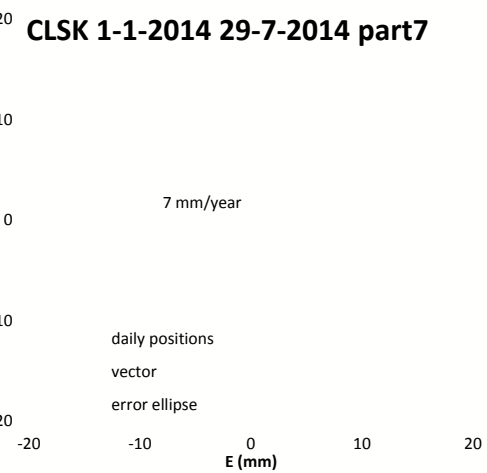
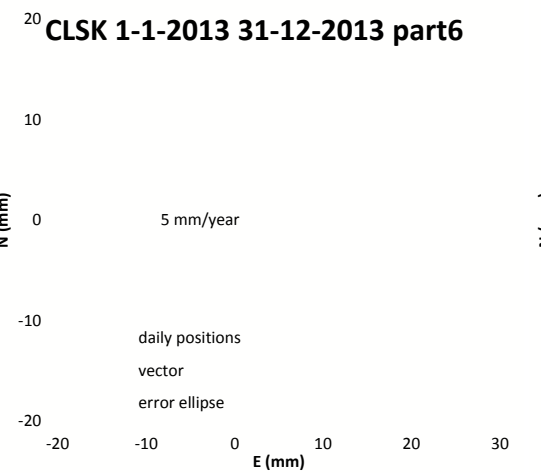
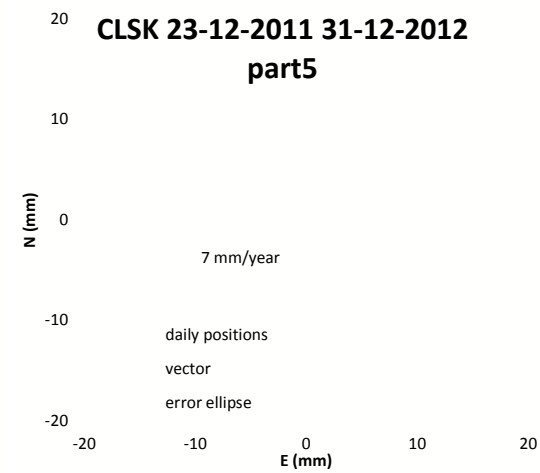
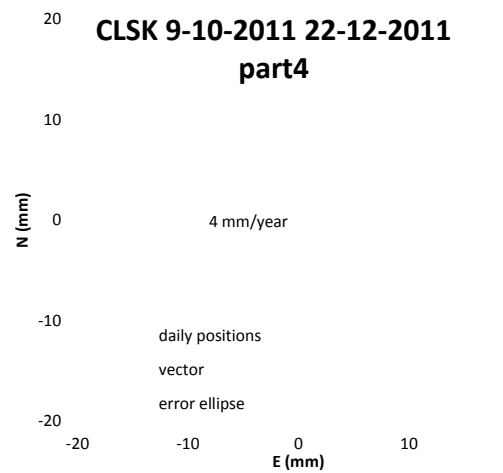
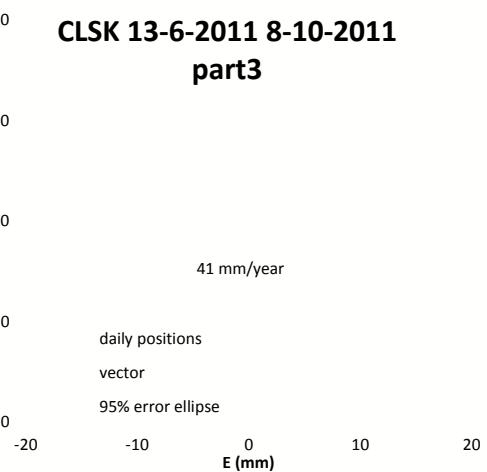
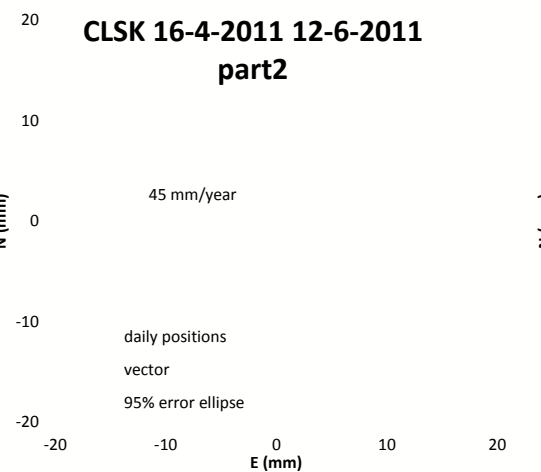
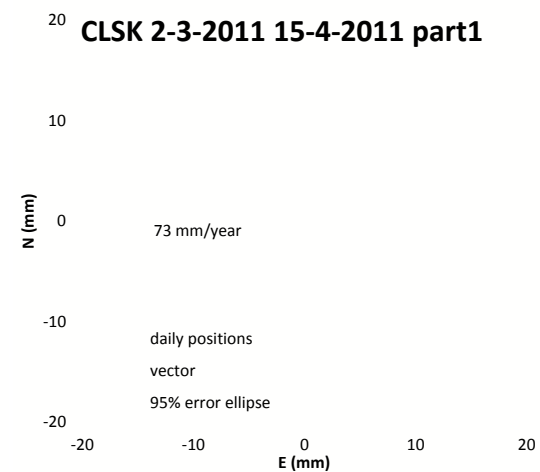
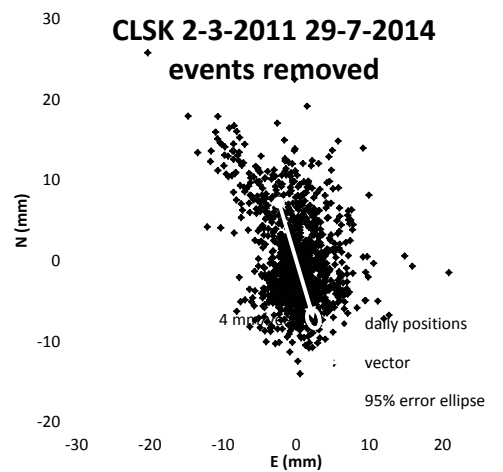
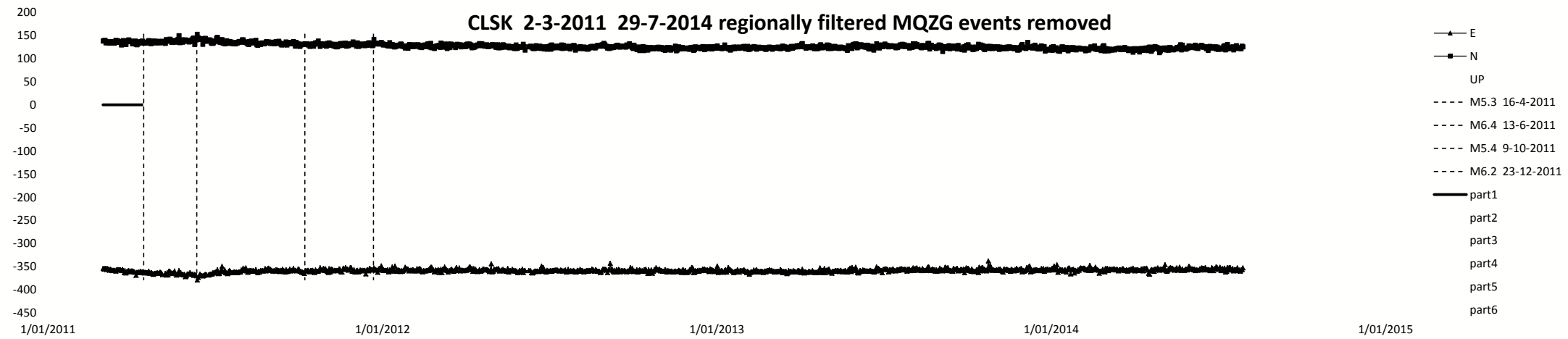
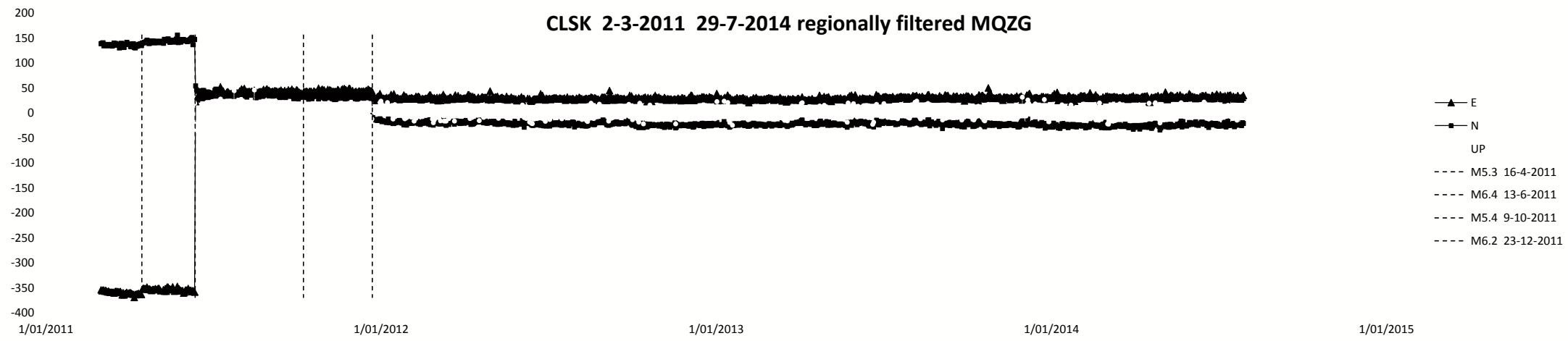


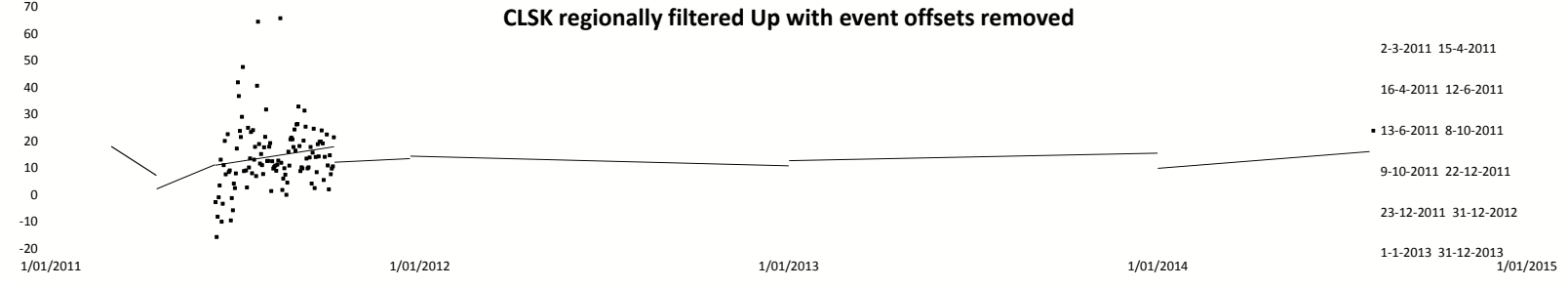
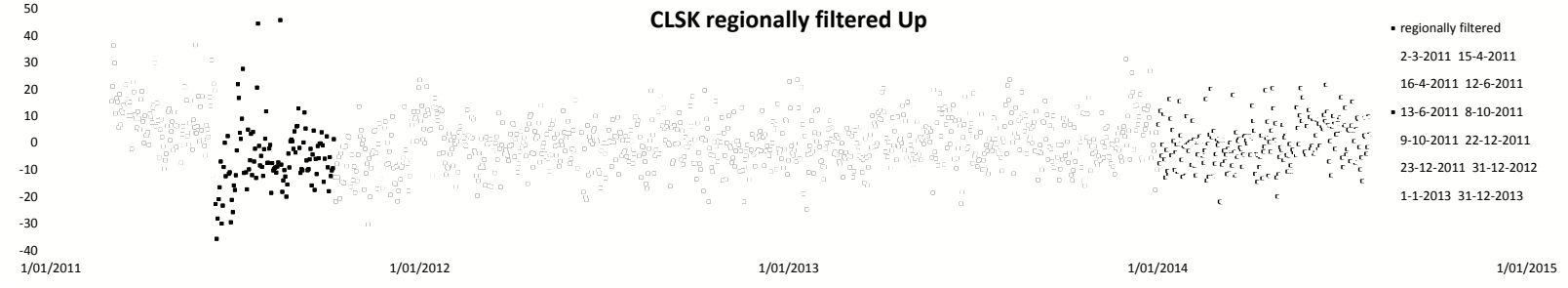
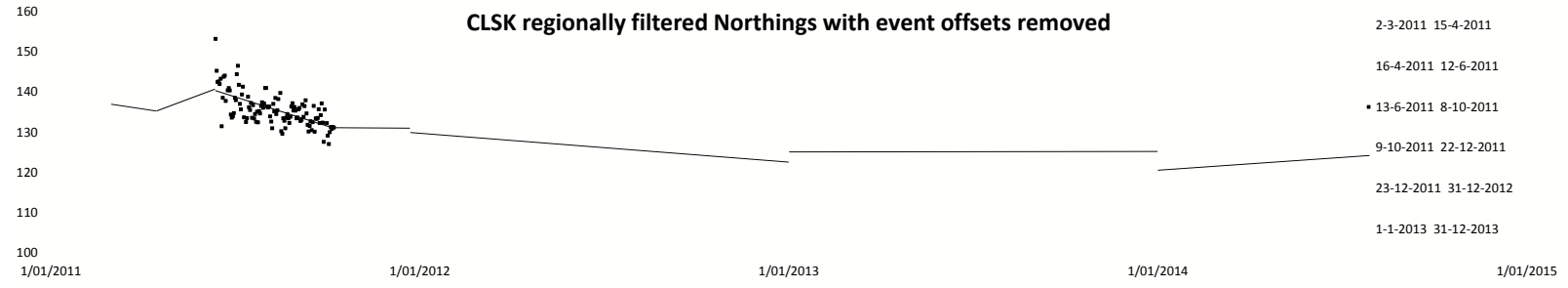
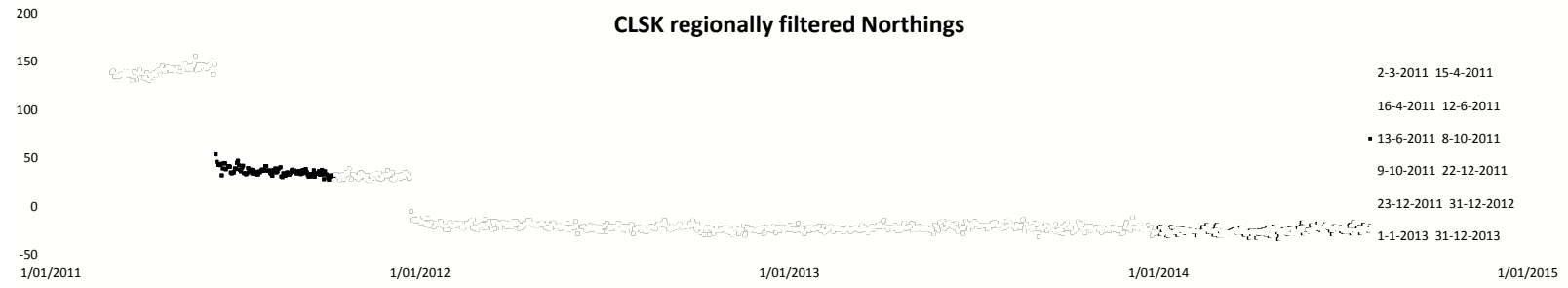
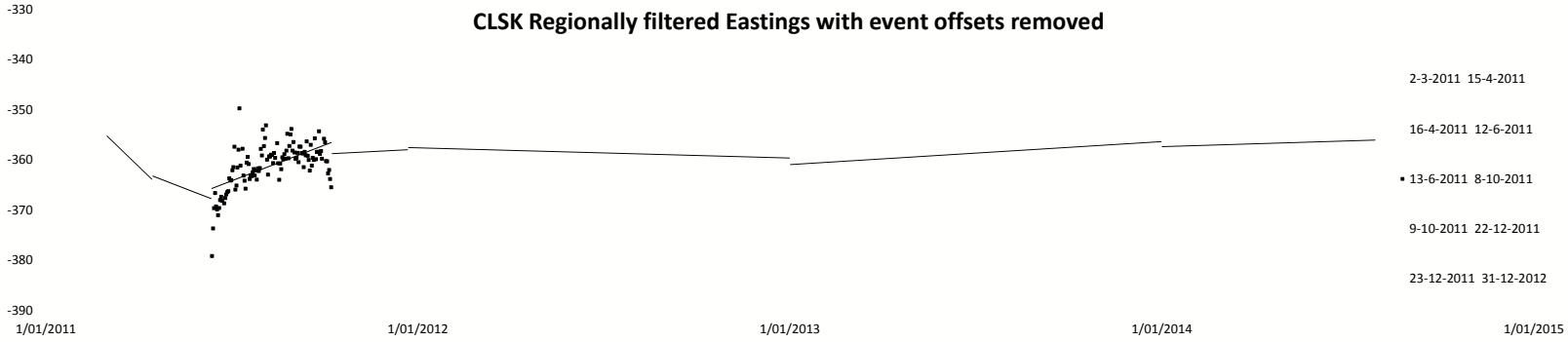
SCALE BAR: 0 50 100 m			<b>MOVEMENT VECTORS</b> <b>Monitoring and cGPS Marks (Source: Aurecon, GeoNet)</b> <b>Filtered Linear Movement*</b>		<b>APPENDIX 2</b> Map 7	
EXPLANATION: * Movement with assumed earthquake induced landslide movement and tectonic (earthquake) movement removed. Movement estimated from least squares adjustment (assuming a linear trend). ** Taken from the report CR2012/317 Background shade model derived from NZAM post earthquake 2011c (July 2011) LiDAR survey resampled to a 1 m ground resolution. Roads and building footprints provided by Christchurch City Council (20/02/2012). PROJECTION: New Zealand Transverse Mercator 2000						
		DRW: BL CHK: CM, GA, FDP			REPORT: CR2014/76	DATE: August 2014



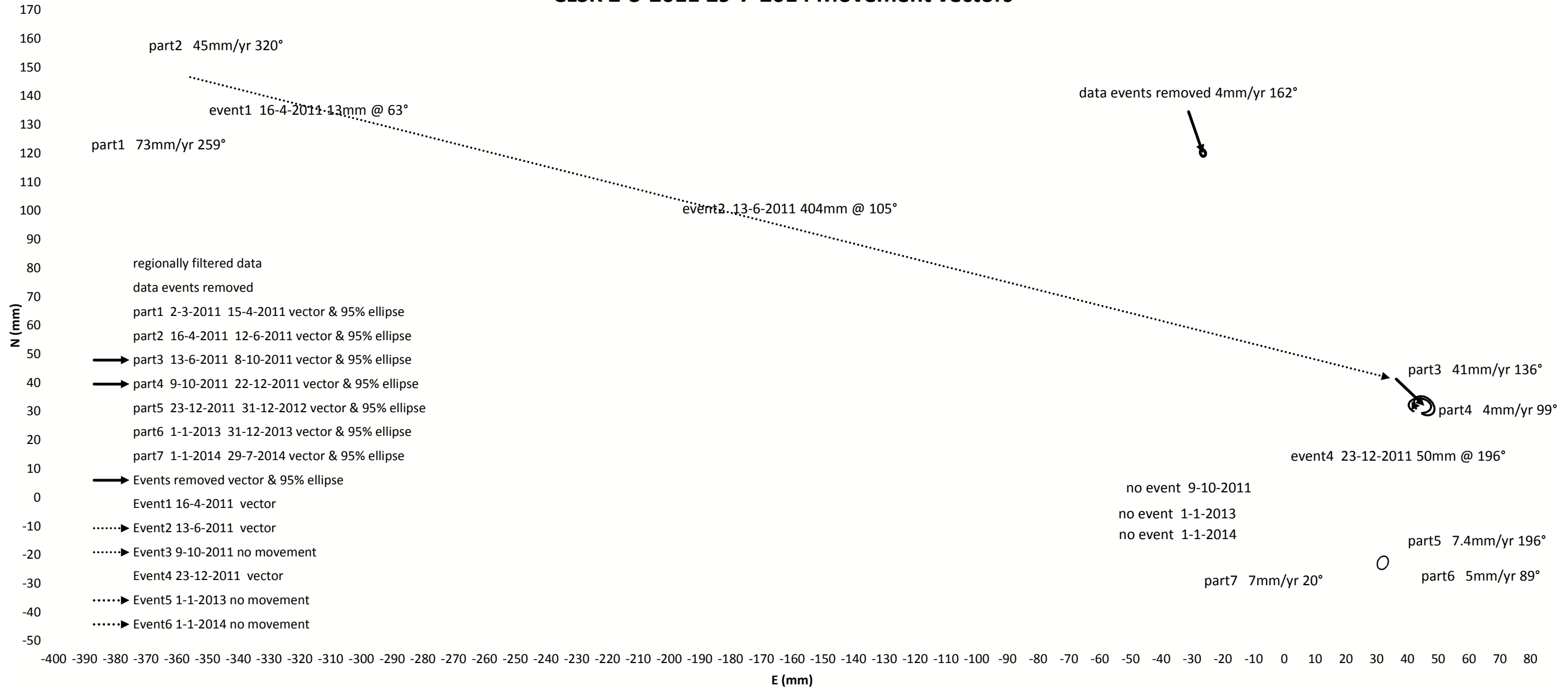
## **A3 APPENDIX 3: CONTINUOUS GPS TIME-SERIES DATA**





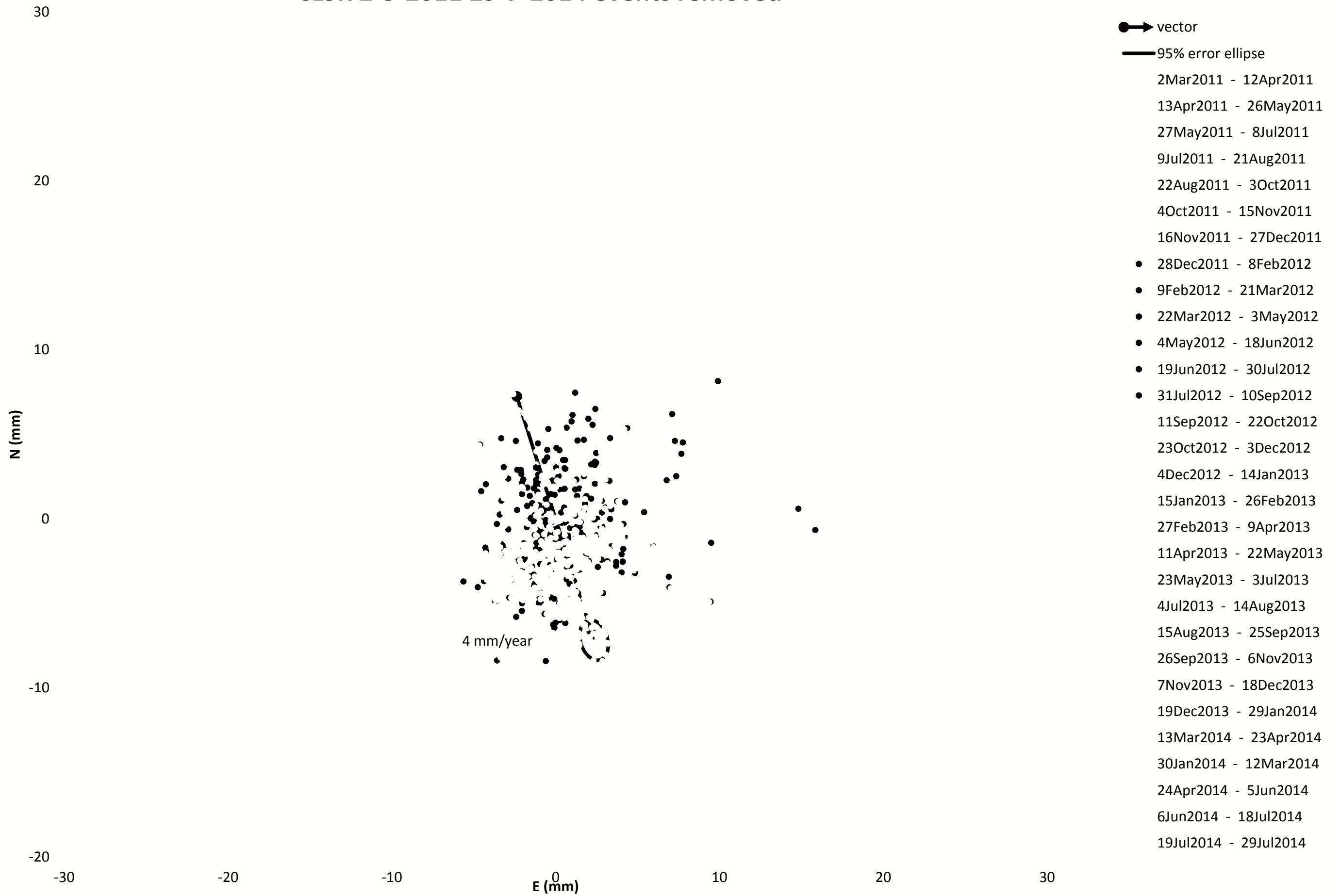


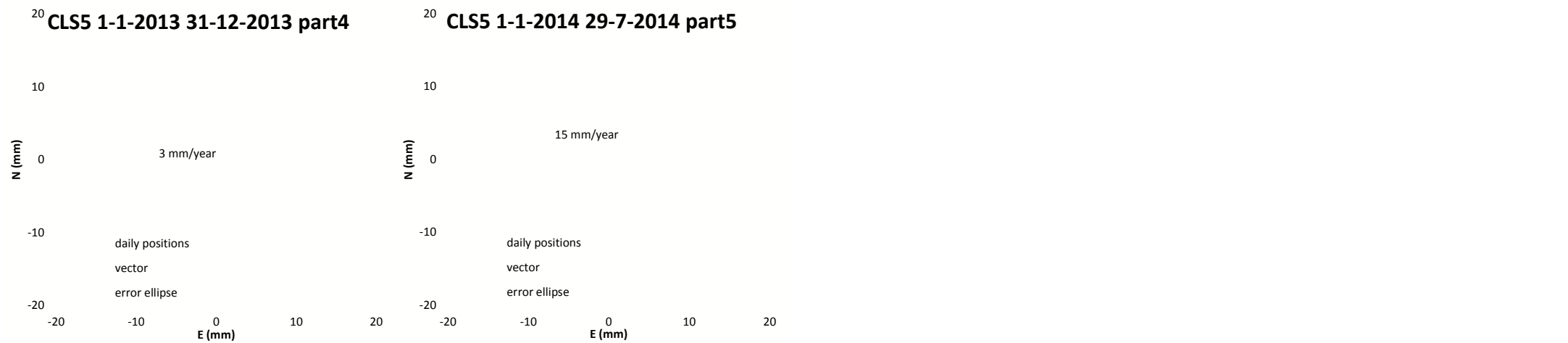
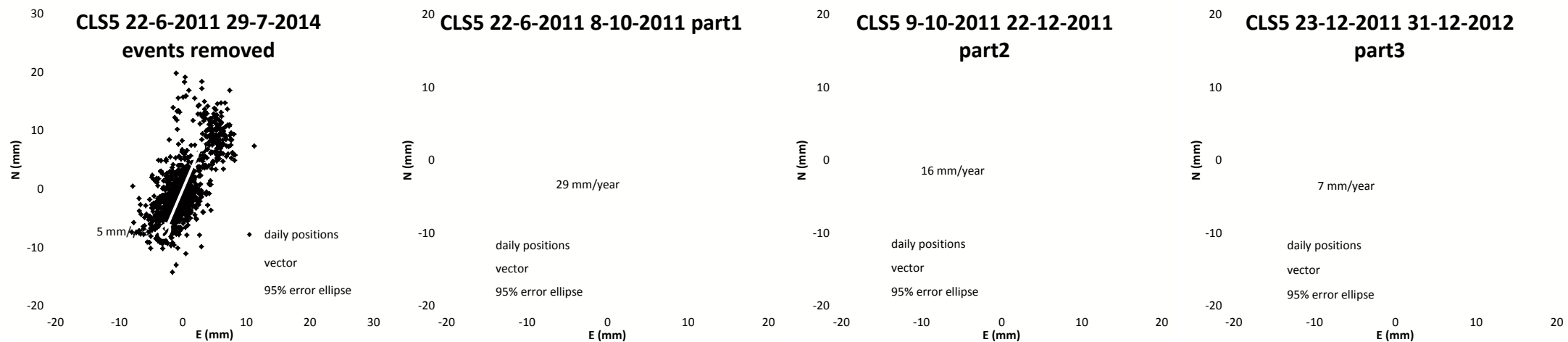
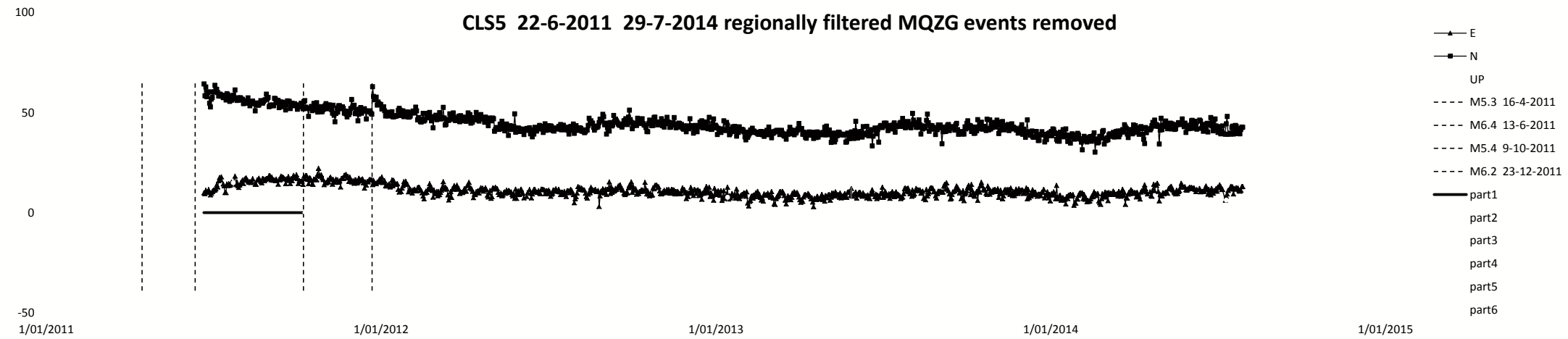
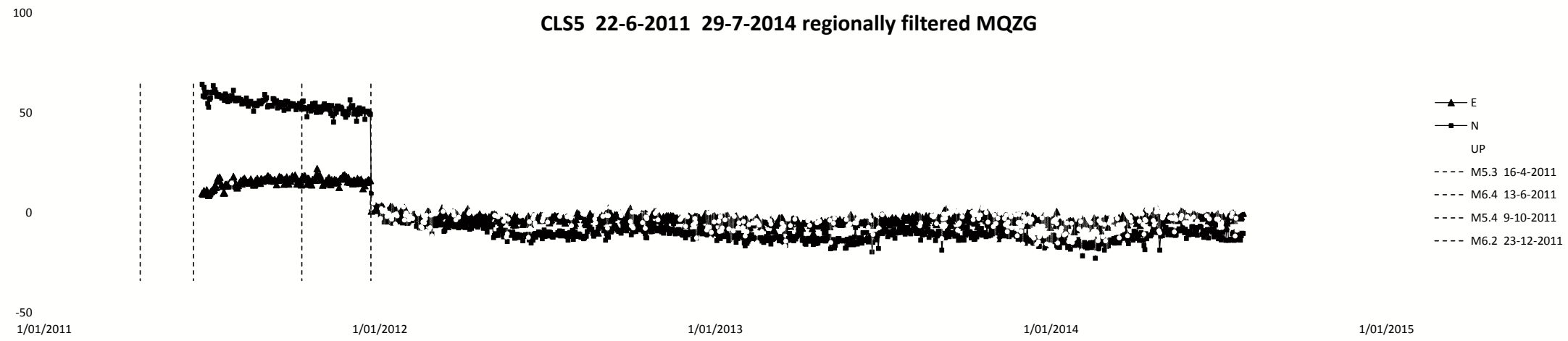
### CLSK 2-3-2011 29-7-2014 Movement vectors

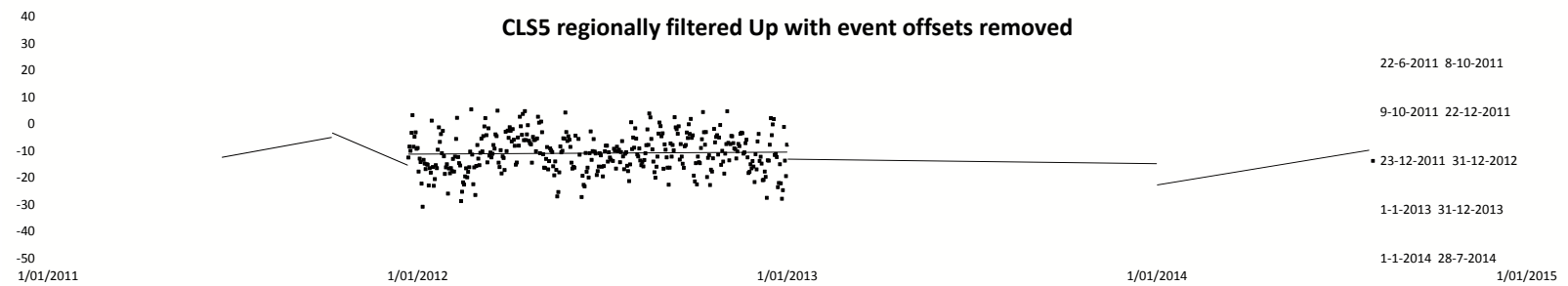
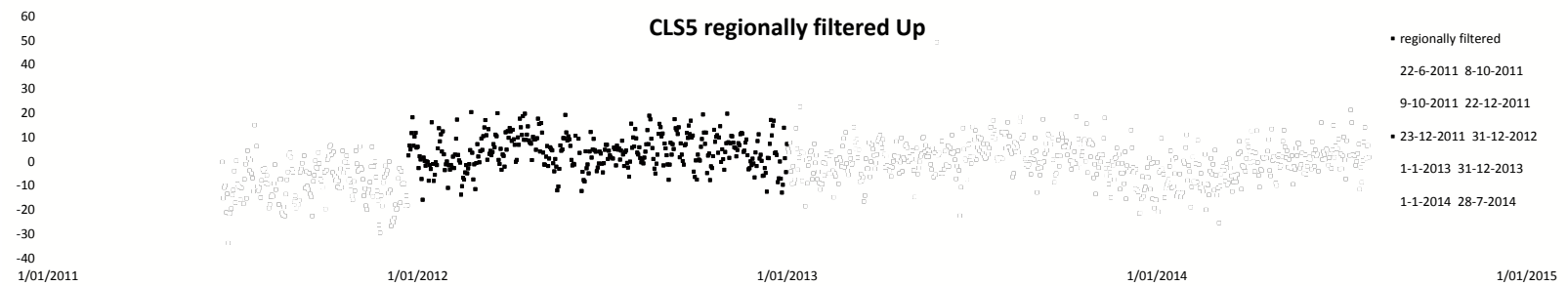
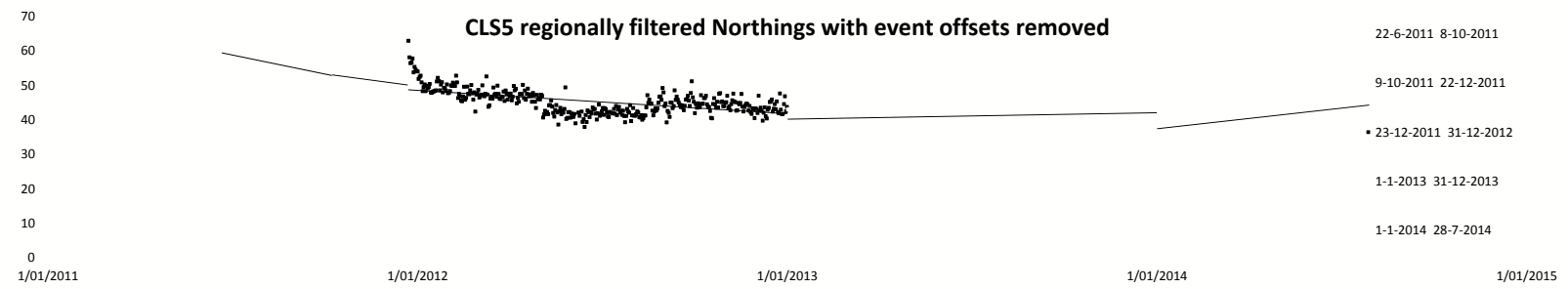
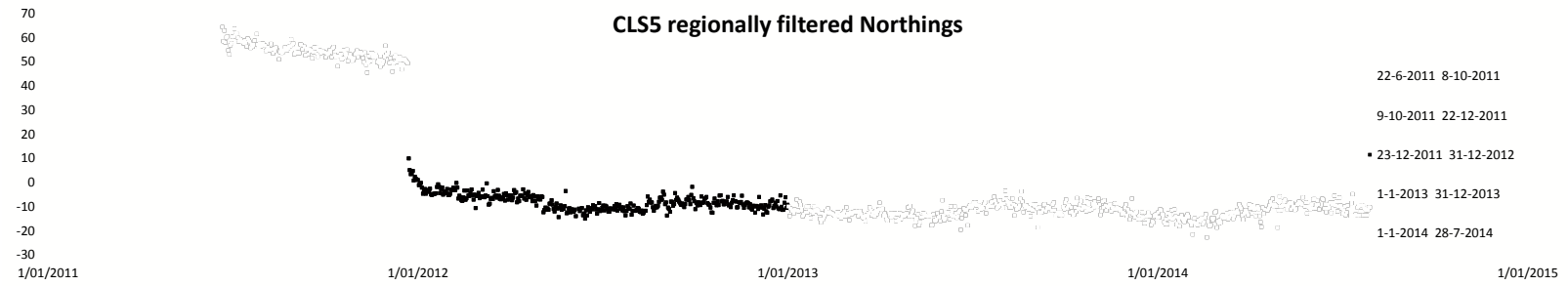
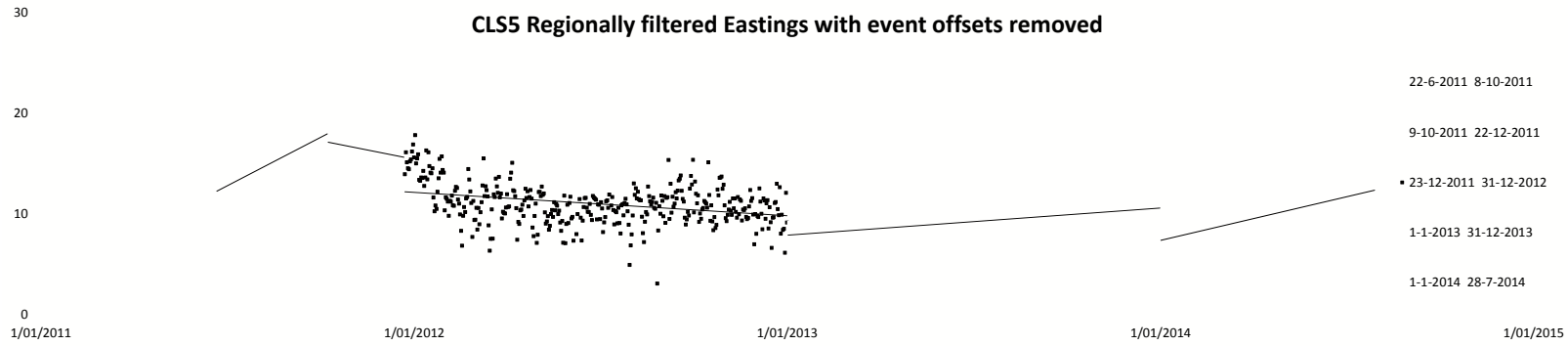
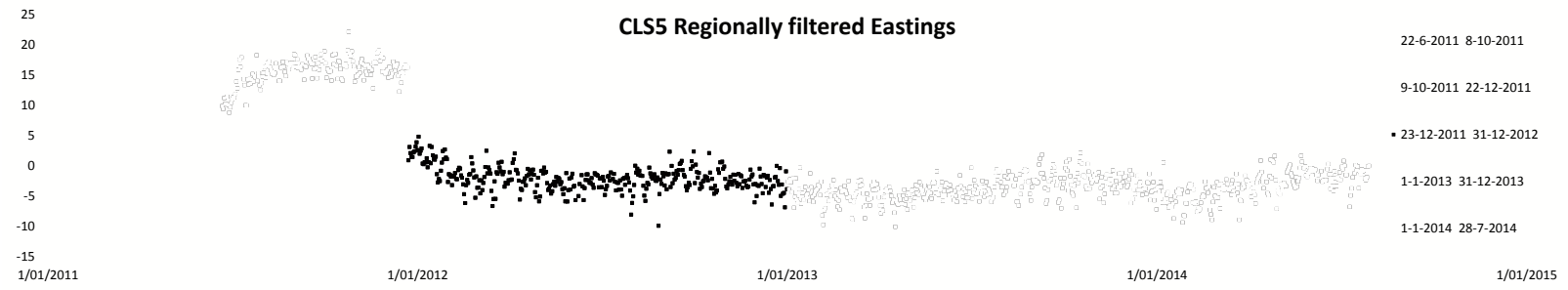


CLSK	offset (mm)	bearing (deg)	up (mm)	comments	date	event	
Event1	13	63			16/04/2011	M5.3	
Event2	404	105	20		13/06/2011	M6.4	
Event3					9/10/2011	M5.4	
Event4	50	196	-7		23/12/2011	M6.2	
Event5					1/01/2013		
Event6					1/01/2014		
	rate (mm/yr)	bearing (deg)	95% CE (mm)	#days	#obs	startdate	enddate
Part1	73	259	33	45	45	2/03/2011	15/04/2011
Part2	45	320	27	58	56	16/04/2011	12/06/2011
Part3	41	136	12	118	114	13/06/2011	8/10/2011
Part4	4	99	18	75	74	9/10/2011	22/12/2011
Part5	7.4	196	2	375	369	23/12/2011	31/12/2012
Part6	5	89	2	365	363	1/01/2013	31/12/2013
Part7	7	20	4	210	208	1/01/2014	29/07/2014
data events removed	4	162	0	1246	1229	2/03/2011	29/07/2014

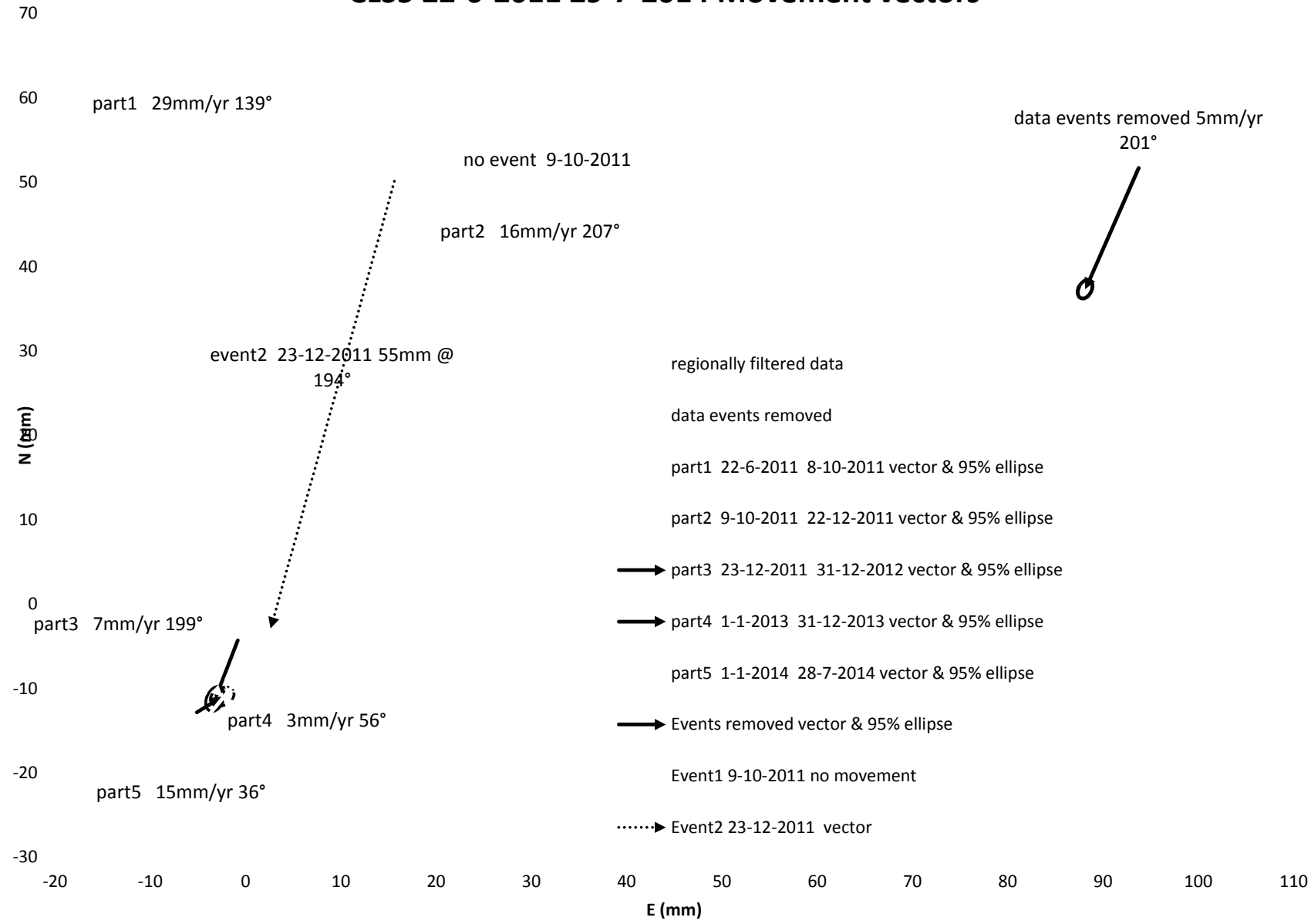
# CLSK 2-3-2011 29-7-2014 events removed







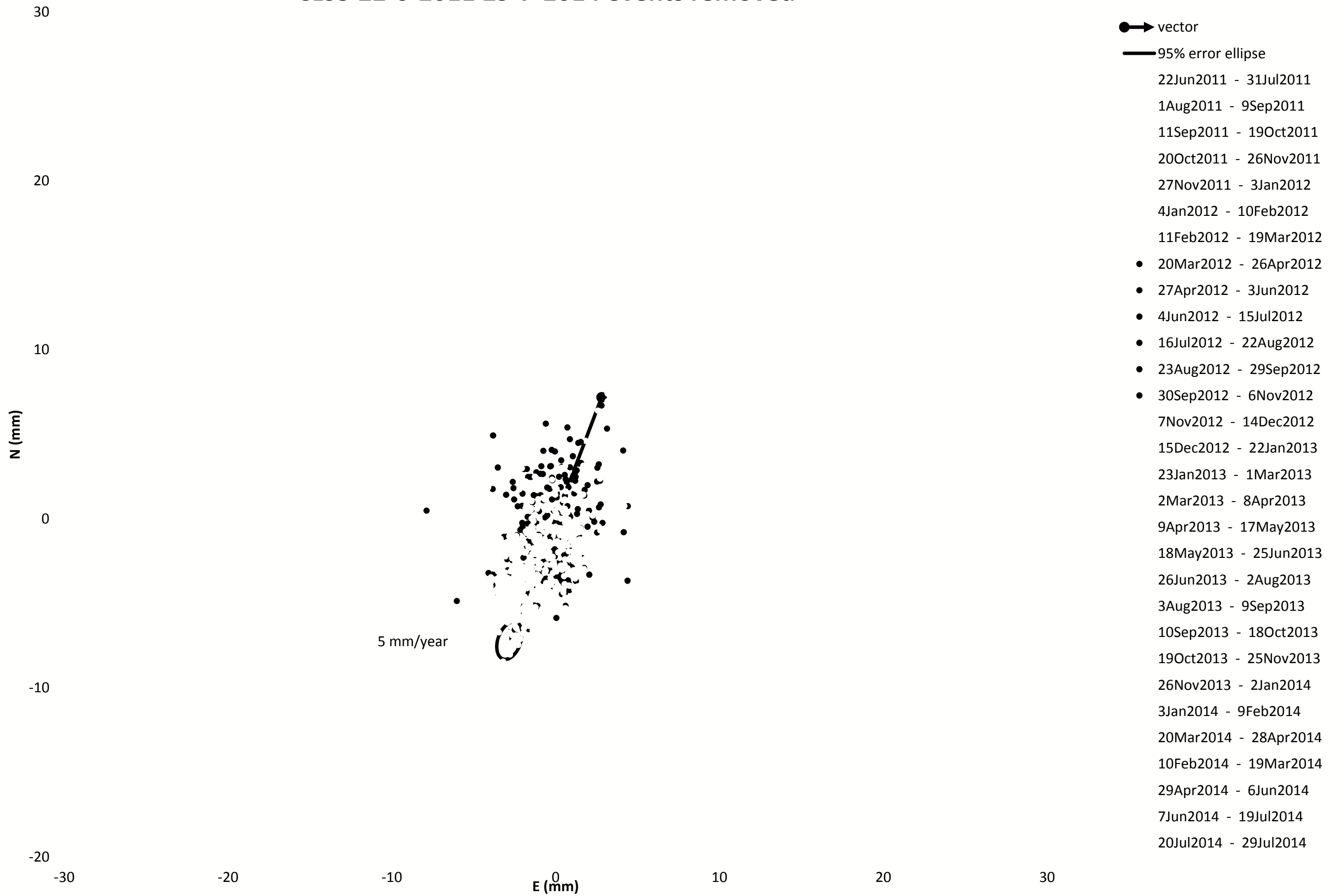
# CLS5 22-6-2011 29-7-2014 Movement vectors

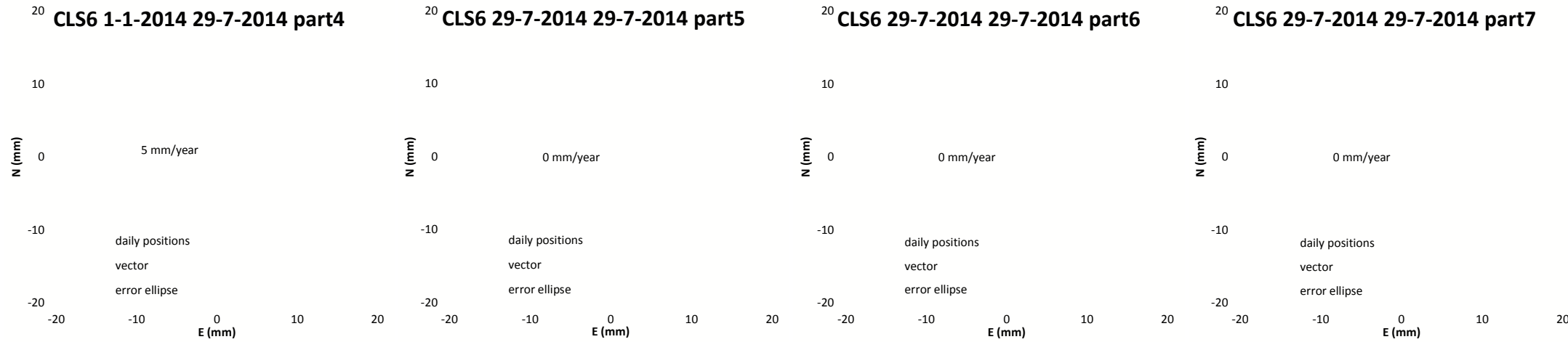
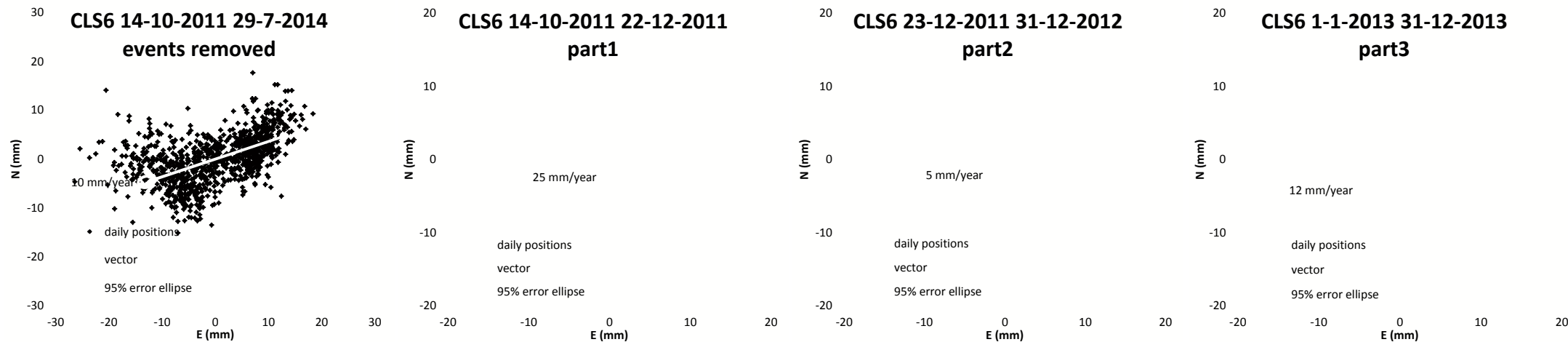
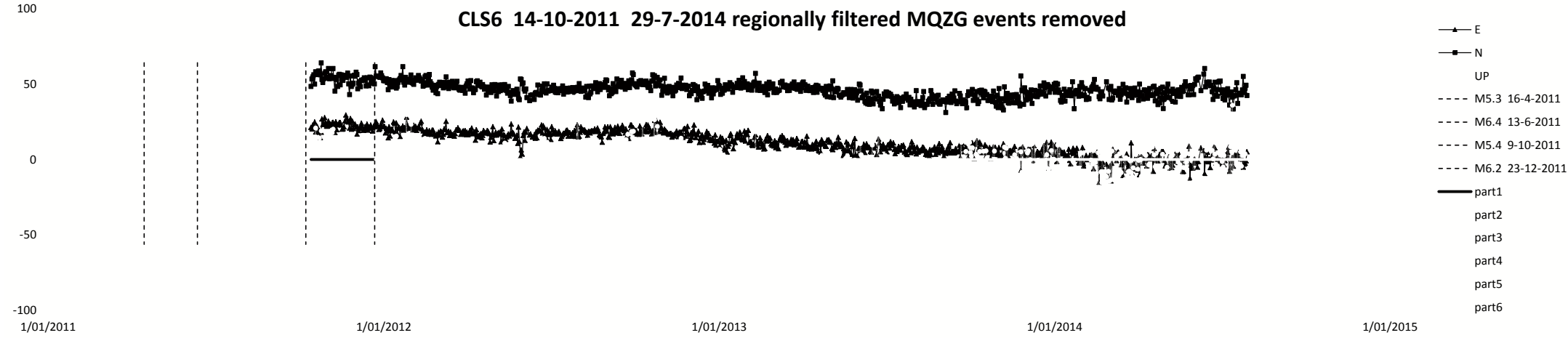
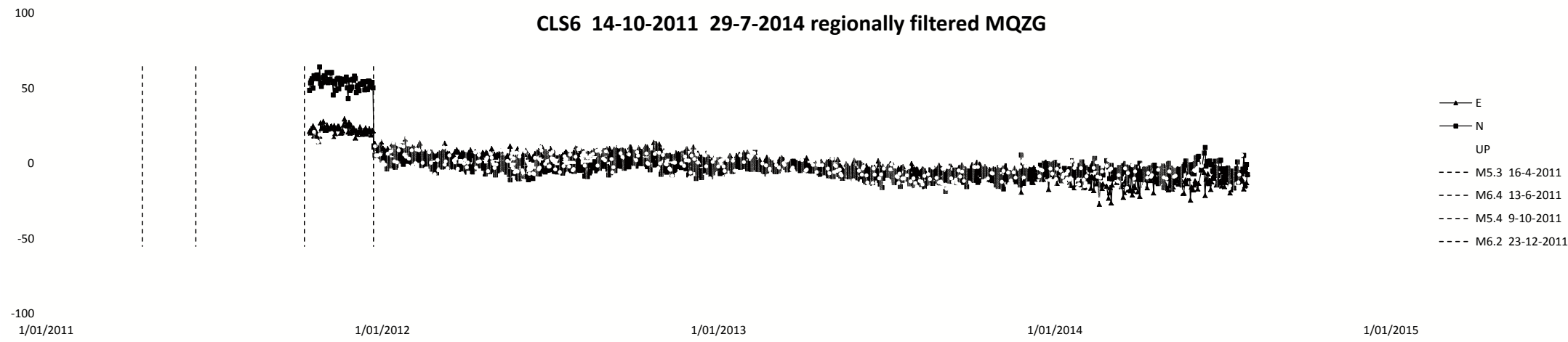


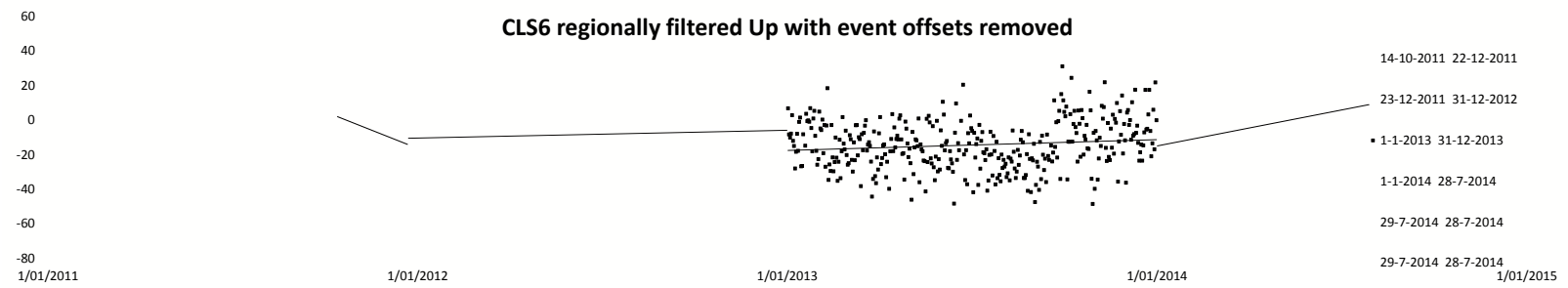
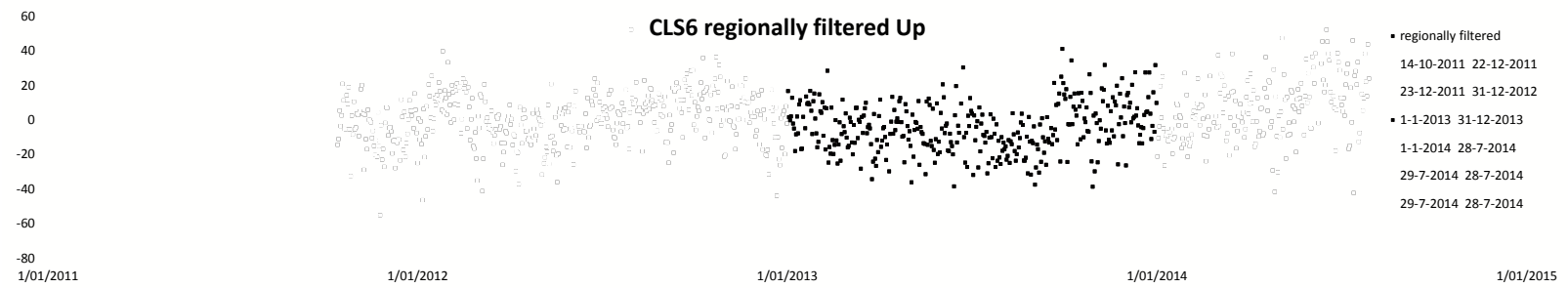
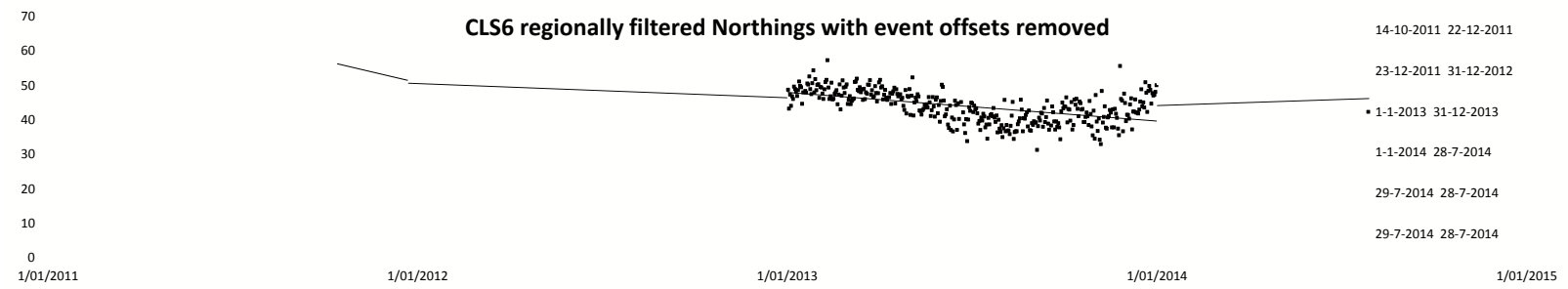
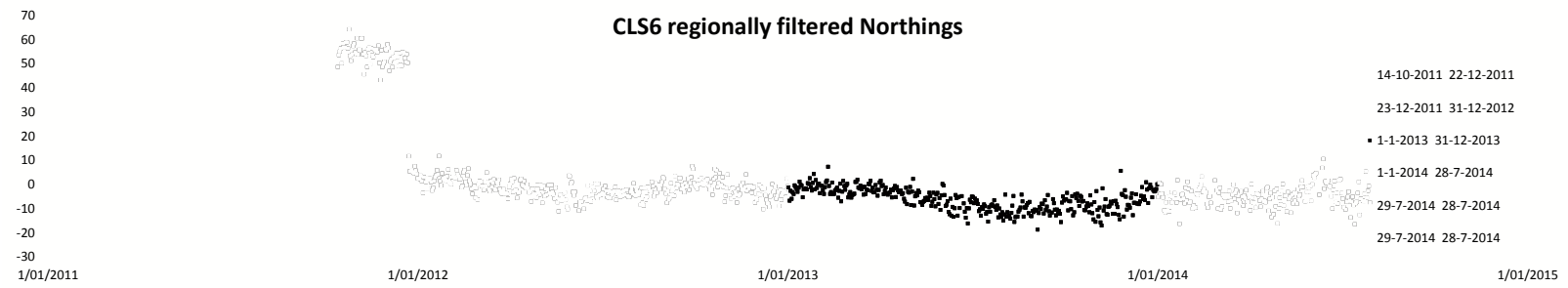
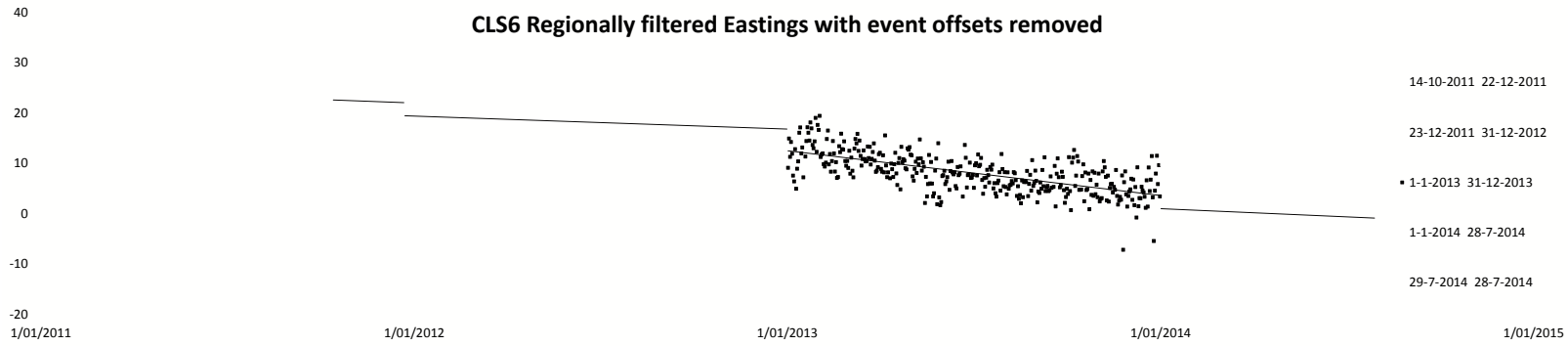
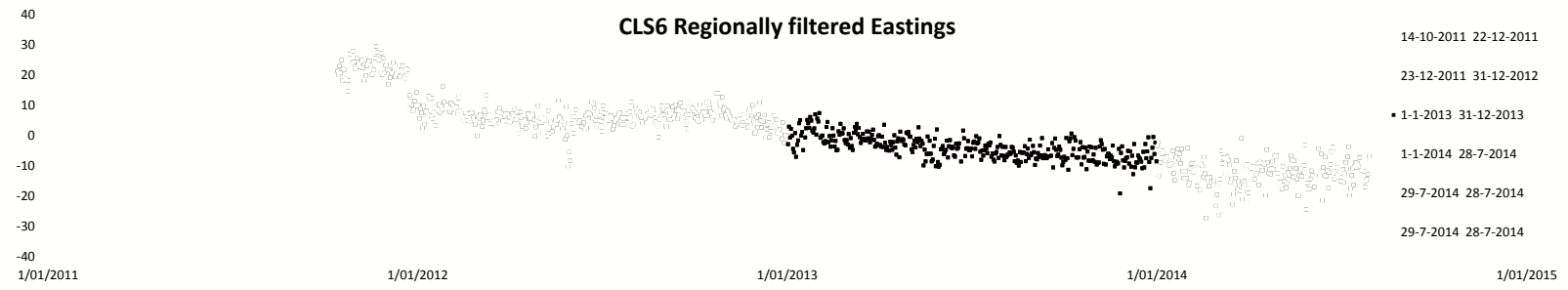
CLS5	offset (mm)	bearing (deg)	up (mm)	comments	date	event
Event1					9/10/2011	M5.4
Event2	55	194	-15		23/12/2011	M6.2

	rate (mm/yr)	bearing (deg)	95% CE (mm)	#days	#obs	startdate	enddate
Part1	29	139	7	109	103	22/06/2011	8/10/2011
Part2	16	207	12	75	75	9/10/2011	22/12/2011
Part3	7	199	1	375	371	23/12/2011	31/12/2012
Part4	3	56	1	365	361	1/01/2013	31/12/2013
Part5	15	36	3	210	202	1/01/2014	29/07/2014
data events removed	5	201	0	1134	1112	22/06/2011	29/07/2014

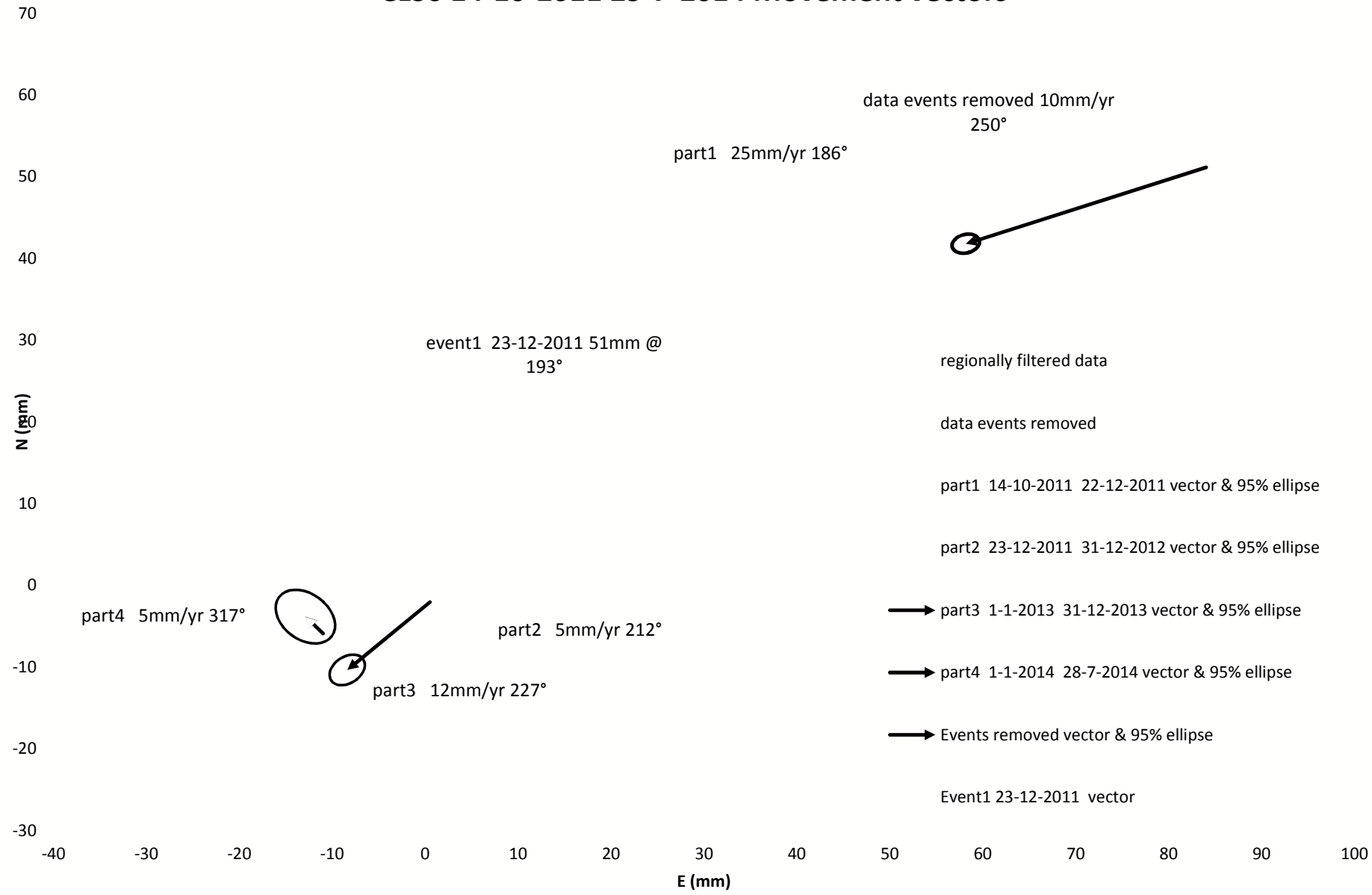
# CLS5 22-6-2011 29-7-2014 events removed





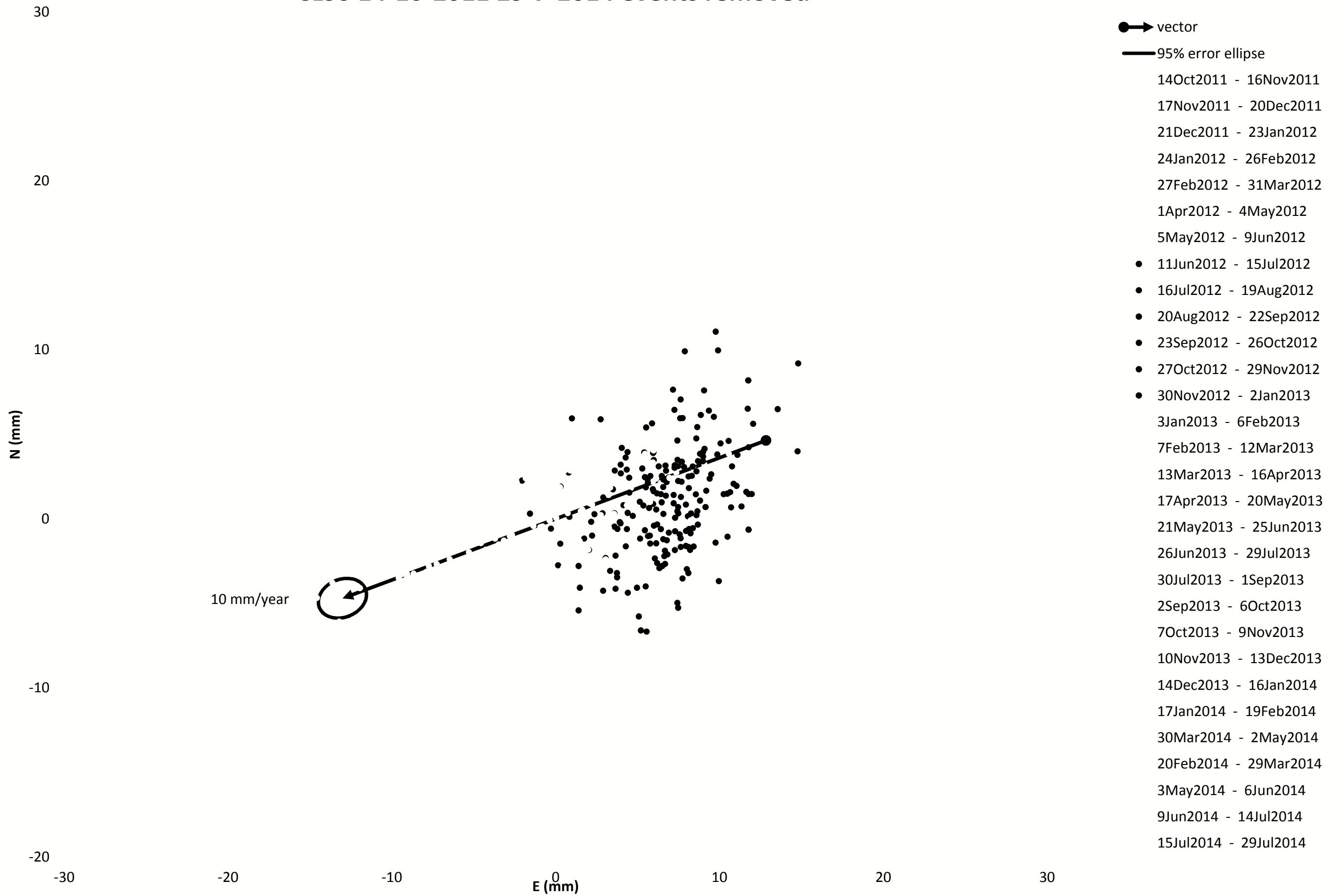


# CLS6 14-10-2011 29-7-2014 Movement vectors



CLS6	offset (mm)	bearing (deg)	up (mm)	comments	date	event	
Event1	51	193	-10		23/12/2011	M6.2	
Event2					1/01/2013		
Event3					1/01/2014		
Event4					29/07/2014		
Event5					29/07/2014		
Event6					29/07/2014		
	rate (mm/yr)	bearing (deg)	95% CE (mm)	#days	#obs	startdate	enddate
Part1	25	186	24	70	70	14/10/2011	22/12/2011
Part2	5	212	2	375	370	23/12/2011	31/12/2012
Part3	12	227	2	365	360	1/01/2013	31/12/2013
Part4	5	317	7	210	200	1/01/2014	29/07/2014
Part5							
Part6							
Part7							
data events removed	10	250	1	1020	1000	14/10/2011	29/07/2014

# CLS6 14-10-2011 29-7-2014 events removed



## A4 APPENDIX 4: RESULTS FROM THE TWO-DIMENSIONAL SITE RESPONSE ASSESSMENT FOR CROSS-SECTION 1

The results from the two-dimensional site response modelling are shown for cross-section 2. The maximum acceleration ( $A_{MAX}$ ) at the slope crest derived from the modelling of each synthetic earthquake time history has been plotted in Figure A4.1. The slope crest is defined as the convex break in slope between the lower steeper slope and the upper less steep slope. Each point on the graph represents the response of this location to a given synthetic free field rock outcrop earthquake input motion (Table A4.1).

The extent of the coseismic landslide, inferred from survey data, crack mapping and slope morphology, is about 130 m in length and about 150 m wide. The modelled peak ground accelerations at the surface across the landslide are, therefore variable given the extent of the landslide. The highest modelled peak ground accelerations during the 22 February 2011 earthquake coincide with the convex break in slope ( $A_{MAX}$ ).

The fundamental frequency of the slope varies from 1.8 to 3.8 Hz based on the equation in Bray and Travasarou (2007), where frequency =  $1/(4 \times H/V_S)$ , and H = slope height of 80 m, and  $V_S$  = average shear wave velocity for the slope of 570–1,200 m/s. The dominant frequency of the input motions is between 3.6 Hz and 5.7 Hz. The “tuning ratio” defined as the ratio between the dominant frequency of the input motion and the fundamental frequency of the slope (Wartman et al., 2013), is about 2.0–3.2 for a shear wave velocity of 570 m/s, and 1.0–1.5 for a shear wave velocity of 1,200 m/s.

Results from the seismic response assessment suggest that the peak ground acceleration amplification factors ( $S_T$ ) for cross-section 2 is about 2.7 ( $\pm 0.2$ ) for horizontal motions, and 1.9 ( $\pm 0.1$ ) for vertical motions – errors at one standard deviation (Figure A4.1).

**Table A4.1** Results from the two-dimensional site response assessment for cross-section 2, using the out-of-phase synthetic free-field rock outcrop motions for the Maffey's Road site by Holden et al. (2014) as inputs to the assessment. PGA is peak ground acceleration.

Earthquake (2011)	Free-field input PGA (horizontal) – $A_{FF}$ (g)	Free-field input PGA (vertical) – $A_{FF}$ (g)	Maximum PGA (horizontal) at convex break in slope – $A_{MAX}$ (g)	Maximum PGA (vertical) at convex break in slope – $A_{MAX}$ (g)
22 February	0.87	0.77	2.50	1.43
16 April	0.05	0.03	0.10	0.07
13 June	0.44	0.30	0.93	0.60
23 December	0.19	0.14	0.36	0.35

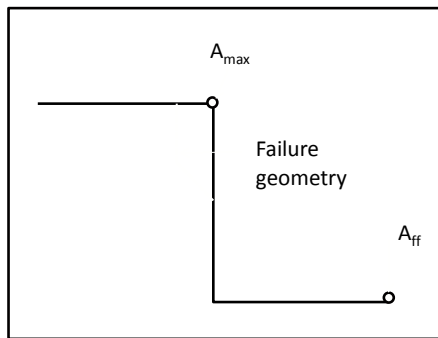
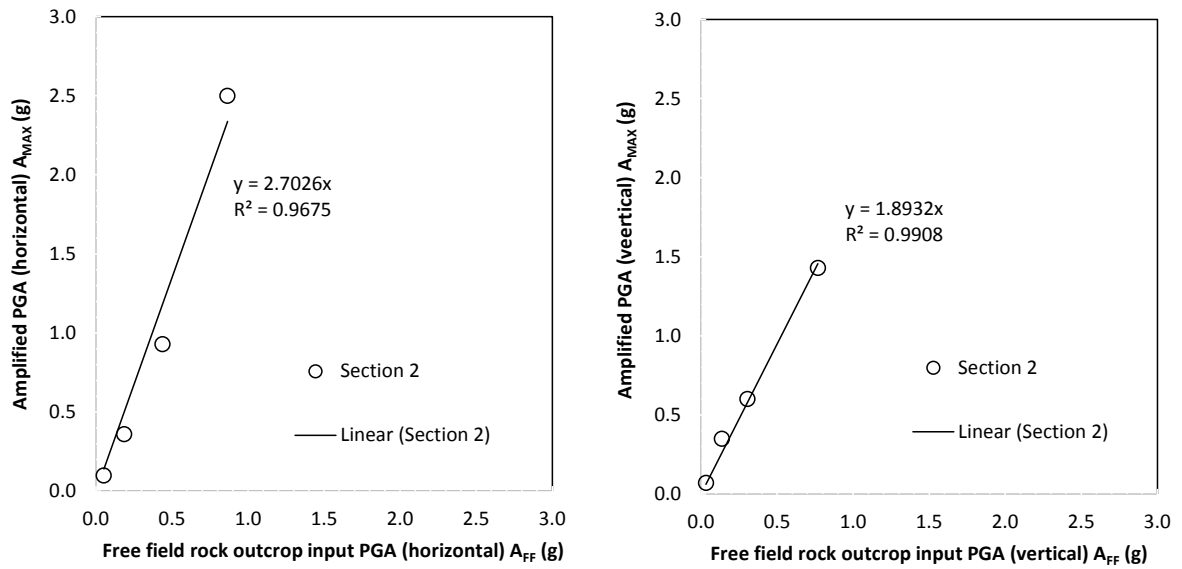


**Figure A4.1** Amplification relationship between the synthetic free-field rock outcrop input motions ( $A_{FF}$ ) and the modelled cliff crest maximum accelerations ( $A_{MAX}$ ) for cross-section 2. A schematic diagram showing the locations of the various recorded accelerations is shown.

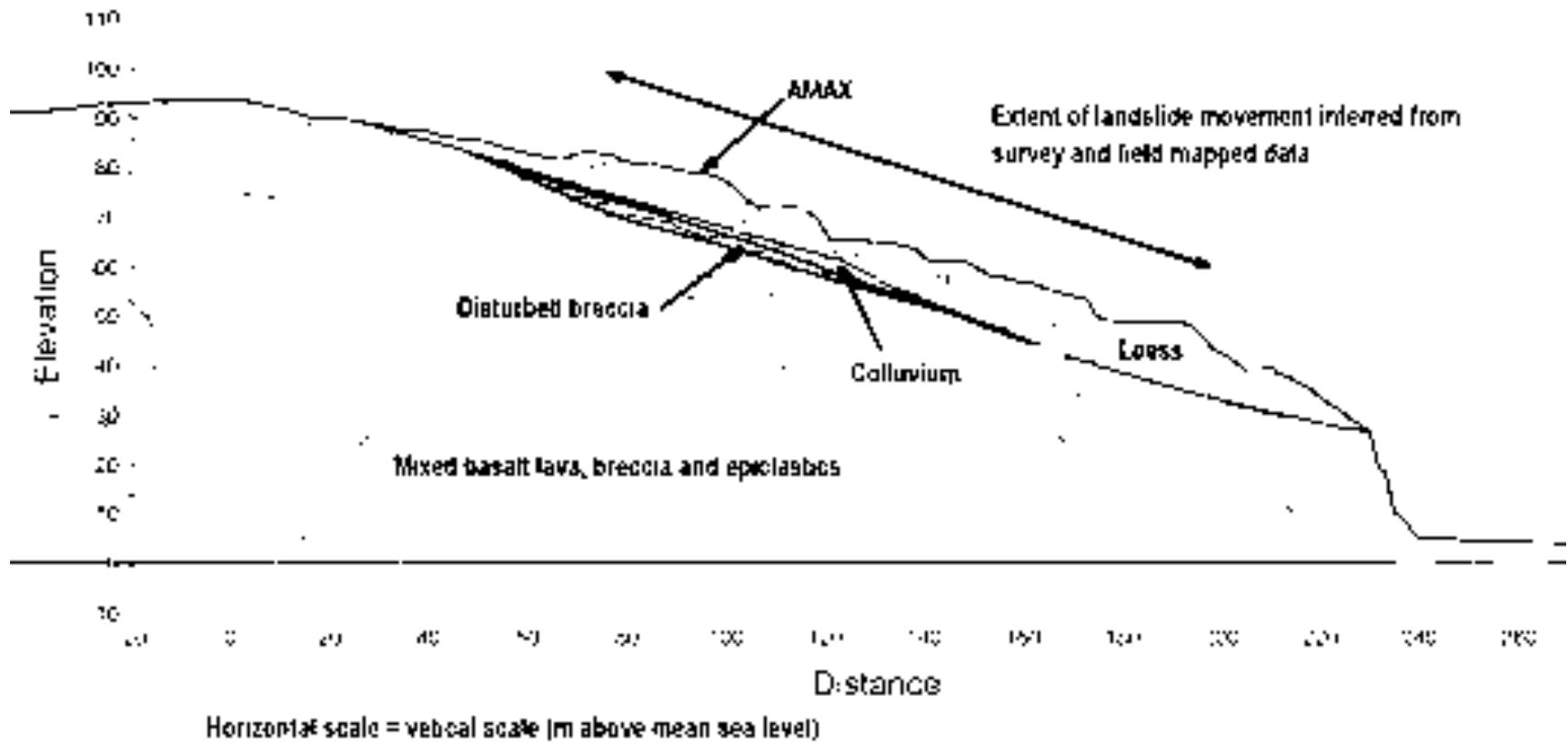


**Figure A4.2** Modelled horizontal peak ground acceleration contours for the 22 February 2011 earthquake at Clifton Terrace, cross-section 2.

The relationship between the modelled vertical and horizontal peak ground accelerations recorded at the slope crest ( $A_{MAX}$ ) is shown in Figure A4.3. The gradient of the linear fit is  $0.59 (\pm 0.03)$  – errors at one standard deviation. The relationship between horizontal and vertical peak ground accelerations appears more curved than linear.

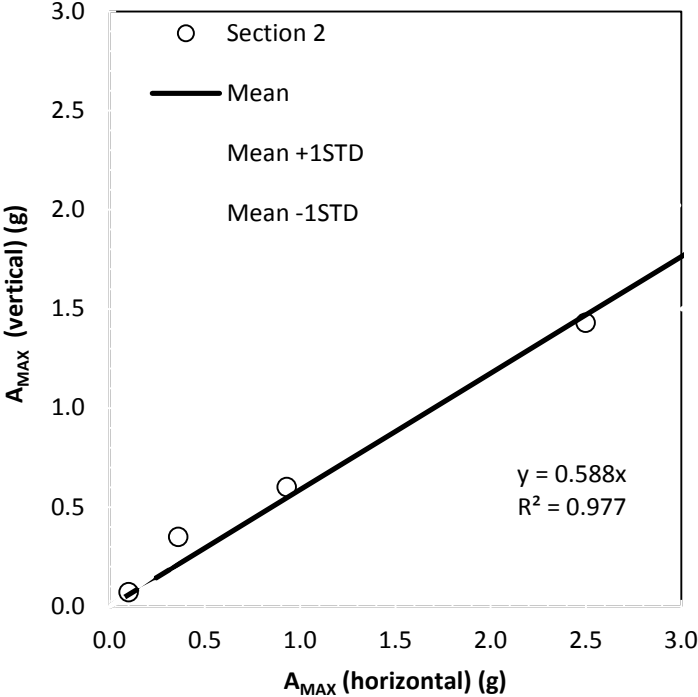


**Figure A4.3** Relationship between the modelled horizontal and vertical maximum accelerations modelled at the convex break in slope ( $A_{MAX}$ ) for cross-section 2, using the synthetic free-field rock outcrop motions for the Clifton Terrace site by Holden et al. (2014) as inputs to the assessment. The mean and standard deviation trend lines are fitted for  $A_{MAX}$  all data. Errors are shown as the mean  $\pm$  one standard deviation (1 STD).

Results from this assessment have shown that the relationship between the peak ground acceleration of the free-field input motion and the corresponding modelled peak acceleration at the slope crest ( $A_{MAX}$ ) is approximately linear. In the range of modelled peak horizontal accelerations, the horizontal amplification factor ( $S_T$ ) is typically in the order of about 2.7 times the input free-field peak horizontal acceleration.

Cross-section 2 comprises about 12 m of loess and colluvium overlying weathered basalt breccia and mixed basalt lava, breccia and epiclastic sequences, where the mean shear wave velocities of the materials change from 570–1,200 m/s in the basalt breccia and lava, to 200–400 m/s in the loess and colluvium (Figure A4.2). The results suggest that the impedance contrasts between the materials contribute most to the amplification of shaking, but that the peak horizontal accelerations (for all modelled earthquakes) concentrate around the convex break in slope, defined as  $A_{MAX}$ .

Results from the assessment of the data collected by the seismic array instruments installed on Clifton Terrace reported by Kaiser et al. (2014) show significant differences in mean peak ground acceleration amplification between stations of up to 1.7 times horizontal and 2.4 times vertical (Figure A4.4). Kaiser et al. (2014) report that there was significant variation in these values across individual events, as seen from the range of values within one standard deviation of the mean shown in Figure A4.4. Furthermore, these values are derived from small to moderate sized earthquakes dominated by high-frequency ground motions and

therefore they cannot be considered appropriate for larger magnitude shaking without further study. However, these results do show that the stations located on source area A (station K1 and K3) have higher amplification factors to the ones located outside the area of cracking (K4 and K5, where K5 is the reference station).

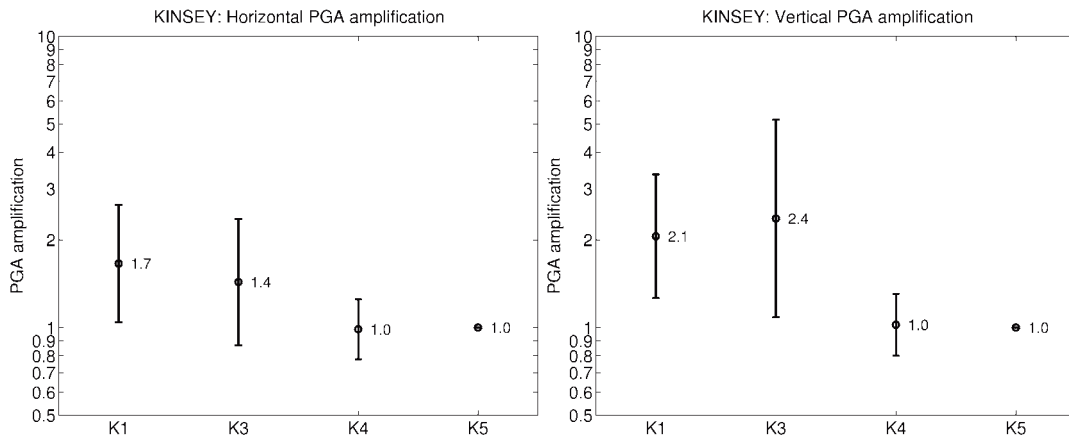


**Figure A4.4** Peak ground amplification (PGA) with respect to the reference station in the horizontal (left) and vertical (right) directions recorded between stations at Clifton Terrace (Figure 6 for instrument locations). The horizontal PGA is taken to be the larger of the two horizontal components. Geometric mean and standard deviations of the amplification factors across individual events are shown as error bars.

These results are similar to those reported by others (e.g., Del Gaudio & Wasowski, 2010), where material impedance contrasts have been shown to have a significant effect on the amplification of shaking. Given the increased amplification of shaking within the loess and colluvium, coupled with the coseismic landslide displacement inferred from surveying, it is likely that the basal slide surface is coincident with the boundary between the colluvium and the underlying rock.

In experimental data, as the slope displaces during an earthquake, the slide surface can “base isolate” the mass above, resulting in lower levels of shaking and displacement. Therefore, the reported amplification factors are near the upper bound of published topographic amplification factors. However, given the impedance contrasts between the loess/fill and rock are so high, this contrast could lead to the trapping of seismic waves within the loess and colluvium. Assessment of this is outside the scope of this report.

Eurocode 8, Part 5, Annex A, gives some simplified amplification factors for the seismic action used in the verification of the stability of slopes. Such factors, denoted  $S_T$ , are to a first approximation considered independent of the fundamental period of vibration and, hence, multiply as a constant scaling factor.

Eurocode 8, Part 5, Annex A recommends:

1. Isolated cliffs and slopes. A value  $S_T \geq 1.2$  should be used for sites near the top edge;
2. Ridges with crest width significantly less than the base width. A value  $S_T \geq 1.4$  should be used near the top of the slopes for average slope angles greater than  $30^\circ$  and a value  $S_T > 1.2$  should be used for smaller slope angles;
3. Presence of a loose surface layer. In the presence of a loose surface layer, the smallest  $S_T$  value given in a) and b) should be increased by at least 20%;

4. Spatial variation of amplification factor. The value of  $S_T$  may be assumed to decrease as a linear function of the height above the base of the cliff or ridge, and to be unity at the base; and
5. These amplification factors should in preference be applied when the slopes belong to two-dimensional topographic irregularities, such as long ridges and cliffs of height greater than about 30 m.

Ashford and Sitar (2002) recommend an  $S_T$  of 1.5 be applied to the maximum free-field acceleration behind the crest based on their assessment of slopes in homogenous materials, typically  $>60^\circ$  to near vertical and of heights (toe to crest) of typically  $>30$  m. This factor is based on the assessment of slopes that failed during the 1989 Loma Prieta  $M_w$  6.9 earthquake.

Results from the seismic response assessment suggest that the horizontal peak ground acceleration amplification factors ( $S_T$ ) for Clifton Terrace are about two to three (cross-section 3) times greater than the free field input motions. These are larger than those values reported by Ashford and Sitar (2002), and are in part a function of the impedance contrasts within the slope, which are not reported to occur in the slopes assessed by Ashford and Sitar (2002). These higher factors may also be a function of the site to earthquake-source distances. In the case of Clifton Terrace, the site is within 5 km of the epicentres of the 22 February, 16 April, 13 June and 23 December 2011 earthquakes, making them all “near-field” earthquakes.





[www.gns.cri.nz](http://www.gns.cri.nz)

#### Principal Location

---

1 Fairway Drive  
Avalon  
PO Box 30368  
Lower Hutt  
New Zealand  
T +64-4-570 1444  
F +64-4-570 4600

#### Other Locations

---

Dunedin Research Centre  
764 Cumberland Street  
Private Bag 1930  
Dunedin  
New Zealand  
T +64-3-477 4050  
F +64-3-477 5232

Wairakei Research Centre  
114 Karetoto Road  
Wairakei  
Private Bag 2000, Taupo  
New Zealand  
T +64-7-374 8211  
F +64-7-374 8199

National Isotope Centre  
30 Gracefield Road  
PO Box 31312  
Lower Hutt  
New Zealand  
T +64-4-570 1444  
F +64-4-570 4657